Probing the Functions of Nek Family Kinases Using Chemical Inhibition

Towards the Development of Potent and Selective Inhibitors of Nek7

Luke Antony Trask

Submitted in accordance with the requirements for the degree of
Doctor of Philosophy

The University of Leeds

School of Molecular and Cellular Biology
School of Chemistry
Astbury Centre for Structural Molecular Biology

Oct, 2021

The candidate confirms that the work submitted is his/her own, except where work which has formed part of jointly-authored publications has been included. The contribution of the candidate and the other authors to this work has been explicitly indicated below. The candidate confirms that appropriate credit has been given within the thesis where reference has been made to the work of others.

Reference(s) for the jointly authored paper(s) include:

S. Chow, A. I. Green, C. Arter, S. Liver, A. Leggott, L. Trask, G. Karageorgis, S. Warriner, A. Nelson, 'Efficient Approaches for the Synthesis of Diverse α-Diazo Amides', *Synthesis.* 2020, 52, A-L

The experimental work, supporting information and initial draft of the manuscript were completed by SC, AIG, CA, SL, AL, GK and the candidate. S.W and A.N supervised the research. A.N prepared the final version of the manuscript for publication.

This copy has been supplied on the understanding that it is copyright material and that no quotation from the thesis may be published without proper acknowledgement.

The right of Luke Antony Trask to be identified as Author of this work has been asserted by him in accordance with the Copyright, Designs and Patents Act 1988.

© 2021 The University of Leeds and Luke Antony Trask

Acknowledgements

Abstract

Understudied protein kinases such as NIMA-related kinases are crucial for cell cycle progression, being involved in the regulation of microtubule-dependent processes. In particular, Nek7 functions in centrosome separation, nuclear envelope breakdown, mitotic spindle assembly and cytokinesis to ensure timely and accurate progression of mitosis. Therefore, many Nek family kinases including Nek7 have been implicated in numerous cancer types. Despite Nek7 being a potential therapeutic target in cancer, no potent and selective inhibitors are available which has limited functional and target validation studies. Therefore, the development of a chemical tool to probe the function of Nek7 and validate this kinase as a therapeutic target in oncology is of great importance.

Previously identified fragments targeting Nek7 provided starting points for elaboration in activity-directed synthesis, four of which were exploited in 272 reactions over two rounds to identify several reactions which gave bioactive product mixtures. Analysis of these few reactions showed them to be non-productive and the reason for bioactivity was not determined.
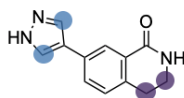
In an effort to identify a suitable chemical probe against Nek7, the structure-activity relationship of a previously developed Nek7 inhibitor (above) was explored further. Firstly, substituents at the 3,5-positions of the pyrazole ring (blue) were varied with 3-methylation proving beneficial. However any substituent larger than a methyl group was detrimental for potency. Next the 3,4-positions of the dihydroisoquinolinone core (purple) were optimised, identifying an amino-group at the 3-position to be beneficial with a diverse range of groups tolerated. Exploration of this azetidine moiety identified methylation which gave a further improvement. Combination of 3,5-pyrazole and 3,4-dihydroisoquinolinone substituents proved beneficial and this work has led to the development of a series of low micromolar affinity inhibitors of Nek7, with up to a 12.5-fold improvement over the starting compound.

Table of Contents

List of Tables

List of Figures

List of Schemes

Abbreviations

ADP	Adenosine Diphosphate
ADS	Activity-Directed Synthesis
ALK	Anaplastic Lymphoma Kinase
AR	Androgen Receptor
ATP	Adenosine Triphosphate
Boc	*tert*-Butoxycarbonyl Protecting Group
Cap	Caprolactamate
CDK	Cyclin-Dependent Kinase
CMD	Concerted Metalation-Deprotonation
CML	Chronic Myeloid Leukaemia
Cp*	1,2,3,4,5-Pentamethylcyclopentadienyl
CTD	*C*-Terminal Domain
Dba	Dibenzylideneacetone
DBU	1,8-Diazabicyclo[5.4.0]Undec-7-Ene
DCC	N,N-Dicyclohexylcarbodiimide
DCE	1,2-Dichloroethane
DCLK	Doublecortin Like Kinase
DFG	Aspartate Phenylalanine Glycine
DFT	Density Functional Theory
DIPEA	N,N-Diisopropylethylamine
DLG	Aspartate Leucine Glycine
DMAD	Dimethyl Acetylenedicarboxylate
DMAP	4-Dimethylaminopyridine

DMF	Dimethyl Formamide
DMSO	Dimethyl Sulfoxide
DNA	Deoxyribonucleic Acid
(S)-DOSP	1-[[4-Alkyl(C11-C13)Phenyl]Sulfonyl]-(2S)-Pyrrolidinecarboxylate
EDG	Electron Donating Group
EDTA	Ethylenediaminetetraacetic Acid
EE	Ethoxyethyl Protecting Group
EGFR	Epidermal Growth Factor Receptor
EMAP	Echinoderm Microtubule-Associated Protein
EML	EMAP-Like Protein
ERK	Extracellular Signal-Related Kinase
EWG	Electron Withdrawing Group
FBDD	Fragment Based Drug Discovery
FDA	Food And Drug Administration
FGFR	Fibroblast Growth Factor Receptor
FLT3	Fms Like Tyrosine Kinase 3
GIST	Gastrointestinal Stromal Tumors
HATU	1-[Bis(Dimethylamino)Methylene]-1*H*-1,2,3-Triazolo[4,5-*B*]Pyridinium 3-Oxid Hexafluorophosphate
HMBC	Heteronuclear Multiple Bond Correlation
HRD	Histidine Arginine Aspartate
HRMS	High Resolution Mass Spectrometry
Hsp	Heat Shock Protein
HTS	High-Throughput Screening
IC50	Half-Maximal Inhibitory Concentration
ICKP	International Centre For Kinase Profiling

IR	Infrared Spectroscopy
JAK	Janus Kinase
K_M	Michaelis-Menten Constant
LE	Ligand Efficiency 1.4(-Logic50)/N
LED	Light Emitting Diode
LRRK	Leucine-Rich Repeat Kinase
MAPK	Mitogen-Activated Protein Kinase
MARK	MAP/Microtubule Affinity-Regulating Kinases
Mklp2	Mitotic Kinase-Like Protein 2
MRC PPU	Medical Research Council Protein Phosphorylation And Ubiquintylation Unit
NBS	*N*-Bromosuccinimide
NEBD	Nuclear Envelope Breakdown
Nek	NIMA-Related Kinase
NIMA	Never-In-Mitosis A
NLRP3	Nlr Family Pyrin Domain Containing 3
NMR	Nuclear Magnetic Resonance
NOESY	Nuclear Overhauser Effect Spectroscopy
NPC	Nuclear Pore Complex
NSCLC	Non-Small Cell Lung Cancer
NTE	*N*-Terminal Extension
Nup	Nucleoporin
Oct	Octanoate
p-ABSA	4-Acetamidobenzenesulfonyl Azide
PCA	Principal Component Analysis
PCy_3	Tricyclohexylphosphine

PDB	Protein Data Bank
PDGFR	Platelet-Derived Growth Factor Receptor
Pfb	Perfluorobutyrate
PI3K	Phosphoinositide 3-Kinases
PKA	Protein Kinase A
PLK	Polo-Like Kinase
RNAi	Rna Interference
rt	Room Temperature
SAR	Structure Activity Relationship
SDS-PAGE	Sodium Dodecyl Sulfate Polyacrylamide Gel Electrophoresis
STAB	Sodium Triacetoxyborohydride
SYK	Spleen Tyrosine Kinase
TACC3	Transforming Acidic Coiled-Coil Containing Protein 3
TFA	Trifluoroacetic Acid
THF	Tetrahydrofuran
TLC	Thin Layer Chromatography

Chapter 1

Biological Role and the Chemical Inhibitors of NIMA-related kinase 7

Protein kinases have become the pharmaceutical industry's most important therapeutic target in oncology[1] and, as a result, the development of kinase inhibitors is at the forefront of research and development. Despite approximately 70 kinase inhibitors approved to date, the majority of kinases have been historically understudied, indicating that the kinase inhibitor discovery field is still immature.[2–4]

Herein, an overview of protein kinases is given focusing on the understudied mitotic kinase Nek7. Known fragments inhibiting Nek7, with the potential to be developed into useful chemical probes, are discussed followed by an outline of the proposed project and its aim to develop a potent and selective Nek7 inhibitor. It is hypothesised this inhibitor could be used as a chemical tool, probing the cellular function of Nek7 to functionally annotate/clinically validate this kinase and stimulate new drug discovery efforts.

1.1   Protein Kinases

Ever since the first phosphorylation event was identified in the 1960s, kinases and the regulation of protein function by phosphorylation has been of interest.[5,6] Protein kinases are one of the largest class of proteins, with the human kinome currently consisting of 518 kinases.[5] Despite this number being about half that predicted prior to cataloguing of the kinome, kinases still constitute around 2% of all human genes.[5,7] Human protein kinases can be classified as serine-threonine or tyrosine kinases with the class denoting which residue of the target protein is phosphorylated. Protein kinases catalyse the transfer of the ATP γ-phosphate to a substrate protein, mediating most of the signal transduction in eukaryotes. Kinases phosphorylate up to one-third of the proteome with virtually every signal transduction process occurring *via* a phosphotransfer cascade.[2,8,9] In doing so, kinases control many cellular

processes such as cell cycle progression, transcription, metabolism, cytoskeletal rearrangement, cell movement, differentiation and apoptosis.

Considering their importance in signal transduction, it is unsurprising that deregulation of kinase function plays an important role in cancer as well as in immunological, inflammatory, neuro-degenerative, metabolic, cardiovascular and infectious diseases.[1,2]

1.1.1 Protein Kinase Structure

Protein kinase A (PKA) was the first crystal structure of a kinase to be published 30 years ago.[10] The structure of many protein kinases has been solved to date, illustrating the now well-known conserved structural core of protein kinases (Fig. 1-1 a-b).[11,12] Furthermore, comparison of the active and inactive conformation of these structures has provided understanding of their regulation (Fig. 1-1 c-d). The protein kinase core consists of an *N*-lobe and a *C*-lobe, with the latter being the larger of the two lobes and the letter denoting the terminus in which the lobe is located. The two lobes are connected by a short, ordered linker sequence, the hinge, the backbone residues of which form two hydrogen bonds to the adenine base of ATP, which binds to the cleft formed between the two lobes. The residue immediately prior to the hinge is the gatekeeper, an important determinant of inhibitor selectivity and Type 1½ inhibition. The *N*-lobe consists of at least one α-helix, the conserved αC-helix, and a 5-stranded anti-parallel β-sheet ($\beta1$-$\beta5$) whereas the *C*-lobe is mostly α-helical with a small β-sheet ($\beta6$-$\beta7$). The dynamic glycine rich *P*-loop, located between $\beta2$-$\beta3$ forms the roof of the ATP cleft and positions the γ-phosphate of ATP for phosphoryl transfer. The αC-helix and activation loop, a dynamic loop involved in substrate recognition and is the site of phosphorylation, must be properly positioned in an active kinase.

Active kinases exhibit a specific conformation in which catalytic and regulatory residues align and function to position the substrate and ATP for catalysis.[11,12] For instance, phosphorylation on the activation loop (either by the kinase itself – autophosphorylation – or a partner protein) is a hallmark of an active kinase. Furthermore, in an active kinase the αC-helix is 'in', packed against the kinase domain, interacting with the phosphorylated activation loop and enabling proper positioning of the regulatory *R*-spine as well as a conserved glutamate-

lysine salt bridge. In an inactive kinase the αC-helix is 'out' away from the kinase domain, disrupting these interactions and opening up an allosteric pocket for exploitation (see Type 1½ and Type III inhibitors) This catalytic lysine residue also interacts with the α and β phosphates of ATP to position them for catalysis. The *R*-spine is another hallmark of the active kinase in which four hydrophobic residues in the kinase core are linearly aligned in a stacked configuration. The residues that make up the *R*-spine are located at the *N*-terminus of the β4 strand (RS1) as well as on the αC-helix (RS2) and in the DFG (RS3) and HRD motifs (RS4). This linear alignment of the *R*-spine functions to align the *N*- and *C*-lobes, is therefore crucial for kinase activity and requires the proper positioning of the DFG and HRD motifs.[13] Furthermore, the *R*-spine serves to position the protein substrate and can be dynamically assembled or disassembled to regulate kinase activity.[12,14] Similarly to the *R*-spine, a catalytic *C*-spine consists of residues from both lobes and is completed by the adenine of ATP and functions to mediate catalysis by positioning ATP. The conserved Asp-Phe-Gly (DFG) motif (or DLG in Nek7) is located at the *N*-terminus of the activation loop and the aspartate points into the ATP binding pocket in an active kinase conformation, DFG-in, and forms interactions with and positions the phosphates of ATP *via* coordinating a divalent magnesium cation. The phenylalanine from this motif points towards the αC-helix in the active conformation and forms part of the *R*-spine. In an inactive conformation, DFG-out, these residues are flipped with the phenylalanine now pointing into the active site and the aspartate pointing away, towards the αC-helix, disrupting the activating interactions. The DFG-out conformation reveals a hydrophobic pocket which can be exploited for drug discovery (see Type II inhibitors). The histidine of the His-Arg-Asp (HRD) motif forms part of the *R*-spine, the aspartate interacts with the hydroxyl group of the peptide substrate to properly position the substrate for catalysis whilst the arginine interacts with the phosphorylated activation loop to stabilise the loop into a more ordered structure and support its active conformation, enabling the substrate to bind.
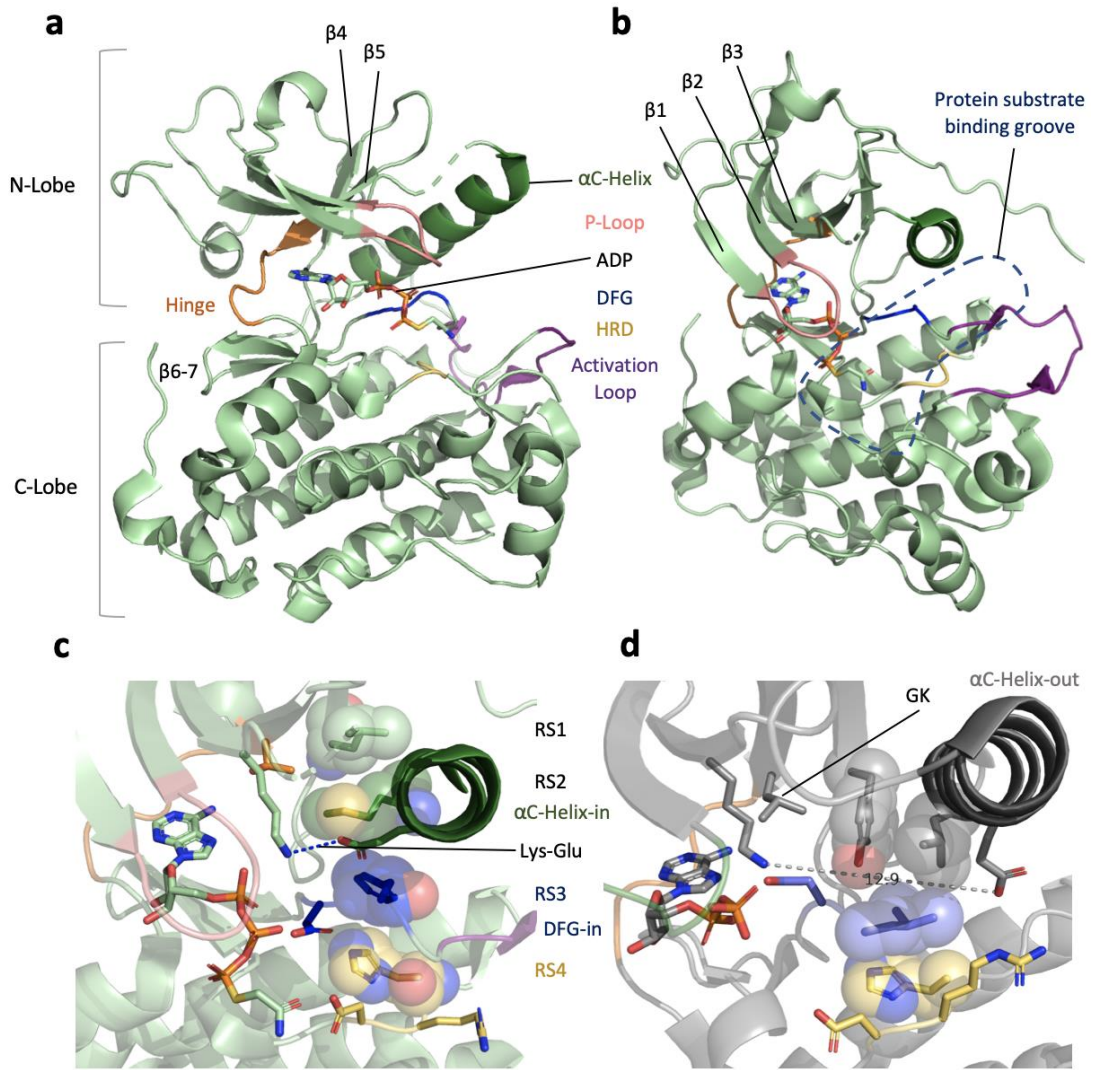
Figure 1-1. Conserved structural features of the kinase domain. (a) EGFR in complex with an ATP analogue (PDB ID: 2GS6) represented as pale green cartoon with the conserved structural features highlighted which is rotated 90 ° about its Y-axis in (b). The active conformation of EGFR is illustrated in (c) and contrasted with the inactive conformation of Nek7 bound to ADP in (d) (PDB ID: 2WQN).

1.2 Mitotic Kinases

Reversible phosphorylation is an important mechanism of mitotic control. For instance, cyclin-dependent kinases (CDKs), along with their corresponding cyclins, regulate phosphorylation of substrate proteins in order to control mitosis.[15] Aurora and Polo-like kinases (PLKs) are also critically involved in the regulation of mitosis. More recently, the less well characterised NIMA-related kinases (Neks) have emerged as having key roles in mitotic regulation.[15,16] The process of segregating duplicated genetic material during cell division is achieved *via* the action of the mitotic spindle, a dynamic bipolar microtubule-based scaffold.[17] Assembly of the mitotic spindle is regulated by protein kinases such as CDKs, PLKs and Neks which phosphorylate spindle-associated proteins on specific regions of the spindle.[18,19] The majority of human cancer cells are aneuploidy and exhibit chromosome instability, enabling the tumour to acquire malignant properties.[16] These defects arise due to errors in chromosome segregation and mitotic spindle assembly resulting in the loss or gain of chromosomes at each cell division. Therefore, targeting mitosis is a validated approach for cancer therapy and Neks are potential therapeutic targets in the treatment of human cancer.

1.2.1 The NIMA-related Kinase Family

The never-in-mitosis A (NIMA) protein was first discovered in *Aspergillus nidulans* and is the founding member of the Nek family.[16,20] Wild-type NIMA was shown to regulate various key mitotic events such as nuclear envelope breakdown, chromosome condensation and mitotic spindle organisation.[21] Neks have been identified in a range of organisms, with the human Nek family consisting of eleven members (Nek1 to Nek11), which are organisationally similar to each other, as well as to NIMA.[15,16] The function of Neks is in the regulation of processes involving microtubule-containing structures such as mitosis and ciliogenesis. Additionally, a few Neks have roles in the DNA damage response and cell cycle checkpoints. The human Nek family is defined by an *N*-terminal catalytic domain, containing the typical features of a serine-threonine kinase, with the exception of the centrally located catalytic domain in Nek10 (Fig. 1-2).[16] The Nek non-catalytic domains are likely responsible for substrate recognition and regulation. A common non-catalytic

region of Nek domain organisation is an oligomerisation motif which is often a coiled-coil and promotes auto-phosphorylation and kinase activation. Several Neks, such as Nek2, also contain degradation motifs within their non-catalytic regions.[22] Nek6 and Nek7 solely contain a short *N*-terminal extension, which may be important for protein partner recognition,[23] and a catalytic domain.[16] The Nek catalytic domains overall are moderately conserved, having approximately 40–50% sequence identity to each other and to that of NIMA. The exception to this is Nek6 and Nek7 as they share more than 85% sequence identity in their kinase domains and are completely identical in the residues that line the ATP binding pocket.[24] Although these kinases are highly similar, they are highly divergent in their *N*-terminal extensions as well as in the residues of the catalytic domain which contact the NTE. Furthermore, depletion of either Nek6 or Nek7 leads to defective mitotic progression suggesting they are not redundant.[18] Because of their similarity, the development of an inhibitor targeting the Nek7 ATP binding site should result in a dual Nek6 and Nek7 inhibitor.

	Activation	Localization	Function
NEK1 (1258 aa)	Genotoxic insults (IR, UV, crosslinking agents, oxidative injury)	Cytoplasm, centrosomes, cilia, sites of DNA damage	Cilia and DDR
NEK2 (445 aa)	S, G2-M	Centrosomes	Mitosis
NEK3 (459 aa)	Prolactin receptor stimulation	Cytoplasm	Prolactin signalling
NEK4 (841 aa)	?	Basal bodies	Cilia
NEK5 (889 aa)	?	?	?
NEK6 (313 aa)	Activated by NEK9, mitosis	Mitotic spindle	Mitosis
NEK7 (302 aa)	Activated by NEK9, mitosis	Weakly to spindle poles	Mitosis
NEK8 (703 aa)	Serum starvation	Nucleus, centrosomes, cilia	Cilia
NEK9 (979 aa)	Mitosis	Cytoplasm, spindle poles	Mitosis
NEK10 (1125 aa)	UV, G2-M	?	DDR
NEK11 (645 aa)	DNA replication inhibitors and genotoxic insults, S to G2-M transition	Nucleus and/or nucleoli	DDR

Figure 1-2. Schematic view of the domain organisation of the eleven human Nek kinases along with a summary of the activation, localisation and function of the kinases, adapted from Fry *et al.* 2012.[16] Shown are the kinase/catalytic domains (purple), coiled coil domain (green), degradation motifs (red), regulator of chromatin condensation 1 (RCC1) domains (light blue) and armadillo repeats (yellow). aa, amino acids.

1.2.2 Structure of the Nek7 Kinase Domain
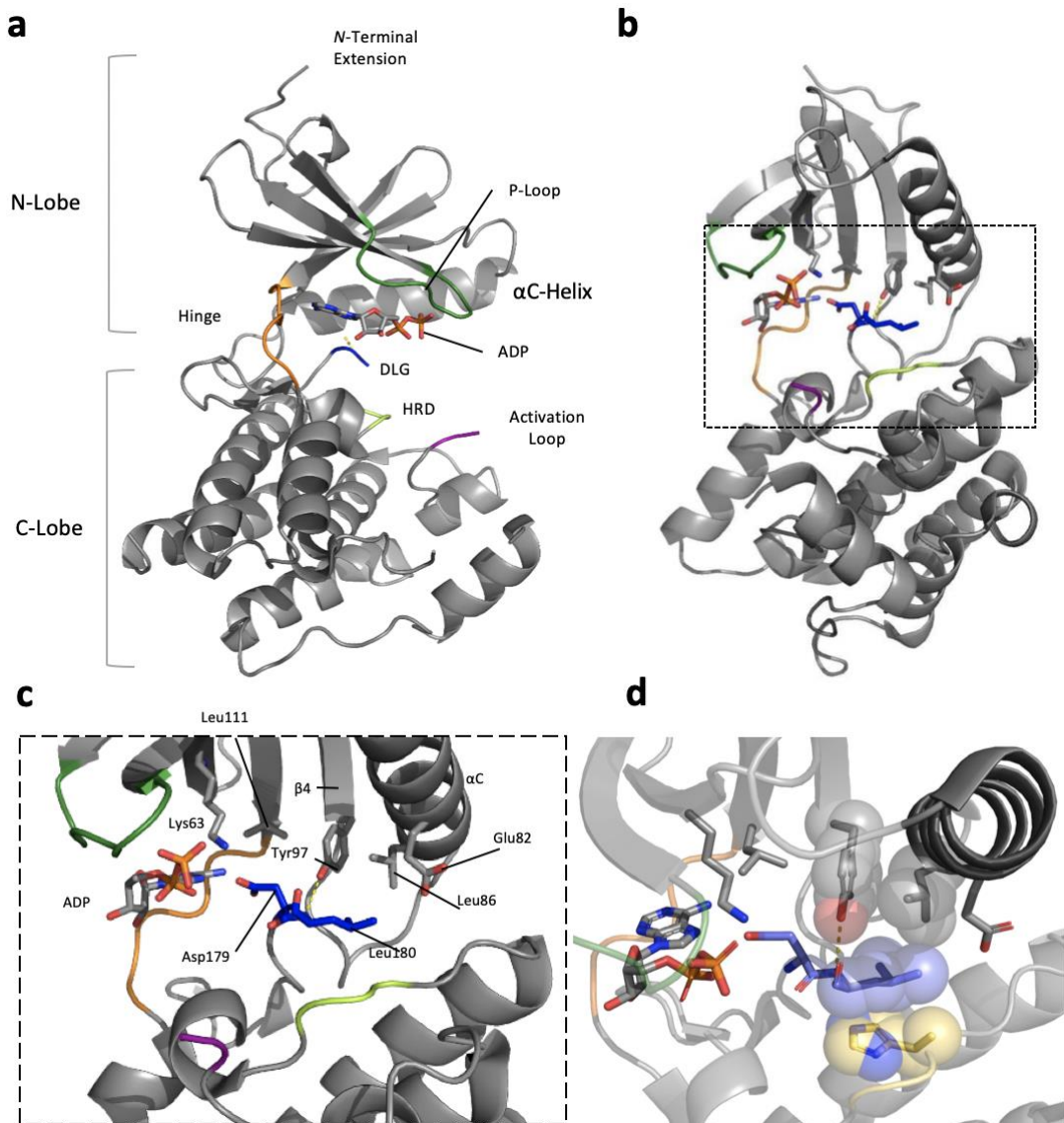
Figure 1-3. Crystal structure of Nek7 bound to ADP (PDB ID; 2WQN) (a) Cartoon representation, highlighting the conserved structural elements of a kinase domain rotated by 90° about its Y-axis in (b). The dashed box indicates the region magnified in (c) highlighting the Tyr-down auto-inhibited conformation. (d) Illustrating the hallmarks of an inactive kinase conformation.

The structure of human Nek7, bound to ADP (Fig. 1-3 a-b) and with a vacant active site, has been determined using X-ray crystallography to 2.3 Å and 2.1 Å resolution, respectively.[24]. The *N*-terminal extension (NTE) of Nek7 sits on a largely hydrophobic surface of the catalytic domain between *β*4 and the *β*2-3 loop and has a structural role, stabilising the catalytic domain and thus contributing to activity.[24] The NTE adopts an unusual extended ordered loop structure which wraps around the side chain of Asn33. As well as giving insight

into the mechanisms by which Nek7 is regulated, its catalytic domain shares common conserved structural elements with other protein kinases (illustrated in Fig. 1-1). These structural elements must be properly positioned to enable catalytic phosphorylation of the peptide substrate. That is, an active kinase consists of: (i) a phosphorylated activation loop, (ii) the *αC*-helix and DFG both 'in', (iii) formation of the Glu-Lys salt bridge and (iv) an aligned *R*-spine.

The overall structure of Nek7 (bound to ADP) shows the hallmarks of an inactive kinase (Fig. 1-3 c-d), consisting of the structural features described above displaced from their usual orientation in an active kinase.[24] That is, the activation loop is un-phosphorylated and the *αC*-helix is 'out', meaning that the Glu-Lys salt bridge and the *R*-spine are broken. Interestingly, Tyr97 is positioned between the *β4* stand and *αC*-helix pointing 'down' into the active site and forms a hydrogen bond between the backbone amide of Leu180 of the DLG motif and its hydroxyl, holding the DLG motif in an inactive conformation. This interaction is important in determining an inactive conformation, possibly by holding the activation loop in an inactive conformation. In an active kinase, the gatekeeper residue Leu111 (in the case of Nek7) would pack with Leu86 (RS2), forming part of the hydrophobic core and enabling the formation of the salt bridge between the catalytically important Lys63 and Glu82. In the Nek7 structure, the aromatic ring of Tyr97 is sandwiched between Leu111 and Leu86 and the *αC*-helix is positioned outwards, twisted away, meaning the Lys63-Glu82 salt bridge cannot form. This Tyr-down conformation disrupts the *R*-spine, blocks the interaction between Leu111 and Leu86, preventing the *αC*-helix adopting an inward conformation and thus preventing the interaction between Lys63 and Glu82, resulting in an inactive kinase. To generate an active Nek7, a substantial conformational change around the *β4* and *αC* helix is required to move from the Tyr-down to the Tyr-up conformation (up on the surface of the kinase).

1.2.3 Activation and Regulation of Nek7

Protein kinases can be activated *via* phosphorylation of their activation loops or by the binding of a protein partner. An additional regulatory mechanism was found to exist in Nek7 in which Tyr97 has an auto-inhibitory function and must be converted from the inhibitory Tyr-down position to the Tyr-up position to

enable catalytic activity.[24] The auto-inhibitory role of Tyr97 was confirmed *via* mutation to Ala, producing the Y97A mutant, which was 5-fold more active than wild-type Nek7.[24] The equivalent residue of Nek6 Tyr108 was also shown to be auto-inhibitory. Mutation of Tyr97 to phenylalanine, the side chain of which can interact with Leu86 and Leu111 but cannot hydrogen bond to the DLG motif, leads to some kinase activation. Therefore, in the auto-inhibited conformation, the hydrogen bond between Tyr97 and the DLG motif and the hydrophobic interaction of Tyr97 with Leu86 and Leu111 are both important for inhibition. Excessive Nek7 activity in interphase is deleterious to cells (Y97A activity increased cell death); therefore it is unsurprising that Nek6 and Nek7 have evolved a stringent auto-inhibitory mechanism to restrict its activity during interphase.
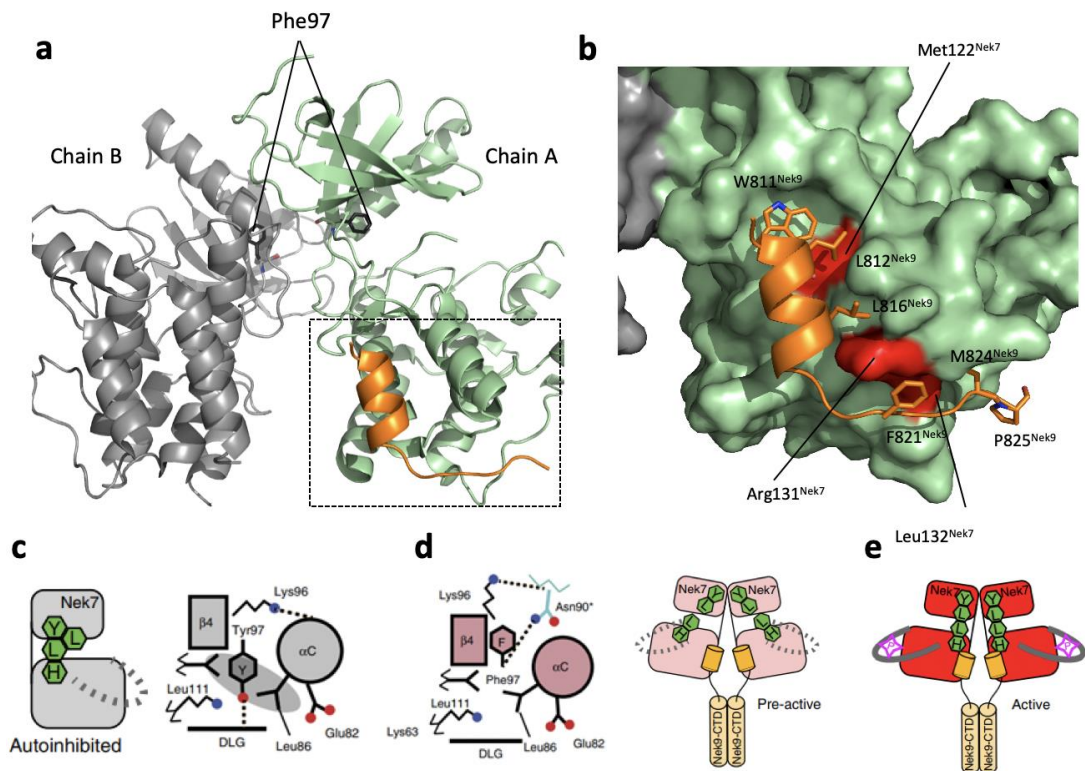
Figure 1-4. Activation of Nek7 by Nek9. (a) Cartoon representation of the crystal structure of Nek9[810-828] (orange) bound to Nek7 Y97F (PDB ID: 5DE2) highlighting the two Nek7 chains and the respective orientation of residue 97 in each (down in chain A and up in chain B). Another molecule of Nek9 is bound to chain B of Nek7 (not shown for clarity). The dashed box represents the region magnified in (b) highlighting the key interacting residues of Nek9 (cartoon representation, orange) binding to Nek7 (surface representation, pale green). (c-e) Schematic of Nek7 activation by Nek9, adapted from Haq *et al.* 2015.[25] Nek7 can slowly become active by auto-phosphorylation however Nek9 binding generates a pre-active state which undergoes rapid auto-phosphorylation to become active.

Additionally to this auto-inhibitory mechanism, Nek6 and Nek7 are regulated by the binding of Nek9.[16,24–26] The Nek9 *C*-terminal domain (CTD) stimulates the activity of wild-type Nek7 to a level similar to that seen for the Nek7 Y97A mutant, yet this domain does not increase the activity of the mutant, suggesting that the Nek9 CTD activation of Nek7 occurs *via* allosteric release of Tyr97 auto-inhibition.[24] To determine the molecular mechanism by which Nek9 activates Nek7, the crystal structure of Nek7 Y97F and Nek9 (residues 810-828, the minimal Nek7 binding region) was determined to 2.78 Å resolution (Fig. 1-4).[25] Nek9[810-828] formed an α-helix, which unexpectedly bound on the *C*-lobe of Nek7 within a groove formed by the hinge region, αD and αE helices and strands β6-β7. Furthermore, the crystal structure revealed two molecules of Nek7 formed a back-to-back dimer, centred around the αC-β4 loops in the vicinity of residue 97 with the ATP binding pockets of each monomer facing away from each other. The structure of Nek7 chain A was similar to that of wild-type Nek7 with residue 97 in the 'down' position, however in chain B this residue was in the 'up' position resulting in twisting of *αC*, bringing the gatekeeper residue Leu111 and Leu86 as well as the salt bridge partners Lys63 and Glu82 closer together. In other words, in chain B, these crucial structural elements are shifted to positions expected in an active kinase. Based on this structure, along with other biochemical studies, the mechanism of Nek7 activation by Nek9 was elucidated (Fig. 1-4 c-e). Nek9 binds to Nek7 *via* its *C*-terminal domain and self-associates through its coiled coil domain bringing two Nek7 monomers together as back-to-back dimers.[25] Back-to-back dimerisation releases Nek7 auto-inhibition *via* a set of conformational changes which switches the conformation of residue 97 resulting in a structure which resembles that of an active kinase. This pre-active state of Nek7 is able to undergo trans auto-phosphorylation (between back-to-back dimers) in a more efficient manner than the auto-inhibited state, resulting in an active kinase. Therefore, Nek9 binding to Nek7 accelerates auto-phosphorylation of Ser195 and kinase activation which is otherwise slow in the absence of Nek9 due to the auto-inhibited state of Nek7.[25,27]

1.2.4 Capturing the Active Nek7 Kinase Domain

At the commencement of this project, there were no crystal structures of Nek7 bound to an inhibitor, limiting the scope for structure-guided design of

inhibitors. Furthermore, the crystallisation conditions identified in the first apo crystal structure of Nek7[24] suffered from reproducibility issues and although crystallisation of Nek7 with Nek9[25] is reproducible, attempts to co-crystallise this complex with inhibitors has also been unsuccessful.[28] In addition, there are no published crystal structures of Nek7 apo or in complex with an inhibitor in which Nek7 is in the active conformation. This also adds difficulty in the design of inhibitors which are tested against active Nek7 in functional assays. To overcome these issues, the composition of the *R*-spine of Nek7 was mutated in order to trap Nek7 in an active conformation and generate an alternative crystal form, more amenable to co-crystallisation studies. Unfortunately, this Nek7 *R*-spine mutant (L86H, Y97F, L180F), whilst displaying a partially stacked *R*-spine, did not exhibit other hallmarks of the active kinase conformation.[28] Nevertheless, co-crystal structures of wild-type Nek7 and the Nek7 *R*-spine mutant were solved in complex with a Nek2 inhibitor in this study.
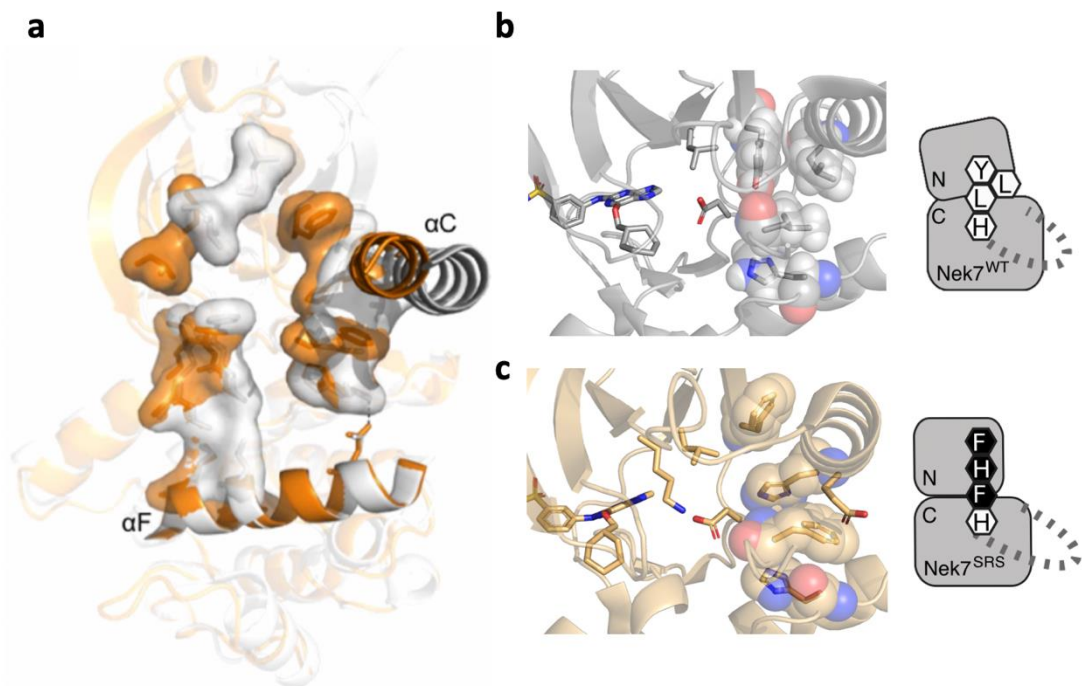
Figure 1-5. Capturing the active Nek7 kinase domain. (a) Nek7^{WT} (grey) and Nek7$^{R\text{-}spine}$ mutant (orange) overlaid, adapted from Byrne *et al.* 2020,[28] illustrating their respective *C*- and *R*-spine positions. (b-c) ATP binding side of Nek7^{WT} (grey) and Nek7$^{R\text{-}spine}$ mutant (orange) with schematics, contrasting the broken and partially stacked *R*-spines.

1.2.5 The Cellular Roles of Nek7

Neks function in many aspects of cell cycle progression including centrosome separation, nuclear pore complex (NPC) disassembly and nuclear envelope breakdown, mitotic spindle assembly as well as contributing to chromatin condensation and cytokinesis (Fig. 1-2).[16] Many of these functions are due to Nek's regulation of microtubule-related structures.[15]

Nek9, Nek6 and Nek7 perform crucial functions in spindle assembly and are part of a signalling pathway which becomes active as cells progress into mitosis.[26] This signalling pathway begins with CDK1, which (along with cyclin B1 and potentially cyclin A) phosphorylates Ser-869 of Nek9, forming a binding site for the polo-box domain of Plk-1.[9, 10] Subsequent binding and phosphorylation of the activation loop residue Thr-210 within the catalytic domain of Nek9 by Plk-1 results in activation of Nek9. It may also be possible that Plk-1 phosphorylates Nek9 outside of the activation loop, releasing Nek9 auto-inhibition, triggering auto-phosphorylation of Thr-210.[29] Nevertheless, the resulting activation of Nek9 prompts auto-phosphorylation of residues within its *C*-terminal non-catalytic region allowing direct binding of Nek9 to Nek6 and Nek7.[26] This leads to activation of Nek6 and Nek7 *via* non-allosteric (Nek9 can phosphorylate activation loop residues of Nek6 and, presumably, Nek7)[16] and allosteric (direct interaction of the Nek9 non-catalytic domain disrupts an auto-inhibitory motif of Nek6 and Nek7, resulting in activation)[24] mechanisms.[26]

1.2.5.1   Nek7 in Centrosome Separation

The expression level and kinase activity of Nek6 and Nek7 is elevated in mitosis owing to the fact that these kinases have a number of mitotic functions.[26] Firstly, downstream of Nek9 in prophase, Nek6 and Nek7 regulate the spindle pole localisation of Eg5, controlling centrosome separation.[26,29,30] The microtubule-associated kinesin Eg5 is a plus-end directed motor that drives spindle poles apart by crosslinking and sliding microtubules, in an anti-parallel manner, across each other.[16] Association of Eg5 to spindles is dependent on phosphorylation of Eg5 at Thr-926 by CDK-1.[26,29,30] This, along with phosphorylation of Eg5 at Ser-1033 by Nek7 causes accumulation of Eg5 around centrosomes, stimulating centrosome separation prior to nuclear

envelope breakdown. Prior to the physical separation of the centrosome, in G_2, Nek2 phosphorylates several key centrosomal proteins to promote dissociation of the inter-centrosomal linker (chromosome disjunction).[31]

1.2.5.2 Nek7 in Nuclear Envelope Breakdown

In the transition from prophase to prometaphase, Nek6 and Nek7 are required for efficient nuclear envelope breakdown *via* phosphorylation of the nucleoporin Nup98.[32] Nup98 is a crucial component of the NPC, acting as a multivalent linker by interacting with and connecting both peripheral and inner ring nucleoporin subcomplexes within the NPC.[33] Hyperphosphorylation of Nup98 causes its dissociation from NPCs, unzipping nucleoporin interactions, leading to NPC disassembly and nuclear envelope breakdown.[12,13] This mechanism of disassembly by phosphorylation explains the rapid nature and the reversibility of this process during mitotic exit.[33] Following nuclear envelope breakdown, Nek6 and Nek7 phosphorylate the EML4 *N*-terminal domain at Ser144 and Ser146 to promote EML4 dissociation from microtubules and chromosome congression.[34]

1.2.5.3 Nek7 in Mitotic Spindle Assembly

In prometaphase and metaphase, Nek6 and Nek7 have important roles in the assembly of a robust mitotic spindle.[18,26] Expression of inactive Nek6 and Nek7 mutants or depletion of these kinases by RNA interference (RNAi) resulted in the formation of short spindles with reduced microtubule density and loss of chromosome alignment, leading to activation of the spindle assembly checkpoint and metaphase arrest.[16,18] Reduced microtubule nucleation at spindle poles is a possible explanation for the resulting fragile spindles upon depletion of Nek6 and Nek7. Indeed, Nek6 and Nek7 predominantly localise to spindle microtubules and spindle poles, respectively, and are both able to phosphorylate microtubules *in vitro*.[18] Furthermore, Nek7 is required to recruit γ-tubulin, a crucial protein for microtubule function,[35] to spindle poles.[18] Therefore, these kinases may function in spindle assembly by promoting microtubule stability or nucleation at spindle poles as well as within the spindle itself *via* the phosphorylation or recruitment of microtubules or their associated proteins.[18] Although the mechanism through which Nek7 contributes to spindle assembly needs further

elucidation, one method in which Nek6 may also promote spindle assembly is *via* phosphorylation of heat shock protein Hsp72.[36] Nek6 phosphorylates Thr66 in the *N*-terminal nucleotide binding domain of Hsp72, localising Hsp72 to spindles. Here, Hsp72 promotes the recruitment of proteins important for microtubule stability and nucleation, ch-TOG and TACC3 to K-fibres.[36–38] K-fibres are the microtubules responsible for connecting spindle poles to kinetochores, protein complexes found at the centromere of chromatids upon which the mitotic spindle attaches, contributing to robust spindle assembly.

1.2.5.4   Nek7 in Cytokinesis

Nek6 and Nek7 are involved in the regulation of cytokinesis.[26] For instance, cells expressing a partially active Nek7 mutant complete sister chromatid separation but fail to undergo abscission, leading to cell arrest during cytokinesis, indicating that a higher level of kinase activity is required to complete cytokinesis.[18] For successful cell abscission and cytokinesis, the microtubule cytoskeleton must reorganise in anaphase to form the central spindle between the two spindle poles at the midzone.[39] Nek6 and Nek7 control distinct kinesins to regulate cytokinesis. Nek6 phosphorylates the kinesin-6 family member Mklp2, controlling its localisation to the central spindle as well as the microtubule bundling activity of the kinesin.[26,39] Similarly, Nek7 phosphorylates the kinesin-3 family member Kif14, stimulating the kinesin to recruit the effector kinase citron to the midzone. In turn, citron kinase is required for proper midbody formation and cell abscission.[39] Therefore, both Nek6 and Nek7 are required in distinct, yet converging, signalling arms for accurate completion of cytokinesis.
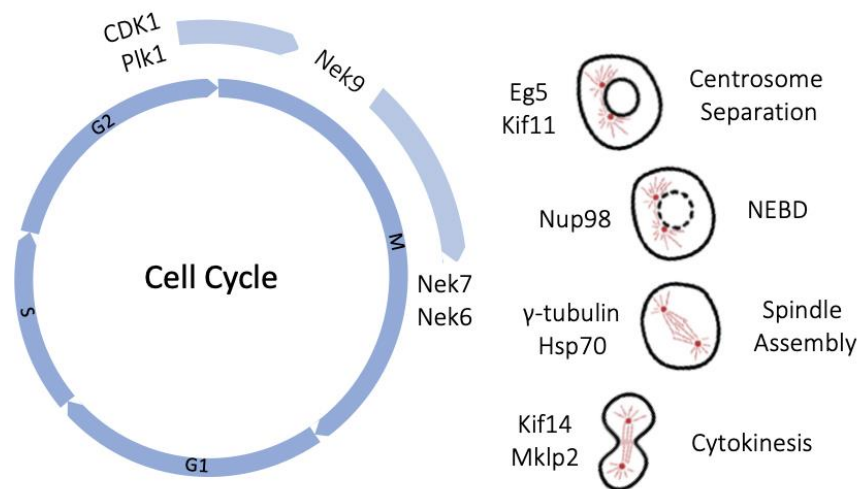
Figure 1-6. Schematic representation of the Nek9-Nek6-Nek7 signalling pathway and a summary of the roles of Nek6 and Nek7 in mitosis.

1.2.5.5   Nek7 in Interphase

Although the kinase activity and expression levels of Nek6 and Nek7 peak in mitosis, there is growing evidence of other functions of these kinases outside of mitosis.[26] For instance, Nek6 and Nek7 are implicated in the control of centrosome duplication and maturation, senescence and the DNA damage response, processes with primarily occur in interphase.[26,40–42] Interestingly, Nek7 was found to be necessary for the activation of the NLRP3 inflammasome, a multi-protein complex which responds to microbes and other danger signals by activating pro-inflammatory caspases and cytokines leading to the induction of programmed inflammatory cell death.[43] In this process, Nek7 acts as a switch between mitosis and inflammasome activation as the level of Nek7 in macrophages is not sufficient to activate both processes. In other words, Nek7 NLRP3 inflammasome activation can only occur during interphase, presumably to ensure this process is mutually exclusive with mitosis.[26,43]

1.2.5.6   The Role of Nek7 in Cancer

Many Nek family kinases have been implicated in cancer.[15] For instance, the majority of human cancer cells are aneuploid and exhibit chromosome

instability, enabling the tumour to acquire malignant properties.[16] These defects arise due to errors in chromosome segregation and mitotic spindle assembly, resulting in the loss or gain of chromosomes at each cell division. Indeed, Nek7 has been shown to be expressed highly in tumour samples from patients with breast and colorectal cancer, cancer of the larynx and melanoma relative to normal tissue from the same patients.[44] Additionally, Nek7 was found to be overexpressed in hepatocellular carcinoma relative to healthy liver tissue.[45] Furthermore, a high level of Nek7 expression was significantly associated with poor prognosis in gallbladder and hepatocellular carcinoma.[45,46] Moreover, Nek7 interference suppressed tumour growth in a mouse model of hepatocellular carcinoma, suggesting Nek7 could be a novel target for this type of cancer.[45] Embryonic fibroblast cells derived from Nek7-null mice showed a variety of mitotic defects and aneuploidy, further suggesting that Nek7 deregulation could induce oncogenesis.[47] Therefore, Nek7 is a potential therapeutic target in the treatment of human cancer. Nek7 has also been suggested as a novel target for the treatment of gout, atherosclerosis, Alzheimer's disease and type II diabetes.[48] Similarly to Nek7, there is a growing body of evidence that Nek6 may be a useful therapeutic target. Nek6 is upregulated in various malignancies such as breast, colon, lung and gastric cancer, melanoma, non-Hodgkins lymphoma and glioblastoma.[44,49,50]

To date, the potential of Neks as anti-cancer targets is underexplored and limited target validation studies have been performed.[16] There is an ever-pressing need for new, effective cancer therapies and, in turn, there has been substantial interest in mitotic kinases as therapeutic targets. Members of the Nek family are attractive drug targets as they are involved in regulating microtubule function, a precedented target pathway for anti-cancer therapy. Mitotic spindle microtubules are one of the most successful targets for anti-cancer therapy.[51] Vinca alkaloids and taxanes suppress microtubule dynamics, leading to inhibition of mitosis and resulting in apoptosis. These are effective treatments in a variety of cancers however their use clinically is limited by side effects such as neuropathy, drug resistance and poor response in some instances. Therefore, patients would benefit from therapies which

trigger a similar response as these microtubule poisons yet are more selective by targeting mitotic kinases.[16,52]

EML4-ALK fusion proteins act as oncogenic drivers in ~5% of NSCLC patients.[53] Recently, it has been identified that expression of EML4-ALK variant 3 in NSCLC patients leads to enhanced stabilisation of microtubules, a spindle-like morphology with extended cytoplasmic protrusions and significantly increased rate of migration which are dependent on Nek9 and Nek7 but not ALK or Nek6.[54] This represents a novel actionable pathway that could drive metastatic disease progression in these NSCLC patients. These protrusions were not affected by treatment with ALK inhibitor crizotinib, potentially explaining why patients with variant 3 respond less well to ALK inhibitors.[54,55] Indeed, standard treatment for NSCLC often involve microtubule poisons, such as vinorelbine or paclitaxel. Alternative targeted therapies would therefore be highly attractive and targeting Nek9 or Nek7 in EML4-ALK positive lung cancer could be beneficial.

1.3 Protein Kinase Inhibitors

For many years, kinases were thought of as difficult to target due to the highly conserved nature of the ATP binding site as well as the millimolar concentrations of ATP in the cell.[1,56] Indeed, early pharmacological kinase inhibitors reached nanomolar affinities but lacked selectivity.[56,57] Obtaining target selectivity, overcoming drug resistance, utilising kinase inhibitors in therapeutic areas other than oncology and validating novel kinase targets have been described as some important challenges in kinase inhibitor discovery.[1,2] Great progress has been made towards achieving these goals, with the field of kinase inhibitor discovery rapidly expanding into disease areas other than oncology. Developing a potent and selective kinase inhibitor remains a challenge, however in most cases these issues have been overcome.[1] For instance, the development of compounds that target hydrophobic pockets in the vicinity of the ATP binding site have allowed a number of potent and selective kinase inhibitors to be identified. Promiscuous inhibitors, *via* high-throughput kinase profiling,[58] can be utilised in the development of a multitude of selective inhibitors for underexplored kinases[59] such as TNK2,[60] PI3K-δ/γ,[61] the Aurora kinases,[62,63] LRRK2,[64] ERK5,[65–67] and DCLK1.[68,69] By utilising kinase-profiling, respectively selective inhibitors targeting a few kinases can be optimised into highly selective inhibitors of those distinct kinases. Furthermore, this promiscuity can also be harnessed in the simultaneous inhibition of several kinases to prevent drug resistance and enable the treatment of multiple cancers using the same molecule. For instance, imatinib[70–73] is approved for the treatment of CML, GIST and myelo-proliferative diseases due to its inhibition of BCR-ABL, c-Kit and PDGFR, respectively.[1] As the first approved kinase inhibitor, imatinib paved the way in the field of kinase inhibitor discovery due to its remarkable selectivity[74,75] and tolerable side-effect profile.[56,76,77] Imatinib has also been termed the 'magic bullet' as it has revolutionised the treatment of CML.[1] Despite several molecular mechanisms of drug resistance having been identified, with point mutations in the ATP binding site common, resistance can also be overcome by the development of drugs which target the resistant mutants.[56,78] Point mutations in the ATP binding site, specifically of the gatekeeper residue

responsible for critical interactions, are common mechanisms of resistance. In the case of BCR-ABL, second generation nilotinib and dasatinib overcome imatinib resistance mutants. Only third generation ponatinib can effectively inhibit the gatekeeper mutant T315I in CML patients.[56,79]

The binding modes of kinase inhibitors with their targets can be used to classify the inhibitors into 6 Types (Fig. 1-7).[14] Type I, I½ and II inhibitors bind to the ATP binding site and compete with ATP. Type III and IV are allosteric inhibitors, are non-competitive with ATP and bind to an allosteric pocket proximal (which is also occupied by Type I½ inhibitors) or distal to the ATP binding site, respectively. Finally Type V inhibitors are bivalent, spanning two regions, whilst Type VI inhibitors bind to the kinase covalently.
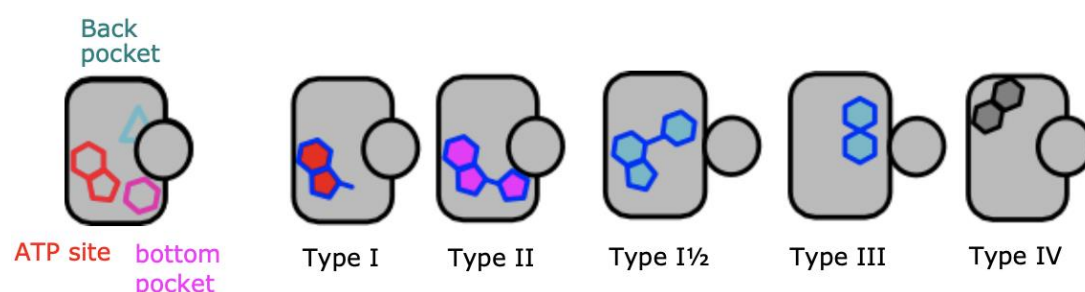
Figure 1-7. Schematic summary of the different types of kinase inhibitor. Type I, I½ and II inhibitors occupy the ATP site and are the focus of this thesis.

1.3.1 Type I and II Inhibitors

Of the 71 clinically approved drugs which target protein kinases to date,[80] the vast majority of them compete with ATP for inhibition and can be classed as Type I, I½ or II kinase inhibitors.[14,81–84] Type I inhibitors (Fig. 1-8) are defined as small molecules that bind to the active conformation of the kinase (DFG-in, *αC*-helix-in), mimicking ATP by making interactions with the hinge region. Type II inhibitors (Fig. 1-11) bind to the inactive DFG-out conformation of the kinase (*αC*-helix in or out), yet still maintain interactions with the hinge and usually display ATP-competitive behaviour similar to that of Type I. The phenylalanine of the DFG-motif is part of the *R*-spine (residue RS2) in an active kinase and transition to the inactive DFG-out conformation exposes a hydrophobic pocket which this residue had previously occupied. Type II inhibitors occupy this now vacant RS2 or 'bottom' pocket which is a result of the DFG-out conformation. Type I½ inhibitors (Fig. 1-10), a subtype of the

Type I inhibitor, bind to the inactive DFG-in, *αC*-helix-out conformation of the kinase and resemble elements of both Type I and II inhibition. Indeed, Type I½ inhibitors bind to the adenine region similarly to Type I inhibitors, establishing interactions with the hinge region, yet extend past the gatekeeper into the RS3 or 'back' pocket and act to push the *αC*-helix-out. This pocket is occupied by the third residue of the *R*-spine, situated on the *αC*-helix and is vacated in the *αC*-helix-out conformation. Type III inhibitors do not make interactions with the adenine region but exploit the resultant, adjacent RS3 pocket to achieve their allosteric mode of action. Therefore, this pocket is sometimes referred to as the 'allosteric' pocket. These pockets are usually named in the context of the study in which they are described and a standard nomenclature would be helpful. Therefore, I have opted to refer to these pockets as RS2 or RS3, being occupied by the second or third *R*-spine residue in an active kinase, respectively, for unambiguity. Nevertheless, these pockets are flexible and an inhibitor may bind to an expanded form of the pocket or occupy more than one pocket.
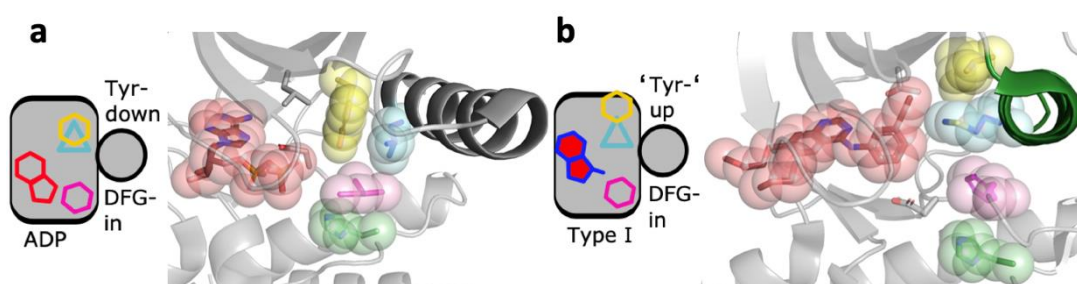
Figure 1-8. Type I kinase inhibitor binding mode, illustrated by the crystal structure and schematic. The ATP site and back and bottom pockets are coloured red, cyan and magenta, respectively with the residues in the crystal structure coloured according to the pocket they occupy. (a) Nek7 bound to ADP (PDB ID: 2WQN). (b) EGFR bound to Type I inhibitor erlotinib (PDB ID: 1M17).

Vemurafenib is a Type I½ inhibitor of B-Raf V600E oncogenic mutant and is the first marketed drug, approved in 2011 for the treatment of melanoma, to have been discovered by fragment-based drug disocovery.[85,86] Previously identified classes of kinase inhibitors were not suitable for inhibition of B-Raf. Therefore, in an attempt to identify a novel kinase hinge binding motif, 20,000 fragments were screened against five kinases and compounds which inhibited at least three were selected for follow-up.[85] This approach of identifying weak,

unselective hits appears to be counter-intuitive for traditional drug discovery efforts but useful for kinase drug discovery. This led to the discovery of the 7-azaindole fragment, a now commonly used hinge binding motif.[85,87] Optimisation was aided by crystallography in Pim1 and FGFR which provided reliable model systems whilst the crystallisation of B-Raf was optimised. This again illustrates how the (un)selectivity of kinase inhibitors and similarity of kinase domains can be an advantage in inhibitor design. Once crystallography, computational simulation, synthetic chemistry and biological assays were adapted to B-Raf, potent and selective compounds were rapidly identified and ultimately led to vemurafenib (Fig. 1-9).[85]

Figure 1-9. Fragment-based discovery of vemurafenib and its modification to PLX7904 which evades the paradoxical MAPK signalling observed with vemurafenib.

Vemurafenib binding causes an outward shift in the αC-helix of B-Raf, a common feature of Type I½ inhibitors, affecting Raf dimerization.[85] This outward shift of the αC-helix of one Raf protomer pushes the αC-helix of the second inward, closing the RS3 allosteric pocket (now occupied by the RS3 residue) and prevents binding of a Type I½ inhibitor to the second protomer.

Therefore, binding of vemurafenib to one protomer induces activation of the second and paradoxically activates MAPK signalling in cells with wild-type B-Raf which depends on dimerization for activation (through upstream Ras).[85,88] The pathway is inhibited with vemurafenib in cells with B-Raf^{V600E}, which is monomeric[89] and constitutively active. To overcome this paradoxical activation of MAPK signalling, vemurafenib was modified to give Type I½ inhibitors that evade the paradox.[90,91] These compounds inhibit B-Raf dimers, interacting with the Leu of the *R*-spine (RS3), potentially causing an outward movement of the *αC*-helix and disruption of the dimer interface.
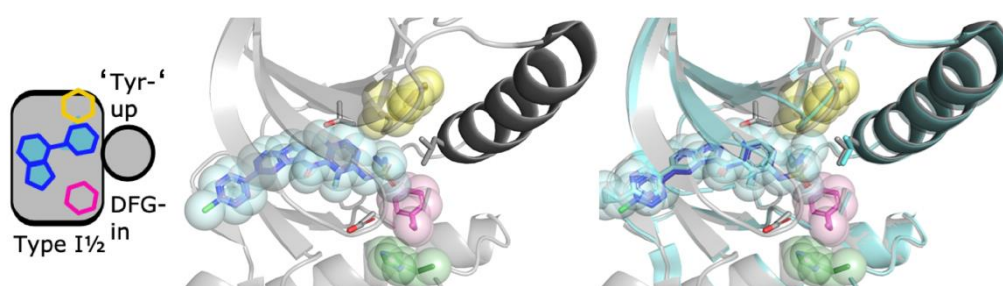
Figure 1-10. Type I½ inhibitor binding mode illustrated by crystal structures of vemurafenib (left) and PLX7904 with B-Raf^{V600E} (PDB IDs: 3OG7 and 4XV1, respectively). Vemurafenib occupies the RS3 allosteric pocket and is therefore coloured cyan. The two structures are overlaid (right) to illustrate the slight outward shift of the *αC*-helix upon PLX7904 binding, which further occupies the RS3 pocket.

An alternative method to target B-Raf dimers is to ensure that the compounds do not displace the *αC*-helix and that both protomers of the dimer are occupied by the inhibitor. Screening of kinase inhibitors against dimeric B-Raf identified ponatinib as a Type II inhibitor of B-Raf that extends into the RS2 pocket of the DFG-out kinase conformation.[92] Structure-guided design identified PHI1 which showed that binding of the inhibitor to the second protomer is preferred following binding to the first protomer.

Ponatinib, as mentioned earlier, along with imatinib, is a Type II inhibitor of BCR-ABL which overcomes resistance inferred by the T315I mutation.[56,79] This mutation removes the hydrogen bond between T315 and imatinib and introduces higher steric demand due to the larger side chain of I315. The acetylene linker in ponatinib overcomes this mutation and is able to inhibit BCR-ABL T315I.
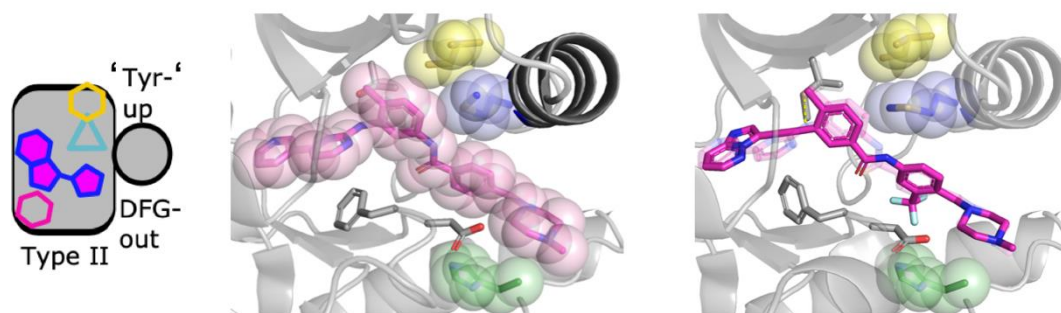
Figure 1-11. Type II inhibitor binding mode illustrated by crystal structures of imatinib (left) and ponatinib (right) with Abl and Abl T315I, respectively (PDB IDs: 1IEP and 3I3K, respectively.) These inhibitors have a Type II binding mode as they bind to the DFG-out conformation and occupy the RS2 pocket. Overlay of imatinib onto the ponatinib Abl T315I structure illustrates how ponatinib overcomes the T315I resistance mechanism.

Despite selectivity being most challenging for these types of inhibitors, due to the conserved nature of the ATP binding site, selectivity is still achievable, especially in the case of Type I½ or II inhibition. This structural similarity of the ATP binding site can be an advantage in that it has provided a wealth of knowledge about inhibiting the kinase domain,[14,81–84] allowing the identification of common hinge binding scaffolds[93] as well as the ability to predict the binding modes and key interactions of novel ligands.[94] This has provided rationale for inhibitor design not only for Type I hinge binding pharmacophores (donor-acceptor-donor hydrogen bonding motif) but also for Type I½ and II inhibitors.[82,83,94,95]

1.3.2 Chemical Inhibitors of Nek7

Nek7 has a role in oncogenesis and therefore is a potentially important target in the treatment of cancer.[44–47] Furthermore, Nek7 has been suggested as a novel treatment for gout, atherosclerosis, Alzheimer's disease and type II diabetes.[48] Despite these indications, and despite the availability of a crystal structure, there are no potent and selective small molecule inhibitors of Nek7.[48] Additionally, because the functions of many Neks, such as Nek7, are poorly characterised, developing selective Nek inhibitors for mechanistic studies is essential to validate these as clinically relevant therapeutic targets and aid our understanding of how these inhibitors may be developed into effective clinical treatments.[16]

Inhibitors developed for a specific kinase often inhibit other kinases, information which can be exploited to identify chemical matter for kinases of which there are none. However, analysis of large sets of screening data revealed that the majority of Nek kinases had hit rates of less than 1%.[48] This gives Nek7 one of the lowest frequency hit rates and means there are relatively few promising starting points for the development of Nek7 inhibitors A few promiscuous kinase inhibitors have activity on a large percentage of the kinome including the Nek family. Tamatinib, a SYK inhibitor, KW-2449, a FLT3 inhibitor, and TG-101348, a JAK2 inhibitor, have been reported to be potent Nek6 and Nek7 inhibitors (11 nM, 210 nM and 160 nM K_d, respectively).[48,96] Follow-up IC_{50} determination of these inhibitors measured values of 6 μM and >100 μM, respectively (Fig. 1-12).[97] Conversely to binding assays, such as the ones which derive K_d, IC_{50} values are dependent on ATP concentration and therefore discrepancy was expected however this illustrates these compounds to be weak Nek7 inhibitors. These large sets of screening data are usually performed at a single concentration and vary in terms of type of data collected (% inhibition, K_d or IC_{50}) and format of the kinase assay (binding *versus* enzyme inhibition)[48] which could go towards explaining the discrepancy.

	Tamatinib	KW-2449	TG-101348
Reported K_d	11 nM	210 nM	160 nM
Measured IC_{50}	6 μM (solubility limiting)	>100 μM	>100 μM
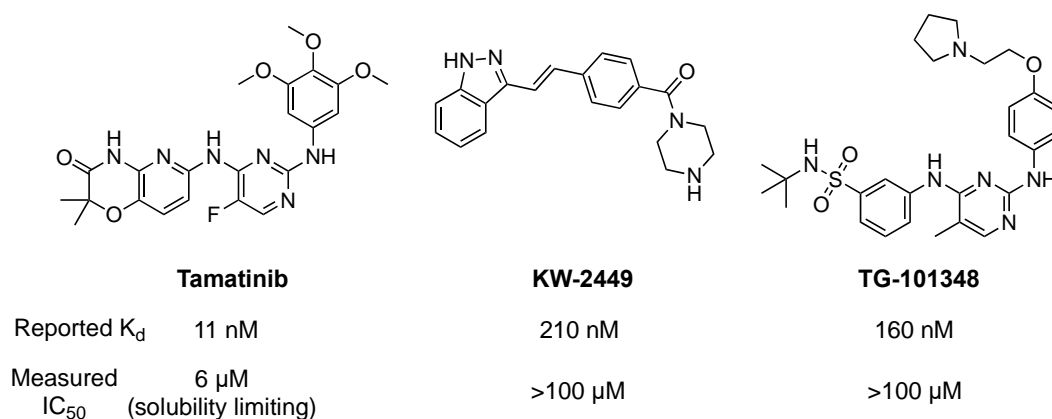
Figure 1-12. Promiscuous kinase inhibitors with reported Nek7 affinity. Subsequent re-screening in a functional biochemical assay illustrated their weak inhibition of Nek7.

Potentially the most promising published compounds against Nek7 were originally synthesised to inhibit JNK family kinases.[48] Examples from this series of compounds demonstrated inhibition of both Nek6 and Nek7 activity

by more than 90% at 10 μM, with varying levels of selectivity. However these molecules have nanomolar affinity for JNK-1, -2 and -3 and are therefore not selective for any Nek family kinase. Furthermore, the inhibitors mentioned so far have been developed for a specific kinase other than Nek7 and only have annotated activity for Nek family kinases from selectivity screens. Therefore, this inhibition data could also suffer from lack of reproducibility as with the compounds above.

JNK-IN-1: R = Me,
56% Nek6, 80% Nek7
JNK-IN-2: R = H,
97% Nek6, 90% Nek7

JNK-IN-7: R = H,
83% Nek6, 93% Nek7
JNK-IN-8: R = Me
0% Nek6, Nek7
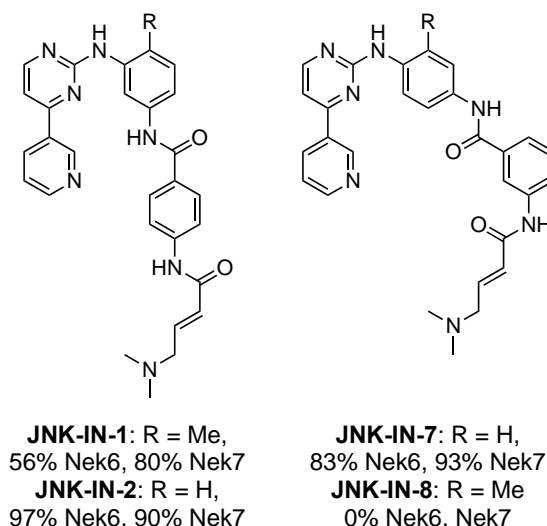
Figure 1-13. Chemical structures of the JNK-1 -2 and -3 inhibitors which also have activity against Nek6 and Nek7.

To overcome these challenges, a dedicated drug discovery program against Nek7 was initiated (Swen Hoelder, ICR in collaboration with Richard Bayliss).[97] Screening of 2466 low molecular weight compounds were tested for functional inhibition of Nek7 *via* a mobility shift assay using a LabChip EZ Reader (see 2.2.2.2). This fragment screen identified eleven hits, ten of which were validated by determining the IC_{50} values for Nek7 (Fig. 1-14). These hits were then triaged based on their ligand efficiency, scope for SAR and synthetic tractability as well as selectivity for Nek7 over the related Nek2 and Plk1 kinases. To assess the scope for SAR and to establish which key moieties of the fragments are essential for binding, 38 commercially available analogues of the four most ligand efficient hits were screened against Nek7. The 6-bromo-quinazolinone and 3-aminophthalimide fragments showed good selectivity for Nek7 and allowed for more efficient analogue synthesis and generation of SAR relative to the pyrrole pyrazine fragment. Therefore the

quinazolinone and phthalimide were chosen as suitable hits for optimisation, first focusing on the quinazolinone as the bromide was not essential for activity and could be used as a synthetic handle to improve potency.
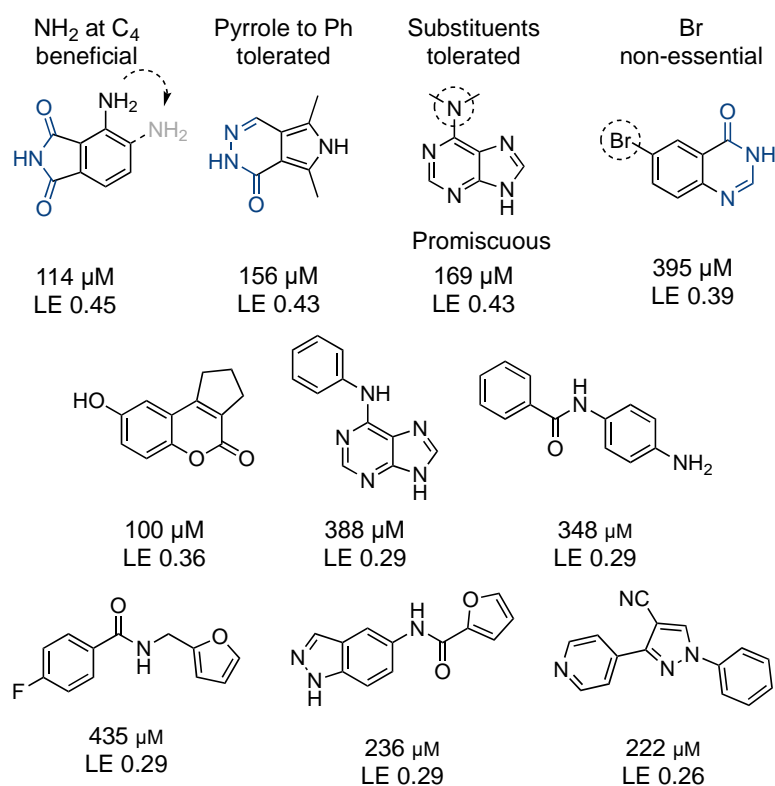
Figure 1-14. Chemical structures of the 10 Nek7 hits with a summary of the SAR learnings from the screening of 38 commercially available analogues of the four most ligand efficient hits. The atoms highlighted in blue represent essential components for binding. C2 methylation of the quinazolinone was detrimental to activity.

Eleven compounds diversifying the C6 position of the 6-bromo-quinazolinone fragment were synthesised and screened against Nek7.[97] Substitution of the bromide with six-membered aromatic rings was not tolerated whereas isoxazole, piperazine and cyclopropyl methylamine had a similar activity to the parent fragment. Interestingly, substitution with 4-pyrazole showed a 16-fold jump in activity. Pyrrole, N-methyl pyrazole and 3-pyrazole all destroyed the activity, showing both nitrogen atoms and substitution at the 4-position of the pyrazole ring are crucial for activity. Furthermore, methylation at the pyrazole 3-position was well tolerated and slightly beneficial for activity.

Further optimisation of the pyrazolyl quinazolinone core was pursued.[97] In general, increasing the size of the substituent at C2 and C8 was detrimental

to activity. Methylation at C2, however, was well tolerated in contrast to C2 methylation of the 6-bromo-quinazolinone fragment hit, which resulted in an inactive compound (Fig. 1-15). This suggests a potential alternative binding mode in which pyrazole is now the hinge binding motif. Further exploration around this core is needed however it was identified that isoquinolinone and quinolinone scaffolds gave a slight improvement in potency compared to the parent quinazolinone. Furthermore, dihydroisoquinolinone had a similar potency as isoquinolinone, yet provided sp^3 hybridised carbon centres for exploration of the Nek7 binding pocket in a more three-dimensional manner than its unsaturated counterparts. These vectors had been unexplored for SAR and could prove to be more beneficial than the equivalent C2 vector of the quinazolinone. In summary, several relatively unselective low micromolar inhibitors of Nek7 have been discovered which provide good starting points for further optimisation.
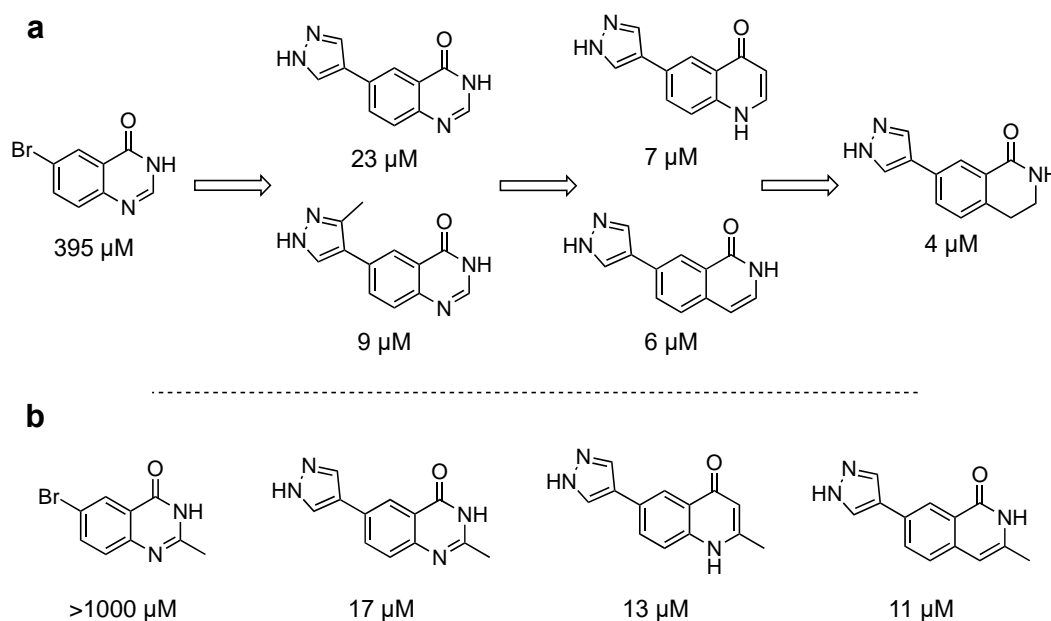
Figure 1-15. Summary of the prior SAR exploration of the bromo-quinazolinone fragment[97] (a) leading to the dihydroisoquinolinone scaffold. (b) Rationale for the hypothesis that pyrazole is the hinge binding motif.

1.4   Summary

In summary, Nek7 is crucial for mitotic progression, having roles in centrosome separation, nuclear envelope breakdown, mitotic spindle assembly and cytokinesis.[15,17,24,27,28,30,37] There are also more and more implications for Nek7 having a role in interphase.[40,41,43] Furthermore, Nek7 has a role in oncogenesis, is upregulated in a number of cells from cancer patients and is required for cell migration in EML4-ALK NSCLC patients.[44–47,54] Therefore, Nek7 could potentially become an important target for the treatment of cancer. Nek7 has also been indicated as a potential therapeutic in a range of diseases such as atherosclerosis, Alzheimer's disease and type II diabetes.[48] Despite this, no selective and potent Nek7 inhibitors have been developed.

The field of kinase drug discovery has explored a very narrow region of "kinase space", focusing on around 40 clinically validated kinases.[3,98] This is unsurprising due to the challenges in target validation. Thus, to fully exploit the therapeutic opportunity of kinases, potent and selective inhibitors will be required for a large number of kinases, including those which are underexplored, both as tool compounds for target validation and as leads for drug development. Nek7 is an underexplored 'dark' kinase which would benefit greatly from the development of a tool compound. Studies on the cellular functions of protein kinases are underpinned by the availability of kinase inhibitors.[3] Therefore, the development of such an inhibitor would enable mechanistic studies of Nek7, further elucidating the role of this kinase in health and diseased states as well as validating Nek7 as a target for drug discovery.[16]

1.5 Project Outline: Probing the Functions of Nek Family Kinases using Chemical Inhibition

The overarching project aim was to develop a suitable chemical tool against Nek7 to probe the cellular functions of this kinase using a chemical inhibitor. As no suitable chemical tool compound is available currently, the function of Nek7 had been previously studied using alternative methods such as RNAi or mutation. These methods are slow whereas a chemical inhibitor is a rapid, direct way to block kinase activity. Therefore, the use of a chemical probe to study the function of Nek7 would complement these previous studies. Given the importance of developing a chemical probe against Nek7, the project had two arms with which it could achieve this goal: (i) activity-directed fragment elaboration to identify a novel ligand series and (ii) structure-activity relationship based improvement of potency of a developed Nek7 chemical series.

1.5.1 Activity-directed Fragment Elaboration to Identify a Novel Ligand Series

Several suitable ligand efficient inhibitors against Nek7 had been identified from a previous fragment screen.[97] The first project aim was to exploit a few of these fragments simultaneously in activity-directed synthesis to potentially discover several useful novel ligand series targeting Nek7. Activity-directed synthesis is a discovery approach which follows the biological activity of catalysed reaction arrays to identify bioactive small molecules (see Chapter 2). It was envisaged that known fragments targeting Nek7 will be elaborated utilising rhodium carbenoid chemistry, using bioactivity to determine productive vectors for fragment elaboration (Fig 2.3). The results towards this first objective will form the basis of Chapter 2.

1.5.2 Improvement of Potency and Selectivity of a Developed Nek7 Chemical Series

The structure-activity relationship of the quinazolinone chemical series had been explored previously, which had led to low micromolar inhibitors of Nek7. These were useful starting points for drug discovery and, in addition to elaborating upon fragments, it was envisaged that this chemical series could

be explored further using the crystal structure of Nek7 in complex with the lead compound from this series to develop a suitable chemical tool for Nek7. The identified chemical probe could then be used in further selectivity, crystallographic and cellular studies to probe the cellular functions of Nek7. The results towards this second objective will form the basis of Chapter 3.

Chapter 2

Activity-Directed Synthesis of Novel Scaffolds as Nek7 Inhibitors

Due to the absence of a Nek7–ligand co-crystal structure at the time, one of the project aims was to use activity-directed synthesis[99,100] to efficiently access novel, alternative ligand series. The results of which will form the basis of this chapter. It was envisaged that several fragments could be exploited in arrays of rhodium catalysed reactions with diverse α-diazo amides, relying on bioactivity to determine productive fragment elaboration. The elaborated ligand series may then be taken forward for further development to generate a toolkit of chemical probes targeting Nek7.

2.1 Activity-Directed Synthesis of Androgen Receptor Agonists

Activity-directed synthesis (ADS) is a novel bioactive small molecule discovery approach developed in the group in which small molecules arise in parallel with their syntheses, driven by the function of the products.[99,100] In the approach, catalysed reactions with alternative outcomes are steered towards bioactive products in a function-driven and structure-blind manner, focusing only on reactions which give interesting products. Activity-directed synthesis involves an iterative approach in which reaction arrays are performed, scavenged to remove the catalyst and assayed against the target of interest as crude reaction mixtures (Fig. 2-1). In each round, the substrates, co-substrates, catalysts and solvent are varied to design reaction arrays in which there are many reactions, all with multiple possible outcomes. The resulting product mixtures are scavenged, evaporated and dissolved in a suitable solvent for assay to circumvent the need to use or develop reactions that work efficiently under biological conditions. The product mixtures are then assayed against the biological target to identify reactions that give active products. In the subsequent round, the reaction array is designed depending on the results of the previous round. There are two mechanisms by which active products can emerge in activity directed synthesis: (i) the structure of the product is

optimised to identify a more active molecule and (ii) the yield of the bioactive molecule is optimised by the varying reaction conditions. After several rounds, only the most active reactions are scaled up and the products are purified, characterised and their activity validated. This process allows many reactions to be performed but only a small number of highly active products are purified.
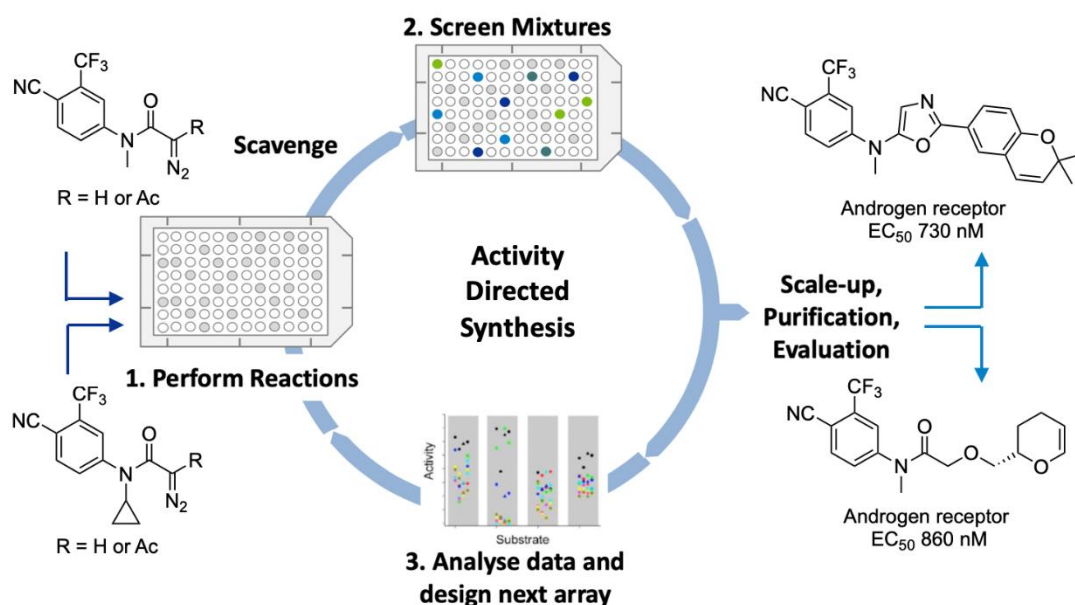
Figure 2-1. Overview of the activity-directed synthesis approach. Rhodium carbenoid chemistry was utilised in this approach.

Metal carbenoid chemistry has been exploited in the activity-directed synthesis of androgen receptor (AR) agonists.[99,100] Four α-diazo substrates were exploited in 326 reactions across three rounds of ADS, yielding a range of increasingly active AR agonists, two of which had high nanomolar activity against the AR (Fig. 2-1). These agonists exhibit novel chemotypes against the AR. Retrospective analysis revealed that structurally diverse yet inactive compounds produced in other reactions during ADS were ignored. Therefore, ADS is a powerful method, enabling the efficient exploration of chemical space to rapidly discover bioactive molecules in parallel with their associated syntheses.

Metal carbenoid species can mediate a wide range of different synthetic transformations such as C–H, N–H and O–H insertions, cyclopropanations, ylide formation and a range of cycloadditions and cascade processes to generate diverse sp^3 rich products.[101,102] This diversity of reactivity makes this

chemical toolbox ideal for ADS. The reactivity of the metal carbenoids is influenced by the nature of the metal catalyst (*i.e.* the ligands surround the dirhodium centre) as well as the substituents adjacent to the carbene carbon atom.[103,104] Regarding the substituents adjacent to the metal carbene, acceptor and acceptor/acceptor carbenes consist of one or two electron withdrawing groups, respectively. These carbenes are therefore more reactive (as the acceptor groups do not stabilise the highly electrophilic carbene centre) than donor/acceptor carbenes which bear both electron withdrawing and donating groups which stabilise the electron-deficient carbene, attenuating its reactivity and improving selectivity (Fig. 2-2a).[104] The effect of altering the ligands surrounding the dirhodium centre is shown in a limited number of representative reactions (Fig 2-2b).[105] Chemoselectivity in these transformations depends on the ligands of the rhodium carbene intermediate, with [Rh$_2$(pfb)$_4$] being more electrophilic than [Rh$_2$(cap)$_4$] resulting in [Rh$_2$(pfb)$_4$] preferring C–H insertion whilst [Rh$_2$(cap)$_4$] favours cyclopropanation.
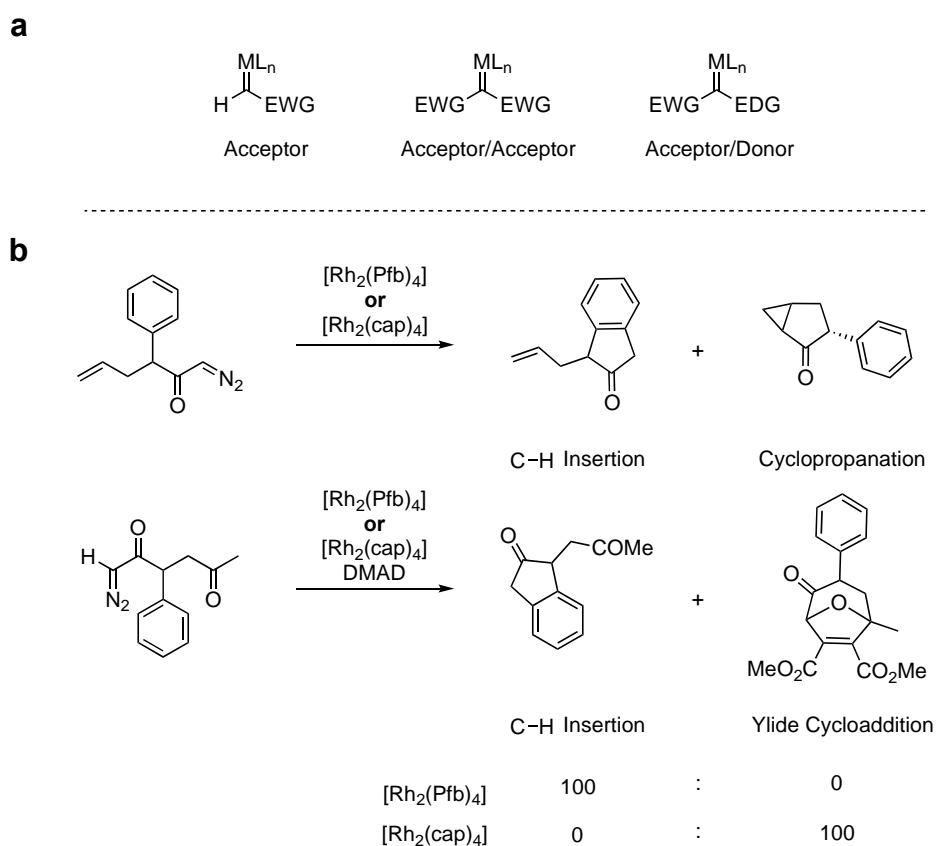
Figure 2-2. Factors which influence the reactivity of metal carbenoids. (a) Substituents surrounding the carbene and (b) ligands surrounding the metal catalyst.

2.2   Activity-Directed Synthesis of Nek7 Inhibitors

2.2.1 Reaction Array 1 Design

Four ATP-competitive fragments that had been shown to inhibit Nek7[97] (Fig. 2-3) were chosen for exploitation in activity-directed synthesis based on their ligand efficiencies and suitability for metal catalysed reaction arrays. That is, rhodium catalysed reactions of fragments **2-1**–**2-4** with α-diazo amides could react at various possible sites on the fragments (Fig. 2-3, blue), giving rise to distinct bioactive chemotypes. This type of chemistry is ideal in activity-directed synthesis as many alternative outcomes are possible yet these outcomes may be controlled through judicious choice of catalyst and reaction conditions. Assaying of the possible outcomes for each reaction could then lead to novel bioactive small molecule(s) in the absence of structural information.
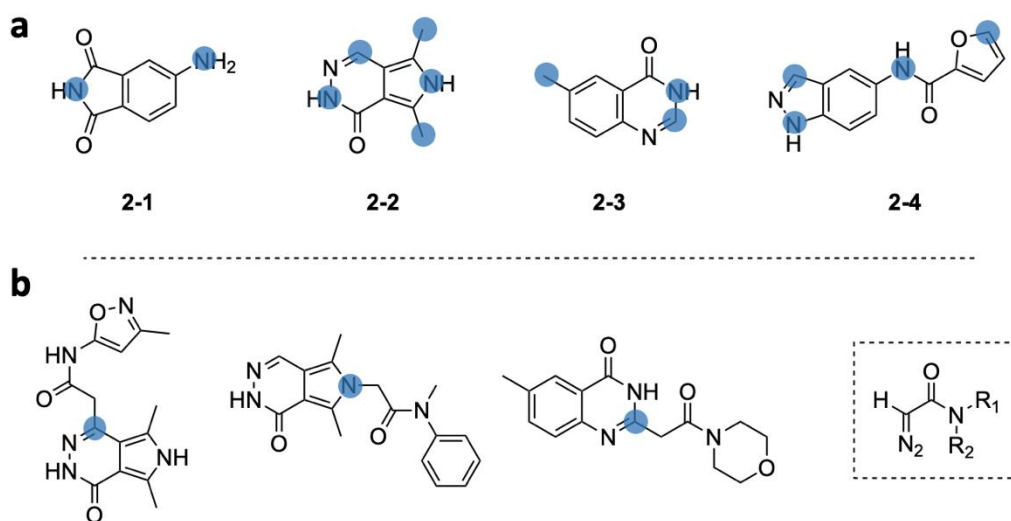
Figure 2-3. The four fragments chosen for elaboration driven by activity-directed synthesis (a). Blue represents possible reactive sites on the fragments using rhodium carbenoid chemistry. (b) Possible products following reaction with diverse α-diazo amides (boxed) and a dirhodium catalyst.

a) Fragments

2-1	2-2	2-3	2-4

b) α-Diazo Amides

2-5	2-6	2-7	2-8
2-9	2-10	2-11	2-12

c) Catalysts

| [Rh₂(OAc)₄] | [Rh₂((S)-DOSP)₄] | [Rh₂(cap)₄] | [Rh₂(pfb)₄] |
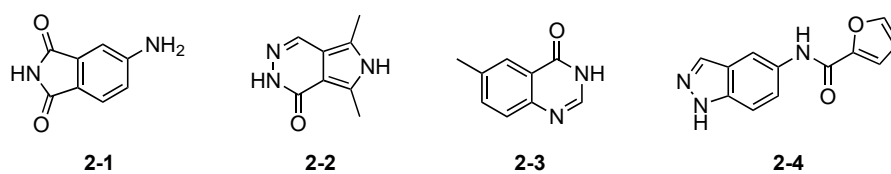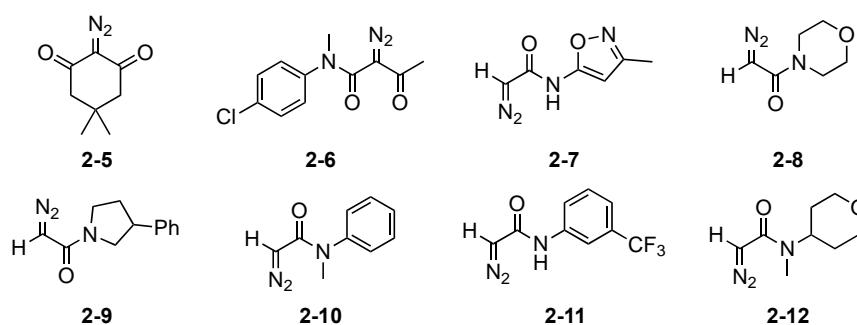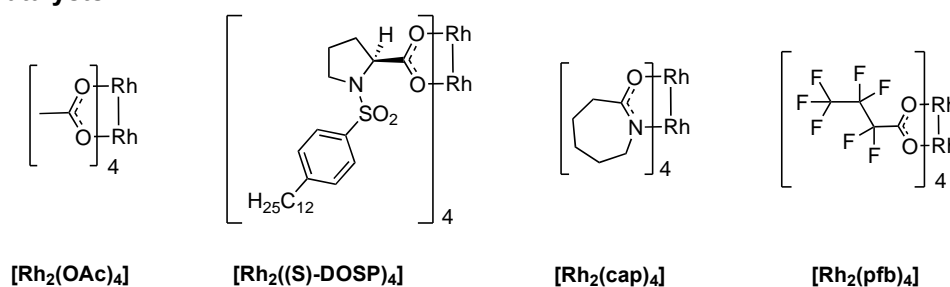
Figure 2-4. The fragments, α-diazo amides and catalysts exploited in the first reaction array. An exhaustive array of all 128 combinations was performed.

With the Nek7 fragments chosen for the array, we turned our attention to the α-diazo amide reactants, which were chosen from a diverse library previously enumerated within the group. The α-diazo amides were chosen based on: (i) the diversity of their chemical structures, (ii) their molecular properties such as a heavy atom count of less than 16 (excluding N_2 as this is lost in any reaction) and lipophilicity and (iii) synthetic tractability. Similarly, previous DFT modelling and principal component analysis of dirhodium catalysts[106] within the group illustrates catalyst (dis)similarity, enabling the rational selection of catalysts for inclusion in a reaction array. The catalysts were chosen based on their diversity with respect to their structure and reactivity. For instance, bidentate carboxylate (*O,O*) ligands are distinct from bidentate carboxamidate (*O,N*) ligands. Furthermore, fluorinated *O,O* ligands are sufficiently different

from other *O,O* ligands. Distinct catalysts, which potentially have different modes of reactivity (C–H insertion *versus* cyclopropanation) or prefer different sites of reactivity, are preferred in early rounds of ADS to give diverse products. Contrastingly, similar catalysts are preferred in later rounds to optimise the already identified bioactive scaffold. An exhaustive array of every possible combination of 4 fragments, 8 α-diazo amides and 4 dirhodium catalysts in CH_2Cl_2 (Fig. 2-4) was performed: a total of 128 reactions.

It was aimed to have a high diversity of reactants and catalysts for the first round of activity-directed synthesis. Any reactions which gave rise to bioactive product mixtures could then inform the choice of similar reactants and catalysts in future iterations.

2.2.2 Synthesis of Substrates for Reaction Array 1

2.2.2.1   Synthesis of Nek7 Fragments

Fragment **2-1** was commercially available. The synthesis of **2-2** began with carboxylic acid **2-13** which was subjected to modified Steglich esterification conditions[107,108] to produce ethyl carboxylate **2-14** in 55% yield. Catalytic DMAP was included as it has been reported to accelerate the DCC-activated esterification and suppresses side product formation[107]. The pyrrole **2-14** was then subjected to modified Vilsmeier–Haack conditions[109] to achieve formylation of the pyrrole ring at the C-4 position in 82% yield. The resultant product was cyclised using excess hydrazine under reflux to give the fragment **2-2**, in 84% yield.
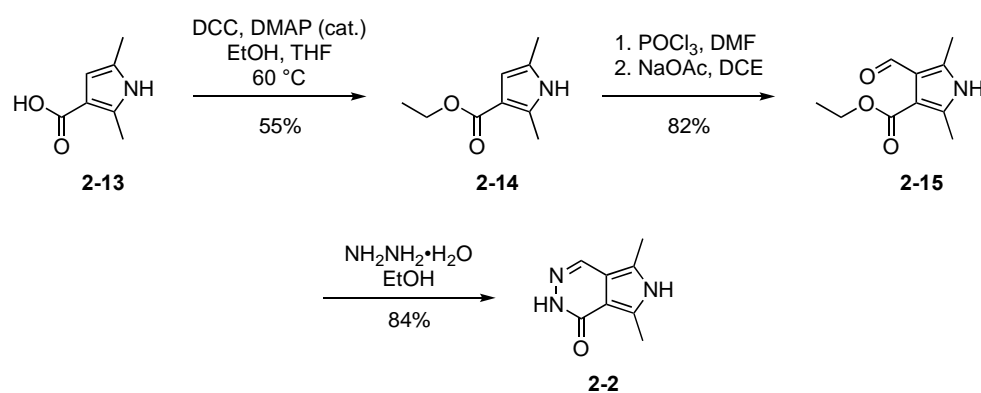
Scheme 2-1. Synthesis of **2-2** *via* Steglich esterification with ethanol, Vilsmeier Haack formylation and cyclisation with hydrazine.

The final two fragments were synthesised *via* one-step syntheses (Scheme 2-2). Anthranilic acid **2-16** was subjected to Niementowski condensation conditions[110] *via* reaction with excess formamide to give **2-3**, which conveniently precipitated out of solution upon production, in 58% yield. Finally, amine **2-17** was reacted with acyl chloride **2-18** and the crude product treated with TFA to give **2-4** in 73% yield (over two steps). It was opted to use the Boc-protected indazole in this instance to avoid the formation of the amide at this position.
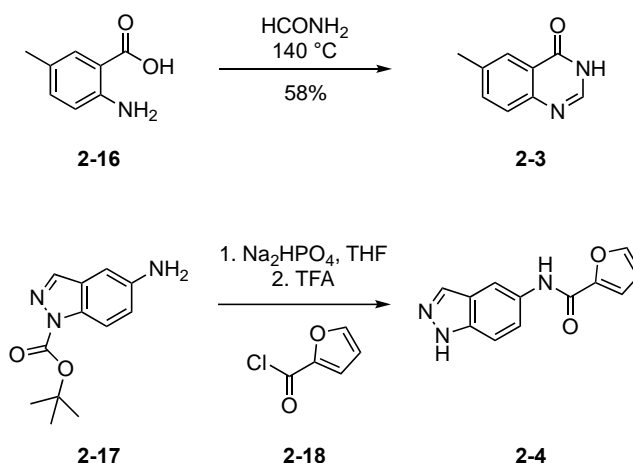
Scheme 2-2. Synthesis of fragments **2-3** and **2-4**.

2.2.2.2   EZ Reader II Mobility Shift Assay

In order to determine the activity of any synthesised fragments for Nek7, as well as to screen the resulting product mixtures from a reaction array, a robust biochemical assay is needed.

The assay chosen for both purposes is a mobility shift assay using the LabChip® EZ Reader (Caliper Life Sciences) which uses the principles of electrophoresis in a microfluidic chip to separate molecules based on size and charge (Fig. 2-5).[111–113] The mobility shift assay enables the analysis of enzymatic reactions without the need for coupled reactions.[114] Using vacuum pressure, enzymatic reactions are 'sipped' from 96- or 384-well microtitre plates into the microfluidic channels. In this case, the kinase catalyses the phosphorylation of a fluorescently labelled peptide substrate. Application of an electrical potential across the channel causes separation of phosphorylated and non-phosphorylated peptide, with the former moving

more quickly towards the positive electrode due to the large, negatively charged phosphoryl group. The now separated products are detected *via* LED-induced fluorescence. For kinetic analysis, the reaction is monitored by sequentially sipping samples at specified time intervals. Percentage conversion is then calculated from the relative heights of the substrate and product peaks and plotted against time. The initial rate is then used for IC_{50} determination or reaction array analysis.
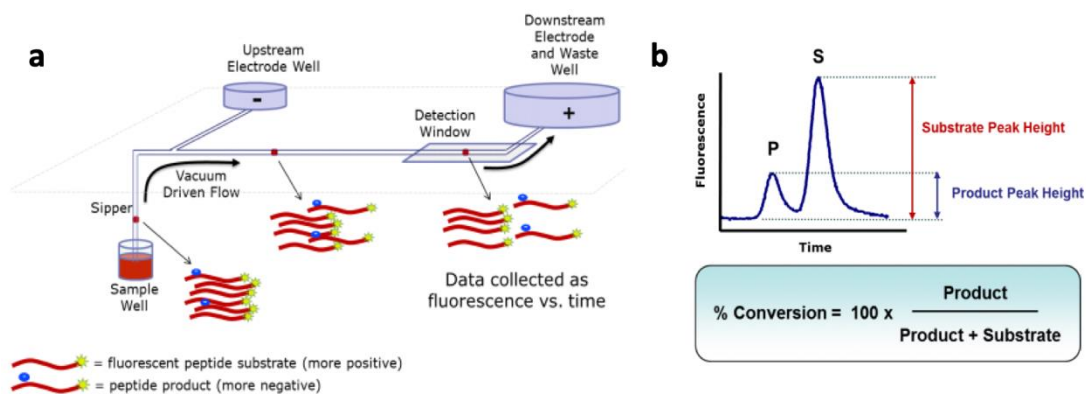
Figure 2-5. Schematic of the EZ Reader mobility shift assay. (a) Illustrating the principles of assay and (b) Example data output of the assay alongside how the EZ Reader software calculates percentage conversion of the peptide substrate.

Prior to the testing of any compounds or reaction arrays, the optimum concentration of Nek7 and ATP for the assay was established (see Appendix A.1). To determine the optimal kinase concentration, a two-fold six-point serial dilution of Nek7 (with the concentration ranging from 500 nM to 16 nM) was performed and the conversion of the fluorescent peptide substrate monitored over time. As the optimal enzyme concentration had to be determined prior to the optimal ATP concentration, the concentration of ATP used in this assay was at the ATP K_M previously determined in the group by Byrne *et al* (45 μM).[28] An enzyme concentration of 250 nM was chosen for use in all future assays as it gave a linear response (R^2 0.996) up to approximately 20% conversion over 40 minutes (Appendix A.1). This linear response corresponds to the initial rate of the enzyme. Furthermore, the rate at this enzyme concentration would enable kinetic data from screening of large reaction arrays to be obtained.

Following the determination of the optimal enzyme concentration for the assay, the optimal ATP concentration, *i.e.* the ATP K_M for Nek7, was

determined as 32 ± 4 µM (Appendix A.1). Using a 250 nM Nek7 concentration, a three-fold, 12-point serial dilution of ATP (from 3 mM to 17 nM final concentration) was performed and the conversion of the fluorescent peptide substrate was monitored over time. The slope of the linear response at each concentration was calculated and plotted against the corresponding ATP concentration (Appendix A.1). This allowed the K_M of ATP for Nek7 to be determined and a final ATP concentration of 30 µM was used in all future assays. Performing the assay using an ATP concentration at the K_M allows the most sensitive detection of Nek7 ATP-competitive inhibitors. High ATP concentrations can preclude the detection of weakly binding fragments whilst lower ATP concentrations can lead to artificially low IC_{50} values which will poorly reflect the activity of the fragments for Nek7, thereby resulting in a poor translation of the fragment into a cellular environment where the ATP concentration is in the low mM range.[97,115]
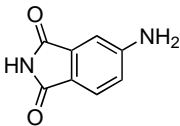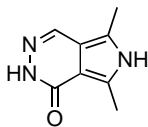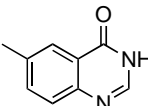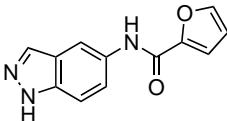
2.2.2.3 Activity Determination of Nek7 Fragments

With the fragments **2-1**–**2-4** in hand, the inhibition of these fragments against Nek7 was determined to validate the previously reported affinities.[97] The inhibition of each fragment was measured in a 10-point 3-fold dilution series from 3 mM top concentration (Appendix A.2). The IC_{50} values measured here would also determine the screening concentration for the reaction array product mixtures. If the screening concertation was too high, residual, unreacted fragment would give rise to inhibition, resulting in difficult identification of more active reaction mixtures.

The determined activities, despite having an increased IC_{50}, showed a similar trend and generally agreed with the previously reported values. The method used here was the same as the one which previously determined the inhibition of these fragments. The small discrepancy in activity of the fragments observed by this work relative to the previously reported values is likely due to the higher enzyme and hence ATP concentrations used here. Based on the measured activities, the reactions resulting from fragments **2-2**–**2-4** were screened at 100 µM (relative to the initial fragment concentration in the reaction). Screening at 100 µM would allow an increase in activity to be observed whilst rendering any residual fragment inactive. However as

fragment **2-1** has an IC_{50} of approximately 100 μM, reactions from this fragment were screened at 30 μM to avoid significant inhibition by any residual fragment.

Table 2-1. Measured Activities of Previously Reported Nek7 Fragments

Entry	No.	Fragment	Reported[97] IC_{50} (μM)	Measured IC_{50} (μM)[a]	Measured LE
1	**2-1**		32	101 ± 9	0.47
2	**2-2**		156	510 ± 95	0.38
3	**2-3**		361	190 ± 43	0.43
4	**2-4**		236	620 ± 58	0.26

[a]n = 2. The small discrepancy observed is due to a higher enzyme and therefore ATP concentration (at K_M) used here. The method used was the same as previously reported.

2.2.2.4   Synthesis of α-Diazo Amides

As **2-8**–**2-10** and **2-12**[116] had been synthesised in the group and **2-5** was commercially available, **2-6**–**2-7** and **2-11** required preparation. A one-pot synthesis of α-diazo amides based on an established synthesis of α-diazoacetic esters[117–120] and from readily available amines was developed.[116] Glyoxylic acid **2-19** was reacted with tosylhydrazide to give the hydrazone **2-20** in 56% yield. After trituration with water and vacuum filtration, the hydrazone was heated with thionyl chloride to generate the corresponding acyl chloride. The crude acyl chloride was immediately reacted with the

desired amine followed by treatment with triethylamine to give the α-diazo amides **2-7** and **2-11** over three steps.
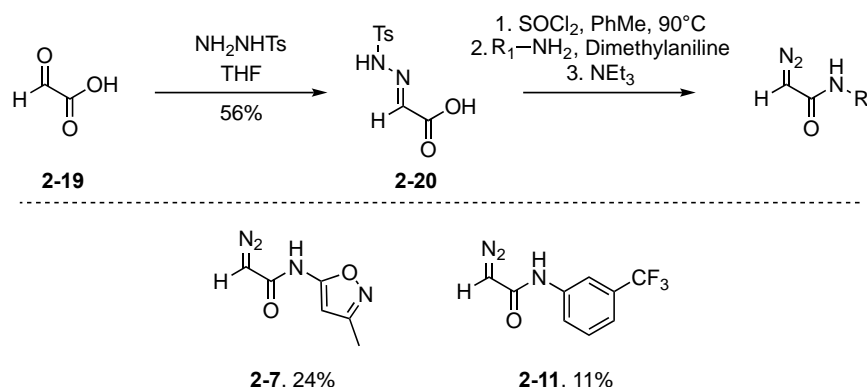
Scheme 2-3. Synthesis of α-diazo amides **2-7** and **2-11** by acylation and elimination. Yields refer to the second synthetic sequence (over three steps).

The remaining α-diazo amide was synthesised *via* acylation of aniline **2-21** with dioxinone **2-22** under microwave irradiation[121] to give **2-23** which was expected to be a substrate for diazo transfer. The synthesis of such compounds by diazo transfer has been demonstrated with a range of substrate classes.[122,123] Previous reports[99,100,116] had shown it was possible to telescope the acylation with a subsequent diazo transfer reaction. Accordingly, treatment of crude **2-23** with *p*-ABSA and triethylamine at 0 °C gave the desired α-diazo amide **2-6** in 36% yield over two steps. The use of triethylamine, rather than DBU, as the base enabled more facile purification. Indeed, under these conditions, diazo transfer was accompanied by precipitation of 4-acetamidobenzenesulfonamide.[124]
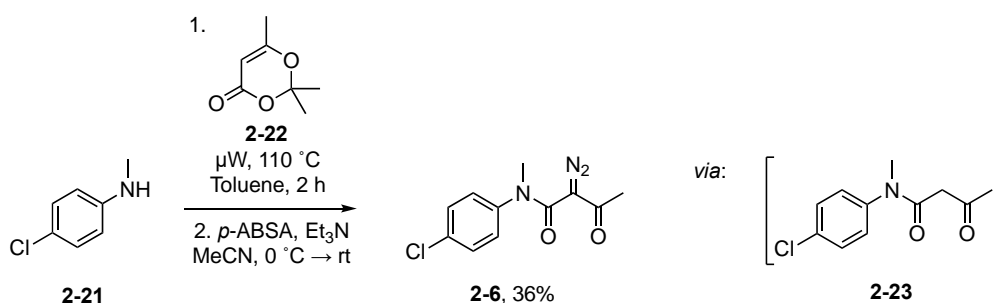
Scheme 2-4. Synthesis of **2-6** *via* acylation and diazo transfer.

2.2.3 Reaction Array 1 Mock Array

Prior to an actual reaction array, a 'mock array' was performed in which the individual components of the reaction array (fragments, α-diazo amides and catalysts) alone as well as each α-diazo amide combined with each catalyst were subjected to the ADS workflow. These are then screened at the desired screening concentration to ensure that no individual component or combination of components are active at that concentration and therefore an identified hit reaction will likely to be due to a productive reaction. Despite the *α*-diazo amides not having precedent for Nek7 activity, all possible combinations of the *α*-diazo amides and catalysts are included as controls in the mock array to demonstrate that any hit reaction identified is not due to intramolecular reactions involving the *α*-diazo amide. The workflow during the mock array is the same as the reaction array. Each individual component is dissolved to the desired concentration (substrate 100 mM, co-substrate 110 mM and catalyst 2.5 mM) in CH_2Cl_2 and left at room temperature for 48 h. Each 'reaction' is then scavenged with the thiourea QuadraPure TU resin for 24 h followed by filtration and concentration of the product mixtures. The resultant solids are then re-dissolved in DMSO to 100 mM total product concentration and screened against Nek7 at the desired screening concentration (100 µM except the 4-aminophthamidide which was screened at 30 µM). All the individual components and combinations of catalyst and co-substrate were inactive against Nek7 at the desired screening concentration (see Appendix A.3). With this result at hand, the actual reaction array was performed.

2.2.4 Reaction Array 1 Execution

With the Nek7 fragments and α-diazo amides in hand, an exhaustive array of 128 reactions (illustrated in Fig. 2-4) stemming from all possible combinations of four fragments, **2-1**–**2-4**, eight α-diazo amides, **2-5**–**2-12**, and four dirhodium catalysts in one solvent (CH_2Cl_2) was performed (see experimental for details). The reactions (50 μl, in CH_2Cl_2) were performed in borosilicate glass micro-vials in which the fragment (100 mM), α-diazo amide (110 mM) and dirhodium catalyst (2.5 mol%) were varied. After 48 h at room temperature, the crude reaction mixtures were scavenged (QuadraPure TU,

30 mg) to remove metal catalysts. After a further 24 h, the mixtures were filtered, evaporated and re-dissolved in DMSO (50 µl) to give a total product concentration of 100 mM (with respect to the fragment). These crude product mixtures were then assayed for inhibition of Nek7 (Fig. 2-6).
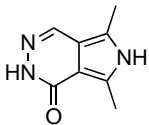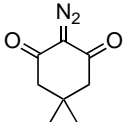
Figure 2-6. Activity of product mixtures derived from reaction array 1. Biological activity is expressed relative to 3 mM **3-3**, which represents 100% inhibition in the centre, purple. The outer edge represents 0% inhibition (normalised to 2% DMSO buffer). The mixtures were assayed for inhibition of Nek7 at a single concentration of 100 µM total product concentration except for reactions with 4-aminophthalimide as the fragment which were screened at 30 µM. The slope of Nek7 activity over time was plotted, with the error bars indicating the standard error, n = 2.

Interestingly, fragment **2-2** yielded active products when reacted with α-diazo amides **2-5** and **2-6** using [Rh$_2$(cap)$_4$] or [Rh$_2$(pfb)$_4$] as the catalyst (Table 2-2). The crude product mixtures from these four reactions inhibited Nek7 by approximately 50% at 100 μM total product concentration. The remaining reactions with fragment **2-2** (and indeed all other fragments) gave rise to no bioactivity, suggesting bioactivity of the product mixtures is dependent on the specific reaction components used. For instance, reactions of fragment **2-2** with only specific combinations of α-diazo amide and catalyst were steered towards bioactive products. Crucially, it had been established that the individual components of the reaction array in isolation as well as combinations of α-diazo amide and catalyst were inactive under the assay conditions (see Appendix A.3). This inactivity suggested that the crude product mixtures which gave rise to bioactivity did so only when all three components were combined.

Table 2-2. Active Combinations from the First Reaction Array

Entry	Fragment	α-Diazo amide	Catalyst	Percentage Inhibition[a]
1		**2-5**	[Rh$_2$(cap)$_4$]	50
	2-2		[Rh$_2$(pfb)$_4$]	41
2		**2-6**	[Rh$_2$(cap)$_4$]	53
			[Rh$_2$(pfb)$_4$]	59

[a]Percentage inhibition (%) of Nek7 at 100 μM total product concentration.

At this point, the most bioactive reactions from the first array were not scaled-up to isolate any bioactive products. Instead, the fragment, α-diazo amides

and catalysts which yielded active products were fed into the design of a subsequent reaction array.

2.2.5 Reaction Array 2 Design

The second reaction array was designed based on the results of the first and consisted of 144 reactions (Fig. 2-7) stemming from an exhaustive combination of 1 fragment, 9 α-diazo amides and 4 catalysts in 4 different reaction solvents. In this case, the α-diazo amides chosen were structurally related to **2-5** and **2-6**, which gave rise to bioactivity in the first round, in an attempt to optimise the bioactive structures produced. This is indeed one of the methods in which activity-directed synthesis can give rise to bioactive products. The second method is by varying the reaction conditions, the yield of the bioactive products may be optimised. We opted to keep catalyst diversity high by including catalysts which are able to perform the desired transformation but are distinct, with respect to their structure and reactivity, from the two which gave rise to bioactive product mixtures in the first array. We hoped that maintaining a high catalyst diversity would not only generate diverse products, but also increase reaction yields. For instance, an alternative dirhodium carboxylate catalyst to [$Rh_2(OAc)_4$] was included ([$Rh_2(oct)_4$]) as well as a gold catalyst which has also been shown to be a useful catalyst in the generation of a metal carbenoid from an α-diazo carbonyl compound.[125,126] We opted to pre-form the cationic gold species, postulated to be the active catalyst,[127] prior to addition into the reaction array. This was achieved by mixing of the corresponding neutral gold complex (coordinated to a chloride ligand) with $AgSbF_6$ and benzonitrile in CH_2Cl_2 (to the desired stock concentration) followed by filtration of the AgCl by-product. Similarly as with the choice of catalysts, we chose to vary the solvent in this array in an attempt to optimise reaction yields. Fragment **2-2** was partially insoluble in CH_2Cl_2 and so polar protic and aprotic solvents were chosen for the array in hope of solubilising the fragment and improving reaction yields.

a) Fragments

2-2
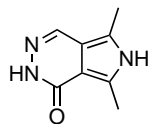
b) α-Diazo Amides
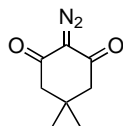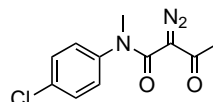
2-5   **2-6**
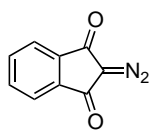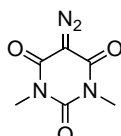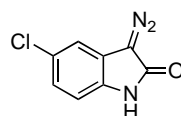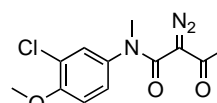
2-5a   **2-5b**   **2-6a**   **2-6b**
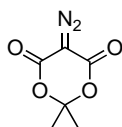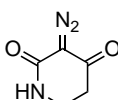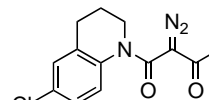
2-5c   **2-5d**   **2-6c**

c) Catalysts
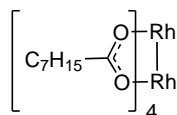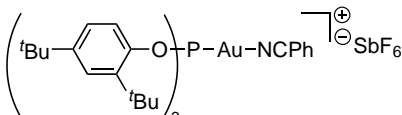
[Rh₂(oct)₄]   **(2,4-ᵗBu₂C₆H₃O)₃PAuNCPh**   **[Rh₂(cap)₄]**   **[Rh₂(pfb)₄]**
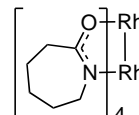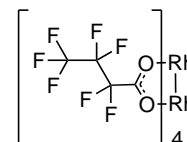
d) Solvents

CH₂Cl₂   MeOH   DMF   THF

Figure 2-7. The fragments, α-diazo amides, catalysts and solvents exploited in the second reaction array. An exhaustive array of all 144 combinations was performed.

2.2.6 Synthesis of Substrates for Reaction Array 2

2.2.6.1   Synthesis of α-Diazo Amides

With **2-5** and **2-6** previously prepared or acquired for the first reaction array, **2-5a**–**2-6d**[116] required synthesis. With the exception of **2-6a**, **2-5a**–**2-6d** were prepared in a similar manner as described for **2-6** (see 2.2.2.4), the results of which are shown in Table 2-3. In the case of the cyclic 1,3-dicarbonyl

compounds **2-5a–2-5d**, a prior acylation step was not necessary and the corresponding α-diazo amides could be prepared from simple diazo transfer. Diazo transfer onto cyclic 1,3-dicarbonyl compounds was found to be more optimal at lower temperatures (-10 °C → rt) and shorter reaction times (~30 min), suggesting a higher reactivity, compared with the acyclic variants (0 °C → rt, ~4 h).

Table 2-3. Synthesis of α-Diazo Amides *via* Diazo Transfer
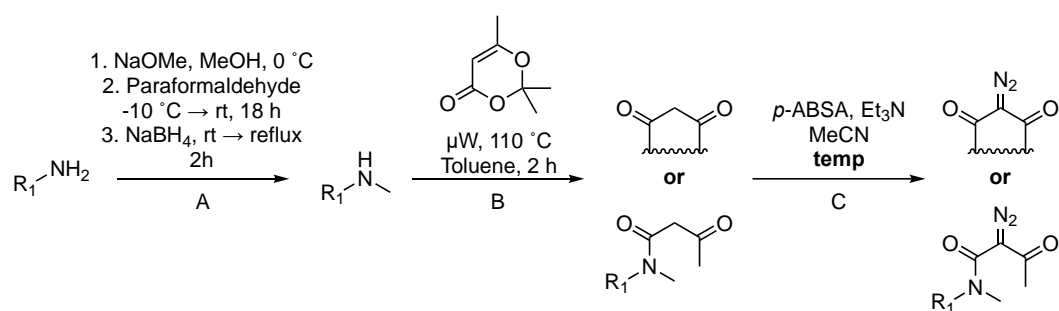
Entry	No.	Starting Material	Method	No.	Product	Yield (%)
1	**2-24**		C (**-10 °C → rt**)	**2-5a**		76%
2	**2-25**		C (**-10 °C → rt**)	**2-5b**		88%
3	**2-26**		C (**-10 °C → rt**)	**2-5c**		91%
4	**2-27**		C (**-10 °C → rt**)	**2-5d**		33%
5	**2-28**		A,B,C (**0 °C → rt**)	**2-6b**		82 (A) 42 (B,C)
6	**2-29**		B,C (**0 °C → rt**)	**2-6c**		67 (B,C)

Cyclic α-diazo amides **2-5a–d** were prepared in yields of 76-91% with the exception of **2-5d** (33%, due to purification issues). Acyclic α-diazo amides **2-6b** (following methylation in 82% yield) and **2-6c** were prepared in yields of 42-67% (telescoped over two steps).

1. NH$_2$NHTs
   THF
   65 ˚C, 1 h
2. NaOH
   65 ˚C, 1 h

82%

2-30   **2-6a**
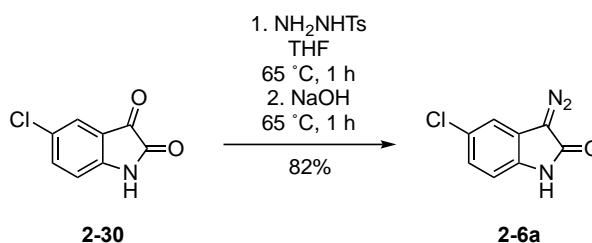
Scheme 2-5. Synthesis of **2-6a** *via* condensation tosylhydrazide and elimination with NaOH.

The final α-diazo amide requiring preparation, **2-6a**, was achieved cleanly and in 82% yield over two steps *via* reaction of isatin **2-30** with tosylhydrazide followed by elimination with NaOH.

2.2.7 Reaction Array 2 Mock Array

As with round 1, a mock array was also performed prior to the execution of round 2. Again, this was to establish that the individual components of the reaction array, as well as combination of components, were inactive under the screening conditions and that an identified hit reaction will likely to be due to a productive reaction. This mock array was performed only in a single solvent (CH$_2$Cl$_2$) and the workflow was the same as the mock array for round 1 (see 2.2.3). All the individual components and combinations of catalyst and α-diazo amide were inactive against Nek7 at the desired screening concentration, except for when α-diazo amide **2-5d** was combined with [Rh$_2$(cap)$_4$] which gave rise to 80% inhibition. This led us to be wary of any active reaction between the fragment, **2-5d** and [Rh$_2$(cap)$_4$], however as all the other individual components or combinations thereof were inactive, reaction array 2 was performed (see Appendix A.3).
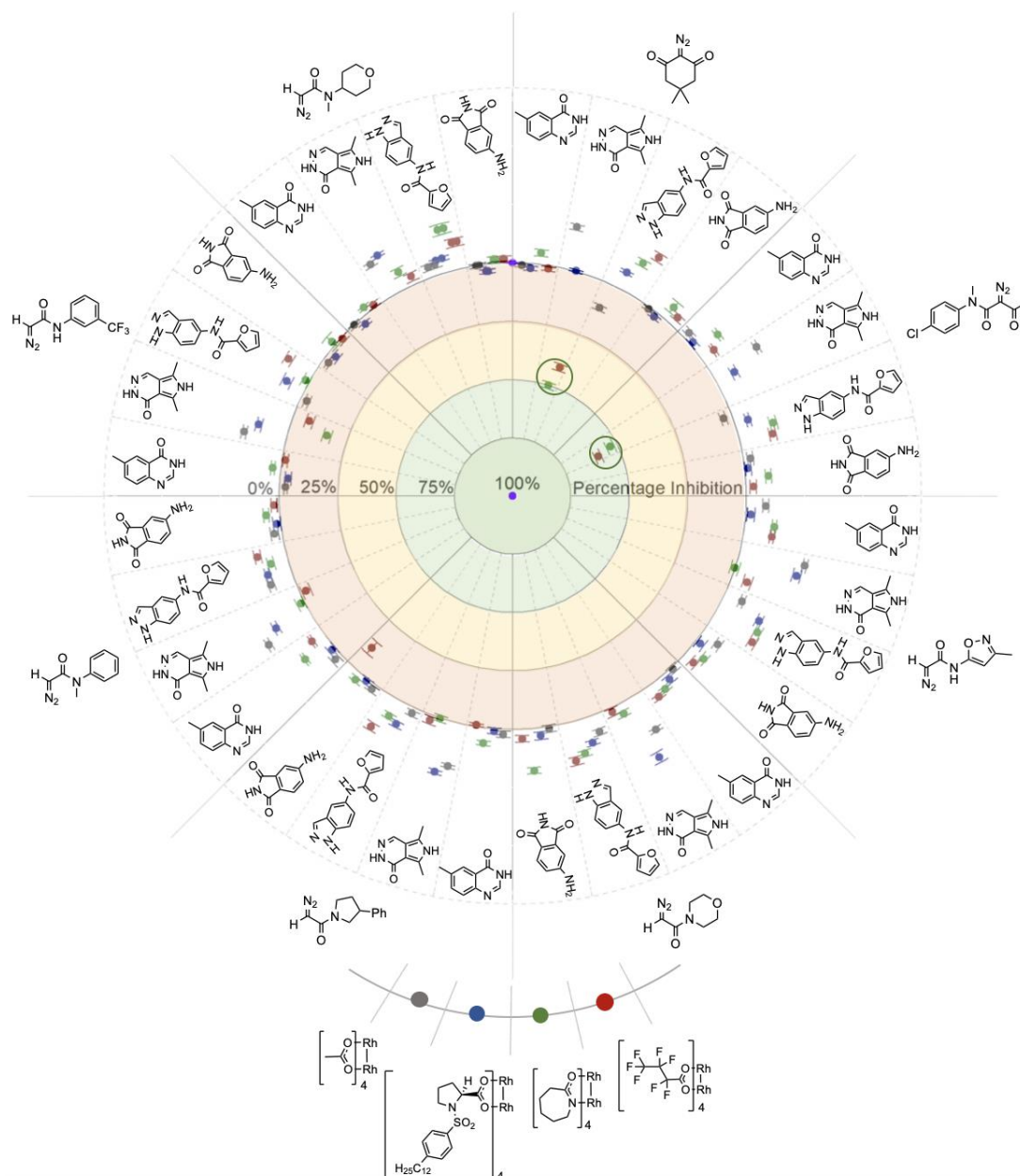
2.2.8 Reaction Array 2 Execution
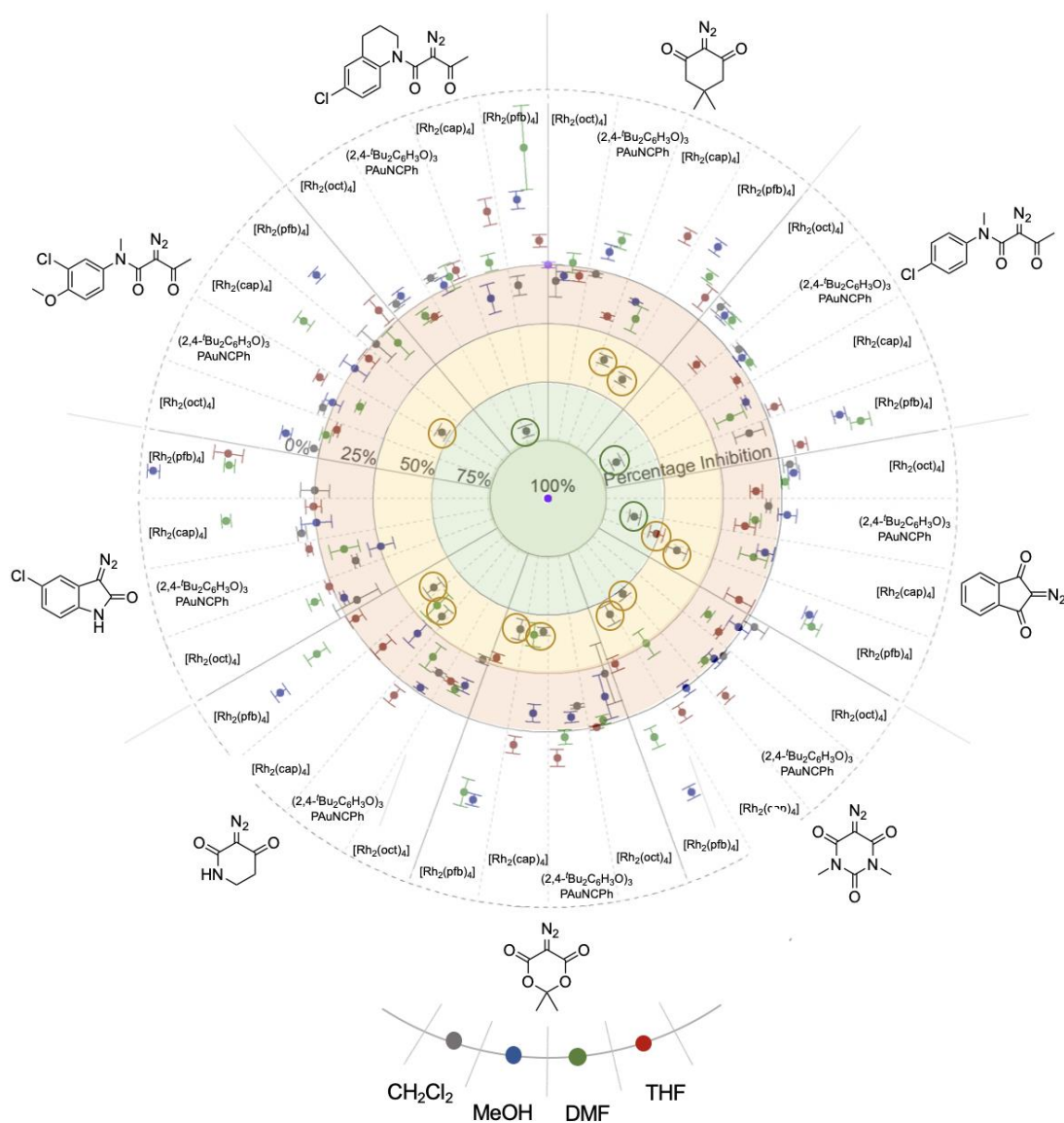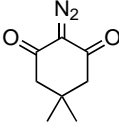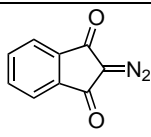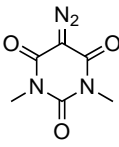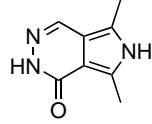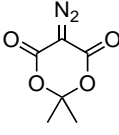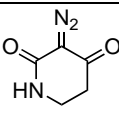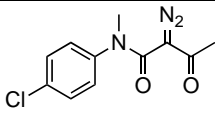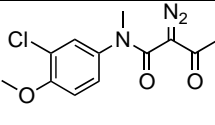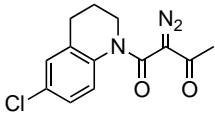
Figure 2-8. Activity of product mixtures derived from reaction array 2. Biological activity is expressed relative to 3 mM **3-3**, which represents 100% inhibition in the centre, purple. The outer edge represents 0% inhibition (normalised to 2% DMSO buffer). The mixtures were assayed for inhibition of Nek7 at a single concentration of 100 μM total product concentration. The slope of Nek7 activity over time was plotted, with the error bars indicating the standard error, n = 2.

With the fragment and α-diazo amides from the first reaction array as well as the ones prepared above in hand, an exhaustive array of 144 reactions (illustrated in Fig. 2-7) stemming from all possible combinations of one fragments, **2-2**, nine α-diazo amides, **2-5**–**2-6**, four catalysts (three dirhodium and one gold) in four solvents (CH_2Cl_2, MeOH, DMF and THF) was performed as described in 2.2.4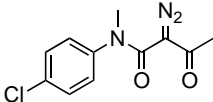. The crude product mixtures were then assayed for inhibition of Nek7 at 100 μM, the results of which are shown above (Fig. 2-8). Crucially, as in round 1, it had been established that the individual components of the reaction array in isolation as well as combinations α-diazo amide and catalyst were inactive under the assay conditions (see Appendix A.3).

A higher range of bioactivities was observed from the product mixtures of array two when compared with the first reaction array. This increased number of active product mixtures may be due to the use of analogous α-diazo amides to the ones which gave rise to activity in the first array. For instance, the reaction of **2-2** and **2-5** with [$Rh_2(cap)_4$] or [$Rh_2(pfb)_4$] in CH_2Cl_2 gave rise to a similar level of Nek7 inhibition as seen in the first array, validating the initial result. Furthermore, fragment **2-2** in combination with analogues of **2-5**, **2-5a**–**2-5d**, using the same catalysts and in the same solvent (as well as in DMF and THF in some cases) gave similar or higher levels of Nek7 inhibition. As shown by the mock array, the activity of the reaction between the fragment, **2-5d** and [$Rh_2(cap)_4$] could be due to the α-diazo amide and the catalyst themselves and should be disregarded. The first array result involving the fragment and **2-6** was also validated here, which gave a higher level of Nek7 inhibition in the second array compared to that observed in the first array. Furthermore, reactions with analogues of **2-6, 2-6b** and **2-6c** also provided bioactive reaction mixtures. Therefore, not only did we identify product mixtures which gave similar levels of Nek7 inhibition as in the first array, we also observed an enrichment of bioactivity with **2-5a** and **2-6c** (as well as **2-6**) giving rise to increased Nek7 inhibition.

Table 2-4. Active Combinations from the Second Reaction Array

Entry[a]	Fragment	α-Diazo amide	Catalyst	Solvent	Percentage Inhibition
1		**2-5**	**[Rh₂(cap)₄]**	**CH₂Cl₂**	**36**
			[Rh₂(pfb)₄]		**40**
2		**2-5a**	[Rh₂(cap)₄]	CH₂Cl₂	62
				THF	51
			[Rh₂(pfb)₄]	CH₂Cl₂	40
3		**2-5b**	[Rh₂(cap)₄]	CH₂Cl₂	48
			[Rh₂(pfb)₄]		44
4	**2-2**	**2-5c**	[Rh₂(cap)₄]	CH₂Cl₂	43
				DMF	41
			[Rh₂(pfb)₄]	CH₂Cl₂	43
5[b]		**2-5d**	[Rh₂(cap)₄]	CH₂Cl₂	32
				DMF	34
			[Rh₂(pfb)₄]	CH₂Cl₂	38
6		**2-6**	**[Rh₂(cap)₄]**	**CH₂Cl₂**	**67**
7		**2-6b**	[Rh₂(cap)₄]	CH₂Cl₂	46

Entry[a]	Fragment	α-Diazo amide	Catalyst	Solvent	Percentage Inhibition
8		\n\n**2-6c**	[Rh$_2$(cap)$_4$]	CH$_2$Cl$_2$	70

[a]Entries 1 and 6 were also active in round 1. [b]**2-5d** combined with [Rh$_2$(cap)$_4$] in CH$_2$Cl$_2$ in the absence of fragment in the mock array gave rise to 80% inhibition however no inhibition was observed in the mock array when [Rh$_2$(pfb)$_4$] was used.

The combination of fragment **2-2** with α-diazo amides **2-5a**, **2-6** and **2-6c** using [Rh$_2$(cap)$_4$] as the catalyst and CH$_2$Cl$_2$ as the solvent yielded the most active product mixtures, inhibiting Nek7 between 62-70% at 100 μM. Therefore, these three most active combinations across both reaction arrays were taken forward for isolation, characterisation and validation.

2.2.9 Identification of Bioactive Product(s)

At this point, the small molecule or molecules responsible for the inhibition of Nek7 were unknown. Therefore, the three most active reaction combinations above from the second reaction array (Table 2-4, Entries 2, 6 and 8, Scheme 2-6) were repeated on a larger (50-fold) scale to provide enough material for characterisation and validation once isolated. The scale-up reactions were performed using the same workflow as previously described (see 2.2.4) but on a 50-fold scale, *i.e.* in a total volume of 2.5 ml as opposed to 50 μl. The workflow was followed closely to repeat the microscale reactions but on a larger scale, the only difference being the larger glass vials required. After the reactions were performed, scavenged and filtered, they were purified by silica flash column chromatography. Despite the scaled-up reactions still showing activity against Nek7 (see Appendix A.4), no products resulting from a reaction were isolated from any of the three reaction mixtures. This lack of bioactive product isolation, and inconclusive LCMS data, led us to investigate the reactions on an NMR scale.
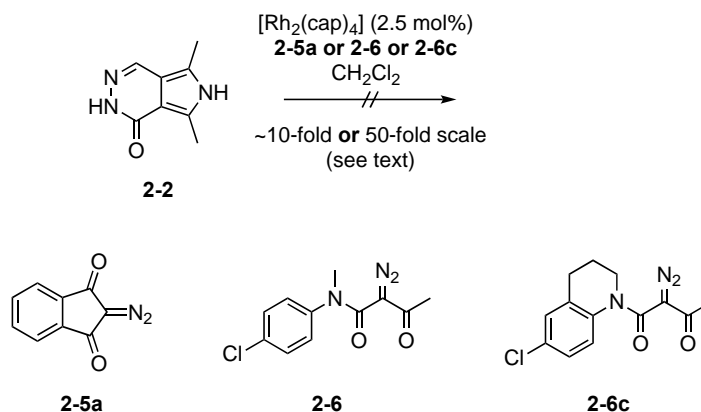
Scheme 2-6. Most active combinations over two rounds of activity-directed synthesis which were scaled-up for identification of bioactive product(s).

The three most active reactions were repeated on a 600 μl total volume (~10-fold) scale. An exhaustive combination of two of the three components, *i.e.* fragment-α-diazo amide, α-diazo amide-catalyst and fragment-catalyst, were performed alongside as controls. After the reactions were performed, scavenged and filtered, they were re-dissolved in the same volume (600 μl) of *d₆*-DMSO. Upon NMR analysis, a spectrum of the α-diazo amide was observed for all three 'active' combinations suggesting no detectable reaction had occurred (the fragment was likely removed during the scavenging and filtering phase due to its insolubility in CH_2Cl_2), see Appendix A.5. The NMR spectrum was altered only in the case of **2-6** (which is able to react intramolecularly) when combined with catalyst in the absence of fragment, suggesting the presence of the fragment may prevent a catalysed reaction from occurring. Surprisingly, for **2-5a** and **2-6c**, no reaction appeared to occur even when the α-diazo amide was simply mixed with the catalyst in CH_2Cl_2.

The unsuccessful isolation of bioactive product(s), *i.e.* the unidentified reason for the observed bioactivity, along with a newly solved Nek7-fragment crystal structure led us to pursue a more conventional ligand optimisation approach which forms the basis of the next chapter.

2.3 Conclusions on the Use of Activity-Directed Synthesis for the Development of Novel Nek7 Inhibitors

We opted to develop previously identified fragments with annotated activity against Nek7 using an activity-directed synthesis approach. This approach was undertaken due to the absence of structural information at the time and in the hope of quickly and efficiently improving the potency of several Nek7 fragments simultaneously to generate novel, alternative starting points for further drug discovery.

With this in mind the Nek7 fragments were reacted with a diverse array of α-diazo amides and dirhodium catalysts, of which, four crude product mixtures gave rise to bioactivity in the form of increased Nek7 inhibition. This activity was followed in a second reaction array, hoping for a further enrichment of activity, by using analogous components to those which gave inhibition in round one. In the second reaction array, 16 crude product mixtures gave rise to Nek7 inhibition at a similar or higher level when compared to round one. Control experiments in both rounds indicated the bioactivity is only observed when all three components (fragment, α-diazo amide and catalyst, usually in CH_2Cl_2) are combined. The bioactive product(s) of the most active three reactions were investigated, yet their identification was unsuccessful. Scale-up of these reactions showed that no reaction had occurred, returning only the α-diazo amide. Following the identification of active reaction mixtures in round 1, it would have been useful to add further validation steps. For instance it would have been useful to scale-up the reactions at this stage and attempt to isolate bioactive material. Furthermore, performing NMR analysis at this stage would have led to the conclusion that no detectable reaction had occurred after round 1.

Activity-directed synthesis has been successful for the identification of high nanomolar active small molecules for the androgen receptor[99,100] and p53/hDM2 protein-protein interaction.[128] In both of these cases, the chemistry was tuned, through judicious choice of components, towards success. The fragment known or theorised to inhibit the target protein was the α-diazo component which was reacted with an array of diverse reactants. The

approach in this work was the reverse – the fragment known to target Nek7 was reacted with an array of α-diazo amides. It is probable then, based on the results observed upon scale-up, that activity-directed synthesis was unsuccessful in this case due to the unproductive nature of the reactions themselves. Of course it is possible that any productive reactions simply formed inactive products or extremely active products in very small quantities, however the latter is unlikely. Nevertheless validation of bioactive product mixtures in this case was key. Although only scaling-up after 3 rounds of ADS was successful for AR inhibitor discovery, this was not successful for Nek7 and bioactive product mixtures from round 1 should have been validated by scale-up and characterisation. ADS is a challenging approach but could be adapted to identify and purify intermolecular products prior to biological testing, instead of testing product mixtures, to improve the chances of activity-directed fragment elaboration being successful in the future.

The lack of success with ADS for discovery of Nek7 inhibitors, along with the recently solved Nek7-Ligand crystal structure, led us to turn our attention to a more conventional ligand optimisation approach which will be discussed in the following chapter.

Chapter 3

Towards the Development of a Suitable Chemical Probe against Nek7

The structure-activity relationship of the pyrazolyl-dihydroisoquinolinone scaffold was developed. To this end, based on structural information, analogues with varying groups at the 3,5-positions of the pyrazole ring and 3,4-dihydroisoquinolinone positions were synthesised and evaluated, the results of which will form the basis of this Chapter. It was envisaged that the synthesised analogues would elucidate productive binding interactions, serving to optimise potency for Nek7.

3.1   The Pyrazolyl Dihydroisoquinolinone Scaffold

Prior to commencement of the project, the screening of approximately 2500 fragments against Nek7 led to the identification of eleven inhibitors (1.3.2).[97] Activity determination confirmed ten of these hits, which were then triaged further based on their ligand efficiency, scope for analogue synthesis and selectivity for Nek7 over the related Nek2 and Plk1 kinases. Intensive SAR exploration of **3-1** led to the discovery of several, relatively unselective, low micromolar inhibitors of Nek7, the most potent of which was **3-3** (Fig. 3-1). Therefore **3-3** was chosen for further exploration in this work, the results of which will form the basis of this Chapter.
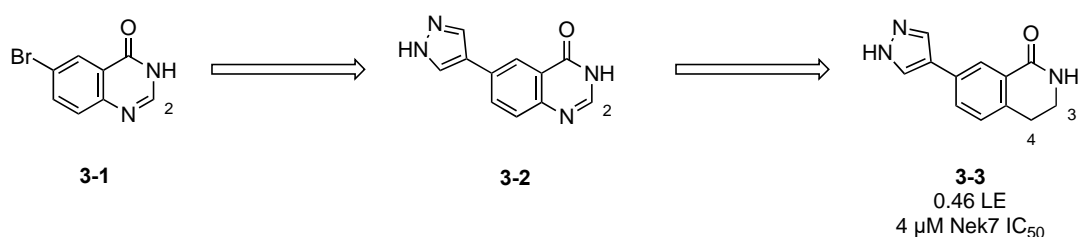
Figure 3-1. SAR exploration of **3-1** which led to **3-3**, the starting point for further exploration in this work. Ligand efficiency (LE) calculated by equation (see abbreviations).

3.1.1 Rationale for the Design of Analogues

The rationale for the design of analogues was based on the crystal structure of **3-3** in complex with Nek7 (Fig. 3-2) which had been previously solved to

2.8 Å as a homotetramer. As the electron density for the ligand was best resolved in chain B, only the structure of **3-3** bound to chain B was considered further. The electron density was ambiguous for which orientation the ligand bound at the hinge of Nek7. However, previous SAR exploration (Chapter 1) led us to hypothesise that the pyrazole was responsible for binding at the hinge of Nek7. The crystal structure with the ligand modelled in this way revealed two hydrogen bonds, one from the pyrazole N–H to the backbone carbonyl of Glu112 and one from Ala114 backbone N–H to the pyrazole acceptor nitrogen atom.

The structure of **3-3** in complex with Nek7 led us to hypothesise that the 3- and 5-positions of the pyrazole ring would be productive vectors for SAR exploration (Fig. 3-2c). Adding substituents in these positions would enable growth of the molecule along the hinge region either towards solvent or the hydrophobic pocket near the gatekeeper residue (Leu 111). With the hinge-binding motif contributing the majority of the binding affinity of a fully elaborated kinase inhibitor,[95] it was envisaged that making additional interactions in the extended hinge region or hydrophobic pocket would boost affinity. Analogues for synthesis were designed in two ways: (i) addition of hydrogen bond donor groups in the 3-pyrazole position to satisfy the donor-acceptor-donor hinge binding motif and (ii) computational docking of a library generated from commercially available pyrazoles.

It was also envisaged that the 3,4-positions of the dihydroisoquinolinone scaffold would be productive vectors for SAR exploration. Adding diverse substituents in these positions would enable growth of the molecule further into the ATP-binding site, towards the αC-helix between the P-loop and DLG motifs which create a suitable pocket for binding (Fig. 3-2d). In addition, the 3,4-dihydroisoquinolinone positions are yet to be explored, offering novel vectors for SAR investigation. Previous work which led to **3-3** performed limited SAR exploration on the related quinazolinone scaffold (**3-2**, Fig. 3-1) at the sp^2 hybridised 2-position with little success.[97] Methyl and ethyl substituents were tolerated at the quinazolinone 2-position however further increase in steric bulk led to a sharp decrease in activity. The sp^3 hybridised dihydroisoquinolinone 3,4-positions offer distinct vectors for growth, which could potentially allow greater substituent tolerance, to that of the

quinazolinone scaffold, which only offers vectors for growth in the plane of the ring.
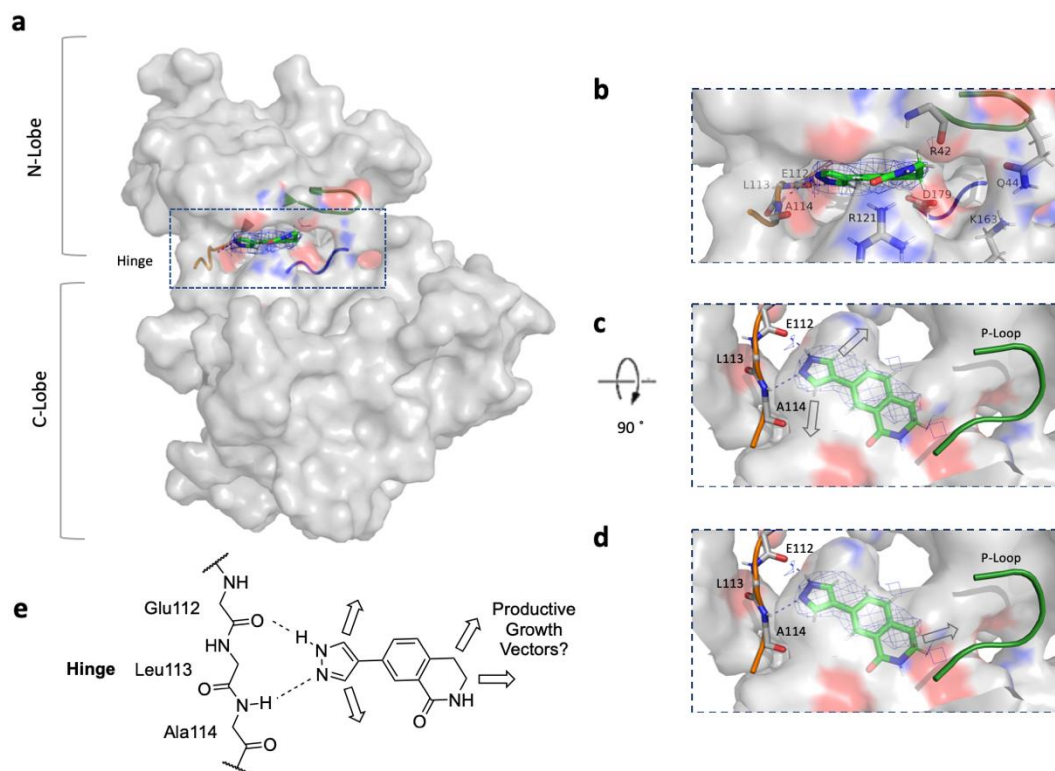
Figure 3-2. Crystal structure of 3-3 in complex with wt Nek7 represented as surface, grey, with labelled residues in the ATP-binding site coloured by element (C, grey; N, blue and O, red).

The hinge, P-loop and DLG are shown as cartoon, coloured orange, green and blue, respectively. The ligand is represented as sticks coloured by element (C, green; N, blue and O, red) with the electron density map (2mFo-DFc) shown as blue wiremesh contoured at 1.0 σ. (a) Structure of Nek7 chain B. The dashed box indicates the region magnified in (b) highlighting the binding pose of 3-3 and the pocket aimed to grow into (green spherical mesh), with potential residues to target for interaction shown as sticks. The binding pose in (b) is rotated by its *y*-axis 45° in (c) and by its *x*-axis 90° in (d) illustrating the size of the pocket surrounding the dihydroisoquinolinone 3,4-position and the vector for growth (arrow). (e) Schematic representation of the binding pose of 3-3 and our hypothesis for SAR exploration. Hinge side chains are excluded for clarity.

3.2 Structure-Activity Relationship Exploration of the Pyrazole Ring

3.2.1 3,5-Pyrazolyl Analogue Design

To satisfy the donor-acceptor-donor hinge binding motif and potentially make an additional interaction in the extended hinge region of Nek7, such as with Ala114, the 3,5-pyrazoles below were designed (Fig. 3-3a, **3-4**–**3-12**). Methyl analogues were also designed as methylation of the pyrazole ring of **3-2** was shown previously to give a small boost in affinity.[129]
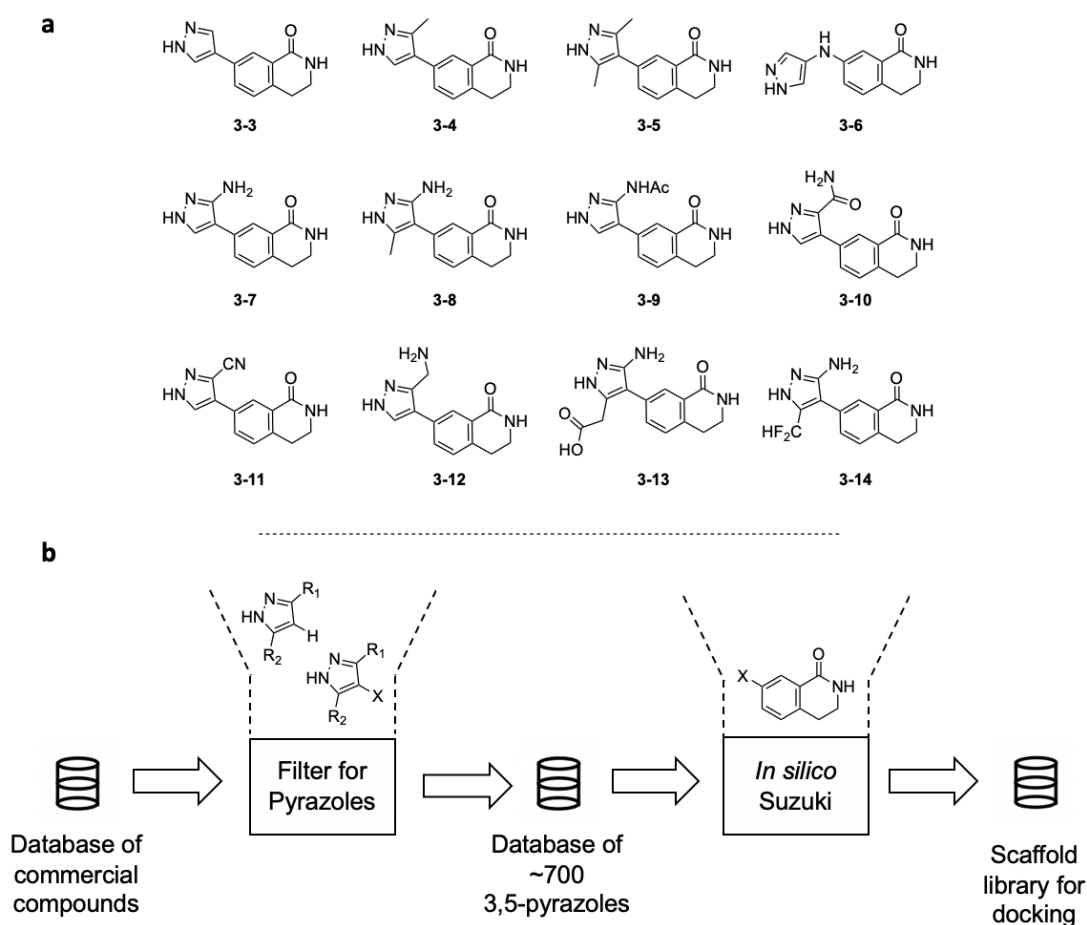
Figure 3-3. 3,5-Pyrazole library for synthesis. Designed by (a) rationale of the hinge binding motif and (b) workflow for the enumeration of a ~1200 compound library following LigPrep (Maestro) for docking (Glide).

To complement this approach, Knime was also used to generate a pyrazole library for docking (Fig. 3-3b). A database of commercially available compounds were filtered for 3,5-substituted pyrazoles followed by an *in silico* Suzuki coupling to install the dihydroisoquinolinone core and give the

corresponding library for docking into the Nek7 crystal structure using Maestro (Schrodinger Suite). In a pragmatic approach, the structures of ten compounds with the top docking scores were inspected. It was clear that hydrophobic groups, especially fluorination, were preferred computationally as many 3,5-disubstiued amino-fluoromethyl pyrazoles appeared (Appendix B.2). A few of these compounds were also chosen for synthesis (Fig. 3-3a, **3-13**–**3-14**). Fluorination can increase binding affinity[130] and as halogenation has been exploited to target the extended hinge region in other kinase inhibitors[131] and methylation was known to be useful,[129] we thought it was a logical approach to synthesise a fluorinated analogue.

It was envisaged that Suzuki coupling would be the most obvious and efficient way to synthesise analogues of **3-3** for testing against Nek7. The Suzuki cross coupling reaction is a powerful approach for forming carbon-carbon bonds and has become one of the most common reactions in the medicinal chemists toolbox.[132,133] A general mechanism[134] of the process is highlighted below (Scheme 3-1).
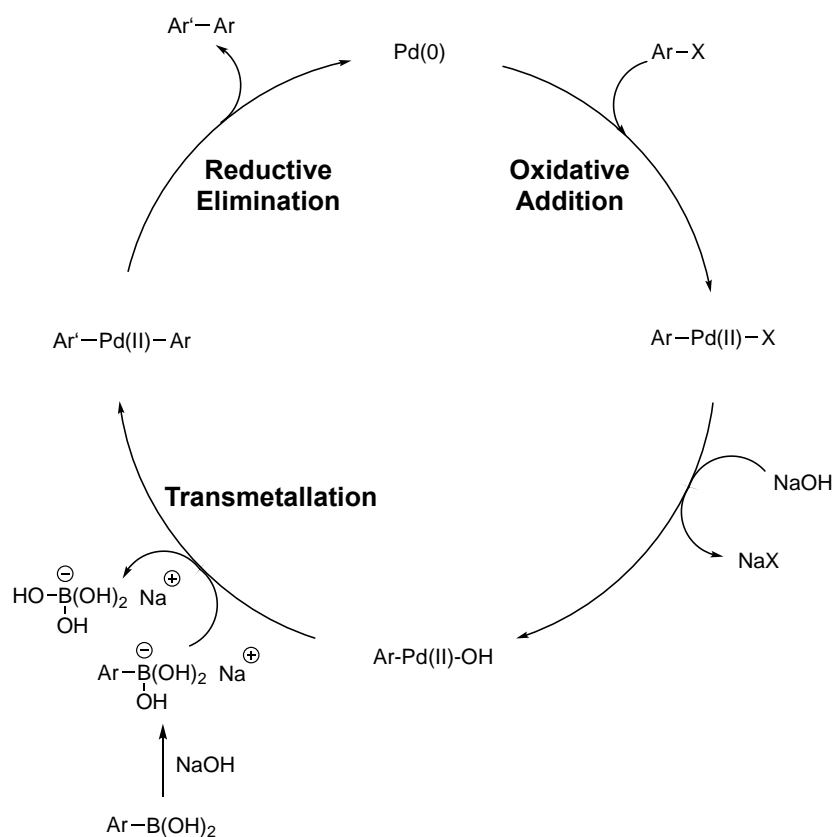
Scheme 3-1. General Mechanism for the Suzuki–Miyaura Cross Coupling.

3.2.2 Synthesis of Pyrazolyl Halides for Suzuki Coupling

Before the designed library of 3,5-pyrazoles could be synthesised, the corresponding pyrazole halides for use in the Suzuki coupling also required synthesis. As 3,5-substituted pyrazoles were more commercially available as halides, bromo-dihydroisoquinolinone **3-15** was converted to the boronate ester **3-16** *via* Miyaura borylation in moderate yield. The Suzuki coupling of **3-16** was then tested with unprotected or ethoxyethyl protected pyrazolyl halides. This reaction was unsuccessful using the unprotected pyrazole but gave the desired product **3-17** in 90% yield with the protected pyrazole.
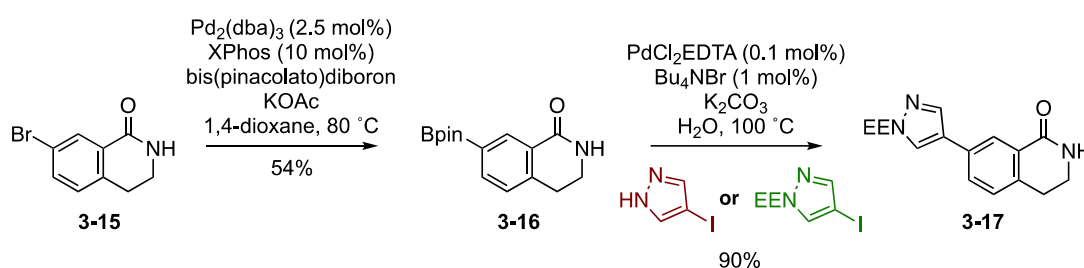
Scheme 3-2. Synthesis of **3-17** in order to determine the suitability of pyrazole protection for Suzuki coupling. The reaction was successful only with a protected pyrazole.

The small library of purchased 3,5-substituted pyrazole halides was then reacted with ethyl vinyl ether under acidic conditions to afford the ethoxyethyl protected pyrazoles in yields of 37% to quantitative (Scheme 3-3). The yield of the reaction was decreased with disubstituted pyrazoles containing an electron-withdrawing group (**3-22**).The ethoxyethyl protecting group was chosen because it is relatively easy to install and remove, is stable under the conditions of the Suzuki coupling and is used to protect a pyrazole prior to Suzuki coupling in the literature.[135] These reactions were rapid with unsubstituted or methylated pyrazoles however were sluggish when electron-withdrawing groups were installed on the pyrazole ring, resulting in the need for higher reaction temperatures. The regioselectivity observed is as shown (Scheme 3-3) however we were aware this group would be removed in the final compound. The nitrile of ethoxyethyl protected **3-20** was hydrolysed to the corresponding amide, **3-23**, using hydrogen peroxide in 87% yield.
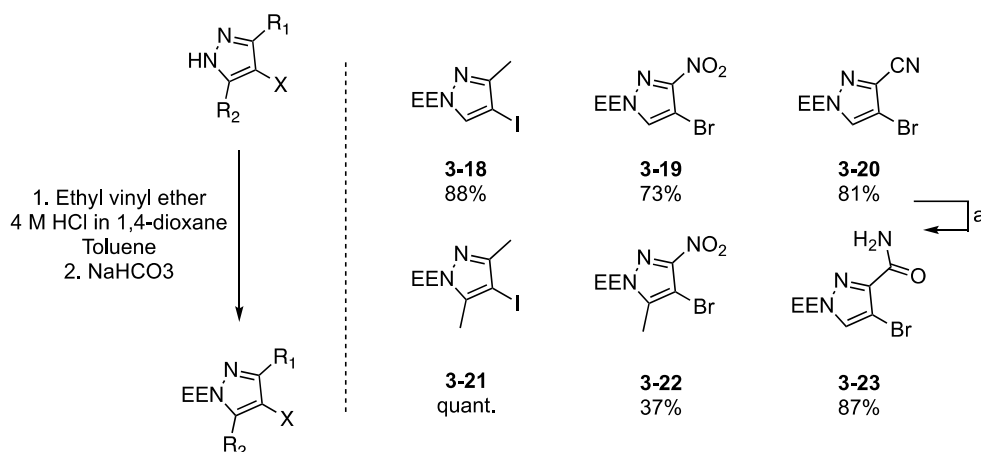
Scheme 3-3. Protection of the small library of commercially available 3,5-substituted pyrazole halides with ethyl vinyl ether. (a) K_2CO_3, H_2O_2 (30% aq.), DMSO. Regioselectivity observed is as shown.

For the synthesis of **3-13**–**3-14**, the corresponding pyrazole heterocycles for the Suzuki coupling required a more in-depth synthetic sequence. **3-26** was synthesised *via* Scheme 3-4 below. **3-24** was first brominated using NBS in THF followed by protection of the carboxylic acid as the ethyl ester using ethanol and sulfuric acid to give **3-25** in 32% yield over two steps. This was then fully protected by reaction with di-tert-butyl dicarbonate using triethylamine and catalytic DMAP to give **3-26**. In the absence of DMAP, a mixture of regioisomers which are singly protected on different positions of the ring is afforded.
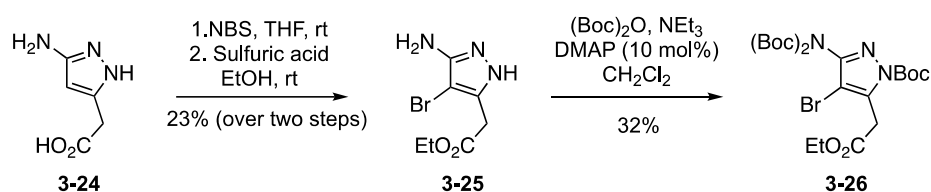
Scheme 3-4. Synthesis of **3-26** *via* bromination and Boc protection prior to Suzuki coupling.

The synthesis of fluorinated pyrazole halides is shown in Scheme 3-5. First, n-BuLi was cooled to -78 °C. Acetonitrile was added and stirred at -70 °C before reaction with difluoroethyl acetate at -45 °C. Following completion of the reaction, the intermediate was cyclised with hydrazine in ethanol to give the difluoroamino pyrazole. As above, **3-28** was then protected as the di-tert-butyl carbamate and the pyrazole ring was brominated using NBS to give **3-**

29 for coupling. Conversely to above, the 3-amino position in this case was only singly protected. Similarly, difluoroacetic anhydride was reacted with ethyl vinyl ether followed by cyclisation with hydrazine to give difluoromethyl pyrazole **3-31**, which was isolated by vacuum distillation. NBS was unsuccessful for the bromination of **3-31** in this case, however the use of bromine gave the desired product **3-32**. Nitration of the pyrazole ring using nitric and sulfuric acid followed by protection with ethyl vinyl ether as performed previously afforded **3-33**. Unfortunately, nitration and protection with ethyl vinyl ether was unsuccessful for the trifluoromethyl variant and therefore **3-34** was protected using di-tert-butyl dicarbonate to give the desired product for Suzuki coupling **3-35** in quantitative yield.
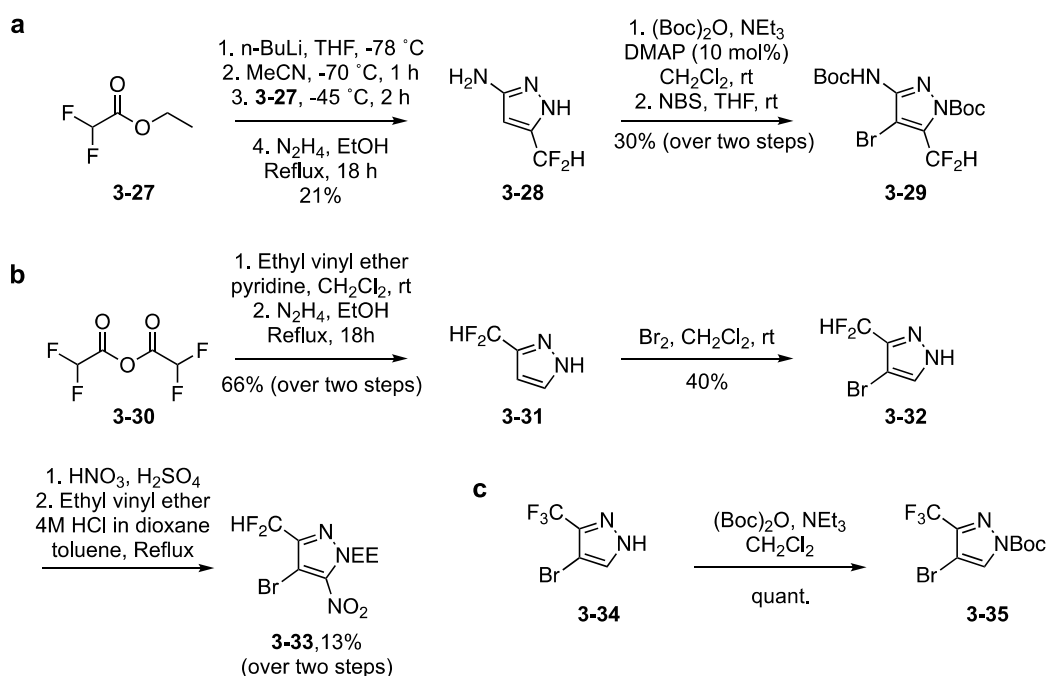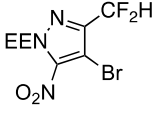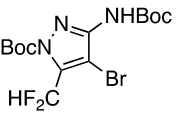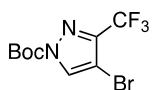
Scheme 3-5. Synthesis of fluorinated heterocycles prior to Suzuki coupling. (a) Synthesis of **3-29**, (b) synthesis of **3-33** and (c) synthesis of **3-35**.

3.2.3 Synthesis of 3,5-Pyrazolyl Analogues

With the protected pyrazole heterocycles in hand, a number of Suzuki coupling reactions were performed (Table 3-1) with the dihydroisoquinolinone core to synthesise the desired compounds for testing.

Table 3-1. Synthesis of 3,5-Pyazolyl Analogues

Entry	Starting Material	Method	No.	Product	Yield (%)
1		A,D	**3-4**		92
2		B,D	**3-5**		35
3		A,D	**3-10**		80
4		B,D	**3-11**		42
5		A,D	**3-13**		75
6		A	**3-36**		87
7		B	**3-7**		7[a]

Entry	Starting Material	Method	No.	Product	Yield (%)
8		A or B	-	-	-
9		A or B	-	-	-
10		A or C	-	-	-

(a) Pd$_2$(dba)$_3$ (5 mol%), PCy$_3$ (12 mol%), K$_3$PO$_4$, 1,4-dioxane–H$_2$O, 100 °C; (b) PdCl$_2$EDTA (0.1 mol%), K$_2$CO$_3$, H$_2$O, 100 °C; (c) Pd(dppf)Cl$_2$:CH$_2$Cl$_2$ (10 mol%), K$_3$PO$_4$, 1,4-dioxane–H$_2$O, 80 °C; (d) TFA, CH$_2$Cl$_2$. [a]Yield following hydrogenation (see Scheme 3-7).

Two Suzuki conditions were used for these couplings, either with a Pd$_2$(dba)$_3$ and PCy$_3$[136] or PdCl$_2$EDTA[135] as the precatalyst. The latter was chosen as the preferred catalyst initially due to its use in the synthesis of **3-17** (and **3-56**, 3.3.2) however the Pd$_2$(dba)$_3$ and PCy$_3$ system was generally higher yielding and more tolerable to various substitutions. For instance, the synthesis of **3-4** was unsuccessful with PdCl$_2$EDTA however was produced in a 92% yield (over two steps, following deprotection) when using Pd$_2$(dba)$_3$ and PCy$_3$. Indeed, this system was developed for coupling of electron deficient heterocycles.[136]

Unfortunately, any Suzuki coupling condition tried with a fluorinated pyrazole was unsuccessful. Specifically, both the nitro and boc-protected amino difluoromethyl pyrazoles (Entry 8 and 9) were unsuccessful under two different Suzuki conditions. With the synthesis of the trifluoromethyl pyrazole analogous to **3-33** unsuccessful even prior to Suzuki coupling, the simple 3-trifluoromethyl substituted pyrazole was attempted. Despite the 3-amino-5-fluoromethyl substituents being preferred computationally, it was envisaged that these analogues could be pursued further if the simple trifluoromethyl substituent was beneficial for activity. Unfortunately this was also unsuccessful as a coupling partner in the Suzuki reaction (Entry 10).

Therefore, the 3-trifluoromethyl pyrazole analogue **3-40** was synthesised by an alternative route (Scheme 3-6) and it was envisaged that other fluorinated analogues could be made in a similar fashion if **3-40** showed promising Nek7 inhibition. The synthetic sequence started from bromo-dihydroisoquinolinone **3-15** which was converted to **3-37** *via* Suzuki coupling with vinyl boronic anhydride. The corresponding alkene was then oxidised to aldehyde **3-38** using osmium tetroxide followed by reaction with nitromethane to give nitro-olefin **3-39**. Finally, trifluoroethyl amine was converted to the corresponding diazo prior to cycloadditon with **3-39** and oxidation with Ag$_2$O to give the desired trifluoromethyl pyrazole **3-40**. This reaction was quenched prior to consumption of the starting material by TLC which explains the low yield of 8% however enough material was produced for testing against Nek7.
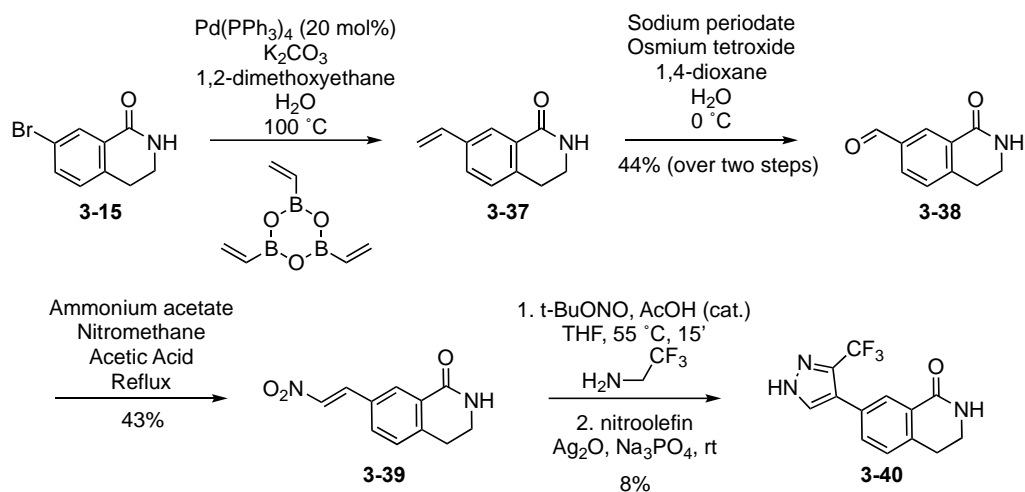
Scheme 3-6. Alternative syntheses to fluorinated pyrazolyl analogues.

The nitro and nitrile substituted pyrazoles were then reduced *via* hydrogenation using an atmosphere of hydrogen (balloon) and Pd/C to give the corresponding amines (**3-7–3-8** and **3-12**) followed by deprotection, if necessary. In the case of **3-8**, the slightly acidic nature of the hydrogenation was enough to deprotect the ethyoxyethyl group without the use of TFA. The 3-amino pyrazolyl analogue was also acetylated using acetic anhydride, giving **3-9**, to probe whether growth by acetylation at this position is possible for inhibitor design. Acetylation only at the 3-amino position was achieved by acetylating both positions with 2 equiv. of acetic anhydride followed by

selective de-acetylation of the pyrazole N-acetyl group using sodium hydrogen carbonate.
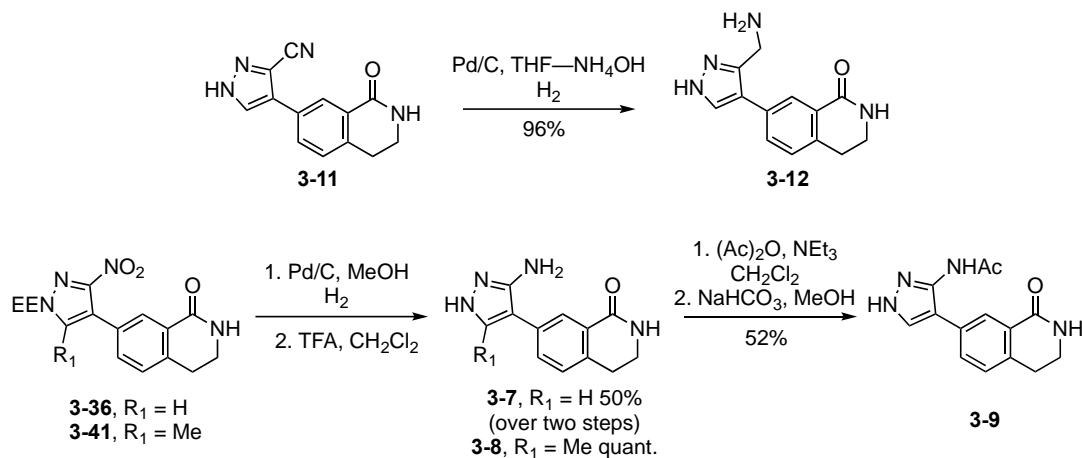
Scheme 3-7. Derivative syntheses of **3-12** and **3-7**–**3-8** leading to **3-9**.

Finally, **3-6** was synthesised *via* Buchwald-Hartwig amination of **3-15** with 4-aminopyrazole in 15% yield. The conditions used were the first attempted in an optimisation of the reaction which found *t*-butanol the preferred solvent.[137] However due to insolubility of the starting materials in *t*-butanol, and its melting point around room temperature, 1,4-dioxane and water were used as an alternative.
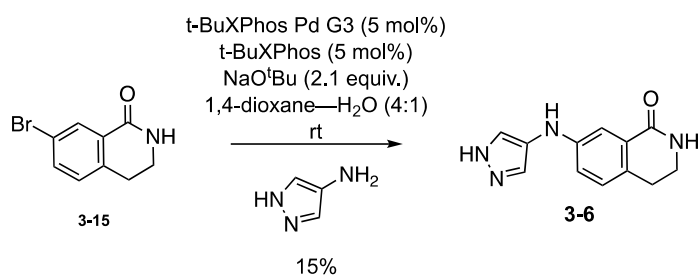
Scheme 3-8. Synthesis of **3-6** *via* Buchwald-Hartwig amination.

3.2.4 Biological Evaluation of 3,5-Pyrazolyl Analogues

With the 3,5-pyrazole analogues successfully synthesised, they were tested for inhibition of Nek7. As a positive control, and for informed comparison of inhibitory concentrations, **3-3** was synthesised *via* the Suzuki coupling shown in Scheme 3-9 below. **3-3** was tested for inhibition of Nek7 using the Caliper EZ Reader II mobility shift assay (see 2.2.2.2) in a 10-point, 3-fold serial dilution from 3 mM (Table 3-2, Entry 1).
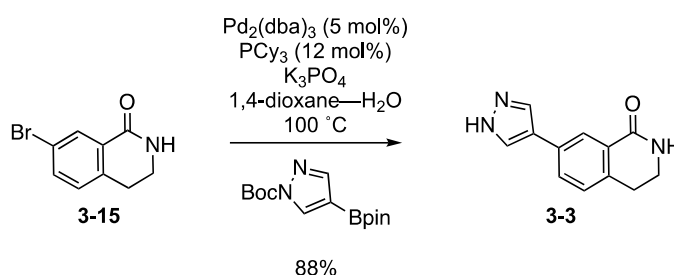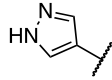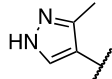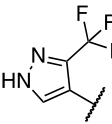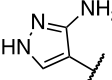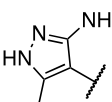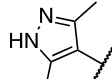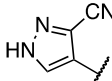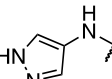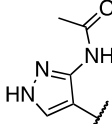
Scheme 3-9. Synthesis of **3-3** *via* Suzuki coupling for use as a positive control and comparison of IC_{50} values of derivatised compounds.
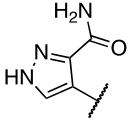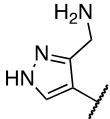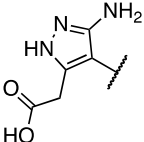
The testing of these analogues, along with the positive control, against Nek7 was outsourced to the International Centre for Kinase Profiling (MRC PPU, University of Dundee) which employ a radioactive filter binding assay using ^{33}P ATP.[138] The compounds were tested in a 10-point, 3-fold dose-response from a top concentration of 1 mM. The activity of Nek7 at each concentration was measured as the amount of radioactivity (counts) incorporated into the peptide substrate from transfer of the ^{33}P γ-phospate of ATP. This assay allows the determination of IC_{50} and the results are shown in Table 3-2.

The previously reported IC_{50} of **3-3** for Nek7 was 4 ± 2 μM.[97] Despite the small discrepancy, the value measured here using the Caliper and the value measured at the ICKP are in agreement with the previously reported value, as well as each other. The small increase in the IC_{50} values here was expected, as a higher Nek7 and therefore ATP concentration was used despite using the same Caliper mobility shift assay as the previously reported value. Furthermore, the ICKP operates an entirely different assay than the mobility shift assay and so a different value was expected. Nevertheless, the values obtained from the same assay *i.e.* ICKP or Caliper can be compared with one

another, allowing conclusions to be drawn about the effect of substitution at the 3,5-positions of the pyrazole ring.

Table 3-2. Biological Evaluation of 3,5-Pyrazolyl Analogues

Entry	No.	R_1	Nek IC$_{50}$ /μM		LE[a]
			ICKP	Caliper	
1	**3-3**		11 ± 6	25 ± 1[b]	0.40
2	**3-4**		14 ± 2	9 ± 1	0.42
3	**3-41**		>1000	-	-
4	**3-7**		40 ± 4	-	0.36
5	**3-8**		70 ± 9	-	0.32
6	**3-5**		144 ± 23	-	0.30
7	**3-11**		282 ± 24	-	0.29
8	**3-6**		>1000	-	-
9	**3-9**		>1000	-	-

Entry	No.	R$_1$	Nek IC$_{50}$ /μM		LE^a
			ICKP	Caliper	
10	**3-10**		>1000	-	-
11	**3-12**		>1000	-	-
12	**3-13**		>1000	-	-

n = 2 unless otherwise stated. ^{a}Ligand efficiency calculated from Caliper data where possible, using the ICKP data where Caliper data is not available. ^{b}n = 6.

Methylation at the 3-position of the pyrazole ring was well tolerated (Entry 2, ICKP), giving an IC$_{50}$ similar to that of the parent compound within error. This substitution also showed a slight improvement over the parent compound when validated in our mobility shift assay (Entry 2, Caliper). Surprisingly, trifluoromethylation at the pyrazole 3-position, despite being of a similar size to a methyl group, resulted in an inactive compound suggesting fluorination of the ring is unfavourable for binding (Entry 3). Unfortunately whilst the addition of a hydrogen bond donor in the 3-position of the pyrazole ring was tolerated (Entry 4), the potential to make an additional hydrogen bond to the hinge region did not provide the affinity boost hoped for. In light of the activities of **3-41** and **3-7** (Entries 3 and 4), it is unlikely that the combination of these substituents would be beneficial for activity as the computational model suggested. 3,5-disubstituted pyrazoles with small groups such as NH$_2$ or methyl were less well tolerated (Entries 5-6). Indeed, larger substituents, including di-substitution with larger groups, rendered the molecules inactive against Nek7 (Entries 7-12).

It was difficult to provide an explanation in the absence of structural information as to why any substitution larger than a methyl seems to have a detrimental effect on the activity of these compounds. It was postulated that

either a steric clash with the protein or the torsion angle between the two rings becoming too large resulted in potential disruption of hydrogen bonding interactions and loss of activity. In the case of the former, it may be beneficial to explore alternative hinge binding motifs which allow growth along the extended hinge towards solvent without disruption of any already present interactions.

3.3   Conclusions on the Structure-Activity Relationship of the Pyrazole Ring

In conclusion, a small library of pyrazoles with varying substituents at the 3,5-position were designed, synthesised and tested for inhibition of Nek7. Unfortunately, none of the compounds tested gave a 'jump' in activity compared to the parent compound which was unsubstituted in the 3,5-position. Methylation at the 3-position provided similar levels of inhibition as the parent compound within error with the radiolabelled assay (ICKP) and gave a slight improvement (almost 3-fold) in activity with the mobility shift assay. The addition of hydrogen bond donor groups at the 3-position did not provide an additional hydrogen bonding interaction with the extended hinge region of Nek7 as hypothesised as a boost in affinity was not observed. Indeed, this was actually detrimental to activity and these compounds were worse than the parent compound at inhibiting Nek7.

Much is known about the ATP-binding site of kinases and the most common hinge scaffolds, along with their hydrogen bonding patterns which allows rational design of kinase inhibitors.[87,94,95] 3-aminopyrazole is one of the most common hinge scaffolds and attempting to increase the number of hydrogen bonds between ligand and protein is a viable approach for affinity optimisation. However, there is no clear correlation between ligand affinity of approved kinase inhibitors and number of hinge hydrogen bonds. Indeed, most approved kinase inhibitors form only one hydrogen bond with the hinge. Therefore, the addition of hydrogen bond donor groups at the 3-position of the pyrazole ring clearly is not beneficial for binding in this case.

It seems addition of anything larger than a methyl group to the pyrazole ring is detrimental for activity. Therefore, a deeper optimisation of the hinge binding motif of these inhibitors is necessary to provide a more optimal vector to allow growth along the extended hinge region and into the hydrophobic pocket around the gatekeeper.

Clearly the use of structural information to guide design was not beneficial in this instance as the computational model was not predictive of binding affinity. Indeed, the computationally predicted affinities were compared to the

measured binding affinities which showed no correlation (R^2 0.02, see Appendix B.3). This could be explained by the fact that Nek7 was crystallised in an inactive conformation (αC-helix-out, Tyr-97-down and Lys63–Glu82 salt bridge and R-spine broken) yet is active in the biological assay and re-arrangement of the binding pocket occurs during activation. Work is currently underway to crystallise Nek7 in an active conformation with some of the compounds reported here however our attention was next turned to exploration of alternative vectors of the parent compound which are previously unexplored.

3.4 Structure-Activity Relationship Exploration of the Dihydroisoquinolinone Core

3.4.1 3,4-Dihydroisoquinolinone Analogue Design

With exploration around the hinge binding motif not as productive as hoped, it was envisaged that addition of substituents to the 3,4-position of the dihydroisoquinolinone core would provide the desired potency optimisation. These positions had been previously unexplored for SAR and it was hoped that growth out of the plane of the molecule would be beneficial. The crystal structure of **3-3** in complex with Nek7 gave residues which could be targeted for interaction however as the structure of the kinase was in an inactive conformation, re-organisation of the motifs important for kinase activity upon activation would likely cause a shift in the positioning of these residues. Furthermore as evidenced by the SAR exploration around the pyrazole ring above, the computational model was not predictive of real life binding. Therefore more generalised SAR approach was taken, incorporating diverse groups at the 3,4-position and groups which seemed to be beneficial were explored further.

Although palladium catalysis has proved to be an effective approach to the synthesis of a range of heterocycles, including isoquinolines and pyridines,[139] indoles,[140] azaindoles[141] and dihydroisoquinolinones,[142,143] the required halogenated substrate can be expensive or challenging to prepare.[144] An alternative to this is to use a nitrogen-containing directing group to enable C–H insertion followed by cyclisation to give the desired heterocycle. Rhodium(III) was found to be a competent catalyst for this transformation, enabling the synthesis of indoles,[145] pyrroles,[146] pyridones,[147] isoquinolines[148] and isoquinolinones[149] using a stoichiometric external oxidant. Glorius[150] and Fagnou[151] reported the use of a hydroxamate ether as a directing group and internal oxidant for C–H functionalisation and the synthesis of isoquinolinones, respectively. Cleavage of the N–O bond contained in the substrate circumvented the need for stoichiometric quantities of an external oxidant. The use of related pivaloyl-protected hydroxamates enabled the synthesis of dihydroisoquinolinones.[144,150] Their methods allow for improved yields, reactivity and selectivity, milder reaction conditions, an expanded reaction

scope and mono- over di-substituted products. Fagnou optimised the conditions further, reducing the catalyst loading and temperature of the reaction. This work has recently been expanded to allow regio- and diastereoselective syntheses of dihydroisoquinolinones.[152–155]
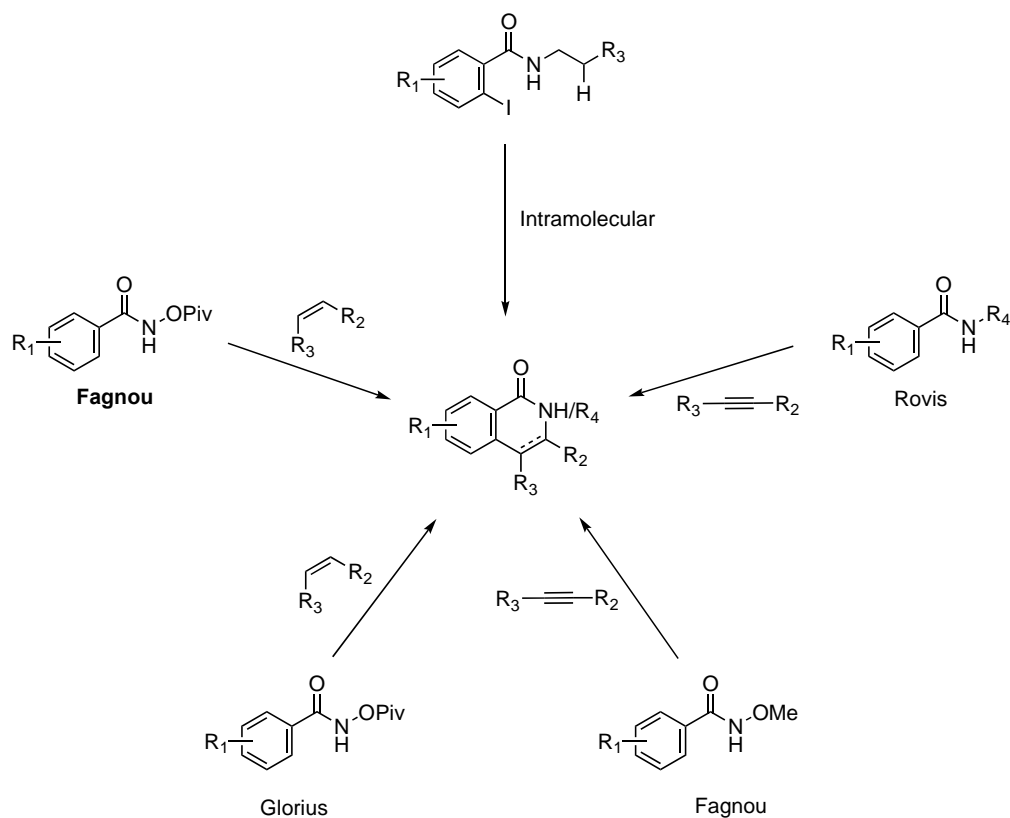
Figure 3-4. Overview of the transition metal-catalysed methods for synthesis of isoquinolinones.

Experimental investigations, corroborated by DFT calculations on surrogates **Ia** and CpRh(OAc)$_2$ for simplification, led Fagnou to propose the catalytic cycle[144] (Scheme 3-10). The calculated cycle starts from, assuming the calculations would be the same, RhCp*(OAc)$_2$, presumably formed from [Cp*RhCl$_2$]$_2$ and CsOAc, which coordinates to deprotonated **Ia** with loss of acetic acid. Calculations conducted with non-deprotonated **Ia** led to a higher energy pathway which was consequently ruled out.[144] C–H bond cleavage via a concerted metalation-deprotonation (CMD) affords intermediate **III**. Ligand (AcOH) dissociation and coordination of the alkene (acetylene was used in the calculations) gives intermediate **V**. Insertion of ethylene into the Rh–C bond gives the seven-membered rhodacycle **VI** which undergoes reductive elimination to afford the C–N bond formation and give intermediate **VII**. N–O

bond oxidative addition forms intermediate **VIII** which, finally, is protonated by acetic acid yielding the desired product **VIIIa** and regenerating the catalyst.
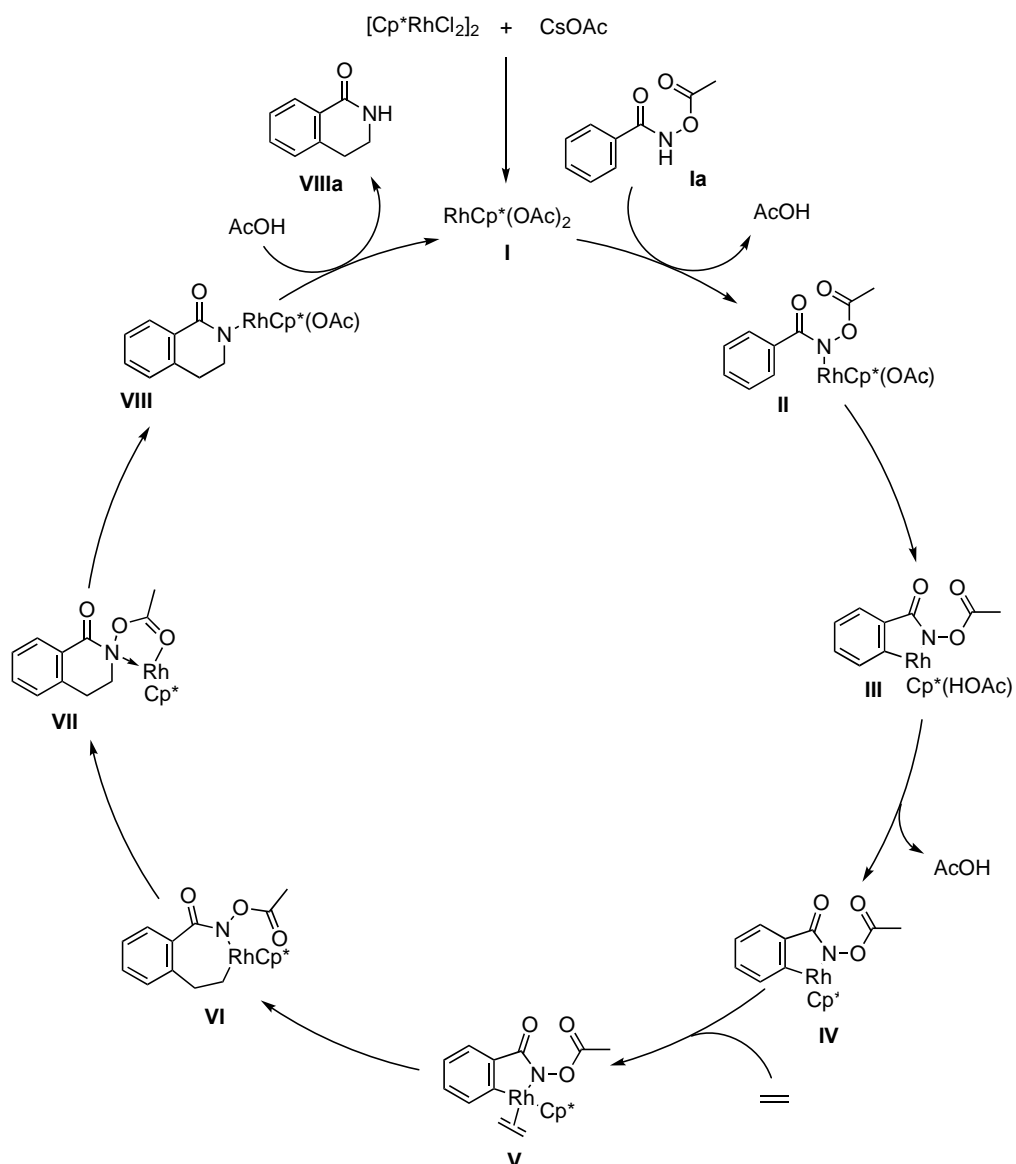
Scheme 3-10. Catalytic cycle for the synthesis of dihydroisoquinolinones using Rh(III) annulation chemistry, proposed by Fagnou.[144]

Due to its advantages over previous methods and success within a collaborator's group,[156] it was envisaged that 3,4-dihydroisoquinolinones could be synthesised from a common intermediate bearing a pivaloyl protected hydroxamate as the directed group as reported by Fagnou. This common intermediate could be cyclised with a variety of alkenes to enable efficient SAR exploration. Furthermore this method allows access to both the 3- and 4-substituted dihydroisoquinolinones simultaneously, an advantage for our purposes as it potentially provides information on not only which substituents are beneficial for activity but in which position. The next section describes the synthesis of the common intermediate which could be synthesised *via* an amide and Suzuki coupling with two possible orders of these synthetic steps.

3.4.2 Synthesis of the Pivaloyl-protected Hydroxamate

To enable the efficient and rapid synthesis of analogues for SAR exploration around the 3,4-position of the dihydroisoquinolinone core, the synthesis of a multi-gram quantity of **3-42** was required (Fig. 3-5a). It was envisaged that **3-42** could then be reacted with a variety of different alkenes to produce the desired analogues in a divergent manner. However the literature precedent for this reaction with the pyrazole substituent was lacking and the use of acidic, nitrogen-rich heterocycles in transition metal catalysed reactions can prove challenging.[157] An alternative, yet less efficient, method for SAR exploration is to synthesise a multi-gram quantity of **3-43** which is reacted with various alkenes, reactions in which the bromo-substituent is known to be tolerated.[158] This could then be followed by installation of the pyrazole by Suzuki coupling, in a more linear manner (divergence occurs earlier in the synthesis resulting in twice the number of synthetic steps).
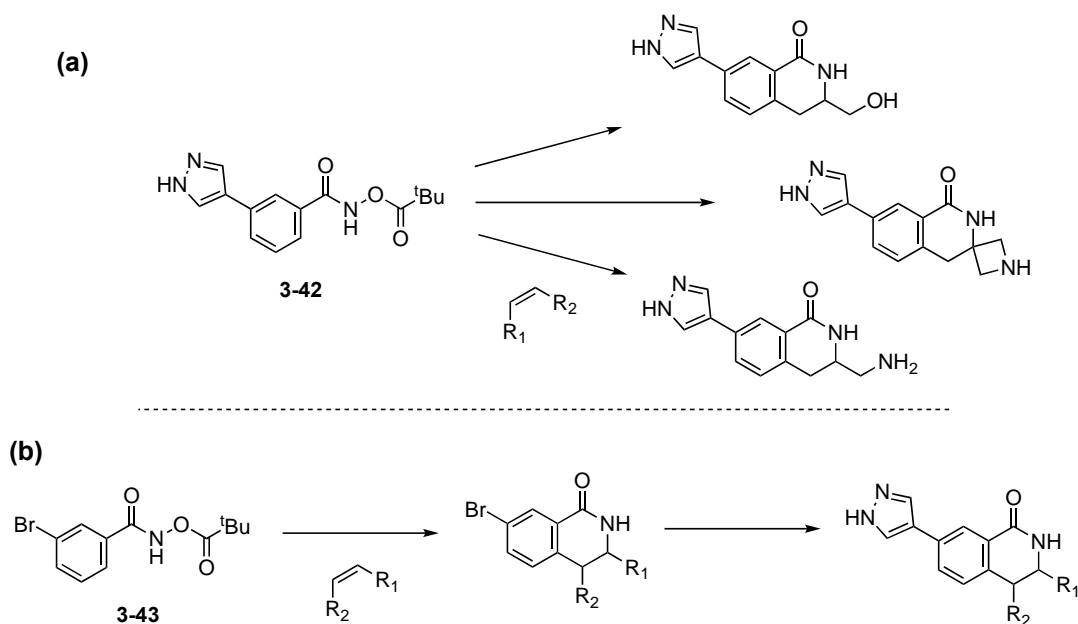
Figure 3-5. Two possible routes for SAR exploration of the dihydroisoquinolinone 3,4-position. (a) The most efficient method in which divergence occurs at a later synthetic step from a common intermediate or (b) a more linear (earlier divergence) route with good precedence for the bromo-substituent.

Initially, attempts to synthesise **3-42** began by reacting **3-44** with hydroxylamine hydrochloride followed by pivaloyl chloride to give the pivaloyl-protected hydroxamate in 58% yield. As expected with the hydroxamate functioning as a strong directing group,[144] installation of the pyrazole by Suzuki coupling as the final step failed even when using palladium pre-catalysts which allow efficient generation of the phosphine-ligated Pd(0) species.[159] The attempted conditions all returned starting materials, suggesting the palladium was sequestered by the directing group.

Therefore the synthesis of **3-42** was investigated by an initial Suzuki step, installing the directing group later. Attempts began with coupling of heteroaryl boronate ester **3-48** to **3-45** (bromobenzoic acid) or **3-46** (methyl bromobenzoate) with little success. Pleasingly, coupling of **3-48** with the ethyl ester **3-47** proceeded in 77% yield, with the protecting group removed from the pyrazole during the reaction conditions. Attempts to perform a direct hydroxyaminolysis on **3-49** in methanol simply resulted in the methyl ester (LC-MS). Exchanging the base to KOH and solvent to pyridine gave the desired hydroxamic acid. The methyl ester was more reactive under these conditions, being consumed in 6 hours versus 72 hours for the ethyl ester.

The hydroxamic acid was immediately reacted with pivaloyl chloride in a two-step manner to give **3-51**. An excess of pivaloyl chloride was used in an attempt to protect the pyrazole N–H prior to the cyclisation with Rh(III) and unexpectedly resulted in the formation of **3-52**. The low yielding (attributed to the formation of **3-52**) and sluggish (when using the ethyl ester) nature of this reaction prompted the identification of an optimised synthetic route, allowing for a multi-gram synthesis of **3-42** or **3-51**.
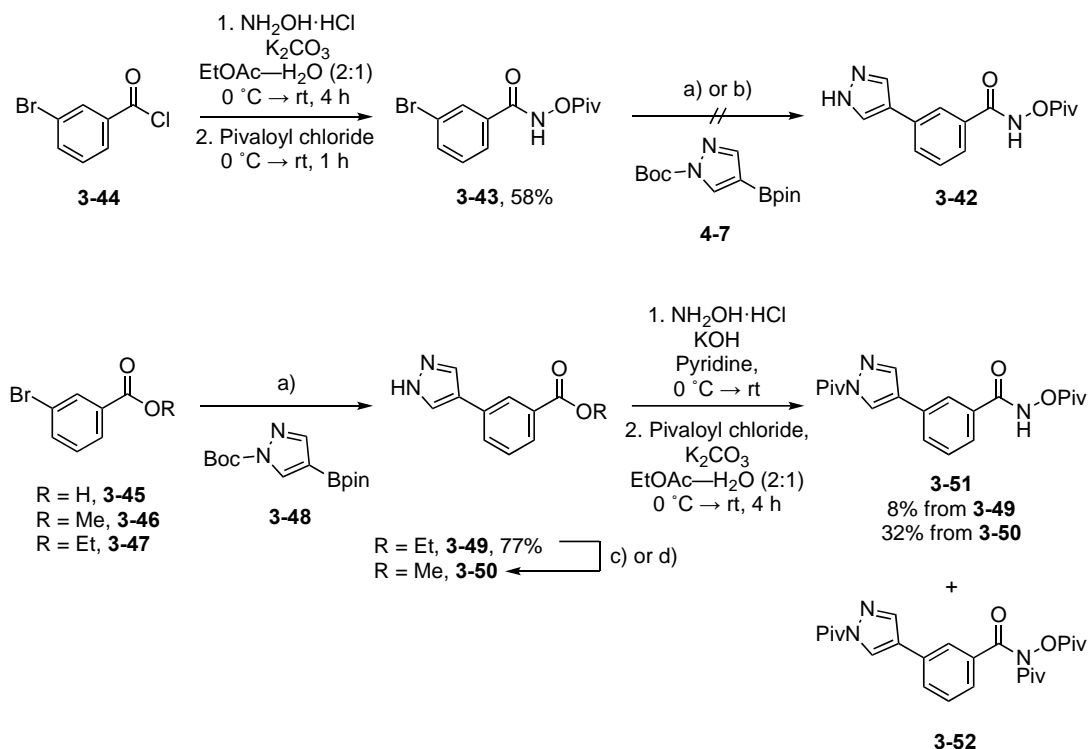
Scheme 3-11. Initial syntheses of **3-42** and **3-51**. Reagents and conditions: (a) Pd$_2$(dba)$_3$ (5 mol%), PCy$_3$ (12 mol%), K$_3$PO$_4$, H$_2$O/1,4-dioxane, 100 °C, 24 h, (b) XPhos Pd G4 (6 mol%), XPhos (6 mol%), K$_3$PO$_4$ H$_2$O/1,4-dioxane, (c) NH$_2$OH (50% aq. soln.), DBU, MeOH, 0 °C → rt, (d), hydroxylamine hydrochloride, KOH, MeOH, 0 °C → rt.

An optimised synthetic route was partly achieved by hydrolysing **3-49** to the corresponding carboxylic acid **3-53** followed by amide coupling with *O*-(pivaloyloxy)ammonium triflate and HATU to give **3-42** in an overall yield of 37%. It was later discovered that the pyrazole N–H could be selectively protected over the hydroxamate N–H by replacing the base with sodium hydrogen carbonate. Employment of this base with pivaloyl chloride following hydroxyaminolysis may have prevented the formation of **3-52**. Nevertheless, Suzuki conditions were found which enabled cross-coupling of **3-54** and **3-55**

to give the carboxylic acid **3-56** directly, circumventing the hydrolysis step to give the final optimised synthetic route, with an overall yield of 51% (from the Suzuki coupling), allowing for multi-gram quantities of **3-57** to be produced for SAR exploration.
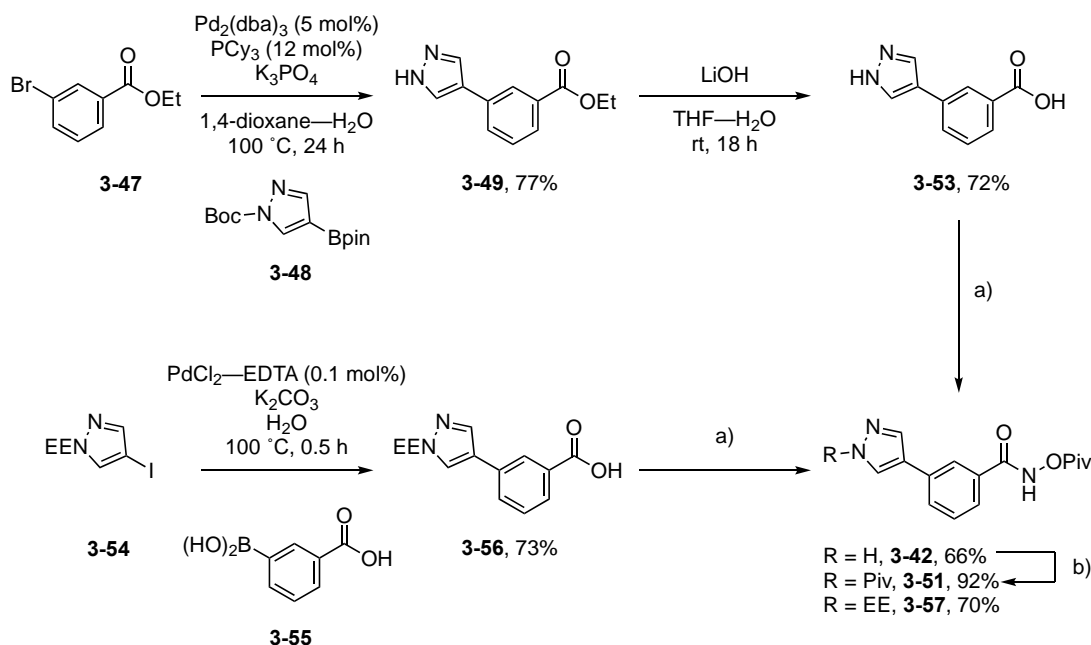
Scheme 3-12. Summary of practical syntheses of **3-42, 3-51** and **3-57**. Reagents and conditions: (a) HATU, DIPEA, DMF, 5 min then TfOH·NH$_2$OPiv, DIPEA, DMF, rt, 1 h, (b) Pivaloyl chloride, NaHCO$_3$, EtOAc–H$_2$O (2:1), 0 °C → rt, 1h.

3.4.3 Synthesis of 3,4-Dihydroisoquinolinone Analogues

There are a few reports of the Rh(III) methodology being applied to thiophenes and furans (and their benzo- derivatives), pyridines, indoles and quinolines[156,160] as well as thiazoles[158] however the scope of the methodology from a fragment perspective is limited[158] and, to the best of our knowledge, we were not aware of the method being applied to phenyl pyrazoles. To test whether the methodology tolerated a 3-pyrazolyl substituent, two reactions were performed (Scheme 3-13). 3-Bromo **3-43** and 3-pyrazolyl **3-51** were reacted with styrene using the most optimised conditions by Fagnou.[144] Unfortunately the reaction with **3-51** was unsuccessful, only returning deprotected starting material. Although the methodology has been applied to pyridines, it has been met with limited success due to the potential detrimental coordination of the Rh(III)[156] or the lower reactivity of these electron deficient systems which, in some cases, was overcome by the formation of a pyridine

N-oxide to increase reactivity.[158,161] It was also observed that the lower reactivity of these systems can be overcome to some extent by increasing the temperature and catalyst loading.[158] Therefore to overcome the electron deficient nature and lower reactivity potentially caused by the pyrazolyl substituent, the temperature and catalyst loading were increased (from room temperature to 65 °C and 1 mol% to 3.5 mol%, respectively). Pleasingly, this gave the dihydroisoquinolinone **3-60** in 40% yield.
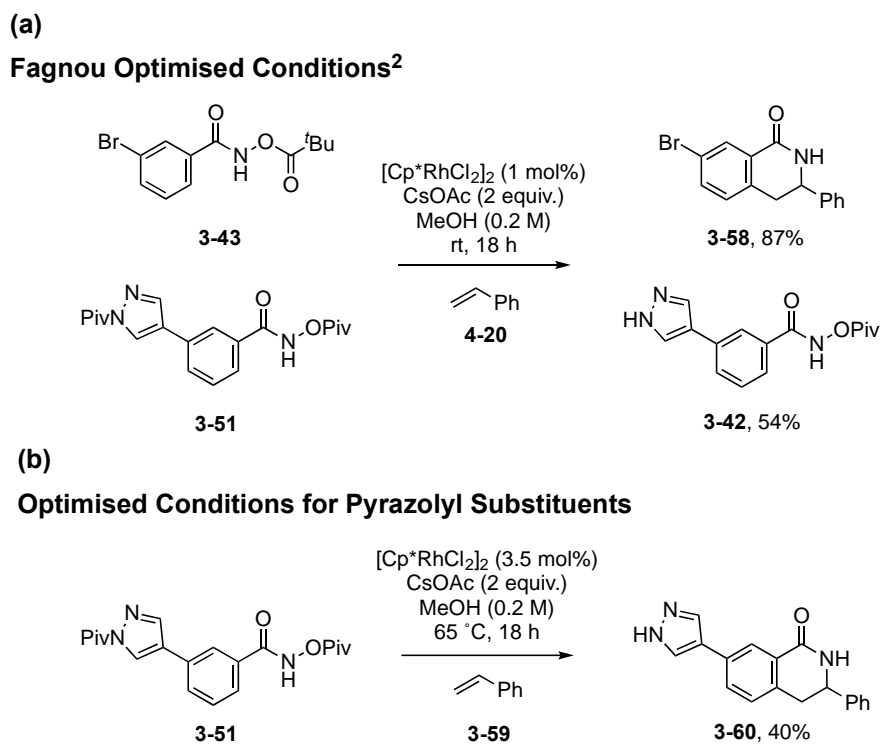
Scheme 3-13. Optimisation of the Rh(III) methodology for pyrazolyl substituents.

With a large enough quantity of material in hand for divergent analogue synthesis and optimised conditions for the Rh(III) cyclisation, we sought to establish the SAR around the previously unexplored 3,4-position of the dihydroisoquinolinone scaffold. Under the optimised conditions, **3-42, 3-51** and **3-57** were reacted with a broad range of alkenes, the results of which are summarised in Table 3-3, to probe the functional group tolerance around the 3,4-position and incorporate handles for subsequent transformations.

Generally, It is worthwhile noting that, the reaction proceeded whether the pyrazole N–H was unprotected (**3-42**), protected with a group which was labile during the reaction conditions (pivaloyl, **3-51**) or protected with a stable group

(ethoxyethyl, **3-57**). However the reaction seemed to proceed more cleanly and in higher yield (Entries 10a-10b and 11a-11b) when the pyrazole N–H was protected throughout the reaction. Typically, the unsuccessful or low yielding annulation reactions can be explained by return of starting material (i.e. no reaction) and/or the formation of two side-products (as evidenced by LCMS data): (1) loss of OPiv to give the corresponding benzamide **3-61** and (2) methyl carbamate **3-62** presumably formed *via* Lossen rearrangement[162,163] followed by trapping of the resultant isocyanate with methanol. Webb,[156] during the synthesis of isoquinolinones under very similar conditions as used here reported a carbamate side product resulting from a Lossen rearrangement which could explain the observation of **3-62** in this work. Interestingly, the Lossen rearrangement identified by Webb only occurred in the presence of [Cp*RhCl$_2$]$_2$ (and was substantially retarded at lower temperatures) whereas the classic Lossen rearrangement requires acylated hydroxamate derivatives, base and heat.[163,164]
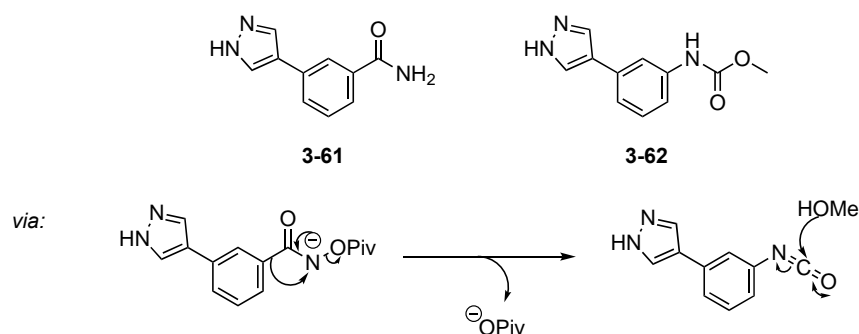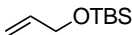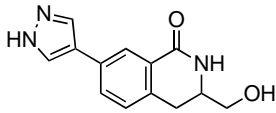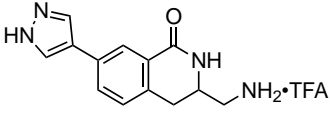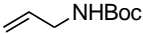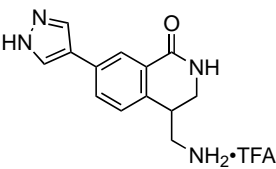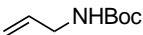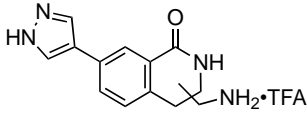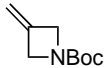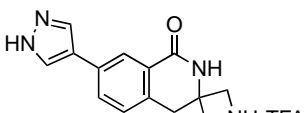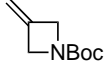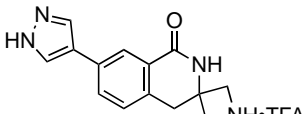
Scheme 3-14. Side products identified during the Rh(III) annulations. **3-62** is presumably formed *via* a Lossen-type rearrangement followed by trapping with methanol.

Under the optimised conditions pivaloyl protected hydroxamate **3-42** reacted with styrene to give the 3-substituted dihydroisoquinolinone **3-60** in 40% yield. The use of allylbenzene, which has a rotatable, sp^3, centre between the phenyl ring and alkene, gave **3-63** as a 35:65 mixture of regioisomers. Fagnou[144] identified a similar mixture of regioisomers when using allylbenzene, albeit with reversed selectivity. Pleasingly 4-vinylpyridine was tolerated, giving **3-64** in 13% yield however reaction with 1-vinylimidazole, consisting of a more basic heterocycle versus pyridine, was unsuccessful.

Table 3-3. Synthesis of 3,4-Dihydroisoquinolinone Analogues

[Cp*RhCl$_2$]$_2$ (3.5 mol%)
CsOAc (2 equiv.)
MeOH (0.2 M)
65 °C, 18 h

R$_1$ = H, **3-42**
R$_1$ = Piv, **3-51**
R$_1$ = ethoxyethyl, **3-57**

3-60—3-70

Entry	Pyrazole	Alkene	Product	Yield[a] (%)	Ratio[b] (R$_2$:R$_3$)
1	**3-42**	⟋Ph	**3-60**	40	
2	**3-42**	⟋⟍Ph	**3-63**	8[c]	35:65
3	**3-42**	(4-pyridyl vinyl)	**3-64**	13	
4	**3-42 or 3-51**	(1-vinylimidazole)	-	-	-
5	**3-42**	(methyl acrylate)	**3-65**	70	
6	**3-42**	(acrylamide)	-	-	-
7	**3-51**	(N-benzyl acrylamide)	**3-66**	55	

Entry	Pyrazole	Alkene	Product	Yield[a] (%)	Ratio[b] (R₂:R₃)
8	**3-42**	OH	-	-	-
9	**3-42**	OTBS	**3-67**	4[d]	
10a[e]	**3-57**	NHBoc	**3-68**	40[d]	
			3-69	51[d]	50:50
10b	**3-51**	NHBoc	**3-68 : 3-69 (50:50 rr)**	47[c,d]	50:50
11a[e]	**3-57**	NBoc	**3-70**	94[d]	
11b	**3-51**	NBoc	**3-70**	28[d]	

[a]Isolated yields are reported. [b]Ratio of isolated products estimated by yield (which is affected by purification and therefore does not reflect the true regioselectivity of the reaction. Unless otherwise stated, a single regioisomer (>95:<5) was isolated. [c]Isolated yield of both regioisomers. [d]Isolated yield after deprotection (over two steps). [e]Reaction performed with 3 mol% [Cp*RhCl₂]₂.

Reaction of **3-42** with methyl acrylate under our conditions of elevated temperature gave **3-65** as a single regioisomer in 70% yield. The formation of the 3-substituted product is in contrast with Fagnou's report for a 4-position preference (1:4.5 mixture, R_2:R_3), although the starting benzamide is unsubstituted and the reaction is run at room temperature in the latter case.[144] Whilst reaction with acrylamide (Entry 6) did not proceed to the expected product, the use of benzyl-protected acrylamide gave **3-66** in 55% yield. It was envisaged that **3-66** could be deprotected to give the desired acrylamide however this was met with little success. The use of Pd(OH)$_2$/C or PtO$_2$[165] under hydrogen atmosphere (balloon, rt) returned only starting material. The same result was also obtained when using *p*-TsOH in toluene under reflux, despite reports of these conditions being successful when catalytic hydrogenation was unsuccessful.[166] To overcome this, the methyl acrylamide, analogous to the methyl acrylate, was synthesised from **3-65** and methylamine.
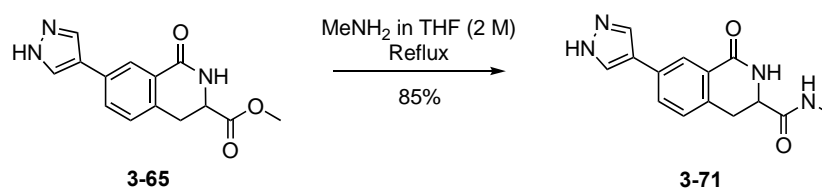
Scheme 3-15. Synthesis of the amide analogue of **3-65**.

As with acrylamide (Entry 6), the reaction of **3-42** with allyl alcohol (Entry 8) was also unsuccessful, thought to be due to the relatively low boiling point of the alkene. To overcome this, the alcohol was TBS-protected and gave **3-67,** after deprotection with HF•Pyridine complex, as a single regioisomer in 4% yield. We opted to use HF•Pyridine for deprotection of the silyl-protected alcohol to avoid the formation of the *tetra*-butyl ammonium methanolate which persisted even after column chromatography. Rees[158] reported mixtures of regioisomers when using TBS protected allyl alcohol although, again, the reactions proceeded at ambient temperature with different (hetero)aromatic starting pivolates than used here. Boc-protected allyl amine gave the corresponding cyclic products after deprotection in good yields and as an equal mixture of regioisomers (Entry 10). Despite the Boc-group having the

potential ability to coordinate to Rh(III) as proposed by Webb,[156] sterics may balance electronics in this case, resulting in an equal mixture. Exocyclic boc-protected methylene azetidine was well tolerated giving **3-70** as the single product after deprotection in excellent yield.

3.4.3.1   Regiochemical Considerations

The C–H activation always occurred at the less hindered position *para*- to the phenyl substituent, with none of the *ortho*- insertion product identified. The regioselectivity around the 3,4-dihydroisoquinolinone position is influenced by the alkene reactant. Steric and electronic effects control insertion, with larger groups preferring the 4-position (steric effects) and electron donating groups, able to coordinate to Rh(III), favouring the 3-position.[167] However, alkenyl C–H insertion gives products with lower regioselectivies compared to alkynes, presumably due to smaller steric interactions.[167] Following the trend identified by Fagnou,[144] conjugated terminal alkenes gave 3,4-dihydroisoquinolinones with that substituent generally in the 3-position (Table 3-1, Entries 1, 3, 5 and 7). With alkyl-substituted terminal alkenes, sterics effects resulted in a mixture of regioisomers (Entries 2 and 10-11) unless the alkene bared an allylic electron donating group in which case, the 3-substituted dihydroisoquinolinone was produced (Entry 9). The inherent selectivity of the reaction broadly reflected the ratio of the isolated products obtained (illustrated by comparison of entries 10a and 10b), with any discrepancies being due to loss of material during purification.

The regiochemical outcome of the reaction was determined by NMR analysis with **3-68** and **3-69** used as exemplar cases for illustration (Fig. 3-6). In all cases, ^{1}H and ^{13}C HMBC and ^{1}H NOESY NMR spectra revealed two key interactions: (1) through-bond correlation between the isoquinolinyl 3–H and the amide carbon atom and (2) through-space correlation between the isoquinolinyl 4–H and an aromatic proton (isoquinolinyl 5–H). Specifically, for the case of **3-68**, a CH, appearing as a triplet of triplets (δ 4.01 ppm), correlated through-bond with the amide carbon atom whilst two CH$_2$ protons (δ 3.26 and 2.97 ppm), both appearing as doublet of doublets, correlated through-space with an aromatic proton, appearing as a large doublet. With **3-69**, the CH proton appeared upfield (δ 3.29 ppm), relative to that in **3-68**, and

overlapped with a CH_2 proton of the methylamine substituent. Both the CH (δ 3.29 ppm) and CH_2 protons of the methylamine substituent correlated through-space with an aromatic proton, appearing as a large doublet. One proton of the isoquinolinyl CH_2 in this case (δ 3.77 and 3.57 ppm) correlated through-bond with the amide carbon atom. The diagnostic couplings presented here, and the relative shifts of the isoquinolinyl CH and CH_2 protons (a downfield shift indicating a deshielded position adjacent to an electronegative group such as the amide) suggests the structural assignments illustrated in Fig. 3-6.

NOESY and HMBC correlations
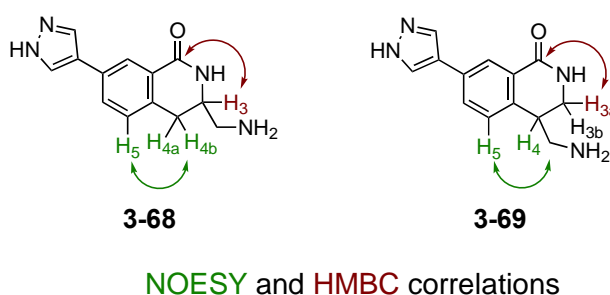
Figure 3-6. Determination of the regiochemical reaction outcome. The NOESY and HMBC correlations observed in **3-68** and **3-69** were used as illustration.
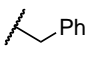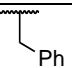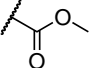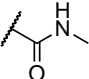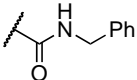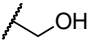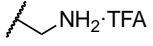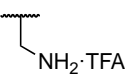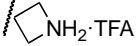
3.4.4 Biological Evaluation of 3,4-Dihydroisoquinolinone Analogues

With the small library of 3,4-substituted dihydroisoquinolinones in hand, their inhibition of Nek7 activity was determined using the Caliper EZ Reader II to probe the SAR around these positions (10-point, 3-fold dose-response from 3 mM, see Chapter 2 or 5 for details). The library was initially synthesised from a range of alkenes, chosen to allow introduction of functional groups into the scaffold which could be useful for subsequent transformations or binding interactions with the kinase. As the SAR of the 3,4-positions of the scaffold had previously been unexplored, it was unknown which groups in this position would make beneficial interactions with and increase the affinity for Nek7. Therefore, the alkenes used in the synthesis had a diverse range of functional groups: hydrogen bond donor/acceptor, hydrophobic or aromatic groups to probe the functional group tolerance around the 3,4-position. The activities of this initial diverse set of 3,4-dihydroisoquinolinones against Nek7 are shown in Table 3-4 (Caliper).

Table 3-4. Biochemical Structure-Activity Relationship for 3,4-Dihydroisoquinolinone Analogues

| Entry | No. | R_1 | R_2 | Nek7 IC$_{50}$/μM $(n)^a$ | | Ligand Efficiency^b |
				ICKP	Caliper	
1	**3-3**	H	H	12 ± 4	25 ± 1 (6)	0.40
2	**3-60**	Ph	H	246 ± 39	377 ± 25	0.22
3	**3-64**	(pyridin-4-yl)	H	-	>1000	<0.19

Entry	No.	R$_1$	R$_2$	Nek7 IC$_{50}$/μM (n)^a		Ligand Efficiency^b
				ICKP	Caliper	
4	**3-63^c**	Ph	Ph	116 ± 21	76 ± 3	0.25
5	**3-65**	O-O	H	54 ± 10	98 ± 6	0.28
6	**3-71**	H N-O	H	>1000	125 ± 7	0.28
7	**3-66**	H N Ph O	H	-	774 ± 49	0.17
8	**3-67**	OH	H	76 ± 13	53 ± 5	0.33
9	**3-68**	NH$_2$·TFA	H	5 ± 0.8	9 ± 0.5 (6)	0.39
10	**3-69**	H	NH$_2$·TFA	25 ± 5	41 ± 0.2 (4)	0.34
11	**3-70**	NH$_2$·TFA	H	3 ± 0.6	12 ± 0.6 (6)	0.36

^{a}Unless otherwise stated, n = 2. Error is shown as SEM. ^{b}Calculated from Caliper measured data. ^{c}Screened as a 35:65 mixture (R$_2$:R$_3$) of regioisomers.

Our starting point for optimisation, **3-3**, was determined to have an IC$_{50}$ for Nek7 of 25 μM. Substitution of the R$_2$ position with phenyl (Entry 2) was not tolerated, reducing the affinity for Nek7 by 15-fold whilst 4-pyridyl (Entry 3) resulted in inactivity at 1 mM. However, having a rotatable methylene linker between the dihydroisoquinolinone scaffold and phenyl group (Entry 4) resulted in the aromatic ring being tolerated and an IC$_{50}$ of 80 μM for Nek7. It is worthwhile noting that **3-63** was screened as a 35:65 mixture of regioisomers so the activity of the individual regioisomers requires further elucidation.

Generally, substitutions at the R_2 position such as methyl carboxylate (Entry 5), methyl amide (Entry 6) and alkyl alcohols (Entry 8) were tolerated. The range of groups tolerated at the R_2 position suggests a sizeable space in the Nek7 ATP-pocket around this position. However large, potentially rotationally restricted, substituents reduced the affinity for Nek7 by 30-fold (Entry 7). Spiro-fused azetidine (Entry 11) at R_2 seems to be somewhat productive, increasing the affinity for Nek7 by around 2-fold. Similarly an amino-group at the R_2 position (Entry 9) increased the affinity for Nek7 by almost 3-fold, more than 4-fold better than its R_3 counterpart (Entry 10), suggesting a hydrogen bond donor in this position may be important.

Compounds which showed inhibition of Nek7 were sent to the International Centre for Kinase Profiling (ICKP, University of Dundee) for validation (Table 3-4, ICKP). In general, except **3-71** which was inactive at 1 mM, the values determined by the ICKP and the ones measured here were in good agreement and even slightly more potent in the case of **3-70**. Whilst a few of the substituents cause a dramatic reduction in activity (Entries 2, 3 and 7), most of the substitutions have only a moderate affect with no larger increases in potency observed which would guide an obvious direction for further SAR. Nevertheless, the activity of **3-68** and **3-70** (Entries 9 and 11) prompted us to explore these functionalities further.

3.4.5 Synthesis of 3,4-Dihydroisoquinolinone Analogues: Second Generation Library

With **3-68** and **3-70** giving moderate increases in potency, they were chosen for further exploration in the hope of gaining additional increases in activity. The analogues designed in this case aimed to incorporate amino-groups into similar positions on the dihydroisoquinolinone scaffold in an attempt to optimise any productive affinity increases. To achieve this, **3-42**, **3-51** and **3-57** were reacted with a range of acyclic, cyclic and exocyclic allyl amines, the results of which are summarised in Table 3-5.
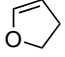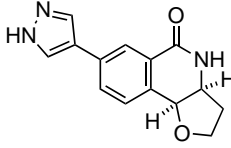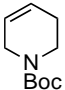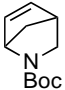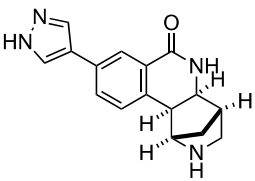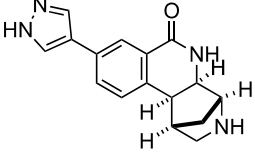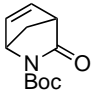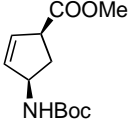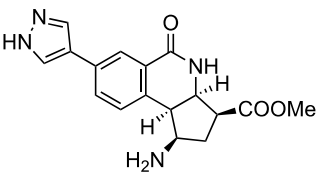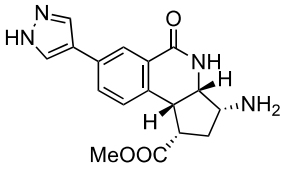
Similarly as with the synthesis of **3-68** and **3-69**, Boc-protected methyl allyl amine gave the corresponding products **3-72** and **3-73** after deprotection in good yields also as an equal mixture of regioisomers (Entry 1). Again, the sterically demanding Boc-group resulted in a mixture. Dimethyl allyl amine
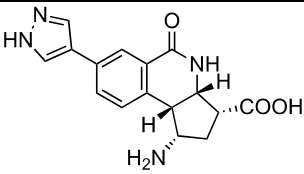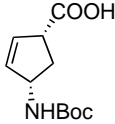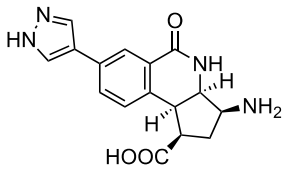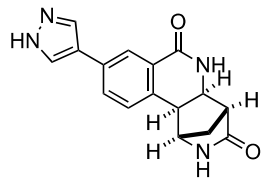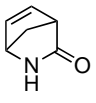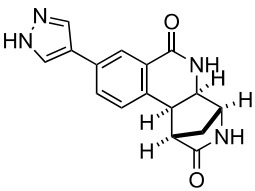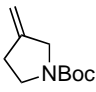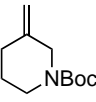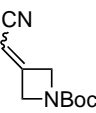
(Entry 2) gave a similarly good yield as the Boc-protected derivatives, although as a single regioisomer possibly due to the basic amine coordinating to Rh(III)[158] but without the Boc-group influencing sterics.
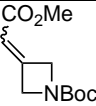
Table 3-5. Synthesis of Second Generation 3,4-Dihydroisoquinolinone Analogues

Entry	Pyrazole	Alkene	Product	Yield[a] (%)	Ratio[b] (R$_2$:R$_3$)
1	**3-57**		**3-72**	43	50:50
			3-73	52	
2[c]	**3-57**		**3-74**	71	
3	**3-51**		-	-	-
4	**3-42** or **3-51**		-	-	-
5	**3-57**		-	-	-

Entry	Pyrazole	Alkene	Product	Yield[a] (%)	Ratio[b] (R₂:R₃)
6[c,d]	**3-57**		**3-75**	61	
7	**3-57**		**-**	-	-
8	**3-57**		**3-76**	12	50:50
			3-77	16	
9	**3-57**		**-**	-	-
10	**3-57**		**3-78**	23	65:35
			3-79	12	

Entry	Pyrazole	Alkene	Product	Yield[a] (%)	Ratio[b] (R$_2$:R$_3$)
11	**3-57**		**3-80**	16	
			3-81	21	
12	**3-57**		**3-82**	54	75:25
			3-83	17	
13	**3-57**	**4-64**	-	-	-
14	**3-57**	**4-65**	-	-	-
15	**3-57**	**4-66**	-	-	-

Entry	Pyrazole	Alkene	Product	Yield[a] (%)	Ratio[b] (R_2:R_3)
16	**3-57**	CO$_2$Me NBoc **4-67**	-	-	-

[a]Isoated yields after deprotection with TFA (over two steps) are reported. [b]Ratio of isolated products estimated by yield (which is affected by purification and therefore does not reflect the true regioselectivity of the reaction. Unless otherwise stated, a single regio- or diastero-isomer (>95:<5) was isolated. [c]Reaction performed at 45 °C. [d]Reaction performed with 3.5 mol% [Cp*RhCl$_2$]$_2$.

In accordance with Fagnou,[144] unactivated cyclic alkenes, *N*-Boc pyrrole and derivatives therof, (Entries 3-5 and 7) were unsuccessful in our hands despite reports of such alkenes being used to give the hemiaminal product.[156,168] We therefore investigated the use of 2,3-dihydrofuran which gave **3-75** as the sole product in 61% yield. **3-75** was the opposite regioisomer identified with Fagnou's[144] use of 2,3-dihydrofurn but in accordance with Webb's,[156] whose product was confirmed by X-ray crystallography. Webb also found n-butyl and ethyl vinyl ethers gave the benzylic ether product preferentially over the aminoacetal, which eliminated thermally or under acidic (silica) conditions to give the corresponding isoquinolinone.[156,168] She therefore postulated that enol ethers favour the benzylic ether product, as seen in this work, by a mechanism in which Rh(III) migrates to the more electron-rich carbon atom, β to oxygen.[156,168] Webb also found *N*-Boc pyrrole to give solely the hemiaminal product, suggesting the regioselectivity is reversed (to the 3-position) when coordinating groups are present on the heteroatom,[156,168] as mentioned earlier. Unactivated cyclic alkenes may have been unsuccessful in our case however strained cyclic alkenes readily provided tricyclic dihydroisoquinolinones (Entries 8-10). As these alkenes are almost symmetrical, mixtures of regioisomeric products were returned. For instance, reaction of **3-57** with boc-azabicycloheptene gave the corresponding tricyclic products **3-76** and **3-77** in a moderate yield. Surprisingly, the use of boc-protected vince lactam (Entry 9) resulted in a postulated annulation and ring

opening with methanol to give the corresponding fused cyclopropyl amino carboxylates after deprotection. It was hypothesised that each regioisomer in this case an unidentified mixture of diastereomers. Therefore, these compounds were made intentionally from the corresponding starting material to give **3-78** and **3-79** as single products (Entry 10). Pleasingly, synthesis of the analogous acids **3-80** and **3-81** was also successful indicating a free carboxylic acid is tolerated in the reaction (Entry 11). Ring opening was not observed when the unprotected vince lactam was used in the reaction, which resulted in **3-82** and **3-83** in a combined yield of 71% (Entry 12), suggesting protection of the amide increased susceptibility to nucleophilic attack.

Expanding the butane ring of methylene azetidine to its corresponding 5- and 6-membered analogues, respectively, was unsuccessful in the reaction (Entries 13 and 14). As with strained cyclic alkenes, the reduction in ring strain as the size of the ring increases could explain the reaction failure. Again, similarly to Fagnou,[144] acyclic internal alkenes (i.e. disubstituted alkenes, Entries 15 and 16) were unsuccessful under our reaction conditions. Since Entries 3-5, 7 and 15-16 were performed, the methodology has been extended to unactivated and acyclic internal alkenes by using $[Cp^fRhCl_2]_2$ as the catalyst or TFE as the solvent, respectively.[169]

3.4.5.1 Regiochemical and Stereochemical Considerations

Interestingly, reaction of **3-57** with boc-protected vince lactam gave two regioisomers, as expected, yet a single diastereomer for each regioisomer. As the nature of the reaction with *cis* or cyclic alkenes results in *cis* annulated products, there were two possible diastereomeric outcomes: ring junction and bridge in a *cis* or *trans* configuration. The sole product obtained was that of the *cis* product, possibly as an effort to minimise unfavourable interactions between the ring junction and bridgehead protons which are on opposite faces.

The regiochemical outcome of the reaction was determined as outlined previously (see section 3.3.3.1). For the cases with internal cyclic alkenes (Table 3-5, Entries 6, 8 and 10-12), the diastereomeric outcome of the reaction was also determined by NMR analysis. Using the relative stereochemical assignments of **3-82** and **3-83** as examples (Fig. 3-7), two CH_2 protons (δ 1.53

and 1.76 ppm) correlated through-bond to two CH protons (δ 2.62 and 3.85 ppm). The downfield, more deshielded proton (δ 3.85 ppm) correlated through-space to an amide N–H proton, the carbon atom of which appeared downfield relative to the benzylic amide carbon atom usually seen in these molecules, the N–H of which correlated through-space to the CH proton at δ 2.62 ppm. The CH proton at δ 3.85 ppm also correlated through-space to an aromatic proton, appearing as a large doublet. These correlations suggested regioisomer **3-82** with the CH protons (δ 2.62 and 3.85 ppm) assigned as H_{12} and H_1, respectively. H_1 and H_{12} correlated through-space (and -bond) to an apparent doublet at δ 3.49 ppm and a doublet of triplets at δ 4.00 ppm, respectively. These protons were deemed to be H_2 and H_{11}, respectively, and coupled to each other with a coupling constant of 9 Hz suggesting a *cis* configuration in a bridged, strained system such as illustrated in Fig 4-6. This coupling constant, along with the through-space correlations outlined above, suggested diastereomer **3-82**. This process was repeated to determine the relative assignment of **3-83** and the key correlations are illustrated in Fig. 3-7.

NOESY and HMBC correlations
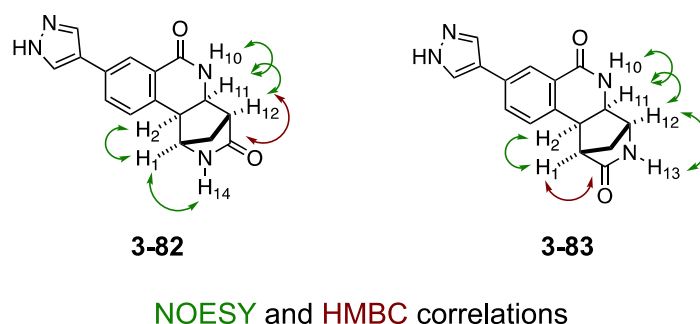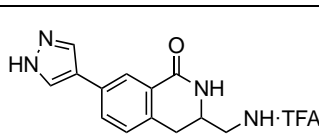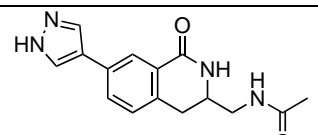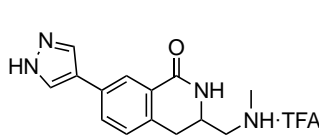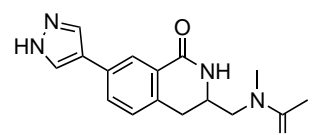
Figure 3-7. Determination of the regio- and stereo-chemical outcome. The NOESY and HMBC correlations observed in **3-82** and **3-83** were used as illustration.
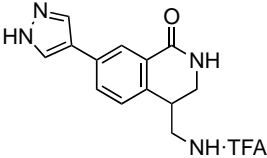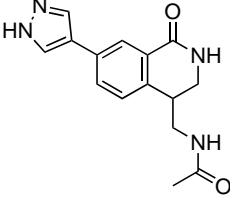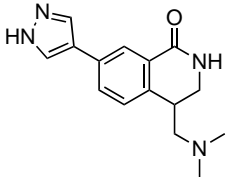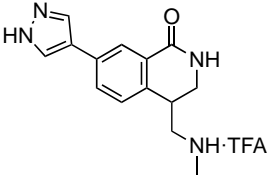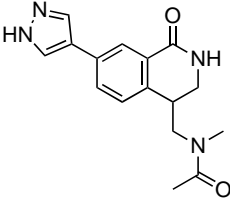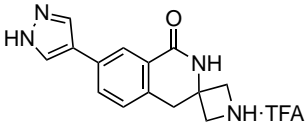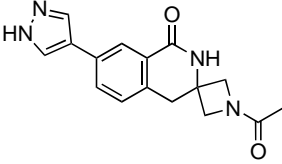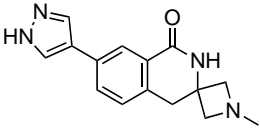
3.4.5.2 Elaboration *via* Methylation and Acetylation

Methylated or acetylated analogues of **3-68** and **3-70** were also synthesised (Table 3-6) to probe whether the N–H is required for a hydrogen bond and if the group can be used as a handle for subsequent transformations whilst retaining the small increase in activity.

3-68–**3-69**, **3-70** and **3-72**–**3-73** were acetylated in 26% to 80% yield. An excess of acetic anhydride was used to completely acetylate both the amine and the pyrazole nitrogen. We then exploited the difference in conditions required to remove an acetyl group from these two groups, selectively de-acetylating the pyrazole ring using $NaHCO_3$ in methanol at room temperature. Similarly, **3-69** and **3-70** were methylated with an excess of formaldehyde followed by reduction with STAB to give **3-87** and **3-90**, respectively, albeit in low yields. The low yield was later attributed to methanol as the reaction solvent and the use of DCE gives improved yields (see 3.3.7).

Table 3-6. Elaboration of amino-functional group handles by acetylation and methylation.

Entry	Starting Material	Method	Product	Yield[a] (%)
1	**3-68**	A)	**3-84**	77
2	**3-72**	A)	**3-85**	80

Entry	Starting Material	Method	Product	Yield[a] (%)
3a		A)	**3-86**	71
3b	**3-69**	B)	**3-87**	12
4	**3-73**	A)	**3-88**	67
5a		A)	**3-89**	26
5b	**3-70**	B)	**3-90**	3

[a]Isolated yields are reported.
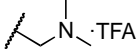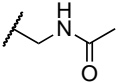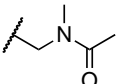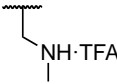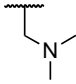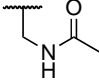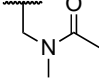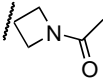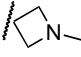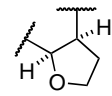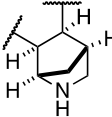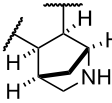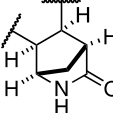
3.4.6 Biological Evaluation of 3,4-Dihydroisoquinolinone Analogues: Second Generation Library
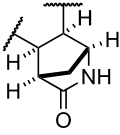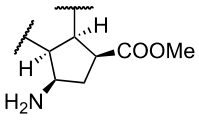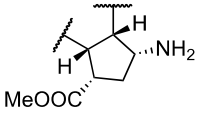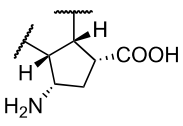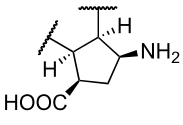
With the second generation library of 3,4-substituted dihydroisoquinolinones in hand, their inhibition of Nek7 activity was determined to probe the SAR around the amino-group. Furthermore, this would establish whether the group can be used as a handle for subsequent transformations whilst retaining the small increase in activity. This library was synthesised from analogous alkenes as the ones which showed promise previously, in an effort to build further potency gains. The activities of these 3,4-dihydroisoquinolinones exploring the role of the amino-group are shown in Table 3-7.

Table 3-7. Biochemical Structure-Activity Relationship for Second Generation 3,4-Dihydroisoquinolinones Analogues

Entry	No.	R_1	R_2	Nek7 IC$_{50}$/μM (n)[a]		Ligand Efficiency
				ICKP	Caliper	
1	**3-3**	H	H	12 ± 4	25 ± 1 (6)	0.40
2	**3-68**	$\diagdown$NH$_2$·TFA	H	5 ± 0.8	9 ± 0.5 (6)	0.39
3	**3-70**	$\diagdown$NH$_2$·TFA	H	3 ± 0.6	12 ± 0.6 (6)	0.36
4	**3-69**	H	$\diagdown$NH$_2$·TFA	25 ± 5	41 ± 0.2 (4)	0.34
5	**3-72**	$\diagdown$NH·TFA	H	33 ± 7	19 ± 4	0.35

| Entry | No. | R₁ | R₂ | Nek7 IC$_{50}$/μM (n)[a] | | Ligand Efficiency |
				ICKP	Caliper	
6	**3-74**		H	69 ± 17	6 ± 1	0.37
7	**3-84**		H	371 ± 42	-	0.23
8	**3-85**		H	138 ± 23	-	0.25
9	**3-73**	H		379 ± 88	529 ± 161	0.24
10	**3-87**	H		121 ± 21	-	0.27
11	**3-86**	H		178 ± 45	53 ± 3	0.29
12	**3-88**	H		915 ± 180	167 ± 12	0.24
13	**3-89**		H	>1000	333 ± 24	0.22
14	**3-90**		H	8 ± 2	4 ± 0.5	0.38
15	**3-75**			38 ± 8	25 ± 2	0.34
16	**3-76**			42 ± 8	-	0.31
17	**3-77**			157 ± 38	-	0.25
18	**3-82**			9 ± 1	13 ± 0.9	0.31

Entry	No.	R₁	R₂	Nek7 IC$_{50}$/µM (n)[a]		Ligand Efficiency
				ICKP	Caliper	
19	**3-83**			14 ± 3	20 ± 1	0.30
20	**3-78**			>1000	-	<0.18
21	**3-79**			>300	-	<0.23
22	**3-80**			>1000	-	<0.18
23	**3-81**			30 ± 4	-	0.30

[a]Unless otherwise stated, n = 2. LE was calculated from Caliper data where possible.

As with the previous set of compounds, this small library was assayed using the Caliper EZ Reader II as well as being sent to the ICKP for validation. Only some compounds here were assayed on the Caliper, due to the COVID-19 pandemic and a machine fault.

Methylation of **3-68** was tolerated (Entry 5, Caliper) with the dimethyl variant (Entry 6, Caliper) approximately five-times more potent than the starting dihydroisoquinolinone **3-3** which lacks any substituent. However, methylation of **3-68** was shown to be less well tolerated from the ICKP data with the dimethyl variant over 10-fold worse than its unmethylated analogue (Entries 5 and 6, ICKP). Similarly, acetylation of this amino group was detrimental for activity (Entries 7 and 8). Methylation and acetylation of the amino group of **3-69** followed a similar trend and was also detrimental to activity (Entries 9-12). In this case however, methylation and acetylation, **3-88**, proved worse than its

unmethylated analogue, **3-86**, the trend of which was reversed for their 3-position regioisomer, **3-84** and **3-85**. Acetylation of **3-70** was also detrimental to activity (Entry 13), showing that these amino groups are unsuitable for use as synthetic handles *via* acetylation. Pleasingly, methylation of **3-70** was tolerated (Entry 14, ICKP) and even improved 4-fold (6-fold over **3-3**) when assayed on the Caliper (Entry 14, Caliper). Therefore, the azetidine nitrogen has potential for use as a synthetic handle *via* reductive amination and alkylation reactions. In general, ring fusion was well tolerated (Entries 15-19) even with relatively bulky bridged-ring systems (entries 16-19). Interestingly, the nitrogen atom seemed to be preferred in the 14 position of **3-76** with its regiomeric counterpart **3-77** detrimental for activity. This preference was not observed in the amide variants **3-82** and **3-83** which have similar activities within error. However a large reduction in activity was seen for **3-78**, **3-79** and **3-80** (Entries 20-22), an interesting result when compared to the activity of **3-81** (Entry 23).

We next turned our attention to **3-70** and methylation of the azetidine **3-90**. With methylation of **3-70** showing promise for inhibition of Nek7, it was envisaged that **3-70** could be grown *via* reductive amination or alkylation in an attempt to gain additional binding interactions and an improvement in potency.

3.4.7 Synthesis of 3,4-Dihydroisoquinolinone Analogues: Exploration of the Azetidine

With **3-70** showing increased potency against Nek7 and methylation of the azetidine in **3-90** giving similar or even improved levels of inhibition, these compounds were chosen for further exploration in the hope of gaining additional increases in potency. It was envisaged that this could be achieved in two ways: (i) combination of favourable 3,5-pyrazole substituents (see 3.2.4) with azetidines **3-70** and **3-90** and (ii) growth of **3-70** and **3-90** by addition of substituents at the azetidine nitrogen position. In order to achieve the latter, a series of reductive amination reactions were performed and the results are shown in Table 3-8.

Table 3-8. Exploration of the Azetidine by Reductive Amination

1. Et₃N, DCE—MeOH
2. Aldehyde or ketone, acetic acid (0-1 equiv.) then STAB, rt, 18 h

3-70 → 3-91—3-97
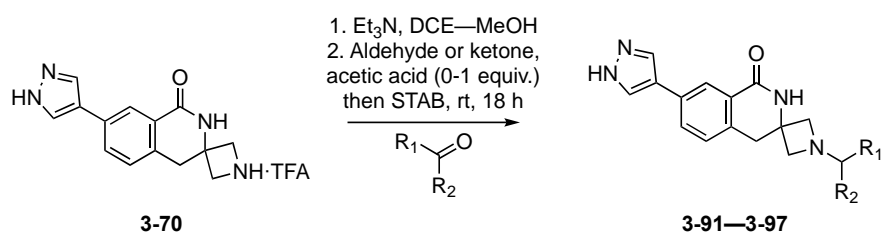
Entry	Carbonyl	No.	Product	Yield (%)
1[a]		**3-91**		17
2[a]		**3-92**		27
3		**3-93**		42
4		**3-94**		55
5		**3-95**		36
6		**3-96**		45
7		**3-97**		76

[a]Synthesised from the free base without the use of NEt₃.

Work was underway to improve the crystallographic model of Nek7, however we were still unable to capture the active structure of the kinase. The aldehydes and ketones chosen for this reaction were therefore done so in the absence of structural information, as the inactive structure of Nek7 bound to the parent compound of this series was not a reliable model for predicting binding (see 3.3). To aid the decision making, the Topliss Tree[170] was used to explore this previously unexplored vector in a systematic way.

Initially, acetone and tetrahydropyran-4-carbaldehyde were reacted with **3-70** using the above conditions but in methanol with an equivalent of acetic acid. This reaction was unsuccessful and starting material was re-purified from this mixture, now as the free base, and the reaction was attempted again. This attempts was also unsuccessful and the cause was quickly attributed to the use of methanol as the sole solvent. The mixture was concentrated and the reaction successfully performed in DCE, which has been identified as the preferred solvent for reductive aminations.[171] The remaining aldehydes or ketones were reacted with **3-70** in DCE with minimal amount of solubilising methanol (**3-70** is insoluble in DCE) to give the desired products in 36% to 76% yield. During the synthesis it was identified that acetic acid was not required for these reactions and additional equivalents of STAB can be added as required.

3-98 was also synthesised by reaction of **3-70** with bromoethyl methyl ether using DMF as the solvent and sodium hydrogen carbonate as the base to prevent alkylation at the pyrazole nitrogen (c.f. acetylation of **3-42** with sodium hydrogen carbonate and potassium carbonate, see 3.3.2).
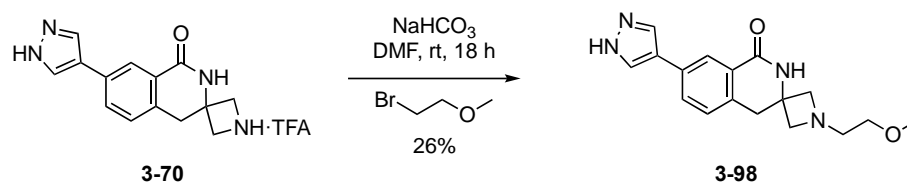
Scheme 3-16. Synthesis of **3-98** *via* alkylation of **3-70** with bromoethyl methyl ether.

With a small library of substituted azetidine compounds in hand, we next turned our attention to the combination of **3-70** and **3-90** with favourable 3,5-pyrazole substituents. As 3-methyl pyrazole was the only promising substitution (see 3.2.4), this was combined with **3-70** and **3-90**. These analogues were synthesised *via* the scheme below in which it was opted to perform the Suzuki coupling last, rather than first as previously performed, to expedite the combination of future 3,5-substituted pyrazoles with 3-azetidine dihydroisoquinolinones.
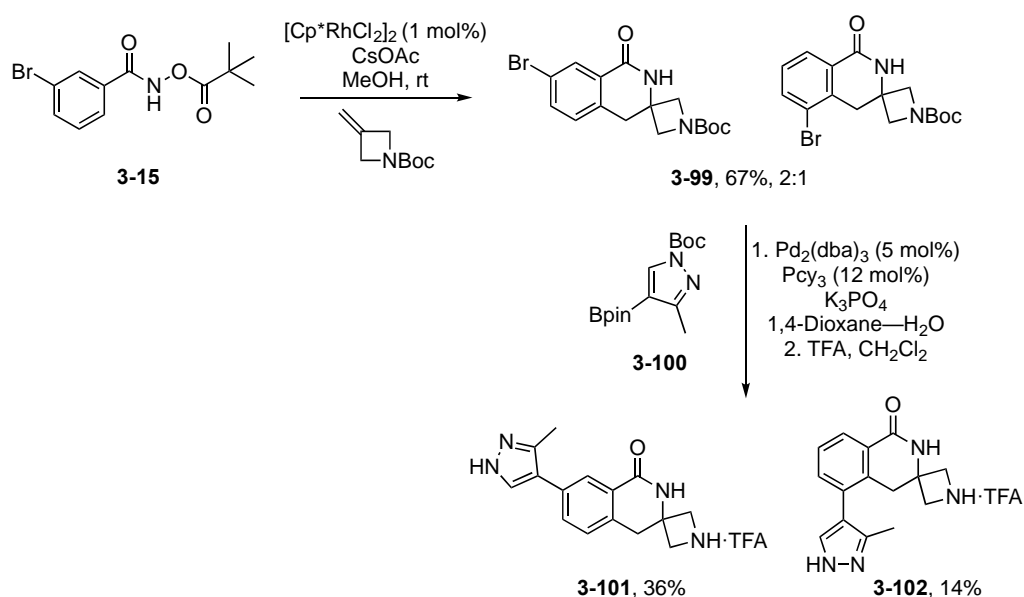
Scheme 3-17. Synthesis of **3-101**. Annulation of **3-15** was performed using rhodium catalysis followed by Suzuki coupling to install the pyrazole ring.

The synthesis of **3-101** began with synthesis of dihydroisoquinolinones **3-99** *via* reaction of **3-15** with boc-protected methylene azetidine under rhodium catalysis, this time at room temperature (elevated temperatures was unnecessary due to **3-15** known to undergo these reactions at room temperature[158]). Surprisingly, an inseparable mixture of regioisomers from C–H insertion *para* or *ortho* to the bromide was produced from this reaction in a 2:1 ratio, respectively. This is in contrast to when this reaction was performed on **3-51** or **3-57**, with a pyrazole in place of the bromide, which gave only a single regioisomer. A possible explanation is the increased steric demand of the pyrazole ring prevents *ortho* C–H insertion. The regioisomers given here were both 3-substituted dihydroisoquinolinones and no 4-azetidine

dihydroisoquinolinone was observed. **3-99** was coupled with **3-100** under palladium catalysis to install the 3-methyl pyrazole ring and give the desired product **3-101** and **3-102**, resulting from Suzuki coupling with the undesired regioisomer. It was hoped that Suzuki coupling on this undesired regioisomer would be unsuccessful, thereby separating the regioisomers, due to the *ortho* position of the bromide. Unfortunately this was not the case, however the products following the Suzuki coupling were separable and **3-101** and **3-102** were isolated by column chromatography, albeit in diminished yield due to the difficult separation. The splitting pattern and coupling constants of the phenyl ring led to the determination of the regioisomers in **3-99** but also allowed determination of which regioisomer is which in the products **3-101** and **3-102**.

Finally, **3-101** and **3-102** were methylated using the conditions above in 45% and 38% yield, respectively. Again, this was to determine the effect of methylation of the azetidine in the presence of the 3-methyl substituted pyrazole.
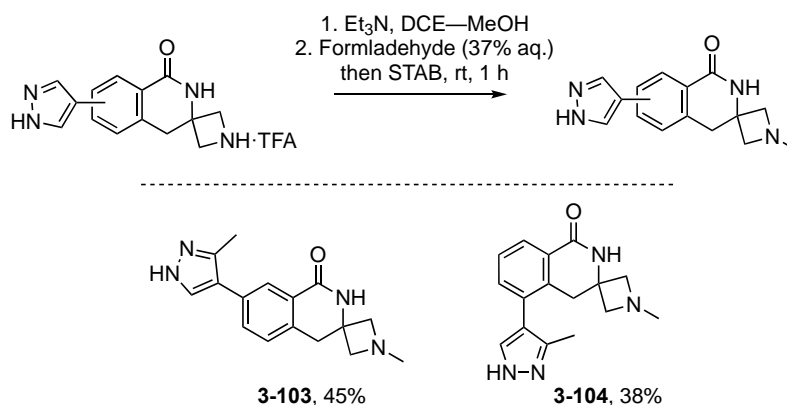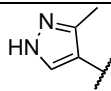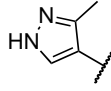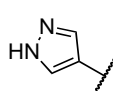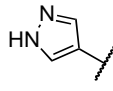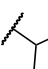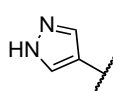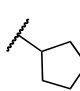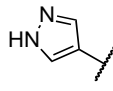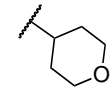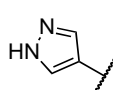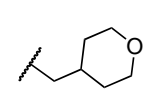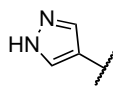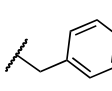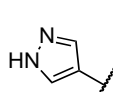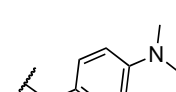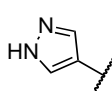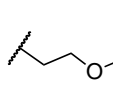
Scheme 3-18. Synthesis of **3-103** and **3-104** by reductive amination with formaldehyde.

3.4.8 Biological Evaluation of 3,4-Dihydroisoquinolinone Analogues: Exploration of the Azetidine

With the library of 3,4-dihydroisoquinolinone azetidine analogues in hand, their inhibition of Nek7 activity was determined by the ICKP. The library was synthesised from a diverse range of aldehydes and ketones (and an alkyl bromide) to probe the SAR around the azetidine and use it as a handle for potency gains. Furthermore, promising pyrazole substituents (3-methylation, 3.2.4) were combined with the 3,4-dihydroisoquinolinone azetidine substituent. It was hoped that these two approaches would lead to the development of a compound with suitable potency for use as a chemical tool against Nek7. The activities of these 3,4-dihydroisoquinolinones are shown in Table 3-9.

Table 3-9. Biological Evaluation of the 3,4-Dihydroisoquinolinone Azetidine Analogues

Entry	No.	R_1	R_2	R_3	Nek7 IC_{50} (μM) ICKP	Caliper	LE
1[a]	**3-70**		H	NH•TFA	3 ± 0.6[b] 13 ± 3[c]	12 ± 0.6 (6)	0.36
2	**3-105**		H	NH	9 ± 0.4	-	0.37
3	**3-90**		H		8 ± 2[b]	4 ± 0.5	0.38
4	**3-101**		H	NH•TFA	6 ± 1	9 ± 0.6	0.35
5	**3-103**		H		8 ± 4	2 ± 0.2	0.38

Entry	No.	R_1	R_2	R_3	Nek7 IC$_{50}$ (μM)		LE
					ICKP	Caliper	
6	3-102	H		NH•TFA	86 ± 7	-	0.28
7	3-104	H			152 ± 10	-	0.25
8	3-93		H		19 ± 3	-	0.31
9	3-91		H		47 ± 9	-	0.28
10	3-97		H		44 ± 5	-	0.25
11	3-96		H		319 ± 9	-	0.20
12	3-92		H		105 ± 9	-	0.21
13	3-94		H		158 ± 19	-	0.20
14	3-95		H		9 ± 0.4	-	0.24
15	3-98		H		88 ± 0.7	-	0.25

[a]8 ± 5 (n = 4). [b]Previously measured value by ICKP. [c]Value measured upon re-sending to ICKP. n = 2 unless otherwise stated.

The previously reported IC$_{50}$ by the ICKP for the parent azetidine compound, **3-70**, was 3 μM. This compound, along with all other compounds from the previous generation libraries (3.3.4 and 3.3.6) were sent as a single batch to the ICKP for validation and comparison to the Caliper measured values, the results of which led to the exploration of the azetidine and the synthesis of the

library here. This library, exploring the SAR around the azetidine, was sent to the ICKP for IC_{50} determination against Nek7, along with the parent azetidine compound again for comparison. Unexpectedly, the ICKP determined the IC_{50} of **3-70** to be 13 μM in this screen and therefore this was the value used for comparison for the rest of this library.

Combination of 3-methyl pyrazole with the azetidine and methyl azetidine substituents (Entries 4 and 5, ICKP) gave a similar, if not slightly improved, activity compared to the parent azetidine compound (Entry 1). Clearly, the pyrazole ring is detrimental to activity when moved to the R_2 position (Entries 6 and 7) as a drop-off in activity is observed compared to their R_1 analogues (Entries 5 and 6). For the compounds with varying substituents off the azetidine nitrogen atom (Entries 8-15) it seems the larger the substituent, the worse the activity. For instance, the methyl (Entry 3), ethyl (Entry 8) and isopropyl (Entry 9) have increasingly worse IC_{50} values for Nek7 however these substituents are still tolerated. As potentially expected, cyclopropyl (Entry 10) gave a similar activity to isopropyl (Entry 9) however tetrahydropyran gave a sharp decrease in activity (Entry 11). This drop-off was slightly reversed when a carbon was introduced between the pyran and the azetidine (Entry 12), however this was still considerably worse than the parent compound. This was also the case for the benzyl substituent (Entry 13) however, interestingly, activity could be restored with a *p*-dimethylamino substituent on the ring (Entry 14). **3-95** actually gave a similar, if not slightly improved, IC_{50} value to the parent azetidine. Despite this restoration of activity, **3-95** was not pursued further due to its decreased ligand efficiency.

The most promising compounds as determined by the ICKP were then assayed using the Caliper mobility shift assay to validate the IC_{50} values. This assay was in-house and also provided more consistent values between runs, giving a higher confidence in the measured IC_{50}. As determined previously (see 3.3.6), methylation of the azetidine (Entry 3, Caliper) gave a 3-fold improvement over the parent compound. The values determined by the ICKP for the compounds which combined the 3-methyl pyrazole and azetidine were validated upon Caliper assay (Entries 4 and 5, Caliper). 3-methyl pyrazole azetidine (Entry 4, Caliper) had a similar activity to the parent compound whilst methylation of this series (Entry 5, Caliper) gave a 6-fold improvement over

the parent azetidine and more than a 12-fold improvement over **3-3**, our starting point for this work (2 μM *versus* 25 μM).

3.4.9 Selectivity over the Kinome

The selectivity of compounds, **3-70**, **3-101** and **3-103** for Nek7 against the kinome was tested in an Express Screen (ICKP) comprising 50 key enzymes that provide a representative sampling of the human kinome (Fig. 3-8 b-d, Appendix B.4). These compounds were tested at a concentration of 1 μM (n = 2) and the average percentage inhibition plotted. The Express Screen did not contain Nek7, but did contain Nek6 which we expected the compounds to inhibit to a similar level as Nek7 as these two kinases are identical in the residues that line the ATP binding site. The selectivity of these compounds were compared with the selectivity of **3-3** which had been tested against 30 kinases previously using the SelectScreen Kinase Profiling Service (Life Technologies).[129] Despite using a different assay at a different compound concentration against fewer and different kinases, a broad comparison of selectivity can be observed between our starting compound (Fig. 3-8 a) and the ones developed by this work (Fig. 3-8 b-d). This is especially true when comparing the respective inhibition for similar or the same kinases. In general the compounds developed here were not selective for Nek6 or Nek7, inhibiting around 50% of the kinases assayed to greater than 90% at 1 μM. This included PLK1, a mitotic kinase with similar structural features as Nek7 (Leu gatekeeper, Phe at base of active site), which was fully inhibited by all three compounds at 1 μM. These compounds could therefore be used as starting points for optimisation into potent and selective compounds for a variety of kinases in a similar fashion to that achieved by high-throughput kinase profiling.[58] One such kinase which may be of interest for this effort is MARK3, an understudied kinase responsible for phosphorylating microtubule-associated proteins such as tau which is the principal component of tangles in Alzheimer's Disease.[4,172,173] All three compounds fully inhibit MARK3 at 1 μM. Interestingly, **3-70** and **3-101** inhibited Nek6 to a similar level at 1 μM as Nek7 (as determined from ICKP IC$_{50}$ determination), as expected, however **3-103**, our most potent compound against Nek7, was inactive against Nek6.

Either this an anomaly across both replicates or methylation of the azetidine provides selectivity for Nek7 over Nek6.
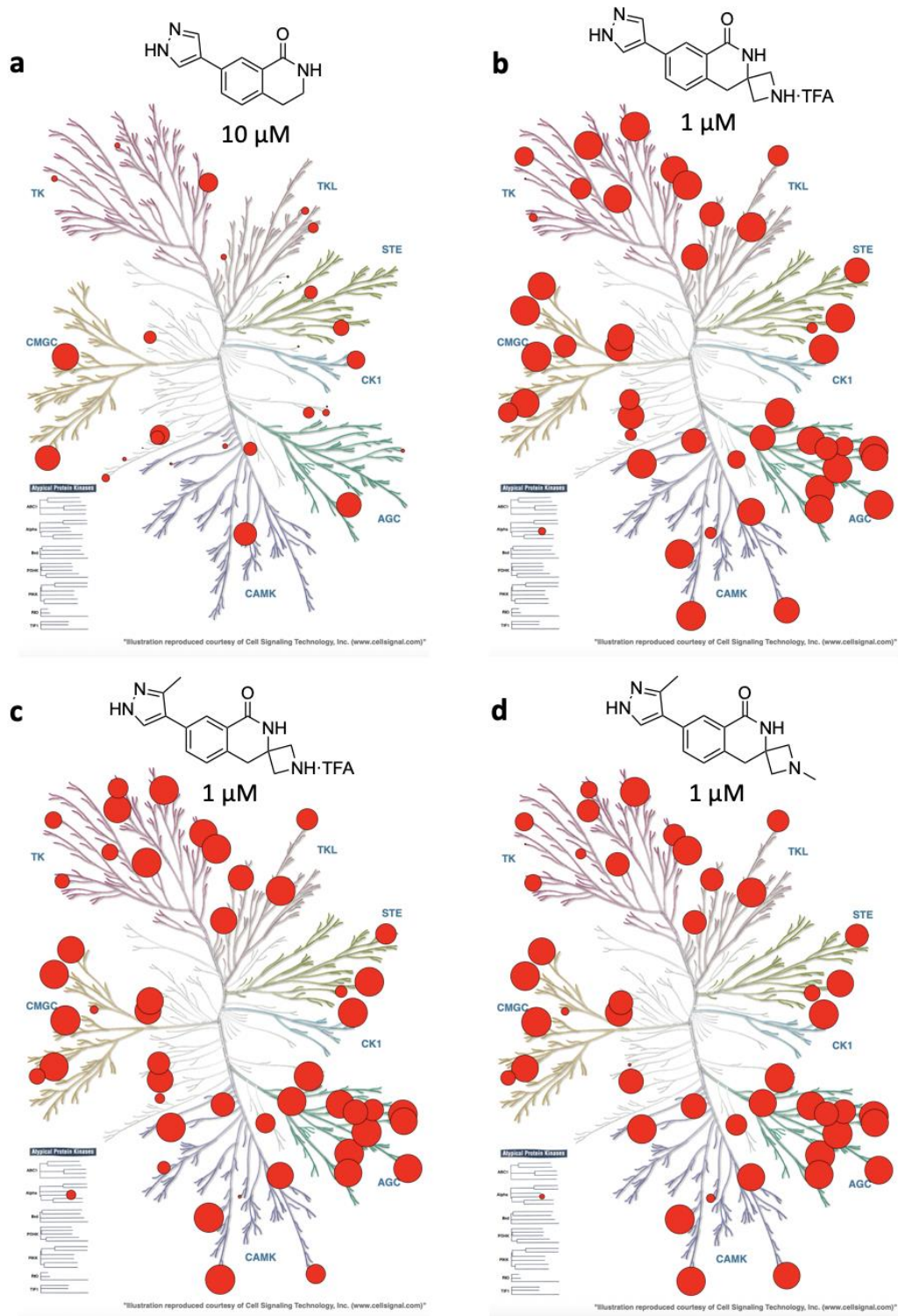
Figure 3-8. Selectivity across the kinome; red circles represent inhibition with the larger the circle, the higher the percentage inhibition.

A few similarities can be made between the development of inhibitors for Braf and Nek7. Firstly the inhibitors of Braf were developed by fragment-based drug discovery, as were the origins of the inhibitors here. Furthermore, Braf forms dimers and the αC-helix out conformation of the kinase was targeted in its inhibition. Nek7 is known to form dimers upon Nek9 binding and all the crystal structures solved to date show a αC-helix out conformation. It may be a useful approach then, to develop Type 1½ inhibitors for Nek7 which may also address some of the selectivity issues. For instance, the structures in the PDB of PLK1 exhibit a αC-helix in conformation. Therefore, the development of a Type 1½ inhibitor for Nek7 may abolish binding to PLK1.

3.4.10　　　Probing the Cellular Function of Nek Family Kinases

As mentioned in Chapter 1, Nek6 phosphorylates Hsp72 to promote microtubule stability and nucleation in mitotic spindle assembly.[36–38] Furthermore, Nek6 and Nek7 are identical in the residues that line the ATP binding pocket and so any inhibitor developed here should also target Nek6 to a similar level (corroborated by the above selectivity screen). HeLa cells were treated with **3-70**, **3-101** and **3-103** in an 8-point 2-fold dilution series from 50 μM over 4 hours and the level of phosphorylated Hsp72 was observed (Fig. 3-9, Josephina, Bayliss Group).

Whilst **3-101** and **3-103** inhibited the phosphorylation of Hsp72 from concentrations upwards of 6.25 μM and 3.125 μM, respectively, treatment with **3-70** seemed to increase phosphorylation of Hsp72 which could be an indicator of mitotic arrest. However because of the promiscuity of these compounds, this cellular data is challenging to interpret. These compounds do exhibit cellular based activity targeting this pathway however despite their inhibition of Nek6, they more potently inhibit the upstream kinase PLK1.
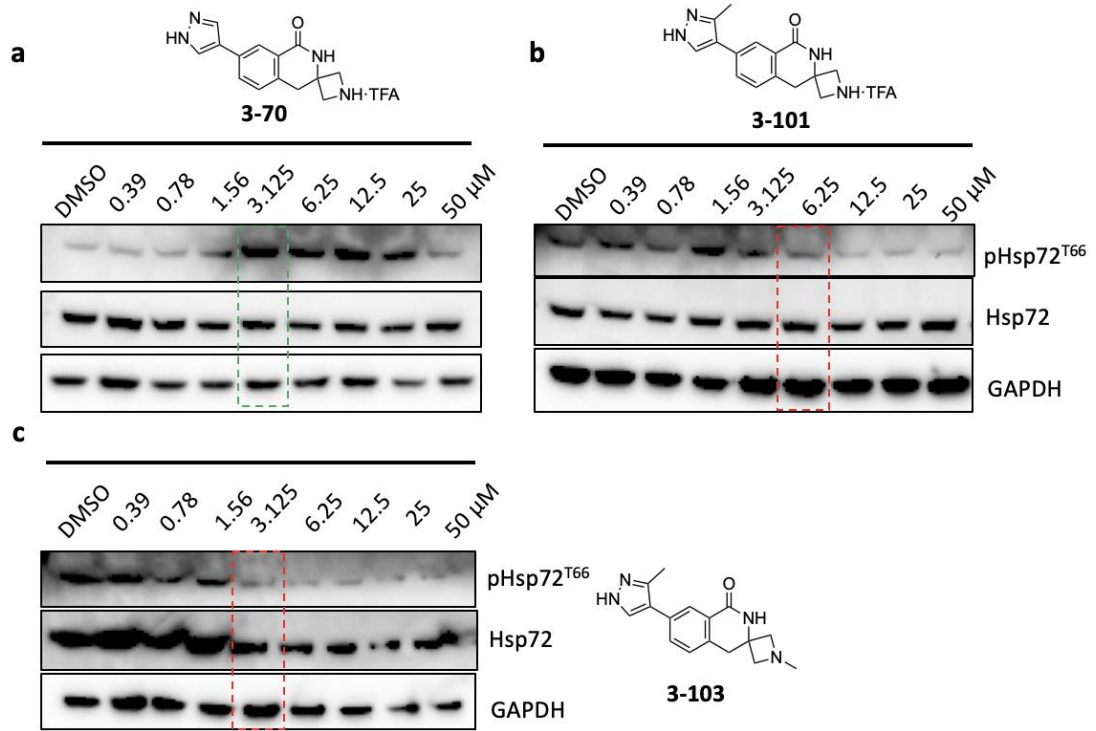
Figure 3-9. Probing phosphorylation of Hsp72 after treatment of HeLa cells with (a) **3-70**, (b) **3-101** and (c) **3-103**.

3.5 Conclusions on the Structure-Activity Relationship of the Dihydroisoquinolinone core

In general, most substitutions at the 3,4-position of the dihydroisoquinolinone core of **3-3** were tolerated, having a moderate effect on potency. It is possible that the binding pocket around the 3,4-position is large or solvent exposed and an improved crystallographic model would allow a more in depth hypothesis. In a few cases, large drops in activity were observed providing information on which groups are unproductive in these positions. Conversely, two examples bearing a nitrogen substituent in the 3-position, **3-68** and **3-70**, provided moderate increases in activity we deemed worth pursuing. A second generation library synthesised on the basis of these two compounds again showed the tolerable nature of the binding pocket with large, bridged, fused ring systems giving a similar potency to our starting compound. Dimethylation of **3-68** was beneficial upon Caliper assay but detrimental when assayed by the ICKP. Pleasingly, methylation of **3-70** was tolerated and even slightly improved indicating reductive amination or simple alkyl halide substitution reactions as methods for improving the activity further. To this end, a third generation library exploring the SAR of the azetidine was synthesised. It seemed addition of substituents to the azetidine larger than a methyl was less tolerated as the size increased and detrimental to activity with larger groups. Benzylation was detrimental to activity however, interestingly, *p*-dimethyl-aminobenzyl restored activity and exploration around this group could be beneficial for future work. Additionally, the 3-methyl pyrazole substituent was combined with the most promising dihydroisoquinolinone variants in an effort to develop a compound which can be used as a chemical probe against Nek7. Combination of variants was well tolerated an even gave a slight improvement in activity leading to **3-103** with 2 μM IC$_{50}$ against Nek7, 12.5-fold improvement over our starting compound (Fig. 3-10).

Despite the development of a series of low micromolar affinity compounds for Nek7 by this work, **3-70**, **3-101** and **3-103** were promiscuous across the kinome and not selective for Nek7. We thought a quality chemical probe should have 30-fold selectivity over other targets with 100 nM *in vitro* potency (low micromolar cellular activity). Therefore, there is still work to be done to

improve the selectivity and potency of these compounds for use as a chemical probe. Despite this, the compounds are still relatively small, being less than 300 molecular weight, and so there is scope for improvement. It is possible the selectivity will be improved as the potency of these compounds for Nek7 is developed to a level suitable for use as a probe. On the other hand, it may be more practical to develop the selectivity and allow potency to follow as a consequence. Alternatively, a more selective chemical series could be sought as a starting point for further development. Nevertheless for an understudied kinase with no published chemical probes against, these compounds provide a basis for the development of more potent and selective inhibitors as well as for preliminary cellular studies in an attempt to elucidate the potential benefits of inhibiting Nek7 in a clinical setting.
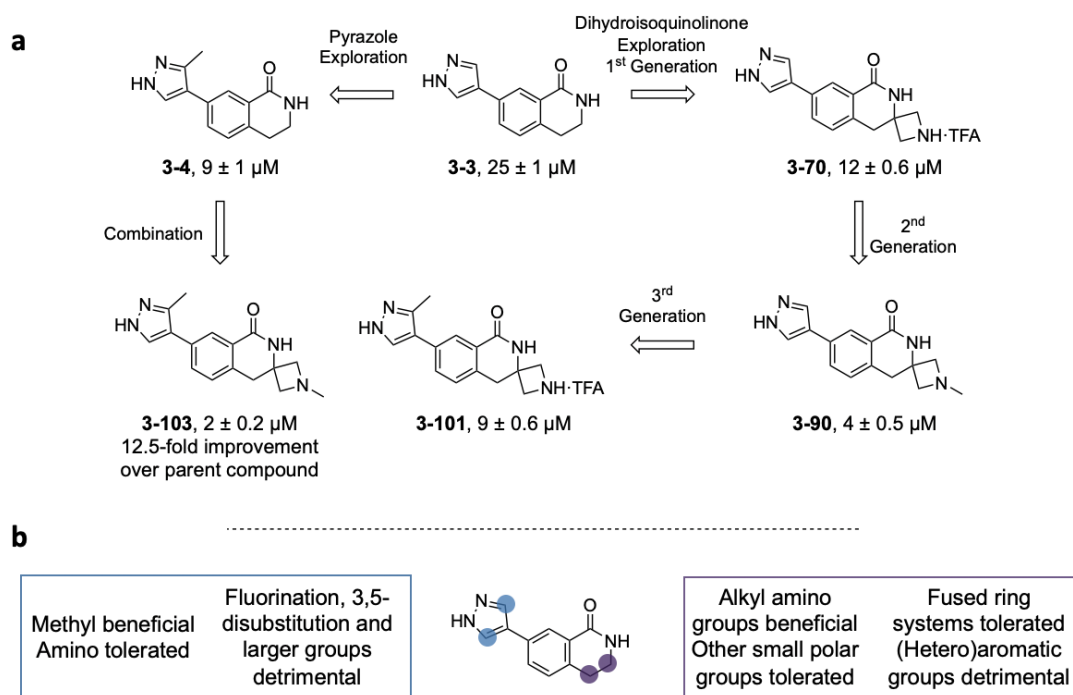
Figure 3-10. Summary of SAR by this work, leading to a 12.5-fold improvement over **3-3** and a low micromolar affinity compound for Nek7. A larger number of diverse groups were tolerated at the 3,4-dihydroisoquinolinone positions.

Chapter 4
Conclusions and Future Work

4.1   Summary and Conclusions

The overall aim of this project was to develop a suitable chemical tool against Nek7 which can be used to probe the cellular functions of this kinase. It was hoped that in developing a chemical tool, the scientific community could validate Nek7 as a clinical target and drug discovery programmes could be initiated. A summary of the project milestones is shown above (Fig. 3-10) and a few of these compounds were tested for selectivity against the kinome as well as used in cellular studies to probe the function of Nek7, thereby working towards the project aim.

To achieve our aim, the project had two overarching arms. Prior to a Nek7-Ligand co-crystal structure, the first arm was exploitation of fragments with Nek7 activity in activity-directed synthesis. To this end, four fragments were simultaneously exploited in 272 reactions over two rounds of ADS in the hope of potentially discovering several novel starting points for further drug discovery efforts. Whilst bioactive reaction product mixtures were identified, the reason for the improved activity was unable to be identified and no bioactive small molecules were isolated.

The second arm of the project was optimisation of a developed Nek7 chemical series through SAR expansion, aided by a solved Nek7-Ligand crystal structure. This developed chemical series was a useful starting point for our optimisation and it was envisaged that this series could be explored to develop a suitable chemical tool for Nek7. To this end, the SAR of the 3,5-positions of the pyrazole ring were explored in the synthesis and testing of 11 analogues and methylation was found to be beneficial for activity. Unfortunately, anything larger than a methyl seemed to be detrimental for activity and the structural model used for docking studies to aid analogue design was deemed to be not suitable for this purpose. This model was not predictive of real-life binding which could be due to the inactive conformation of the kinase in the model. Alternatively, the pyrazole library used to evaluate the computation model was a small one. Furthermore, our docking studies assumed pyrazole to be the

hinge binding motif and so exploration of the dihydroisoquinolinone amide as playing the role of this motif may be necessary.

Nevertheless our attention turned to the 3,4-positions of the dihydroisoquinolinone core which had yet to be explored for SAR. In an effort to develop the SAR at this position, diverse groups were introduced in 10 distinct analogues and testing revealed nitrogen-based substituents to be beneficial for activity. A further 20 analogues based on these substituents were synthesised to develop the SAR. Methylation of the azetidine nitrogen was found to be beneficial for activity and led to the synthesis of 9 further compounds exploring the azetidine further. Furthermore, combination of pyrazole 3-methylation with these promising dihydroisoquinolinone substitutions led to the discovery of a few low micromolar inhibitors of Nek7, one of which, **3-103**, had an IC_{50} of 2 μM, a 12.5-fold improvement over our starting compound. Unfortunately, these compounds were promiscuous across the kinome but were very potent against interesting, understudied kinases where selectivity could be tuned to a specific kinase. Furthermore whilst the selectivity profiles were not ideal, these relatively small compounds have scope for further development and it is anticipated that improved selectivity will be achieved as the potency of these compounds for Nek7 is developed or *vice versa*. Work is currently underway with a few of these most potent compounds to probe the function of Nek7 in a cellular model.

4.2   Future Work

The development of a reliable structural model to allow docking studies is of top priority to enable the potency and selectivity of these compounds to be efficiently improved. Furthermore, the development of a confident Nek7-Ligand co-crystal structure, preferably with the kinase in an active conformation, will validate the binding mode orientation of our starting compound. This will also enable rationale behind the binding mode of the compounds developed here and explain why such a large variety of groups were tolerated at the 3,4-dihydroisoquinolinone positions. The compounds developed here, despite being more potent than the starting compound lacked selectivity. It may be useful to gain selectivity data for other chemical series developed by this work to identify a more selective starting point for

optimisation. Alternatively, structure-based optimisation of the most potent compounds developed here may lead to a simultaneous improvement in selectivity. As any substituent larger than a methyl group at the azetidine was not tolerated, exploration of alternative positions of the dihydroisoquinolinone core, such as the amide nitrogen which is previously unexplored, may be beneficial. This is with the exception of the dimethylaminobenzyl substituent which restored affinity compared to benzylation alone and, despite a decreased ligand efficiency, may be worth exploring further.
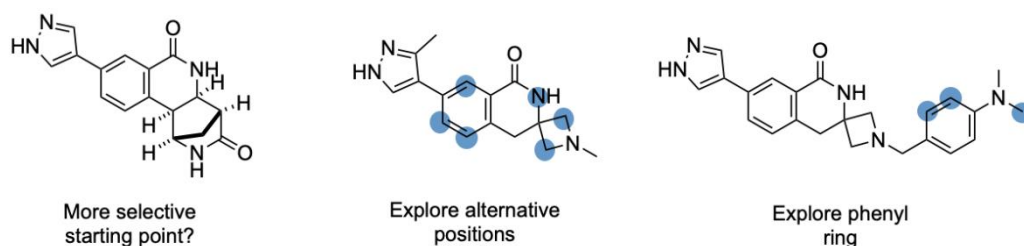
Figure 4-1. Potential approaches for further exploration of the dihydroisoquinolinone SAR developed here.

Structural information would also help explain why the addition of any substituent larger than a methyl group onto the pyrazole ring is detrimental for activity. Only a relatively small library varying the 3,5-positions of the pyrazole ring was synthesised here. Therefore, the synthesis of a larger library, exploring different groups may be beneficial. As mentioned previously, alternative heterocycles other than pyrazole have yet to be explored. These alternative motifs may allow growth along the extended hinge region without disruption of any already present interactions. Optimisation of the pyrazole ring itself could be achieved by exploring common hinge scaffolds or merging the hinge binding motifs of other known Nek7 inhibitors (Chapter 1) with the dihydroisoquinolinone core.
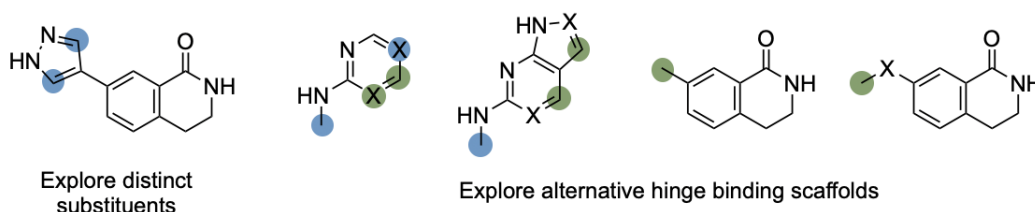
Figure 4-2. Potential approaches for further exploration of the pyrazole SAR developed here.

Chapter 5
Experimental

5.1 Experimental for Compound Synthesis

5.1.1 General Experimental

Commercially available starting materials were obtained from Sigma-Aldrich, Alfa Aesar, Fluorochem, Enamine BB (EU), Fisher Scientific or Insight Biotechnology. All non-aqueous reactions were carried out under an atmosphere of nitrogen unless otherwise stated and water-sensitive reactions were performed in anhydrous solvents (obtained from a PureSolv MD5 Purification System) in oven- or flame-dried glassware, cooled under nitrogen before use. Anhydrous dimethyl sulfoxide (DMSO), anhydrous 1,2-dichloroethane, anhydrous dimethylformamide (DMF) and anhydrous 1,4-dioxane were obtained from SureSeal bottles from Sigma−Aldrich. All other solvents and reagents were of chromatographic or analytical grade and used as supplied. Ether refers to diethyl ether and petrol refers to petroleum spirit (b.p. 40-60 °C) unless otherwise stated. Solvents were removed under reduced pressure using an IKA RV 10 rotary evaporator with a Vacuubrand PC2001 Vario diaphragm pump.

Flash column chromatography was carried out using silica gel 60 (35-70 μm particles) supplied by Merck. Flash column chromatography was also carried out on Isolera One or Four (Biotage) instruments using SNAP KP-SIL or Sfär silica D duo cartridges 5-50 g, 60 μm. Thin layer chromatography was carried out using commercially available pre-coated aluminium plates (Merck silica gel 60 F254). Ultraviolet lamp (λ_{max} = 254 nm) and $KMnO_4$ were used for visualisation.

Analytical LC-MS was performed using a system comprising an Ultimate3000 HPLC instrument with a Brucker Amazon Speed MS detector with electrospray ionisation. The system ran with a positive and negative switching mode and UV diode array detector using a Phenomenex Kinetex C18 (50 mm × 2.1 mm × 2.6 μm) column and gradient elution with two binary solvent systems: $MeCN/H_2O$ or $MeCN/H_2O$ plus 0.1% formic acid and a run time of

1.7 minutes (1 minute gradient). Preparative LC-MS was performed using an Agilent Technologies Infinity (1260) instrument with a UV diode array detector and an Agilent 6100 series Single Quad MS detector. The system used a Phenomenex Kinetex C18 EVO 21.2 × 250 mm 5 micron column. The general preparation method used a solvent system of 5:95 → 95:5 MeCN/H2O plus 0.1% formic acid and a run time of 15 or 35 minutes (10 or 30 minute gradient). Accurate mass spectrometry was performed using electrospray ionisation on a Bruker MaXis Impact spectrometer.

^{1}H and ^{13}C NMR spectra were collected on a Bruker 300 (AV3 NMR spectrometer operating at 7.0 T and equipped with a 5 mm BBO probe), Bruker 400 (AV3HD NMR spectrometer operating at 9.4 T and equipped with a 5 mm BBO probe) or Bruker 500 (AV-NEO NMR spectrometer operating at 11.7 T and equipped with a 5 mm DCH cryoprobe or BBO probe) MHz spectrometer. Data was collected at 298 K unless otherwise stated. Chemical shifts are quoted in parts per million down field of trimethylsilane and coupling constants (*J*) are given in Hz. Assignment of NMR signals was aided by the use of DEPT 135, COSY, HSQC, HMBC and NOESY. Splitting patterns have been abbreviated as follows: app (apparent), br (broad), s (singlet), d (doublet), dd (doublet of doublets), t (triplet), q (quartet), m (multiplet).

Infrared spectra were recorded on a Bruker Alpha ATR FR-IR spectrometer; absorptions are reported in wavenumber (cm^{-1}).

5.1.2 General Procedures

General Procedure A: Synthesis of 3,4-Dihydroisoquinolinones

According to a modified procedure,[144] and without any precautions to extrude oxygen or moisture, the pivaloyl-protected hydroxamic acid (1 equiv.), [Cp*RhCl$_2$]$_2$ (3-3.5 mol%) and CsOAc (2 equiv.) were added to a screw-top vial equipped with a stir bar. MeOH (0.2 M) was then added followed by the alkene (1.1-1.5 equiv.) (if the alkene was solid, it was added prior to the MeOH). The reaction was sealed with the screw-top septum and stirred at 65 °C. For alkenes with boiling points close to the reaction temperature, the reaction was performed at 45 °C with 3.8 equiv. of alkene (see specific examples below). After 18 hours, the reaction was adsorbed onto silica and purified by flash column chromatography (see specific conditions provided for

each compound). The purified compound was then dissolved in MeCN and washed with petrol to remove residual pivalic acid.

General Procedure B: Deprotection

Trifluoroacetic acid (12.5% v/v) was added to a solution of the protected isoquinolinone (1 equiv.) in CH_2Cl_2 (0.1 M) and the reaction was stirred at room temperature. After consumption of the starting material by TLC, the reaction was concentrated under reduced pressure to give the product which was used without further purification.

General Procedure C: HATU Amide Coupling

According to a modified procedure,[174] DIPEA (1.1 equiv.) was added dropwise to a solution of the carboxylic acid (1 equiv.) and HATU (1.2 equiv.) in DMF (0.145 M) and the mixture was stirred at room temperature. After a few minutes, a solution of the ammonium (1.25 equiv.) and DIPEA (2.5 equiv.) in a minimum amount of DMF (which had previously been stirring for 1 hour at room temperature) was added dropwise to the carboxylate solution. The reaction mixture was stirred at room temperature for an additional 1 hour. After which, the mixture was diluted with EtOAc (7 ml/mmol) and washed with LiCl (3 x, each with 10 x the volume of DMF). The organic layer was dried ($MgSO_4$), filtered and concentrated under reduced pressure to give a crude product.

General Procedure D: Suzuki-Miyaura Coupling

According to a modified procedure,[136] the heteroaryl boronate ester (1.1 equiv.), [Pd_2dba_3] (5 mol%) and PCy_3 (12 mol%) were charged to a reaction vessel with a stir bar in air. The vessel was sealed, flushed with nitrogen for 15 minutes and anhydrous 1,4-dioxane (0.4 M) and the aryl halide (1 equiv.) were added (if the aryl halide was solid, it was added prior to flushing with nitrogen) to give a deep red solution. K_3PO_4 (1.7 equiv.) was dissolved in de-ionised water (1.27 M), which had first been degassed *via* vigorous bubbling with nitrogen, and added to the reaction mixture. The mixture was then heated at 100 °C for 24 hours with vigorous stirring. After which, the mixture was cooled, filtered through a pad of celite (eluting with EtOAc) and concentrated under reduced pressure. The aqueous residue was extracted with EtOAc (3 x

20 ml/mmol) and the combined organics were dried (MgSO$_4$), filtered and concentrated under reduced pressure to give a crude product.

General Procedure E: Suzuki-Miyaura Coupling

According to a modified procedure,[135] the aryl boronate (0.9-1.2 equiv.), K$_2$CO$_3$ (2 equiv.), Bu$_4$NBr (1 mol%) and heteroaryl halide (1 equiv.) were charged to a reaction vessel with a stir bar in air. The vessel was sealed, flushed with nitrogen for 15 minutes and de-ionised water (0.5 M), which had first been degassed *via* vigorous bubbling with nitrogen, followed by PdCl$_2$–EDTA (0.01 M, 0.1 mol%) were added to the reaction mixture. The reaction was heated to 100 °C, upon which the red-brown suspension turned black, for the specified time. After which, a light yellow solution was produced and the mixture was cooled and worked-up using the procedure for the specific examples below to give a crude product.

General Procedure F: Pyrazole Protection

According to a modified procedure,[175] ethyl vinyl ether (1.5 equiv.) was added to a suspension of the pyrazole (1 equiv.) in toluene (0.5 M). The resulting suspension was treated with 4 M HCl in 1,4-dioxane (0.025 equiv.), added dropwise over 5 minutes, and the reaction mixture was heated to 40 °C usually resulting in rapid dissolution of solids to give a clear yellow solution. The mixture was stirred at 40 °C until consumption of the pyrazole by TLC (see specific examples for the reaction times). After which, solid NaHCO$_3$ (0.25 equiv.) was added to the cooled solution and the suspension stirred at room temperature for 1 hour. The mixture was then filtered and concentrated under reduced pressure to give a crude product.

General Procedure G: Acetylation with Acetic Anhydride

Triethylamine (3.5 equiv.) followed by acetic anhydride (2.5 equiv.) was added in a dropwise manner to a solution of the amine or ammonium salt (1 equiv.) in CH$_2$Cl$_2$ (0.2 M) at 0 °C under nitrogen. If an amine is used, only 2.5 equiv. of triethylamine was used. After stirring at room temperature overnight, the reaction was quenched with a sat. solution of NaHCO$_3$ (20 ml/mmol) and diluted with CH$_2$Cl$_2$ (20 ml/mmol). The organic layer was separated, washed with a sat. solution of NaHCO$_3$ (2 x 20 ml/mmol), H$_2$O (20 ml/mmol) and brine

(20 ml/mmol) and dried (MgSO$_4$), filtered and concentrated under reduced pressure. The resultant crude product was re-dissolved in MeOH (0.2 M) and solid NaHCO$_3$ (2 equiv.) was added to remove the acetyl group from the pyrazole. The mixture was stirred overnight at room temperature, filtered and concentrated under reduced pressure to give a crude product.

General Procedure H: Reductive Amination

According to a modified procedure,[ref] without any precautions to extrude oxygen or moisture, triethylamine (1 equiv.) was added to a suspension of the amine or ammonium salt (1 equiv.) in DCE (0.2 M). If the amine is used triethylamine was omitted. Methanol was added dropwise until a clear solution was obtained followed by glacial acetic acid (0-1 equiv.) and the aldehyde or ketone (0.9-1.5 equiv.). The mixture was stirred for 5 min at room temperature before addition of STAB (1-3 equiv.). The mixture was stirred at room temperature until consumption of the ammonium salt by TLC or overnight (additional equivalents of STAB can be added as necessary) and concentrated under reduced pressure to give a crude product.

General Procedure I: Synthesis of Diazo Compounds by Acylation and Elimination

Developed from syntheses of α-diazoacetic esters,[117–120] 2-[(4-methylbenzenesulfonamido)imino]acetic acid, (1 equiv.) was dissolved in anhydrous toluene (0.4 M) and purged with N$_2$ for 5 min. SOCl$_2$ (2 equiv.) was added dropwise at rt and the solution was stirred vigorously and slowly heated to 90 °C over 30 min. After 4 h, the reaction mixture was cooled to rt, the solvent was removed under reduced pressure and the crude product was dried under vacuum. The crude product (1 equiv.) was dissolved in anhydrous CH$_2$Cl$_2$ (0.4 M) and cooled to 0 °C under N$_2$. The amine (1-1.1 equiv.) and dimethylaniline (1-1.5 equiv.) were added simultaneously and the reaction mixture was stirred for 90 min at rt. After which Et$_3$N (5 equiv.) was added dropwise over 10 min at 0 °C. The reaction mixture was allowed to gradually return to rt and the solution was stirred overnight. The reaction mixture was washed with aqueous sodium bicarbonate solution and brine solution successively. The organic layer was collected, dried (MgSO4), filtered and concentrated under reduced pressure to afford the crude diazo amide.

General Procedure J: Diazo Transfer

According to procedures,[116,122,123] a solution of dicarbonyl compound (1 equiv.) and p-ABSA (1.5 equiv.) in anhydrous MeCN was cooled to −10 °C. Et_3N (1.2 equiv.) was added dropwise over 5–10 min and the mixture was stirred at RT under a N_2 atmosphere. After 0.5–1 h (when a solid precipitated out of solution and the starting material had been consumed according to TLC), the solvent was removed under reduced pressure and the crude residue was dissolved in Et_2O (30 mL/mmol), filtered and the resulting solid rinsed with CH_2Cl_2 (30 mL/mmol). The filtrate was concentrated under reduced pressure to give a crude product.

General Procedure K: Acylation Followed by Diazo Transfer

According to procedures,[99,100,116,122,123] whilst stirring at rt, 2,2,6-trimethyl-4H-1,3-dioxin-4-one (1.1 equiv.) was added to a solution of aniline (1 equiv.) in anhydrous toluene and the mixture was reacted under microwave irradiation (110 °C, max 200 W, max 300 psi). After 2 h, the solvent was removed under reduced pressure and p-ABSA (1.5 equiv.) was added followed by anhydrous MeCN (0.12 M) under an atmosphere of N_2. The solution was cooled to 0 °C, Et_3N (1.2 equiv.) was added dropwise over 5–10 min and the mixture was stirred at rt for 4 h. After which, the solvent was removed under reduced pressure to give a crude product.

General Procedure L: Acetylation with an Acyl Chloride

According to a modified procedure,[176] a solution of acyl chloride (1 equiv.) in THF (0.4 M) was cooled to 0 °C under nitrogen. Na_2HPO_4 (2.5 equiv.) was added in one portion followed by the addition of amine (1 equiv.) over 5 min and the mixture was allowed to react at rt. After 1 h, the reaction was quenched with water (10 ml/mmol) and the resulting mixture was extracted with EtOAc (3 x 20 ml/mmol). The combined organic layers were washed with sat. aq. brine soln. (20 ml/mmol), dried ($MgSO_4$), filtered and concentrated under reduced pressure to give a crude product.

5.1.3 Synthesis of Substrates and Co-substrates for Activity-Directed Synthesis

Ethyl 2,5-dimethyl-1*H*-pyrrole-3-carboxylate, 2-14
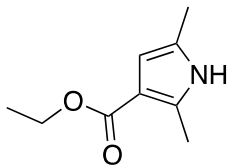
Following a modified procedure,[108] DMAP (4.40 mg, 0.36 mmol) and EtOH (2.10 ml, 36.0 mmol) were added sequentially to a mixture of 2,5-dimethyl-1H-pyrrole-3-carboxylic acid, 17, (500 mg, 3.60 mmol) and DCC (740 mg, 3.60 mmol) in THF (10 ml) under nitrogen. The reaction was heated at 60 °C for 24 h, the reaction was then cooled to room temperature and the precipitate filtered and washed with THF. Water (10 ml) was added to the filtrate and extracted with EtOAc (3 × 10 ml). The combined organics were dried (MgSO$_4$), filtered and concentrated under reduced pressure to give the crude product which was purified by flash column chromatography, eluting with 30:70 EtOAc–petrol to give the *pyrrole-carboxylate*[177] (330 mg, 55%) as a colourless amorphous solid. δ_H (400 MHz, CDCl$_3$) 8.13 (1H, br s, N–H), 6.20 (1H, app dd, *J* 2.9, 1.2, 4–H), 4.25 (2H, q, *J* 7.1, ethyl 1–H), 2.47 (3H, s, methyl 5–H), 2.19 (3H, s, methyl 2–H), 1.32 (3H, t, *J* 7.1, ethyl 2–H). δ_C (101 MHz, CDCl$_3$) 166.0, 134.4, 125.7, 111.7, 107.6, 59.3, 14.6, 13.2, 12.7. IR v_{max} (neat)/cm^{-1} 3288, 3191, 2980, 2923, 2861, 2747, 1656 and 1599. R_F 0.56 (30:70 EtOAc–petrol). HRMS (ESI): C$_9$H$_{13}$NO$_2$ requires [M+Na]$^+$, calculated 190.0844, found 190.0839.

Ethyl 4-formyl-2,5-dimethyl-1*H*-pyrrole-3-carboxylate, 2-15
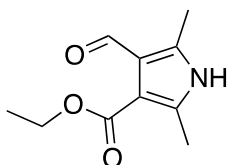
Following a modified procedure,[109] POCl$_3$ (0.74 ml, 7.94 mmol) was added to a solution of DMF (0.77 ml, 9.93 mmol) at 0 °C under a nitrogen atmosphere and stirred for 30 min. 1,2-DCE (3 ml) was added followed by ethyl 2,5-dimethyl-1H-pyrrole-3-carboxylate, (0.83 g, 4.96 mmol) dissolved in 1,2-DCE

(12 ml) and the mixture was heated at reflux for 45 min. After cooling, a solution of NaOAc·3H$_2$O (3.38 g, 24.8 mmol) in water (7.2 ml) was added and the reaction mixture was heated again at reflux for 80 min. The mixture was cooled to room temperature and the product was extracted with CH$_2$Cl$_2$ (3 × 20 ml) and the combined organic layers were washed with water (3 × 10 ml), dried (MgSO$_4$), filtered and evaporated under reduced pressure. The resulting crude product was purified by flash column chromatography eluting, with 50:50 EtOAc–petrol to give the *pyrrole-carboxylate*[109] (0.79 g, 82%) as a light yellow amorphous solid. δ_H (400 MHz, DMSO) 11.78 (1H, br s, N–H), 10.27 (1H, s, formyl–H), 4.21 (2H, q, *J* 7.1, ethyl 1–H), 2.38 (3H, s, methyl–H), 2.37 (3H, s, methyl–H), 1.27 (3H, t, *J* 7.1, ethyl 2–H). δ_C (101 MHz, DMSO) 189.0, 164.8, 135.5, 135.3, 120.0, 111.1, 59.7, 14.7, 13.3, 13.2. IR v_{max} (neat)/cm^{-1} 3084, 2984, 2922, 2849, 1698, 1634 and 1587. R_F 0.46 (50:50 EtOAc–petrol). HRMS (ESI): C$_{10}$H$_9$NO$_3$ requires [M+Na]$^+$, calculated 218.0793, found 218.0790.

5,7-Dimethyl-2*H*,6*H*-pyrrolo[3,4-d]pyridazin-1-one, 2-2
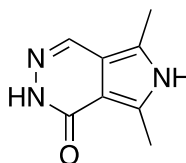
Following a modified procedure,[178] ethyl 4-formyl-2,5-dimethyl-1H-pyrrole-3-carboxylate, (0.82 g, 4.20 mmol) and hydrazine monohydrate (3.40 ml, 42.0 mmol) in EtOH (35 ml) were heated to reflux overnight. After which, the reaction mixture was cooled to room temperature and concentrated under reduced pressure. CH$_2$Cl$_2$ (50 ml) and water (50 ml) were added and the precipitated product was collected, washed with water and dried under reduced pressure. The aqueous filtrate was extracted with CH$_2$Cl$_2$ (3 × 50 ml) and the combined organic fractions were washed with brine (25 ml), dried (MgSO$_4$), filtered and concentrated under reduced pressure. The crude product was purified by flash column chromatography, eluting with 2:98 MeOH–EtOAc concentrated and combined with the precipitated product to give the *pyridazinone*[178] as a colourless amorphous solid (0.57 g, 84%). δ_H (400 MHz, DMSO) 12.02 (1H, br s, pyrrole N–H), 11.12 (1H, s, amide N–H), 7.97 (1H, s, 4–H), 2.52 (3H, s, methyl–H), 2.38 (3H, s, methyl–H). δ_C (101

MHz, DMSO) 160.8, 134.3, 126.5, 121.6, 115.8, 110.8, 12.2, 10.9. IR v_{max} (neat)/cm^{-1} 3395, 3133, 2984, 2853, 1618 and 1580. R_F 0.23 (2:98 MeOH–EtOAc). HRMS (ESI): $C_8H_{10}N_3O$ requires [M+H]$^+$, calculated 164.0824, found 164.0816.

6-Methyl-3*H*-quinazolin-4-one, 2-3
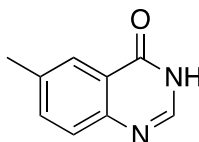
Following a modified procedure,[110] formamide (0.79 ml, 19.8 mmol) was added to 2-amino-5-methylbenzoic acid (500 mg, 3.30 mmol) to produce a thick suspension which was heated to 140 °C for 5 h, during which the solution became clear followed by the gradual precipitation of a solid out of solution. When no liquid remained (after 5 h), ice was added to the reaction mixture and the solid was filtered, washed with water, dissolved in MeOH and concentrated under reduced pressure to give the crude product which was purified by precipitation from EtOH to give the *quinazolinone*[110] as a colourless amorphous solid (310 mg, 58 %). δ_H (400 MHz, DMSO) 12.14 (1H, br s, N–H), 8.03 (1H, s, 2–H), 7.92 (1H, app s, 5–H), 7.62 (1H, app d, *J* 8.1, 7–H), 7.56 (1H, d, *J* 8.1, 8–H), 2.43 (3H, s, methyl–H). δ_C (101 MHz, DMSO) 160.6, 146.7, 144.5, 136.4, 135.5, 127.1, 125.2, 122.4, 20.8. R_F 0.11 (50:50 EtOAc–petrol). IR v_{max} (neat)/cm^{-1} 3125, 3024, 2920, 2795, 2717, 2627, 1689, 1655 and 1607. HRMS (ESI): $C_9H_9N_2O$ requires [M+H]$^+$, calculated 161.0715, found 161.0710.

N-(1*H*-indazol-5-yl)furan-2-carboxamide, 2-4
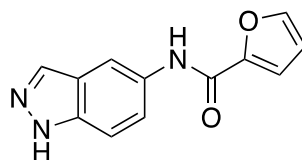
According to general procedure L, furoyl chloride (0.21 ml, 2.14 mmol) with *tert*-butyl 5-aminoindazole-1-carboxylate (0.50 g, 2.14 mmol) gave a crude product which was dissolved in chloroform (26 ml) and TFA (6.6 ml, 86.20 mmol) was added. After stirring overnight, most of the solvent was removed under reduced pressure and the pH was adjusted to 7 with sat. aq. brine soln.

The resulting mixture was extracted with CH_2Cl_2 (3 × 50 ml) and the combined organic layers were washed with sat. aq. brine soln. (15 ml), dried ($MgSO_4$), filtered and concentrated under reduced pressure. The resulting crude product was purified by flash column chromatography, eluting with 2:98 → 10:90 MeOH–CH_2Cl_2 to give the *carboxamide* (355 mg, 73% over two steps) as a light brown amorphous solid. δ_H (400 MHz, DMSO) 13.01 (1H, s, N–H), 10.18 (1H, s, amide N–H), 8.20 (1H, d, *J* 1.8, indazolyl 4–H), 8.06 (1H, s, indazolyl 3–H), 7.92 (1H, dd, *J* 1.7, 0.7, 5–H), 7.63 (1H, dd, *J* 8.9, 1.8, indazolyl 6–H), 7.52 (1H, d, *J* 8.9, indazolyl 7–H), 7.32 (1H, dd, *J* 3.5, 0.7, 3–H), 6.70 (1H, dd, *J* 3.5, 1.7 4–H). δ_C (101 MHz, DMSO) 156.2, 147.7, 145.5, 137.1, 133.5, 131.3, 122.7, 121.4, 114.3, 112.1, 111.3, 110.0. R_F 0.07 (50:50 EtOAc–petrol). IR v_{max} (neat)/cm^{-1} 3259, 2923, 2851, 1759, 1644 and 1595. HRMS (ESI): $C_{12}H_9N_3O_2$ requires [M+Na]$^+$, calculated 250.0593, found 250.0587.

2-[(4-Methylbenzenesulfonamido)imino]acetic acid, 2-20
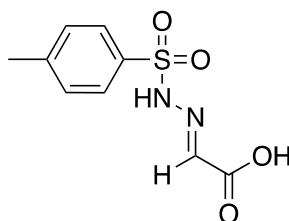
According to a modified procedure,[120,116] glyoxylic acid (7.40 g, 80.6 mmol) followed by *p*-toluene sulfonyl hydrazide (10.0 g, 53.7 mmol) were charged to a round bottom flask and flushed with nitrogen. Anhydrous THF (60 ml) was added and the reaction mixture was stirred at room temperature. After 24 h, the solvent was evaporated under reduced pressure to produce a colourless oil which solidified and the resulting solid was triturated with water (60 ml) to give a suspension which was filtered, washed with water and dried under reduced pressure to give the *acetic acid*[116,120] (7.30 g, 56%) as a colourless amorphous solid. δ_H (400 MHz, Acetone) 8.50 (1H, s, imino–H), 7.70 (2H, d, *J* 8.2, 2– and 6–H), 7.36 (2H, d, *J* 8.2, 3– and 5–H), 2.43 (3H, s, methyl–H). δ_C (101 MHz, Acetone) 144.8, 136.5, 130.3, 129.1, 21.5. IR v_{max} (neat)/cm^{-1} 3549, 3463, 3031, 2864, 2648, 1694 and 1587. HRMS (ESI): $C_9H_{10}N_2O_4S$ requires [M+Na]$^+$, calculated 265.0259, found 265.0252.

2-Diazo-*N*-(3-methyl-1,2-oxazol-5-yl)acetamide, 2-7
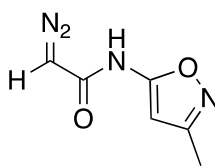
According to general procedure I, 2-[(4-methylbenzenesulfonamido)imino]acetic acid, (2.00 g, 8.26 mmol), 5-amino-3-methylisoxazole (810 mg, 8.26 mmol) and dimethylaniline (1.00 ml, 8.26 mmol) gave a crude dark orange oil which was purified by flash column chromatography, eluting with 4:96 MeOH–CH_2Cl_2 to give the *acetamide*[116] (150 mg, 11%) as a light yellow solid. δ_H (400 MHz, Acetone) 10.18 (1H, br s, N–H), 6.13 (1H, s, oxazolyl–H), 5.59 (1H, s, 2–H), 2.19 (3H, s, methyl–H). δ_C (101 MHz, Acetone) 161.8, 161.3, 160.7, 87.8, 48.4, 10.7. R_F 0.22 (4:96 MeOH–CH_2Cl_2). IR v_{max} (film)/cm^{-1} 3203, 3142, 3103, 3026, 2104, 1646 and 1541. HRMS (ESI): $C_6H_6N_4O_2$ requires [M+H]$^+$, calculated 167.0569, found 167.0531.

2-Diazo-*N*-[3-(trifluoromethyl)phenyl]acetamide, 2-11
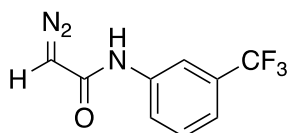
According to general procedure I, 2-[(4-methylbenzenesulfonamido)imino]acetic acid, (2.00 g, 8.26 mmol), 3-(trifluoromethyl)aniline (1.10 ml, 9.10 mmol) and dimethylaniline (1.60 ml, 12.4 mmol) gave a crude dark orange oil which was purified by column chromatography eluting with CH_2Cl_2 to give the *acetamide* (146 mg, 11 %) as a light yellow solid. δ_H (400 MHz, Methanol) 7.96 (1H, app s, phenyl 2–H), 7.66 (1H, d, *J* 8.0, phenyl 6–H), 7.45 (1H, t, *J* 8.0, phenyl 5–H), 7.31 (1H, d, *J* 8.0, phenyl 4–H), 5.33 (1H, s, 2–H). δ_C (101 MHz, Methanol) 167.00, 141.24, 132.18 (q, *J* 32.1), 130.69, 125.5 (q, *J* 271.4), 123.51, 120.70 (q, *J* 4.0), 116.80 (q, *J* 4.0), 49.33. R_F 0.25 (CH_2Cl_2). IR v_{max} (film)/cm^{-1} 3290, 3242, 3163, 3093, 2097, 1598 and 1560. HRMS (ESI): $C_9H_6F_3N_3O$ requires [M+H]$^+$, calculated 230.0541, found 230.0534.

N-(4-chlorophenyl)-2-diazo-*N*-methyl-3-oxobutanamide, 2-6
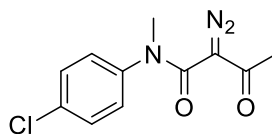
According to a modified procedure,[99,100,116] anhydrous toluene (10 ml) was added to a large microwave vessel and placed under a nitrogen atmosphere. 4-chloro-N-methylaniline (1.70 ml, 14.1 mmol) and 2,2,6-trimethyl-1,3-dioxin-4-one (2.10 ml, 15.5 mmol) were added sequentially whilst stirring. The mixture was then reacted under microwave conditions (110 °C temperature, 200 W maximum power and 300 psi maximum pressure) for 2 h. After which, the solvent was removed under reduced pressure and *p*-ABSA (5.00 g, 21.2 mmol) was added to the resulting solid. The flask was placed under nitrogen atmosphere and anhydrous MeCN (56 ml, 0.25 M) was added. The solution was cooled to 0 °C and NEt_3 (3.93 ml, 28.2 mmol) was added dropwise, the solution became light orange upon addition of NEt_3 and the reaction mixture was left to stir at room temperature overnight. The resulting deep red solution was concentrated under reduced pressure and purified by flash column chromatography, eluting with 50:50 EtOAc–petrol to give the *oxobutanamide*[116] (1.28 g, 36% over two steps) as a light yellow oil which solidified upon standing. δ_H (400 MHz, Acetone) 7.54-7.41 (4H, m, phenyl–H), 3.34 (3H, s, methyl–H), 2.37 (3H, s, oxobutanamide–H). δ_C (101 MHz, Acetone) 190.3, 160.3, 142.5, 132.4, 129.9, 128.0, 73.2, 37.4, 27.3. R_F 0.4 (50:50 EtOAc–petrol). IR v_{max} (neat)/cm^{-1} 3097, 2925, 2106, 1624 and 1586. HRMS (ESI): $C_{11}H_{10}ClN_3O_2$ requires $[M+Na]^+$, calculated 274.0359, found 274.0349.

2-(-λ5-Diazynylidene)-2,3-dihydro-1*H*-indene-1,3-dione, 2-5a
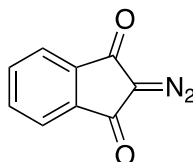
According to General Procedure J, 1H-indene-1,3(2H)-dione (500 mg, 3.4 mmol) gave a crude product which was purified by flash column chromatography, eluting with CH_2Cl_2 to give the *dione*[116,179] (446 mg, 76%) as a yellow amorphous solid. δ_H (500 MHz, CD_2Cl_2) 7.84-7.79 (2H, m, 4– and 7–

H), 7.78-7.74 (2H, m, 5– and 6–H). δ_C (126 MHz, CD_2Cl_2) 182.39, 137.57, 135.17, 122.88, 70.39. R_F 0.4 (50:50 EtOAc–petrol). IR v_{max} (neat)/cm^{-1} 2119, 1688, 1594, 1350, 1329 and 1265. Spectroscopic data match previously reported.[116,179]

5-(-λ5-Diazynylidene)-1,3-dimethyl-1,3-diazinane-2,4,6-trione, 2-5b
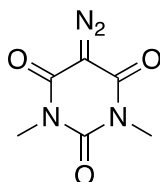
According to General Procedure J, 1,3-dimethyl-1,3-diazinane-2,4,6-trione (1.00 g, 6.4 mmol) gave a crude product which was purified by flash column chromatography, eluting with 50:50 EtOAc–petrol to give the trione[116,179,180] (1.03 g, 88%) as a pale yellow amorphous solid. δ_H (500 MHz, CD_2Cl_2) 3.27 (6H, s, dimethyl–H). δ_C (126 MHz, CD_2Cl_2) 158.5, 150.9, 71.9, 28.6. R_F 0.55 (50:50 EtOAc–petrol). IR v_{max} (neat)/cm^{-1} 2155, 1710, 1638, 1468 and 1415. Spectroscopic data match previously reported.[116,179,180]

5-(-λ5-Diazynylidene)-2,2-dimethyl-1,3-dioxane-4,6-dione, 2-5c
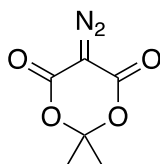
According to General Procedure J, 2,2-dimethyl-1,3-dioxane-4,6-dione (0.50 g, 3.50 mmol) gave a crude product which was purified by flash column chromatography, eluting with CH_2Cl_2 to give the dione[116,179,181,182] (0.54 g, 91%) as a colourless amorphous solid. δ_H (500 MHz, CD_2Cl_2) 1.76 (6H, s, dimethyl–H). δ_C (126 MHz, CD_2Cl_2) 158.65, 107.40, 64.39, 26.95. R_F 0.38

(CH$_2$Cl$_2$). IR v_{max} (neat)/cm^{-1} 2175, 1706, 1308, 1296 and 1191. Spectroscopic data match previously reported.[116,179,181,182]

3-(-λ5-Diazynylidene)piperidine-2,4-dione, 2-5d
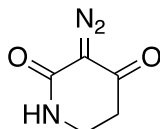
According to General Procedure J, piperidine-2,4-dione (0.50 g, 4.42 mmol) gave a crude product which was purified by flash column chromatography, eluting with 10:90 MeOH–CH$_2$Cl$_2$. Further purification by flash column chromatography, eluting with Et$_2$O gave the *dione*[116,183] (204 mg, 33%) as a colourless amorphous solid. δ_H (500 MHz, CD$_2$Cl$_2$) 6.96 (1H, s, N–H), 3.45 (2H, td, J 6.5, 2.8, 6–H), 2.60 (2H, t, J 6.5, 5–H). δ_C (126 MHz, CD$_2$Cl$_2$) 188.56, 163.72, 75.41, 37.36, 36.68. R_F 0.08 (Et$_2$O). IR v_{max} (neat)/cm^{-1} 3183, 3045, 2905, 2150, 1650, 1461 and 1416. Spectroscopic data match previously reported.[116,183]

5-Chloro-3-(-λ5-diazynylidene)-2,3-dihydro-1*H*-indol-2-one, 2-6a
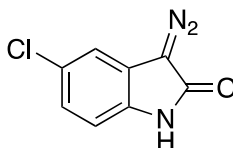
According to a modified procedure,[184] a mixture of 5-chloroisatin (500 mg, 2.75 mmol) and *p*-toluenesulfonyl hydrazide (538 mg, 2.89 mmol) in THF (4 ml, 0.68 M) was stirred at 65 °C for 1 h. After which, the mixture was cooled slightly and filtered whilst still warm. The resultant solid was re-suspended in 0.2 M NaOH (21 ml) and stirred at 65 °C for 1 h. After cooling to rt, the reaction mixture was neutralised with dry ice and filtered to give the *indolone*[185] (436 mg, 82%) as a red-orange amorphous solid which was used without further purification. δ_H (501 MHz, DMSO-d_6) 10.78 (1H, s, N–H), 7.56 (1H, d, J 2.1, 4–H), 7.11 (1H, dd, J 8.3, 2.1, 6–H), 6.89 (1H, d, J 8.3, 7–H). δ_C (126 MHz, DMSO-d_6) 167.86, 131.83, 125.71, 125.20, 119.56, 119.49, 111.48, 61.18. R_F 0.33 (50:50 EtOAc–petrol). HRMS (ESI): C$_8$H$_4$ClN$_3$O requires [M+H]$^+$,

calculated 194.0116, found 194.0112. Spectroscopic data match previously reported.[185]

3-Chloro-4-methoxy-*N*-methylaniline
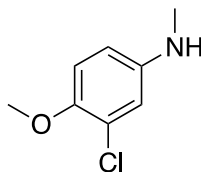
3-chloro-4-methoxyaniline (0.86 ml, 7.00 mmol) was added dropwise over 5 min to a suspension of NaOMe (1.89 g, 35 mmol) in MeOH (12 ml) at 0 °C. The resulting light brown solution was cooled to -10 °C and paraformaldehyde (294 mg, 9.80 mmol) in MeOH (8 ml) was added. After stirring at rt overnight, the mixture was cooled to 0 °C and NaBH$_4$ (206 mg, 7.00 mmol) was added portion-wise over 20 min. The mixture was stirred at rt for 20 min prior to heating at reflux for 2 h. After cooling to rt, 1 M KOH (20 ml) was added and the aqueous phase extracted with Et$_2$O (3 x 50 ml). The combined organics were dried (MgSO$_4$), filtered and concentrated under reduced pressure to give a crude product which was purified by flash column chromatography, eluting with 50:50 Et$_2$O–pentane to give the *methylaniline*[186] (0.98 g, 82%) as a light yellow oil. δ_H (501 MHz, Acetone-d_6) 6.91 (1H, d, *J* 8.8, 5–H), 6.65 (1H, d, *J* 2.7, 2–H), 6.53 (1H, dd, *J* 8.8, 2.7, 6–H), 4.79 (1H, br s, N–H), 3.76 (3H, s, methyoxy–H), 2.74 (3H, d, *J* 5.5, N-methyl–H). δ_C (126 MHz, Acetone-d_6) 147.43, 146.27, 123.78, 115.65, 114.26, 112.03, 57.25, 30.94. R_F 0.58 (50:50 Et$_2$O–pentane). HRMS (ESI): C$_8$H$_{10}$ClNO requires [M+H]$^+$, calculated 172.0524, found 172.0521. Spectroscopic data matched previously reported.[186]

N-(3-chloro-4-methoxyphenyl)-2-diazo-*N*-methyl-3-oxobutanamide, 2-6b
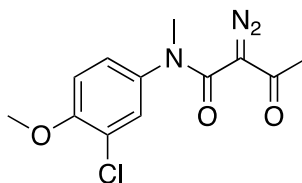
According to General Procedure K, 3-chloro-4-methoxy-N-methylaniline, (600 mg, 3.50 mmol) gave a crude product which was purified by flash column chromatography, eluting with 10:90 Et$_2$O–CH$_2$Cl$_2$ to give the

oxobutanamide[116] as a light yellow, low melting amorphous solid (412 mg, 45% over two steps). δ_H (500 MHz, CD_2Cl_2) 7.27 (1H, d, *J* 2.6, phenyl 2–H), 7.12 (1H, dd, *J* 8.7, 2.6, phenyl 6–H), 6.97 (1H, d, *J* 8.7, phenyl 5–H), 3.91 (3H, s, butanamide–H), 3.29 (3H, s, N-methyl–H), 2.44 (3H, s, methoxy–H). δ_C (126 MHz, CD_2Cl_2) 191.6, 161.1, 155.1, 136.5, 128.7, 126.6, 123.7, 113.2, 74.0, 56.8, 38.7, 28.6. R_F 0.43 (10:90 Et_2O–CH_2Cl_2). IR v_{max} (neat)/cm^{-1} 3360, 2110, 1642, 1499 and 1361. HRMS (ESI): $C_{12}H_{12}ClN_3O_3$ requires [M+Na]$^+$, calculated 304.0460, found 304.0456.

1-(6-Chloro-1,2,3,4-tetrahydroquinolin-1-yl)-2-diazobutane-1,3-dione, 2-6c
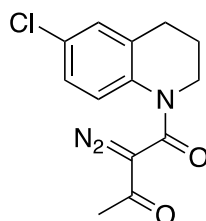
According to General Procedure K, 6-chloro-1,2,3,4-tetrahydroquinoline (500 mg, 3.00 mmol) gave a crude product which was purified by flash column chromatography, eluting with 10:90 Et_2O–CH_2Cl_2 to give the *dione*[116] as a light yellow, low melting amorphous solid (522 mg, 63% over two steps). δ_H (500 MHz, CD_2Cl_2) (1H, d, *J* 8.6, quinolinyl 5–H), 7.25 (1H, d, *J* 2.5, quinolinyl 8–H), 7.17 (1H, dd, *J* 8.6, 2.5, quinolinyl 7–H), 3.75 (2H, t, *J* 6.5, quinolinyl 2–H), 2.74 (2H, t, *J* 6.5, quinolinyl 4–H), 2.32 (3H, s, 4–H), 1.98 (2H, q, *J* 6.5, quinolinyl 3–H). δ_C (126 MHz, CD_2Cl_2) 191.1, 162.5, 138.4, 135.8, 131.7, 129.7, 127.9, 124.9, 77.4, 45.9, 27.6, 27.4, 24.8. R_F 0.43 (10:90 Et_2O–

CH$_2$Cl$_2$). IR v$_{max}$ (neat)/cm^{-1} 2950, 2891, 2107, 1632 and 1484. HRMS (ESI): C$_{13}$H$_{12}$ClN$_3$O$_2$ requires [M+Na]$^+$, calculated 300.0511, found 300.0508.

tris(2,4-Di-tert-butylphenyl)phosphite gold(I) benzonitrile hexafluoroantimonate ([(2,4-(^{t}Bu)$_2$C$_6$H$_3$O)$_3$PAu(PhCN)]SbF$_6$)
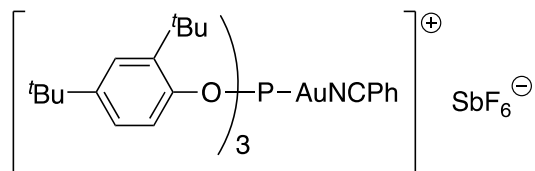
According to a modified procedure,[187] benzonitrile (11 μl, 0.11 mmol) followed by silver hexafluoroantimonate (39 mg, 0.11 mmol) was added to a solution of tris(2,4-di-tert-butylphenyl)phosphite gold(I) chloride (100 mg, 0.11 mmol) in CH$_2$Cl$_2$ (5 ml) and stirred at rt for 1 h. After which, the mixture was filtered to give a colourless solution which was used without further purification.

5.1.4 Synthesis of Compounds for Structure-Activity Relationship Determination

PdCl$_2$ – EDTA

According to procedure,[135] EDTA disodium salt dihydrate (186 mg, 0.5 mmol) and Na$_2$CO$_3$ (106 mg, 1 mmol) were added to a solution of PdCl$_2$ (89 mg, 0.5 mmol) in de-ionised water (5 ml, 0.1M) which had previously been degassed *via* vigorous bubbling with nitrogen and stirred to give a yellow-red solution which was used without further purification.

7-(1*H*-Pyrazol-4-yl)-1,2,3,4-tetrahydroisoquinolin-1-one, 3-3
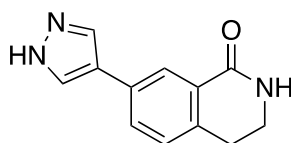
According to General Procedure D, 7-bromo-3,4-dihydro-2H-isoquinolin-1-one (140 mg, 0.62 mmol) gave a crude product which was purified by flash column chromatography, eluting with 0:100 → 10:90 MeOH–CH$_2$Cl$_2$ to give the *isoquinolinone* (116 mg, 88%) as a light yellow amorphous solid. δ_H (400 MHz, DMSO-d_6) 12.97 (1H, s, pyrazolyl N–H), 8.23 (1H, s, amide N–H), 8.03 (1H, d, *J* 1.9, 8–H), 7.94 (2H, br. s, pyrazolyl–H), 7.70 (1H, dd, *J* 7.8, 1.9, 6–H), 7.28 (1H, d, *J* 7.8, 5–H), 3.37 (2H, td, *J* 6.5, 2.9, 3–H), 2.87 (2H, t, *J* 6.5, 4–H). δ_C (101 MHz, DMSO-d_6) 165.0, 137.2, 136.6, 132.0, 130.2, 128.8, 128.4, 126.0, 123.8, 121.1, 39.7, 27.9. R_F 0.30 (10:90 MeOH–CH$_2$Cl$_2$). IR ν_{max} (neat)/cm^{-1} 3471, 3185, 3111, 3051, 2948, 1653 and 1616. HRMS (ESI): C$_{12}$H$_{11}$N$_3$O requires [M+H]$^+$, calculated 214.0975, found 214.0970.

7-(4,4,5,5-Tetramethyl-1,3,2-dioxaborolan-2-yl)-1,2,3,4-tetrahydroisoquinolin-1-one, 3-16
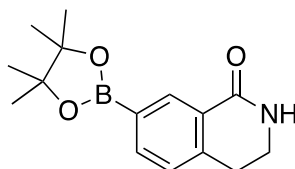
According to a modified procedure,[131] 7-bromo-3,4-dihydro-2H-isoquinolin-1-one (2.50 g, 11.10 mmol), Pd$_2$(dba)$_3$ (0.25 g, 0.28 mmol), XPhos (0.50 g, 1.11 mmol), bis(pinacolato)diboron (3.37 g, 13.27 mmol) and KOAc (3.25 g, 33.18

mmol) were weighed into a round bottom flask fitted with a stir bar in air. The mixture was degassed with nitrogen for 15 minutes before 1,4-dioxane was added. The deep red solution was stirred at 80 °C overnight after which, the reaction mixture was cooled to room temperature, diluted with H_2O (175 ml) and extracted with EtOAc (3 x 250 ml). The combined organics were washed with sat. brine soln. (150 ml), dried (MgSO$_4$), filtered through celite (washing with EtOAc) and concentrated under reduced pressure to give a crude product which was purified by flash column chromatography, eluting with 50:50 → 100:0 EtOAc–petrol to give the isoquinolinone[131] (1.63 g, 54%) as a colourless amorphous solid. δ_H (500 MHz, Methanol-d_4) 8.34 (1H, app. d, J 0.8, 8–H), 7.84 (1H, dd, J 7.5, 1.3, 6–H), 7.30 (1H, app. dq, J 7.5, 0.8, 5–H), 3.50 (2H, t, J 6.7, 3–H), 3.00 (2H, t, J 6.7, 4–H), 1.35 (12H, s, tetramethyl–H). δ_C (126 MHz, Methanol-d_4) 166.8, 142.7, 141.0, 138.1, 133.6, 127.9, 126.7, 83.9, 39.3, 27.8, 23.8. R_F 0.32 (EtOAc). IR ν_{max} (film)/cm^{-1} 3271, 2977, 2941, 1656 and 1608. HRMS (ESI): $C_{15}H_{20}BNO_3$ requires [M+Na]$^+$, calculated 296.1429, found 296.1433.

1-(1-Ethoxyethyl)-4-iodo-1*H*-pyrazole
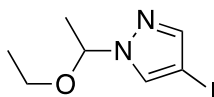
According to General Procedure F, 4-iodopyrazole (5 g, 27.8 mmol), stirring at 40 °C for 30 minutes, gave a crude product which was purified by flash column chromatography, eluting with 10:90 EtOAc–petrol to give the pyrazole[175] (6.2 g, 90%) as a light yellow oil. δ_H (400 MHz, Chloroform-d) 7.58 (1H, s, pyrazolyl–H), 7.42 (1H, s, pyrazolyl–H), 5.42 (1H, q, J 6.0, ethyl 1–H), 3.35 (1H, dq, J 9.5, 7.0, ethoxy 1–H$_A$), 3.23 (1H, dq, J 9.5, 7.0 ethoxy 1–H$_B$), 1.54 (3H, d, J 6.0, ethyl 2–H), 1.04 (3H, t, J 7.0, ethoxy 2–H). δ_C (101 MHz, Chloroform-d) 143.6, 130.6, 87.8, 64.1, 57.5, 22.1, 14.8. R_F 0.36 (10:90 EtOAc–petrol). IR ν_{max} (film)/cm^{-1} 2977, 2935, 2909, 1377, 1305 and 1118. HRMS (ESI): $C_7H_{11}IN_2O$ requires [M+Na]$^+$, calculated 288.9808, found 288.9806.

1-(1-Ethoxyethyl)-4-iodo-3-methyl-1*H*-pyrazole, 3-18
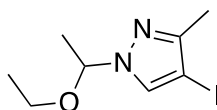
According to General Procedure F, 4-iodo-3-methyl-1H-pyrazole (505 mg, 2.43 mmol), stirring at 40 °C for 2 hours, gave the *pyrazole* (596 mg, 88%) as a colourless amorphous solid, which was used without further purification. δ_H (500 MHz, Chloroform-*d*) 7.38 (1H, s, 5–H), 5.21 (1H, q, *J* 6.0, ethyl 1–H), 3.24 (1H, dq, *J* 9.4, 7.0 ethoxy 1–H_A), 3.14 (1H, dq, *J* 9.4, 7.0, ethoxy 1–H_A), 2.05 (2H, s, methyl–H), 1.42 (3H, d, *J* 6.0, ethyl 2–H), 0.94 (3H, t, *J* 7.0, ethoxy 2–H). δ_C (126 MHz, Chloroform-*d*) 149.9, 131.3, 87.4, 63.9, 60.7, 21.9, 14.7, 13.4. R_F 0.74 (30:70 EtOAc–petrol). IR ν_{max} (film)/cm^{-1} 3184, 2923, 2853, 1658, 1584 and 1433. HRMS (ESI): molecular ion not found.

1-(1-Ethoxyethyl)-4-iodo-3,5-dimethyl-1*H*-pyrazole, 3-21
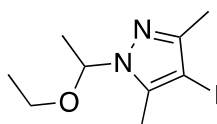
According to General Procedure F, 4-iodo-3,5-dimethyl-1H-pyrazole (540 mg, 2.43 mmol), stirring at 40 °C for 2 hours followed by 50 °C for 1 hour (resulting in dissolution of all solids), gave the *pyrazole* (717 mg, quant.) as a yellow oil, which was used without further purification. δ_H (500 MHz, Chloroform-*d*) 5.45 (1H, q, *J* 6.2, ethyl 1–H), 3.36 (1H, dq, *J* 9.3, 7.0, ethoxy 1–H_A), 3.26 (1H, dq, *J* 9.3, 7.0, ethoxy 1–H_B), 2.33 (3H, s, 5 methyl–H), 2.18 (3H, s, 3 methyl–H), 1.60 (3H, d, *J* 6.2, ethyl 2–H), 1.12 (3H, t, *J* 7.0, ethoxy 2–H). δ_C (126 MHz, Chloroform-*d*) 149.3, 140.2, 87.2, 65.2, 63.5, 21.2, 14.9, 14.1, 12.3. R_F 0.83 (30:70 EtOAc–petrol). IR ν_{max} (film)/cm^{-1} 3400, 2975, 2929, 1534, 1375 and 1324. HRMS (ESI): $C_9H_{15}IN_2O$ requires [M+Na]$^+$, calculated 317.0121, found 317.0112.

4-Bromo-1-(1-ethoxyethyl)-1*H*-pyrazole-3-carbonitrile, 3-20
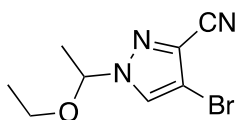
According to General Procedure F, 4-bromo-1H-pyrazole-3-carbonitrile (418 mg, 2.43 mmol) was stirred at 40 °C for 2 hours followed by 45 °C overnight.

An additional 0.5 equiv. ethyl vinyl ether followed by TFA (2 drops) was added and the reaction stirred at 50 °C for 24 hours. A further 1.5 equiv. ethyl vinyl ether and 0.025 equiv. 4 M HCl in 1,4-dioxane were added and the temperature was increased to 60 °C. After stirring for 72 hours at 60 °C, an additional 1.5 equiv. ethyl vinyl ether was added and the reaction was stirred for a further 72 hours at 60 °C. At which point, TLC indicated consumption of the starting material and the crude product was purified by flash column chromatography, eluting with 0:100 → 10:90 EtOAc–petrol to give the *pyrazole* (480 mg, 81%) as a light yellow oil. δ_H (500 MHz, Methanol-d_4) 8.21 (1H, s, pyrazole–H), 5.63 (1H, q, *J* 6.0, ethyl 1–H), 3.55 (1H, dq, *J* 9.4, 7.0, ethoxy 1–H_A), 3.38 (1H, dq, *J* 9.4, 7.0, ethoxy 1–H_B), 1.68 (3H, d, *J* 6.0, ethyl 2–H), 1.18 (3H, t, *J* 7.0, ethoxy 2–H). δ_C (126 MHz, Methanol-d_4) 131.1, 126.9, 113.1, 100.1, 91.0, 65.8, 21.9, 15.0. R_F 0.28 (10:90 EtOAc–petrol). IR ν_{max} (film)/cm^{-1} 3129, 2980, 2932, 2245, 1321 and 1117. HRMS (ESI): molecular ion not found.

4-Bromo-1-(1-ethoxyethyl)-1*H*-pyrazole-3-carboxamide, 3-23
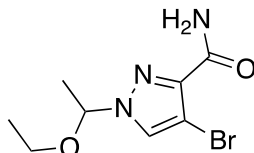
According to a modified procedure,[188] K_2CO_3 (276 mg, 2.00 mmol) followed by H_2O_2 (30% aq. soln., 2 ml, 20.00 mmol) was added to 4-Bromo-1-(1-ethoxyethyl)-1H-pyrazole-3-carbonitrile, (238 mg, 1.00 mmol) dissolved in DMSO (7 ml, 0.15 M). After stirring at rt for 30 min, the off-white suspension resulted in a colourless solution and H_2O (50 ml) and EtOAc (50 ml) were added. The aqueous layer was extracted with EtOAc (3 x 50 ml) and the combined organics were washed with H_2O (25 ml) and brine (sat. aq. soln., 25 ml), dried (MgSO$_4$), filtered and concentrated under reduced pressure to give the *carboxamide* (227 mg, 87%) which was used without further purification. δ_H (500 MHz, Chloroform-*d*) 7.65 (1H, s, 5–H), 6.76 (1H, br s, N–H_A), 6.14 (1H, br s, N–H_B), 5.43 (1H, q, *J* 6.0, ethoxyethyl 1–H), 3.45 (1H, dq, *J* 9.4, 7.0, ethoxy 1–H_A), 3.33 (1H, dq, *J* 9.4, 7.0, ethoxy 1–H_A), 1.62 (3H, d, *J* 6.0, ethoxyethyl 2–H), 1.14 (3H, t, *J* 7.0, ethoxy 2–H). δ_C (126 MHz, Chloroform-*d*) 163.05, 141.15, 129.34, 95.25, 89.17, 64.77, 22.18, 14.81. R_F

0.02 (30:70 EtOAc–petrol). IR ν_{max} (film)/cm^{-1} 3383, 3211, 2980, 1655 and 1608. HRMS (ESI): $C_8H_{12}BrN_3O_2$ requires [M+H]$^+$, calculated 262.0186, found 262.0181.

4-Bromo-1-(1-ethoxyethyl)-3-nitro-1*H*-pyrazole, 3-19
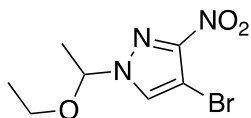
According to General Procedure F, 4-bromo-3-nitro-1H-pyrazole (467 mg, 2.43 mmol), stirring at 40 °C for 2 hours followed by 45 °C for 24 hours, gave a crude product which was purified by flash column chromatography, eluting with 0:100 → 50:50 CH$_2$Cl$_2$–petrol to give the *pyrazole* (465 mg, 73%) as a light yellow amorphous solid. δ_H (501 MHz, Chloroform-*d*) 7.76 (1H, s, pyrazoyle–H), 5.53 (1H, q, *J* 6.0, ethyl 1–H), 3.52 (1H, dq, *J* 9.4, 7.0, ethoxy 1–H$_A$), 3.42 (1H, dq, *J* 9.4, 7.0, ethoxy 1–H$_B$), 1.65 (3H, d, *J* 6.0, ethyl 2–H), 1.18 (3H, t, *J* 7.0, ethoxy 2–H). δ_C (126 MHz, Chloroform-*d*) 151.7, 130.1, 90.9, 90.7, 65.4, 22.4, 14.7. R_F 0.65 (30:70 EtOAc–petrol). IR ν_{max} (film)/cm^{-1} 3131, 2981, 2933, 1543, 1377, 1307 and 1119. HRMS (ESI): $C_7H_{10}BrN_3O_3$ requires [M+Na]$^+$, calculated 285.9798, found 285.9795.

4-Bromo-1-(1-ethoxyethyl)-5-methyl-3-nitro-1*H*-pyrazole, 3-22
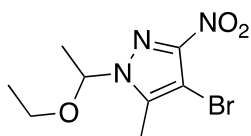
According to General Procedure F, 4-bromo-5-methyl-3-nitro-1H-pyrazole (500 mg, 2.43 mmol) was stirred at 40 °C for 2 hours followed by 45 °C overnight. An additional 0.5 equiv. ethyl vinyl ether followed by TFA (2 drops) was added and the reaction stirred at 50 °C for 24 hours. A further 1.5 equiv. ethyl vinyl ether and 0.025 equiv. 4 M HCl in 1,4-dioxane were added and the reaction was stirred to 60 °C for 72 hours. An additional 1.5 equiv. ethyl vinyl ether was added and the reaction was stirred for a further 96 hours at 60 °C. A further 1.5 equiv. ethyl vinyl ether was added and the reaction stirred for 72 hours at 60 °C followed by an additional 1.5 equiv. ethyl vinyl ether. The reaction was stirred at reflux overnight after which point, TLC indicated

consumption of the starting material. The crude product was purified by flash column chromatography, eluting with 0:100 → 100:0 CH_2Cl_2–petrol and flushing with 5:95 MeOH–CH_2Cl_2 to give the *pyrazole* (251 mg, 37%) as a light yellow oil. δ_H (501 MHz, Methanol-d_4) 5.74 (1H, q, *J* 6.0, ethyl 1–H), 3.51 (1H, dq, *J* 9.2, 7.0, ethoxy 1–H_A), 3.36 (1H, dq, *J* 9.2, 7.0, ethoxy 1–H_B), 2.48 (3H, s, methyl–H), 1.68 (3H, d, *J* 6.0, ethyl 2–H), 1.17 (3H, t, *J* 7.0, ethoxy 2–H). δ_C (126 MHz, Methanol-d_4) 151.5, 141.9, 89.6, 88.9, 64.0, 19.6, 13.7, 9.3. R_F 0.67 (30:70 EtOAc–petrol). IR ν_{max} (film)/cm^{-1} 3129, 2981, 2933, 1545, 1378, 1308 and 1120. HRMS (ESI): $C_8H_{12}BrN_3O_3$ requires [M+Na]$^+$, calculated 299.9954, found 299.9956.

Ethyl 2-(3-amino-4-bromo-1*H*-pyrazol-5-yl)acetate, 3-25
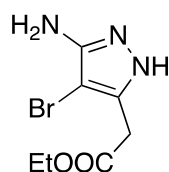
N-Bromosuccinimide (694 mg, 3.9 mmol) was added to a solution of (5-amino-2H-pyrazol-3-yl)-acetic acid (500 mg, 3.54 mmol) in THF (12 ml, 0.3 M) and the mixture was stirred at rt overnight. After which, the mixture was concentrated under reduced pressure and re-dissolved in EtOH (6 ml) prior to addition of sulfuric acid (0.4 ml). The mixture was then heated to reflux until consumption of starting material by TLC. After which, the reaction was cooled to rt and neutralised to pH 7 with bicarb (sat. aq. soln.) and extracted with EtOAc (3 x 50 ml). The combined organics were dried ($MgSO_4$), filtered and concentrated under reduced pressure to give a crude product which was purified by flash column chromatography, eluting with 0:100 → 100:0 EtOAc–petrol to give the *ethyl acetate* (176 mg, 23% over two steps) as a light orange amorphous solid. δ_H (501 MHz, Chloroform-*d*) 4.22 (2H, q, *J* 7.2, ethyl 2–H), 3.64 (2H, s, acetate–H), 1.30 (3H, t, *J* 7.2, ethyl 1–H). δ_C (126 MHz, Chloroform-*d*) 169.44, 151.63, 135.25, 81.78, 61.73, 30.97, 14.13. R_F 0.37 (EtOAc). IR ν_{max} (film)/cm^{-1} 3331, 3216, 2981, 2932, 1732 and 1614. HRMS (ESI): $C_7H_{10}BrN_3O_2$ requires [M+Na]$^+$, calculated 269.9849, found 269.9841.

tert-Butyl   3-{bis[(tert-butoxy)carbonyl]amino}-4-bromo-5-(2-ethoxy-2-oxoethyl)-1_H_-pyrazole-1-carboxylate, 3-26
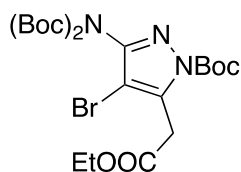
(Boc)$_2$O (120 mg, 0.55 mmol) was added portion-wise to a solution of Ethyl 2-(3-amino-4-bromo-1_H_-pyrazol-5-yl)acetate, (87 mg, 0.25 mmol), triethylamine (0.04 ml, 0.28 mmol) and DMAP (3 mg, 0.025 mmol) in CH$_2$Cl$_2$ (0.63 ml, 0.4 M). The mixture was stirred at rt overnight, after which H$_2$O (25 ml) and CH$_2$Cl$_2$ (25 ml) were added. The aqueous layer was extracted with CH$_2$Cl$_2$ (3 x 25 ml) and the combined organics were washed with bicarb (sat. aq. soln., 25 ml), dried (MgSO$_4$), filtered and concentrated under reduced pressure. The resulting crude product was purified by flash column chromatography, eluting with 0:100 → 10:90 EtOAc–petrol to give the _pyrazole_ (44 mg, 32%) as a colourless amorphous solid. δ_H (501 MHz, Chloroform-_d_) 4.16 (2H, q, _J_ 7.2, ethoxy 1–H), 3.74 (2H, s, oxoethyl 1–H), 1.59 (9H, s, _tert_-butyl–H), 1.40 (18H, s, bis _tert_-butyl–H), 1.24 (3H, t, _J_ 7.2, ethoxy 2–H). δ_C (126 MHz, Chloroform-_d_) 168.32, 148.24, 147.34, 146.16, 137.44, 99.18, 86.64, 83.87, 61.25, 33.81, 27.90, 27.80, 14.19. HRMS (ESI): molecular ion not found.

5-(Difluoromethyl)-_1H_-pyrazol-3-amine, 3-28
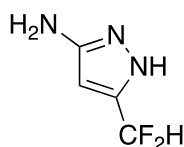
According to procedures,[189,190] n-butyllithium (1.6 M in hexane, 15.2 ml, 24.4 mmol) was added to a flask of anhydrous THF (76 ml) under a nitrogen atmosphere at -78 °C. Acetonitrile (1.12 ml, 21.2 mmol) was added dropwise and the resulting mixture was stirred at -70 °C for 1 h. Ethyl difluoroacetate (1.6 ml, 15.2 mmol) was added to the resultant suspension over 5 min, maintaining the temperature below -69 °C. The reaction mixture was then stirred at -45 °C for 2 h to give a colourless solution which was quenched _via_ the addition of HCl (19.2 ml, 2 M aq. soln.) whilst keeping the temperature below -20 °C followed by warming to rt and concentration under reduced

pressure. The residue was re-suspended in EtOH (50 ml) followed by dropwise addition of hydrazine monohydrate (2.5 ml, 33.50 mmol) at rt. The mixture was then heated at reflux overnight, cooled to rt and concentrated under reduced pressure to give a crude product which was purified by flash column chromatography, eluting with 15:85 → 100:0 EtOAc–petrol to give the *pyrazolamine*[190] (431 mg, 21% over two steps) as a yellow oil. δ_H (501 MHz, Methanol-d_4) 6.57 (1H, t, *J* 55.1, difluoromethyl–H), 5.67 (1H, t, *J* 1.1, 4–H), 5.31 (3H, app br s, 1–H and 3-amine–H). δ_C (126 MHz, Methanol-d_4) 151.44, 146.95 (t, *J* 28.0), 112.47 (t, *J* 232.8), 87.93. R_F 0.46 (EtOAc). Spectroscopic data matched previously reported.[190]

tert-Butyl 4-bromo-3-{[(tert-butoxy)carbonyl]amino}-5-(difluoromethyl)-1*H*-pyrazole-1-carboxylate, 3-29
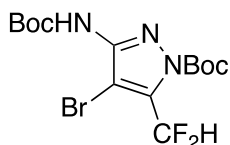
(Boc)$_2$O (428 mg, 1.96 mmol) was added portion-wise to a solution of 5-(difluoromethyl)-1H-pyrazol-3-amine, (120 mg, 0.90 mmol), triethylamine (0.28 ml, 2.00 mmol) and DMAP (11 mg, 0.09 mmol) in CH_2Cl_2 (2.25 ml, 0.4 M). The mixture was stirred at rt overnight, after which H_2O (25 ml) and CH_2Cl_2 (25 ml) were added. The aqueous layer was extracted with CH_2Cl_2 (3 x 25 ml) and the combined organics were washed with bicarb (sat. aq. soln., 25 ml), dried (MgSO$_4$), filtered and concentrated under reduced pressure. *N*-Bromosuccinimide (176 mg, 0.99 mmol) was added to a solution of the crude product in THF (3 ml, 0.3 M) and the mixture was stirred at rt overnight. The resulting crude product was purified by flash column chromatography, eluting with 0:100 → 10:90 EtOAc–petrol to give the *pyrazole* (111 mg, 30% over two steps) as a colourless oil and a 6:5 mixture of rotamers. δ_H (501 MHz, Chloroform-*d*) 6.67 (6H, t, *J* 53.0, difluoromethyl–H$_{Major}$), 6.55 (5H, d, *J* 53.0, difluoromethyl–H$_{Minor}$), 5.49 (11H, s, N–H$_{Major\ and\ minor}$), 1.65 (45H, s, *tert*-butoxy–H$_{Minor}$), 1.61 (54H, s, *tert*-butoxy–H$_{Major}$), 1.41 (99H, s, *tert*-butyl–H$_{Major\ and\ minor}$). δ_C (126 MHz, Chloroform-*d*) 148.15, 146.12 (t, *J* 28.4), 145.74 (t, *J* 29.2), 111.00 (t, *J* 236.2), 110.65 (t, *J* 236.7), 95.13, 87.95, 87.29, 84.49, 72.52, 28.03, 27.94, 27.89. R_F 0.24 (10:90 EtOAc–petrol). IR ν_{max} (film)/cm^{-1}

3193, 2984, 1747, 1623 and 1314. HRMS (ESI): $C_{12}H_{20}BrF_2N_3O_4$ requires $[M+Na]^+$, calculated 434.0497, found 434.0499.

5-(Difluoromethyl)-1*H*-pyrazole, 3-31
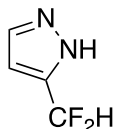
According to a modified procedure,[191] to a solution of pyridine (1.6 ml, 20.0 mmol) and ethyl vinyl ether (2.1 ml, 22.0 mmol) in CH_2Cl_2 (50 ml, 0.4 M) was added difluoroacetic anhydride (2.5 ml, 20.0 mmol) dropwise at -5 °C. The reaction mixture was allowed to slowly warm to rt and stirred at this temperature overnight. After which saturated sodium hydrogen carbonate solution (50 ml) was added, the two phases were separated and the organic phase was washed with H_2O (50 ml), dried (MgSO$_4$), filtered and concentrated under reduced pressure. The resultant crude product (2.43 g, 16 mmol) was then re-dissolved in EtOH (53 ml, 0.3 M) and hydrazine monohydrate (2 ml, 24 mmol) was added dropwise. The mixture was then stirred at reflux overnight followed by cooling to rt and concentration under reduced pressure. The residue was re-dissolved in Et$_2$O (100 ml), washed with H_2O (100 ml) and brine (100 ml), dried (MgSO$_4$), filtered and concentrated under reduced pressure. The crude product was purified by vacuum distillation (~15 mbar, 100 °C). Residual un-distilled crude product was purified by flash column chromatography, eluting with 50:50 EtOAc–petrol and combined with the pure distillate to give the *pyrazole*[192,193] (1.55 g, 66%) as a colourless oil. δ_H (501 MHz, Chloroform-*d*) 7.61 (1H, d, *J* 2.3, 3–H), 6.77 (1H, t, *J* 55.4, difluoromethyl–H), 6.53 (1H, dt, *J* 2.3, 1.1, 4–H). δ_C (126 MHz, Chloroform-*d*) 146.48 (t, *J* 28.5), 130.00, 111.25 (t, *J* 234.2), 103.01 (t, *J* 2.1). R_F 0.20 (20:80 EtOAc–petrol). Note: the product unexpectedly does not fluoresce under UV and must be stained with KMnO$_4$ and sole purification by flash column chromatography would be possible. Spectroscopic data matched previously reported.[193]

4-Bromo-5-(difluoromethyl)-1*H*-pyrazole, 3-32

$$\text{Br} \quad \overset{N}{\underset{CF_2H}{\diagup}} NH$$
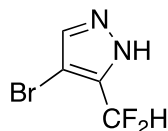
According to a modified procedure,[192] bromine (1.25 ml, 24.40 mmol) was added dropwise to a solution of 3-(difluoromethyl)-1H-pyrazole, (737 mg, 6.24 mmol) in CH_2Cl_2 (20 ml, 0.3 M) and the mixture was stirred at rt for 2 h. After which, the mixture was poured into water (100 ml) and the organic phase was washed with a saturated solution of sodium hydrogen sulfite (100 ml), water (50 ml) and brine (50 ml), dried ($MgSO_4$), filtered and concentrated under reduced pressure. The crude product was purified by flash column chromatography, eluting with 0:100 → 20:80 EtOAc–petrol to give the *pyrazole*[192] as a colourless amorphous solid. δ_H (501 MHz, Chloroform-*d*) 12.26 (1H, s, N–H), 7.70 (1H, t, *J* 1.2, 3–H), 6.80 (1H, t, *J* 53.9, difluoromethyl–H). δ_C (126 MHz, Chloroform-*d*) 142.15, 130.43, 108.96 (t, *J* 236.3), 91.56. R_F 0.25 (20:80 EtOAc–petrol). IR ν_{max} (film)/cm^{-1} 3141, 2977, 2917 1658, 1108 and 1019. HRMS (ESI): $C_4H_3BrF_2N_2$ requires [M+H]$^+$, calculated 196.9520, found 196.9526.

4-Bromo-5-(difluoromethyl)-1-(1-ethoxyethyl)-3-nitro-1*H*-pyrazole, 3-33

$$O_2N \quad \overset{N}{\underset{CF_2H}{\diagup}} \overset{N}{\diagup} \overset{CH_3}{\underset{O}{\diagup}} \diagdown$$
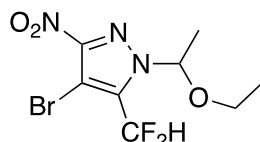
According to a modified procedure,[194] nitric acid (0.13 ml, 3.00 mmol) was added to a solution of 4-bromo-5-(difluoromethyl)-1H-pyrazole, (350 mg, 1.78 mmol) in sulfuric acid (0.8 ml, 16.00 mmol) and the mixture was stirred at 50 °C overnight. After which, the mixture was slowly poured into a cold saturation solution of $NaHCO_3$ until pH 7-8 had been achieved. The aqueous phase was then extracted with EtOAc (3 x 50 ml) and the combined organics were washed with brine (50 ml), dried ($MgSO_4$), filtered and concentrated under reduced pressure. According to General Procedure F, the crude nitrated product (300 mg, 2.00 mmol) at 80 °C gave a crude product which was purified by flash column chromatography, eluting with 0:100 → 10:90 EtOAc–petrol to give the *pyrazole* (62 mg, 11% over two steps) as a light yellow solid. δ_H (501 MHz, Chloroform-*d*) 7.01 (1H, t, *J* 51.7, difluoromethyl–H), 5.84 (1H, q, *J* 6.0,

ethyl 1–H), 3.55 (1H, dqd, J 9.2, 7.0, 0.8, ethoxy 1–H_A), 3.44 (1H, dq, J 9.2, 7.0, ethoxy 1–H_B), 1.74 (3H, d, J 6.0, ethyl 2–H), 1.21 (3H, t, J 7.0, ethoxy 2–H). δ_C (126 MHz, Chloroform-d) 152.00, 135.88 (t, J 26.9), 107.04 (t, J 237.9), 92.21 (t, J 4.9), 91.13 (t, J 1.6), 65.43, 22.12, 14.57. HRMS (ESI): molecular ion not found.

tert-Butyl 4-bromo-3-(trifluoromethyl)-1*H*-pyrazole-1-carboxylate, 3-35
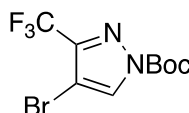
(Boc)$_2$O (1.10 g, 5.00 mmol) was added portion-wise to a solution of 4-bromo-3-(trifluoromethyl)-1H-pyrazole (1.00 g, 4.65 mmol) and triethylamine (0.70 ml, 5.00 mmol) in CH_2Cl_2 (24 ml, 0.2 M). The mixture was stirred at rt overnight, after which H_2O (50 ml) and CH_2Cl_2 (50 ml) were added. The aqueous layer was extracted with CH_2Cl_2 (3 x 25 ml) and the combined organics were washed with bicarb (sat. aq. soln., 25 ml), dried ($MgSO_4$), filtered and concentrated under reduced pressure to give the *pyrazole* (1.47 g, quant.) as a yellow amorphous solid which was used without further purification. δ_H (501 MHz, Chloroform-d) 8.16 (1H, t, J 1.0, 5–H), 1.65 (9H, s, *tert*-butyl–H). δ_C (126 MHz, Chloroform-d) 145.56, 144.25 (q, J 38.1), 133.01, 119.82 (q, J 270.9), 94.60 (q, J 1.2), 87.90, 27.75. R_F 0.60 (10:90 EtOAc–petrol). IR ν_{max} (film)/cm^{-1} 3283, 3157, 2986, 2358, 2085 and 1768. HRMS (ESI): $C_9H_{10}BrF_3N_2O_2$ requires [M-^{t}Bu+H]$^+$, calculated 280.9144 found 280.9137.

7-(3-Methyl-1*H*-pyrazol-4-yl)-1,2,3,4-tetrahydroisoquinolin-1-one, 3-4
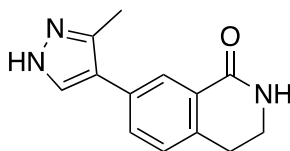
According to General Procedure D, 1-(1-ethoxyethyl)-4-iodo-3-methyl-1H-pyrazole, (70 mg, 0.25 mmol) gave a crude product which was purified by flash column chromatography, eluting with 0:100 → 5:95 MeOH–CH_2Cl_2 to give the ethoxyethyl protected pyrazole (69 mg, 0.23 mmol) which, after being subjected to General Procedure B, gave the *isoquinolinone* (52 mg, 92%) as a yellow amorphous solid. δ_H (500 MHz, Methanol-d_4) 8.09 (1H, s, pyrazolyl

5–H), 8.03 (1H, d, J 2.0, 8–H), 7.61 (1H, dd, J 7.9, 2.0, 6–H), 7.38 (1H, d, J 7.9, 5–H), 3.52 (2H, dd, J 7.1, 6.7, 3–H), 3.01 (2H, t, J 6.7, 4–H), 2.51 (3H, s, methyl–H). δ_C (126 MHz, Methanol-d_4) 166.6, 140.9, 138.3, 133.1, 131.2, 130.5, 129.0, 128.0, 126.0, 120.1, 39.4, 27.3, 9.7. R_F 0.19 (5:95 MeOH–CH$_2$Cl$_2$). IR ν_{max} (film)/cm^{-1} 3211, 2979, 2934, 1658 and 1613. HRMS (ESI): C$_{13}$H$_{13}$N$_3$O requires [M+Na2-H]$^+$, calculated 272.0770, found 272.0772.

7-(3,5-Dimethyl-1*H*-pyrazol-4-yl)-1,2,3,4-tetrahydroisoquinolin-1-one, 3-5
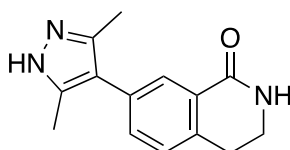
According to General Procedure E, 7-(4,4,5,5-Tetramethyl-1,3,2-dioxaborolan-2-yl)-1,2,3,4-tetrahydroisoquinolin-1-one, **3-16** (75 mg, 0.275 mmol) and 1-(1-ethoxyethyl)-4-iodo-3,5-dimethyl-1H-pyrazole, (90 mg, 0.305 mmol) were stirred overnight at 100 °C. After which, the reaction was cooled, concentrated under reduced pressure and purified by flash column chromatography, eluting with 0:100 → 5:95 MeOH–CH$_2$Cl$_2$ to give the ethoxyethyl protected pyrazole. According to General Procedure B, the ethoxy protected pyrazole (33 mg, 0.105 mmol) gave the *isoquinolinone* (25 mg, 34%) as an orange amorphous solid. δ_H (501 MHz, Methanol-d_4) 7.85 (1H, d, J 1.8, 8–H), 7.43 (1H, dd, J 7.7, 1.8, 6–H), 7.36 (1H, d, J 7.7, 5–H), 3.54 (2H, t, J 6.7, 3–H), 3.02 (2H, t, J 6.7, 4–H), 2.26 (6H, s, dimethyl–H). δ_C (126 MHz, Methanol-d_4) 166.91, 137.46, 132.98, 132.56, 129.18, 128.61, 127.70, 127.51, 117.12, 39.48, 27.33, 9.87. R_F 0.19 (5:95 MeOH–CH$_2$Cl$_2$). IR ν_{max} (film)/cm^{-1} 3246, 2929, 1645 and 1612. HRMS (ESI): C$_{14}$H$_{15}$N$_3$O requires [M+Na]$^+$, calculated 264.1107, found 264.1100.

4-(1-Oxo-1,2,3,4-tetrahydroisoquinolin-7-yl)-1*H*-pyrazole-3-carboxamide, 3-10
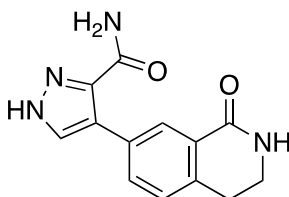
According to General Procedure D, 7-(4,4,5,5-Tetramethyl-1,3,2-dioxaborolan-2-yl)-1,2,3,4-tetrahydroisoquinolin-1-one, **3-16**, (75 mg, 0.275 mmol) and 4-bromo-1-(1-ethoxyethyl)-1H-pyrazole-3-carboxamide, (65 mg, 0.25 mmol) gave a crude product which was purified by flash column chromatography, eluting with 10:90 MeOH–CH$_2$Cl$_2$ to give the ethoxyethyl protected pyrazole (73 mg, 0.22 mmol) which, after being subjected to General Procedure B followed by purification by flash column chromatography, eluting with 0:100 → 10:90 MeOH–CH$_2$Cl$_2$, gave the *pyrazole carboxamide* (33 mg, 52% over two steps) as a yellow amorphous solid. δ_H (501 MHz, Methanol-d_4) 8.08 (1H, d, *J* 1.8, isoquinolinyl 8–H), 7.85 (1H, s, 5–H), 7.72 (1H, dd, *J* 7.9, 1.8, isoquinolinyl 6–H), 7.29 (1H, d, *J* 7.9, isoquinolinyl 5–H), 3.51 (2H, dd, *J* 6.7, 2.7, isoquinolinyl 3–H), 2.99 (2H, t, *J* 6.7, isoquinolinyl 4–H). δ_C (126 MHz, Methanol-d_4) 166.97, 166.34, 141.89, 138.02, 133.01, 131.32, 129.22, 128.16, 127.42, 126.93, 122.31, 39.46, 27.35. R_F 0.21 (10:90 MeOH–CH$_2$Cl$_2$). IR ν_{max} (film)/cm^{-1} 3382, 3252, 2924, 1659 and 1614. HRMS (ESI): C$_{13}$H$_{12}$N$_4$O$_2$ requires [M+Na]$^+$, calculated 279.0853, found 279.0847.

2-[3-Amino-4-(1-oxo-1,2,3,4-tetrahydroisoquinolin-7-yl)-1*H*-pyrazol-5-yl]acetic acid, 3-13
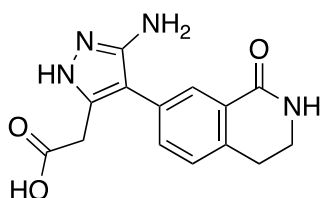
According to General Procedure D, tert-Butyl 3-{bis[(tert-butoxy)carbonyl]amino}-4-bromo-5-(2-ethoxy-2-oxoethyl)-1H-pyrazole-1-carboxylate, (28 mg, 0.05 mmol) and 7-(4,4,5,5-Tetramethyl-1,3,2-dioxaborolan-2-yl)-1,2,3,4-tetrahydroisoquinolin-1-one, **3-16**, (15 mg, 0.055 mmol) gave a crude product which, after being subjected to General Procedure G to ensure complete deprotection, was purified by HPLC, eluting with 5:95 → 95:5 MeCN–H$_2$O plus 1% formic acid to give the *acetic acid* (11 mg, 77%) as a yellow amorphous solid. δ_H (501 MHz, Methanol-d_4) 7.92 (1H, d, *J* 2.0, isoquinolinyl 8–H), 7.50 (1H, dd, *J* 7.9, 2.0, isoquinolinyl 6–H), 7.44 (1H, d, *J* 7.8, isoquinolinyl 5–H), 3.70 (2H, s, 2–H), 3.54 (2H, t, *J* 6.7,

isoquinolinyl 3–H), 3.04 (2H, t, J 6.7, isoquinolinyl 4–H). δ_C (126 MHz, Methanol-d_4) 171.45, 167.89, 141.20, 140.78, 134.44, 133.16, 129.67, 129.37, 108.56, 40.73, 31.24, 28.79. IR ν_{max} (film)/cm^{-1} 3307, 3257, 2983 and 1626. HRMS (ESI): $C_{14}H_{14}N_4O_3$ requires [M+H]$^+$, calculated 287.1139, found 287.1134.

7-(3-amino-5-methyl-1H-pyrazol-4-yl)-1,2,3,4-tetrahydroisoquinolin-1-one, 3-8
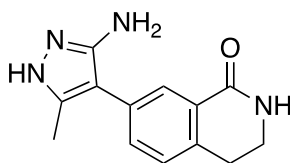
According to General Procedure E, 7-(4,4,5,5-Tetramethyl-1,3,2-dioxaborolan-2-yl)-1,2,3,4-tetrahydroisoquinolin-1-one, (150 mg, 0.55 mmol) and 4-Bromo-1-(1-ethoxyethyl)-5-methyl-3-nitro-1H-pyrazole (127 mg, 0.46 mmol) were stirred overnight at 100 °C. After which, the reaction was cooled and diluted with H_2O (20 ml) and CH_2Cl_2 (20 ml). The phases were separated and the aqueous phase was extracted with CH_2Cl_2 (3 x 20 ml). The combined organics were dried (MgSO$_4$), filtered and concentrated under reduced pressure to give a crude product. Pd/C (10 mg, 10%) was added to a solution of the crude product in MeOH (10 ml) under an atmosphere of nitrogen. The reaction mixture was stirred at room temperature under an atmosphere of H_2 (balloon) overnight. After completion the reaction mixture was filtered through celite, washing with EtOAc, and concentrated under reduced pressure to give a crude product which was purified by flash column chromatography, eluting with 0:100 → 10:90 MeOH–CH_2Cl_2 to give the *isoquinolinone* (8 mg, 7%) as an orange amorphous solid. δ_H (501 MHz, Methanol-d_4) 7.91 (1H, d, J 1.9, 8–H), 7.51 (1H, dd, J 7.8, 1.9, 6–H), 7.36 (1H, d, J 7.8, 5–H), 3.52 (2H, dd, J 7.1, 6.5, 3–H), 3.00 (2H, t, J 6.5, 4–H), 2.24 (3H, s, methyl–H). δ_C (126 MHz, Methanol-d_4) 168.49, 138.36, 133.74, 133.71, 130.11, 129.08, 128.37, 40.90, 28.73, 11.00. R_F 0.30 (5:95 MeOH–CH_2Cl_2). IR ν_{max} (film)/cm^{-1}. HRMS (ESI): $C_{13}H_{14}N_4O$ requires [M+H]$^+$, calculated 243.1240, found 243.1238.

7-[1-(1-Ethoxyethyl)-3-nitro-1H-pyrazol-4-yl]-1,2,3,4-tetrahydroisoquinolin-1-one, 3-36
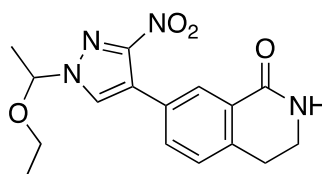
According to General Procedure E, 7-(4,4,5,5-Tetramethyl-1,3,2-dioxaborolan-2-yl)-1,2,3,4-tetrahydroisoquinolin-1-one, (200 mg, 0.732 mmol) and 4-bromo-1-(1-ethoxyethyl)-3-nitro-1H-pyrazole (162 mg, 0.610 mmol) were stirred overnight at 100 °C. After which, the reaction was cooled and diluted with H_2O (20 ml) and CH_2Cl_2 (20 ml). The phases were separated and the aqueous phase was extracted with CH_2Cl_2 (3 x 20 ml). The combined organics were dried ($MgSO_4$), filtered and concentrated under reduced pressure to give a crude product which was purified by flash column chromatography, eluting with 0:100 → 5:95 MeOH–CH_2Cl_2 to give the *isoquinolinone* (146 mg, 72%) as a light yellow amorphous solid. δ_H (500 MHz, Chloroform-*d*) 8.08 (1H, d, *J* 2.0, 8–H), 7.78 (1H, s, pyrazolyl–H), 7.59 (1H, dd, *J* 7.8, 2.0, 6–H), 7.29 (1H, d, *J* 7.8, 5–H), 6.90 (1H, br. s N–H), 5.59 (1H, q, *J* 6.0, ethyl 1–H), 3.61 (2H, td, *J* 6.5, 2.8, 3–H), 3.56 (1H, dq, *J* 9.4, 7.0, ethoxy 1–H_A), 3.48 (1H, dq, *J* 9.4, 7.0, ethoxy 1–H_B), 3.04 (2H, t, *J* 6.5, 4–H), 1.70 (3H, d, *J* 6.0, ethyl 2–H), 1.20 (3H, t, *J* 7.0, ethoxy 2–H). δ_C (126 MHz, Chloroform-*d*) 166.1, 151.2, 139.2, 133.3, 129.2, 128.5, 128.1, 127.6, 119.5, 90.0, 65.3, 40.2, 28.2, 22.5, 14.9. R_F 0.31 (5:95 MeOH–CH_2Cl_2). IR ν_{max} (film)/cm^{-1} 3236, 2978, 2930, 2362, 2342, 1666 and 1525. HRMS (ESI): $C_{16}H_{18}N_4O_4$ requires [M+H]$^+$, calculated 331.1401, found 331.1399.

7-[3-Amino-1*H*-pyrazol-4-yl]-1,2,3,4-tetrahydroisoquinolin-1-one, 3-7
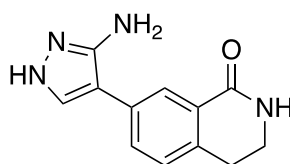
Pd/C (15 mg, 10 wt.% loading on activated charcoal) was added to a solution of 7-[1-(1-ethoxyethyl)-3-nitro-1H-pyrazol-4-yl]-1,2,3,4-tetrahydroisoquinolin-1-one, (146 mg, 0.44 mmol) in EtOH (20 ml, 22 mM) and EtOAc (10 ml, 44 mM) under nitrogen atmosphere. The reaction mixture was stirred at room temperature under an atmosphere of H_2 (balloon) overnight. After completion the reaction mixture was filtered through celite, washing with EtOAc, and

concentrated under reduced pressure to give the amino-pyrazole (132 mg, 0.44 mmol) which, after being subject to General Procedure B and purification by HPLC, eluting with 5:95 → 95:5 MeCN–H_2O plus 1% formic acid, gave the *isoquinolinone* (56 mg, 44%) as an red-orange amorphous solid. δ_H (501 MHz, Methanol-d_4) 8.03 (1H, d, *J* 2.0, 8–H), 7.67 – 7.61 (2H, m, 6–H and pyrazolyl 5–H), 7.32 (1H, app dq, *J* 7.9, 0.8, 5–H), 3.51 (2H, app dd, *J* 7.1, 6.5, 3–H), 2.98 (2H, t, *J* 6.5, 4–H). δ_C (126 MHz, Methanol-d_4) 167.19, 136.48, 132.42, 129.96, 128.69, 127.73, 124.45, 39.51, 27.27. R_F 0.19 (10:90 MeOH–CH_2Cl_2). IR ν_{max} (film)/cm^{-1} 3212, 2961, 2928, 2872, 1650 and 1613. HRMS (ESI): $C_{12}H_{12}N_4O$ requires [M+Na]$^+$, calculated 251.0903, found 251.0895.

N-[4-(1-oxo-1,2,3,4-tetrahydroisoquinolin-7-yl)-1*H*-pyrazol-3-yl]acetamide, 3-9
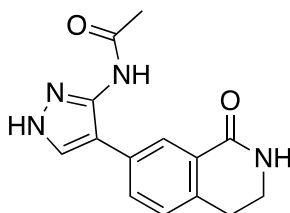
According to General Procedure G, 7-[3-amino-1H-pyrazol-4-yl]-1,2,3,4-tetrahydroisoquinolin-1-one, (55 mg, 0.24 mmol) gave a crude product which was purified by flash column chromatography, eluting with 0:100 → 10:90 MeOH–CH_2Cl_2 to give the *acetamide* (65 mg, quant.) as a yellow amorphous solid. δ_H (501 MHz, Methanol-d_4) 8.06 (1H, d, *J* 2.0, isoquinolinyl 8–H), 7.89 (1H, s, pyrazolyl–H), 7.59 (1H, dd, *J* 7.8, 2.0, isoquinolinyl 6–H), 7.30 (1H, d, *J* 7.8, isoquinolinyl 5–H), 3.50 (2H, t, *J* 6.7, isoquinolinyl 3–H), 2.97 (2H, t, *J* 6.7, isoquinolinyl 4–H), 2.15 (3H, s, acetamide–H). δ_C (126 MHz, Methanol-d_4) 172.20, 166.84, 140.66, 137.64, 131.00, 130.54, 129.58, 128.73, 127.61, 125.34, 115.08, 39.46, 27.29, 21.39. R_F 0.22 (10:90 MeOH–CH_2Cl_2). IR ν_{max} (film)/cm^{-1} 3233, 2951, 1649 and 1614. HRMS (ESI): $C_{14}H_{14}N_4O_2$ requires [M+Na]$^+$, calculated 293.1009, found 293.1007.

4-(1-Oxo-1,2,3,4-tetrahydroisoquinolin-7-yl)-1*H*-pyrazole-3-carbonitrile, 3-11
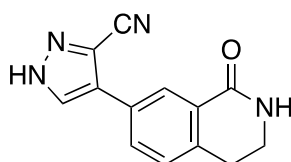
According to General Procedure E, 7-(4,4,5,5-Tetramethyl-1,3,2-dioxaborolan-2-yl)-1,2,3,4-tetrahydroisoquinolin-1-one, (200 mg, 0.732 mmol) and 4-bromo-1-(1-ethoxyethyl)-1H-pyrazole-3-carbonitrile (148 mg, 0.610 mmol) were stirred overnight at 100 °C. After which, the reaction was cooled and concentrated under reduced pressure to give the crude protected pyrazole which, according to General Procedure B, gave a crude product which was purified by flash column chromatography, eluting with 0:100 → 5:95 MeOH–CH$_2$Cl$_2$ to give the *pyrazole* (61 mg, 42% over two steps) as a colourless amorphous solid. δ_H (500 MHz, Chloroform-*d*) 8.23 (1H, d, *J* 2.0, isoquinolinyl 8–H), 8.17 (1H, s, 5–H), 7.82 (1H, dd, *J* 7.9, 2.0, isoquinolinyl 6–H), 7.41 (1H, d, *J* 7.9, isoquinolinyl 5–H), 3.54 (2H, t, *J* 6.7, isoquinolinyl 3–H), 3.03 (2H, t, *J* 6.7, isoquinolinyl 4–H). δ_C (126 MHz, Chloroform-*d*) 167.8, 140.6, 131.5, 130.6, 130.3, 129.5, 129.0, 126.8, 123.1, 119.2, 115.6, 40.7, 28.7. R_F 0.23 (5:95 MeOH–CH$_2$Cl$_2$). IR ν_{max} (film)/cm^{-1} 3346, 2929, 2240, 1660 and 1617. HRMS (ESI): C$_{13}$H$_{10}$N$_4$O requires [M+H]$^+$, calculated 239.0927, found 239.0923.

7-[3-(Aminomethyl)-1*H*-pyrazol-4-yl]-1,2,3,4-tetrahydroisoquinolin-1-one, 3-12
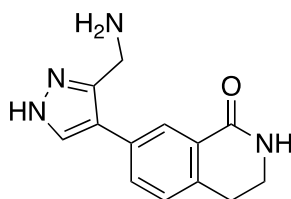
Pd/C (2 mg, 10 wt% loading on activated charcoal) was added to a solution of 4-(1-oxo-1,2,3,4-tetrahydroisoquinolin-7-yl)-1H-pyrazole-3-carbonitrile, (16 mg, 0.067 mmol) in 4:1 THF–NH$_4$OH (1.3 ml, 50 mM) under nitrogen atmosphere. The reaction mixture was stirred at room temperature under an atmosphere of H$_2$ (balloon) overnight. After completion, the reaction mixture was filtered through celite, washing with EtOAc, and concentrated under reduced pressure to give the *isoquinolinone* (23 mg, 96%) as a colourless amorphous solid. δ_H (500 MHz, Methanol-*d*$_4$) 7.94 (1H, d, *J* 2.0, 8–H), 7.90

(1H, s, pyrazolyl–H), 7.57 (1H, dd, *J* 7.8, 2.0, 6–H), 7.38 (1H, d, *J* 7.8, 5–H), 4.24 (2H, s, aminomethyl–H), 3.53 (2H, t, *J* 6.7, 3–H), 3.02 (2H, t, *J* 6.7, 4–H). δ_C (126 MHz, Methanol-d_4) 168.2, 139.4, 132.9, 132.7, 130.3, 129.4, 127.3, 121.6, 120.8, 40.8, 37.2, 28.6. R_F 0.15 (10:90 7M NH$_3$ in MeOH–CH$_2$Cl$_2$). IR ν_{max} (film)/cm^{-1} 3369, 1668, 1486, 1436, 1196 and 1136. HRMS (ESI): C$_{13}$H$_{14}$N$_4$O requires [M+Na]$^+$, calculated 265.1060, found 265.1056.

1-Oxo-1,2,3,4-tetrahydroisoquinoline-7-carbaldehyde, 3-39
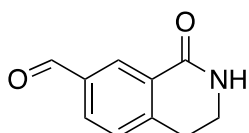
According to a modified procedure,[195] a solution of 7-bromo-3,4-dihydro-1-(2H)-isoquinolinone (1.36 g, 6.00 mmol) and Pd(PPh$_3$)$_4$ (348 mg, 0.30 mmol) in 1,2- dimethoxyethane (60 ml) was stirred at room temperature for 30 min before addition of vinylboronic anhydride pyridine complex (590 mg, 1.4 mmol), K$_2$CO$_3$ (830 mg, 6.00 mmol) and water (20 ml). The reaction was heated at reflux for 1.5 h before cooling to room temperature and addition of water (100 ml). The mixture was extracted with CH$_2$Cl$_2$ (3 x 200ml), the organic layers were combined, dried (MgSO$_4$) and concentrated under reduced pressure. The crude product (1 g, 5.77 mmol) was dissolved in 1,4-dioxane (58 ml) and water (12 ml) and cooled to 0 °C prior to addition of sodium periodate (2.84 g, 13.27 mmol) and osmium tetroxide (5 ml, 4% aqueous solution). The reaction mixture was warmed to room temperature and stirred for 30 min before concentration under reduced pressure. The residue was dissolved in 1,4-dioxane (50 ml) and concentrated again. The mixture was then dissolved in dichloromethane (100 ml), dried (MgSO$_4$) and concentrated under reduced pressure. The crude product was purified by flash column chromatography, eluting with 0:100 → 100:0 EtOAc–petrol to give the *carbaldehyde*[195] (332 mg, 32% over two steps) as a colourless amorphous solid. δ_H (501 MHz, Chloroform-*d*) 10.04 (1H, app d, *J* 0.6, carbaldehyde–H), 8.54 (1H, d, *J* 1.8, 8–H), 7.99 (1H, dd, *J* 7.8, 1.8, 6–H), 7.40 (1H, dp, *J* 7.8, 0.8, 5–H), 7.04 (1H, s, N–H), 3.63 (2H, ddd, *J* 6.8, 6.3, 2.9, 3–H), 3.09 (2H, t, *J* 6.8, 4–H). δ_C (126 MHz, Chloroform-*d*) 191.39, 165.35, 145.44, 135.65,

131.33, 130.99, 129.86, 128.42, 39.79, 28.65. R_F 0.27 (EtOAc). Spectroscopic data matched previously reported.[195]

7-[(1E)-2-Nitroethenyl]-1,2,3,4-tetrahydroisoquinolin-1-one, 3-40
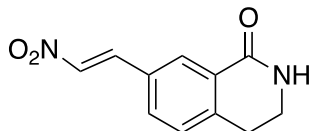
According to a modified procedure,[196] 1-oxo-1,2,3,4-tetrahydroisoquinoline-7-carbaldehyde, (343 mg, 1.96 mmol) was added to a solution of ammonium acetate (362 mg, 4.70 mmol) in nitromethane (3.9 ml) and acetic acid (7.8 ml) and heated at reflux. Upon completion of the reaction, the mixture was cooled, diluted with water (50 ml) and extracted with CH_2Cl_2 (3 x 50 ml). The combined organics were washed with brine (sat. aq. soln., 50 ml), dried (MgSO$_4$), filtered and concentrated under reduced pressure to give a crude product which was purified by flash column chromatography, eluting with 0:100 → 10:90 MeOH–CH_2Cl_2 to give the *isoquinolinone* (260 mg, 61%) as a yellow amorphous solid. δ_H (501 MHz, Chloroform-d) 8.28 (1H, d, J 2.0, 8–H), 8.01 (1H, d, J 13.6, ethenyl 2–H), 7.66 (1H, d, J 13.6, ethenyl 1–H), 7.61 (1H, dd, J 7.9, 2.0, 6–H), 7.34 (1H, d, J 7.9, 5–H), 6.53 (1H, s, N–H), 3.62 (2H, td, J 6.6, 2.9, 3–H), 3.07 (2H, t, J 6.6, 4–H). δ_C (126 MHz, Chloroform-d) 165.26, 142.90, 138.14, 137.78, 132.75, 130.12, 129.37, 128.74, 128.51, 40.04, 28.51. R_F 0.40 (5:95 MeOH–CH_2Cl_2). IR ν_{max} (film)/cm^{-1} 3363, 3077, 1657, 1627, 1608 and 1332. LCMS (ESI): $C_{11}H_{10}N_2O_3$ requires $[2M+H]^+$, calculated 437.15, found 437.03.

7-[3-(Trifluoromethyl)-1*H*-pyrazol-4-yl]-1,2,3,4-tetrahydroisoquinolin-1-one, 3-41
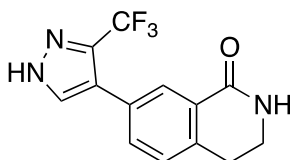
According to a modified procedure[197] and under an atmosphere of nitrogen, *t*BuONO (66 μl, 0.55 mmol) and acetic acid (6 μl, 0.1 mmol) were added to a stirred solution of 2,2,2-trifluoroethylamine (40 μl, 0.5 mmol) in THF (1.25 ml). The solution was heated at 55 °C for 15 min, after which the reaction mixture was cooled to 0 °C and 7-[(1E)-2-nitroethenyl]-1,2,3,4-tetrahydroisoquinolin-

1-one, (54.5 mg, 0.25 mmol), Ag_2O (87.0 mg, 0.38 mmol) and Na_2CO_3 (53.0 mg, 0.5 mmol) were added dropwise as a suspension in THF (1.25 ml) under nitrogen. The resulting suspension was stirred at rt for 6 hours (at which point the reaction was incomplete). After which, the mixture was quenched with TsOH (1.25 ml, 1 M soln. in THF–H_2O, 1:1 mixture) followed by NH_4Cl (1.25 ml, sat. aq. soln.). The resulting insoluble solid was filtered and the filtrated extracted with CH_2Cl_2 (10 ml). The combined organics were dried ($MgSO_4$), filtered and concentrated under reduced pressure to give a crude product which was purified by flash column chromatography, eluting with 0:100 → 10:90 MeOH–CH_2Cl_2 to give the *isoquinolinone* (5.6 mg, 8%) as a yellow amorphous solid. δ_H (501 MHz, Methanol-d_4) 8.02 (1H, d, *J* 2.0, 8–H), 7.96 (1H, d, *J* 1.1, pyrazolyl–H), 7.56 (1H, dd, *J* 7.8, 2.0, 6–H), 7.36 (1H, dq, *J* 7.8, 0.8, 5–H), 3.53 (2H, dd, *J* 7.1, 6.5, 3–H), 3.02 (2H, t, *J* 6.5, 4–H). δ_C (126 MHz, Methanol-d_4) 167.95, 140.20, 133.63 (app d, *J* 1.7), 131.30, 131.08, 130.15, 128.91, 128.64 (app d, *J* 1.4), 123.41 (q, *J* 267.9), 121.74, 40.78, 28.71. δ_F (376 MHz, Methanol-d_4) -60.59. R_F 0.16 (5:95 MeOH–CH_2Cl_2). IR ν_{max} (film)/cm^{-1} 3207, 2945, 1646 and 1613. HRMS (ESI): $C_{13}H_{10}F_3N_3O$ requires [M+H]$^+$, calculated 282.0849, found 282.0846.

7-[(1*H*-Pyrazol-4-yl)amino]-1,2,3,4-tetrahydroisoquinolin-1-one, 3-6
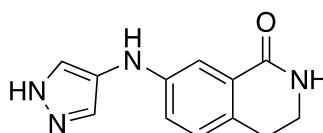
According to a modified procedure,[137] 4-aminopyrazole (62.30 mg, 0.75 mmol), *t*-BuXPhos Pd G3 (29.80 mg, 37.50 μmol), *t*-BuXPhos (16.00 mg, 37.50 μmol), NaO^{t}Bu (152 mg, 1.50 mmol) and 7-bromo-3,4-dihydro-1-(2H)-isoquinolinone (187 mg, 0.83 mmol) were charged to a 20 ml reaction vial which was purged with nitrogen for 15 min followed by addition of 1,4-dioxane and H_2O (7.5 ml, 4:1 mixture). The mixture was stirred at rt for 4 days, at which point the reaction was not complete, and concentrated under reduced pressure prior to addition of H_2O (10 ml), sat. aq NH_4Cl (10 ml) and EtOAc (20 ml). The layers were separated and the aqueous layer extracted with EtOAc (3 x 20 ml). The combined organics were dried ($MgSO_4$) and concentrated under reduced pressure. The crude product was purified by flash column

chromatography, eluting with 0:100 → 10:90 MeOH–CH$_2$Cl$_2$ to give the *isoquinolinone* (26 mg, 15%) as a deep red amorphous solid. δ$_H$ (501 MHz, Methanol-d_4) 7.54 (1H, br s, pyrazolyl–H), 7.38 (1H, d, *J* 2.6, 8–H), 7.07 (1H, dq, *J* 8.2, 0.7, 5–H), 6.93 (1H, dd, *J* 8.2, 2.6, 6–H), 3.44 (1H, dd, *J* 7.2, 6.5, 3–H), 3.35 (1H, s, N–H), 2.83 (1H, t, *J* 6.5, 4–H). δ$_C$ (126 MHz, Methanol-d_4) 168.91, 147.74, 134.94, 130.31, 129.74, 129.30, 126.42, 122.57, 118.95, 112.33, 41.22, 28.13. *R*$_F$ 0.31 (10:90 MeOH–CH$_2$Cl$_2$). IR ν$_{max}$ (film)/cm^{-1} 3200, 2965, 1646, 1610 and 1577. HRMS (ESI): C$_{12}$H$_{12}$N$_4$O requires [M+Na]$^+$, calculated 251.0903, found 251.0900.

(3-Bromophenyl)formamido 2,2-dimethylpropanoate, 3-43
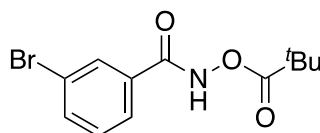
According to procedure,[158] 3-bromobenzoyl chloride (1.20 ml, 9.10 mmol) was added dropwise to a solution of hydroxylamine hydrochloride (0.63 g, 9.10 mmol) and K$_2$CO$_3$ (2.52 g, 18.20 mmol) in a 0.3 M 2:1 biphasic mixture of EtOAc (18.2 ml, 0.5 M) and H$_2$O (9.1 ml, 1 M) at 0 °C. After stirring at room temperature for 4 hours, pivaloyl chloride (1.1 ml, 9.10 mmol) was added dropwise and the reaction stirred for a further 18 hours at room temperature. After which, the reaction was quenched with H$_2$O (20 ml) and EtOAc (20 ml), the phases were separated and the aqueous phase was extracted with EtOAc (3 x 50 ml). The combined organic layers were dried over MgSO$_4$, filtered and concentrated under reduced pressure to give a crude product which was purified by flash column chromatography, eluting with 0:100 → 30:70 EtOAc–petrol to give the propanoate[158] (1.6 g, 58%) as a colourless amorphous solid. δ$_H$ (501 MHz, Methanol-d_4) 7.97 (1H, t, *J* 1.8, phenyl 2–H), 7.79 (1H, ddd, *J* 7.9, 1.8, 1.0, phenyl 4/6–H), 7.75 (1H, ddd, *J* 7.9, 1.8, 1.0, phenyl 4/6–H), 7.42 (1H, t, *J* 7.9, phenyl 5–H), 1.34 (9H, s, *t*butyl–H). δ$_C$ (126 MHz, Methanol-d_4) 176.1, 164.8, 135.0, 133.3, 130.3, 130.2, 125.9, 122.3, 38.0, 26.1. *R*$_F$ 0.22 (10:90 EtOAc–hexane). IR ν$_{max}$ (film)/cm^{-1} 3194, 2975, 2935, 1781, 1664 and 1595. HRMS (ESI): C$_{12}$H$_{14}$BrNO$_3$ requires [M+H]$^+$, calculated 300.0230, found 300.0230.

[3-(1*H*-Pyrazol-4-yl)phenyl]formamido 2,2-dimethylpropanoate, 3-42
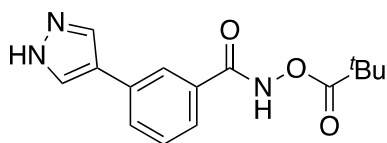
According to General Procedure C, 3-(1H-Pyrazol-4-yl)benzoic acid (1.07 g, 5.67 mmol) gave a crude product which was purified by flash column chromatography, eluting with 0:100 → 5:95 MeOH–CH$_2$Cl$_2$ to give the *propanoate* (1.08 g, 66%) as a colourless amorphous solid. δ_H (500 MHz, Acetone-d_6) 8.13 (1H, td, J 1.8, 0.6, phenyl 2–H), 8.13-8.03 (2H, m, pyrazolyl–H), 7.85 (1H, ddd, J 7.8, 1.8, 1.1, phenyl 4–H), 7.72 (1H, ddd, J 7.8, 1.8, 1.1, phenyl 6–H), 7.50 (1H, td, J 7.7, 0.6, phenyl 5–H), 1.33 (9H, s, ^{t}butyl–H). δ_C (126 MHz, Acetone-d_6) 176.8, 166.4, 136.7, 134.8, 133.1, 130.0, 129.8, 125.8, 125.0, 122.0, 38.9, 27.4. R_F 0.30 (5:95 MeOH–CH$_2$Cl$_2$). IR ν_{max} (film)/cm^{-1} 3183, 2969, 2932, 1634, 1607 and 1584. HRMS (ESI): C$_{15}$H$_{17}$N$_3$O$_3$ requires [M+H]$^+$, calculated 288.1343, found 288.1334.

Ethyl 3-(1*H*-pyrazol-4-yl)benzoate, 3-49
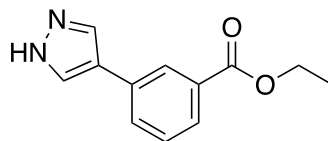
According to General Procedure D, ethyl 3-bromobenzoate (2.5 ml, 15.6 mmol) gave a crude product which was purified by flash column chromatography, eluting with 0:100 → 40:60 EtOAc–petrol to give the *benzoate* (2.6 g, 77%) as a colourless amorphous solid. δ_H (400 MHz, Chloroform-d) 8.19 (1H, t, J 1.6, 2–H), 7.95 (2H, s, pyrazolyl–H), 7.91 (1H, dt, J 7.7, 1.6, 4– or 6–H), 7.69 (1H, dt, J 7.7, 1.6, 4– or 6–H), 7.44 (1H, t, J 7.7, 5–H), 4.41 (2H, q, J 7.1, ethyl–H), 1.42 (3H, t, J 7.1, ethyl–H). δ_C (101 MHz, Chloroform-d) 166.7, 132.8, 131.3, 131.1, 130.0, 128.9, 127.6, 126.7, 121.9, 61.2, 14.4. R_F 0.18 (40:60 EtOAc–petrol). IR ν_{max} (neat)/cm^{-1} 3114, 3067, 2999, 2937, 1713 and 1605. HRMS (ESI): C$_{12}$H$_{12}$N$_2$O$_2$ requires [M+H]$^+$, calculated 217.0972, found 217.0975.

3-(1*H*-Pyrazol-4-yl)benzoic acid, 3-53
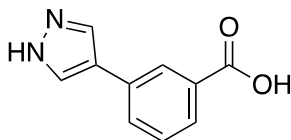
LiOH (0.73 g, 17.4 mmol), dissolved in H_2O (60 ml), was added to a solution of ethyl 3-(1H-pyrazol-4-yl)benzoate (1.88 g, 8.7 mmol) in THF (60 ml) and the mixture stirred at room temperature. After 24 hours, the reaction mixture was concentrated under reduced pressure, re-dissolved in H_2O and the pH was adjusted to 3 using 0.5 M HCl. The aqueous layer was extracted with EtOAc (3 x 100 ml) and the combined organic layers were dried ($MgSO_4$), filtered and concentrated under reduced pressure to give the acid[135] (1.2 g, 72%) as a colourless amorphous solid. δ_H (300 MHz, DMSO) 12.99 (1H, br s, N–H), 8.13 (3H, s, 2– and pyrazolyl–H), 7.85 (1H, dt, J 7.7, 1.3, 4– or 6–H), 7.76 (1H, dt, J 7.7, 1.3, 4– or 6–H), 7.47 (1H, t, J 7.7, 5–H). δ_C (101 MHz, DMSO) 165.9, 130.1, 124.2, 122.7, 119.8, 118.8, 118.7, 117.9, 114.1. IR ν_{max} (film)/cm^{-1} 3246, 2994, 1647, 1576 and 1555. HRMS (ESI): $C_{10}H_8N_2O_2$ requires [M+H]$^+$, calculated 189.0659, found 189.0654.

O-pivaloylhydroxyamine triflic acid
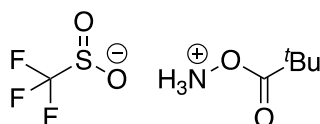
According to a modified procedure,[144] pivalic anhydride (9 mL, 45.06 mmol) was added to a solution of *tert*-butyl hydroxycarbamate (5 g, 37.55 mmol) in chloroform (100 ml, 0.4 M) and he reaction mixture was stirred under reflux. After 16 hours, the mixture was quenched with sat. $NaHCO_3$ (50 ml) and CH_2Cl_2 (50 ml). The phases were separated and the organic layer was washed with sat. $NaHCO_3$ (3 x 50 ml), dried (MgSO4), filtered and concentrated under reduced pressure. The colourless amorphous solid obtained (7.89 g, 36.33 mmol), which can be purified by flash column chromatography, eluting with 0:100 → 5:95 EtOAc–petrol, if desired, was dissolved in ether (90 ml, 0.4 M) and triflic acid (3.21 ml, 36.33 mmol) was added dropwise at 0°C. After the reaction was stirred for 30 minutes at room temperature, petrol (90 mL) was added. The precipitate was collected by filtration to give the ammonium salt[144] (8.55 g, 91% over two steps) as a colourless amorphous solid. δ_H (500 MHz,

Methanol-d_4) 1.33 (9H, s, ^{t}butyl–H). δ_C (126 MHz, Methanol-d_4) 174.5, 120.4 (q, J 318.4), 38.1, 25.6. Spectroscopic data matched previously reported.[144]

{3-[1-(2,2-Dimethylpropanoyl)-1H-pyrazol-4-yl]phenyl}formamido 2,2-dimethylpropanoate, 3-51
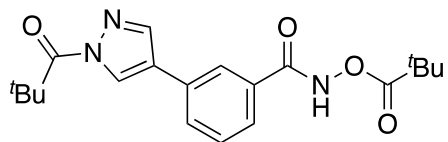
Pivaloyl chloride (123 µl, 1.00 mmol) in EtOAc (0.3 ml) was added dropwise to [3-(1H-pyrazol-4-yl)phenyl]formamido 2,2-dimethylpropanoate, (284 mg, 1.00 mmol) and $NaHCO_3$ (84 mg, 1.00 mmol) in a biphasic mixture of 2:1 EtOAc–H_2O (5 ml, 0.2 M) at 0 °C. The mixture was stirred vigorously for 2 h at rt, after which the reaction was quenched with EtOAc (10 ml) and sat. aq. soln. sodium hydrogen carbonate (10 ml). The aqueous phase was separated and extracted with EtOAc (3 x 25 ml) and the combined organics were washed with sat. aq. soln. sodium chloride (25 ml), dried ($MgSO_4$), filtered and concentrated under reduced pressure to give the *propanoate* (342 mg, 92%) as a colourless amorphous solid which was used without further purification. δ_H (501 MHz, Chloroform-d) 9.38 (1H, s, N–H), 8.53 (1H, d, J 0.9, pyrazolyl–H), 8.00 (1H, dt, J 1.8, 1.2, phenyl 2–H), 7.98 (1H, d, J 0.9, pyrazolyl–H), 7.71 (2H, app tdd, J 8.9, 1.8, 1.2, phenyl 4– and 6–H), 7.49 (1H, t, J 7.8, phenyl 5–H), 1.54 (9H, s, dimethylpropanoyl–H), 1.38 (9H, s, dimethylpropanoyl–H). δ_C (126 MHz, Chloroform-d) 177.24, 176.63, 141.02, 132.13, 131.92, 130.24, 129.67, 126.51, 126.26, 125.35, 123.66, 41.48, 38.64, 27.79, 27.18. R_F 0.94 (50:50 EtOAc–petrol). LCMS (ESI): $C_{20}H_{25}N_3O_4$ requires [M+H]$^+$, calculated 372.19, found 371.95.

3-[1-(1-Ethoxyethyl)-1*H*-pyrazol-4-yl]benzoic acid, 3-56
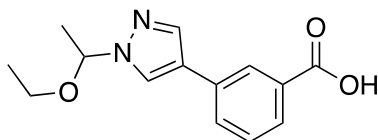
According to General Procedure E, 3-carboxybenzeneboronic acid (3.74 g, 22.50 mmol) and 1-(1-ethoxyethyl)-4-iodopyrazole (5.70 g, 21.42 mmol) were stirred for 30 minutes at 100 °C. After which, the reaction was cooled, filtered

through celite (eluting with H_2O) and acidified to pH 3. The mixture was filtered again, and the filtrate extracted with CH_2Cl_2 (3 x 50 ml). The combined organics were dried ($MgSO_4$), filtered, concentrated under reduced pressure and combined with the filtride to give a crude product which was purified by flash column chromatography, eluting with 0:100 → 5:95 MeOH–CH_2Cl_2 to give the *acid* (4.07 g, 73%) as a colourless amorphous solid. δ_H (500 MHz, Methanol-d_4) 8.22 (1H, t, *J* 1.6, 2–H), 8.18 (1H, s, pyrazolyl 5–H), 7.92 (1H, s, pyrazolyl 3–H), 7.88 (1H, dt, *J* 7.8, 1.6, 6–H), 7.77 (1H, dt, *J* 7.8, 1.6, 4–H), 7.44 (1H, t, *J* 7.8, 5–H), 5.54 (1H, q, *J* 6.0, ethyl 1–H), 3.47 (1H, dq, *J* 9.5, 7.0, ethoxy 1–H_A), 3.32 (1H, dq, *J* 9.5, 7.0, ethoxy 1–H_B), 1.67 (3H, d, *J* 6.0, ethyl 2–H), 1.12 (3H, t, *J* 7.0, ethoxy 2–H). δ_C (126 MHz, Methanol-d_4) 168.3, 136.4, 132.7, 131.2, 129.5, 128.8, 127.4, 126.2, 124.8, 122.6, 87.3, 63.8, 20.8, 13.8. R_F 0.21 (5:95 MeOH–CH_2Cl_2). IR ν_{max} (film)/cm^{-1} 3205, 2992, 2473, 1895, 1673 and 1253. HRMS (ESI): $C_{14}H_{16}N_2O_3$ requires [M+Na2-H]$^+$, calculated 305.0873, found 305.0867.

{3-[1-(1-Ethoxyethyl)-1*H*-pyrazol-4-yl]phenyl}formamido 2,2-dimethylpropanoate, 3-57
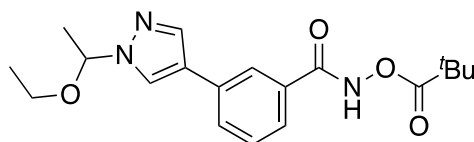
According to General Procedure C, 3-[1-(1-ethoxyethyl)-1H-pyrazol-4-yl]benzoic acid (4 g, 15.50 mmol) gave a crude product which was purified by flash column chromatography, eluting with 0:100 → 30:70 EtOAc–petrol to give the *propanoate* (3.9 g, 70%) as a colourless amorphous solid. δ_H (400 MHz, Chloroform-*d*) 7.94 (1H, t, *J* 1.8, phenyl 2–H), 7.87 (1H, s, pyrazolyl 5–H), 7.78 (1H, s, pyrazolyl 3–H), 7.66-7.61 (2H, m, phenyl 4– and 6–H), 7.41 (1H, t, *J* 7.7, phenyl 5–H), 5.50 (1H, q, *J* 6.0, ethyl 1–H), 3.44 (1H, dq, *J* 9.5, 7.0, ethoxyethyl 1–H_A), 3.33 (1H, dq, *J* 9.5, 7.0, ethoxyethyl 1–H_B), 1.65 (3H, d, *J* 6.0, ethyl 2–H), 1.35 (9H, s, *t*Bu), 1.13 (3H, t, *J* 7.0, ethoxyethyl 2–H). δ_C (101 MHz, Chloroform-*d*) 177.0, 166.7, 136.3, 133.3, 131.6, 129.4, 129.3, 125.2, 124.7, 123.3, 122.6, 87.8, 64.2, 38.5 27.1, 22.1, 14.8. R_F 0.22 (30:70 EtOAc–petrol). IR ν_{max} (film)/cm^{-1} 3210, 2978, 1776, 1656 and 1609. HRMS (ESI): $C_{19}H_{25}N_3O_4$ requires [M+H]$^+$, calculated 360.1918, found 360.1910.

7-Bromo-3-phenyl-1,2,3,4-tetrahydroisoquinolin-1-one, 3-58
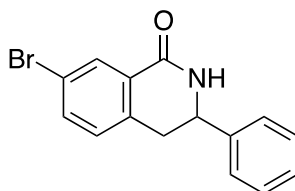
According to a modified procedure,[144] without any precautions to extrude moisture or air, styrene (85 μl, 0.74 mmol) was added to a solution of (3-bromophenyl)formamido 2,2-dimethylpropanoate **3-43** (200 mg, 0.67 mmol), [Cp*RhCl$_2$]$_2$ (4 mg, 6.70 μM, 1 mol%) and CsOAc (257 mg, 1.34 mmol) in MeOH (3.35 ml, 0.2 M). The reaction was stirred at room temperature for 18 hours. After which, the reaction was adsorbed onto silica and purified by flash column chromatography, eluting with 0:100 → 30:70 EtOAc–petrol. The purified compound was then dissolved in MeCN, washed with petrol and concentrated under reduced pressure to give the *isoquinolinone* (176 mg, 87%) as a colourless amorphous solid. δ_H (500 MHz, DMSO-d_6) 8.51 (1H, app. br. d, *J* 2.9, N–H), 7.97 (1H, d, *J* 2.3, 8–H), 7.63 (1H, dd, *J* 8.1, 2.3, 6–H), 7.38-7.28 (5H, m, phenyl–H), 7.23 (1H, d, *J* 8.1, 5–H), 4.83 (1H, ddd, *J* 7.0, 5.6, 2.9, 3–H), 3.28 (1H, dd, *J* 16.1, 5.6, 4–H$_A$), 3.07 (1H, dd, *J* 16.1, 7.0, 4–H$_B$). δ_C (126 MHz, DMSO-d_6) 161.8, 140.2, 135.0, 132.9, 129.4, 128.6, 127.6, 126.7, 125.7, 124.7, 118.1, 51.7, 33.4. R_F 0.30 (30:70 EtOAc–petrol). IR ν_{max} (film)/cm^{-1} 3369, 3063, 2895, 1663 and 1594. HRMS (ESI): $C_{15}H_{12}BrNO$ requires [M+Na]$^+$, calculated 323.9994, found 323.9991.

3-Phenyl-7-(1*H*-pyrazol-4-yl)-1,2,3,4-tetrahydroisoquinolin-1-one, 3-60
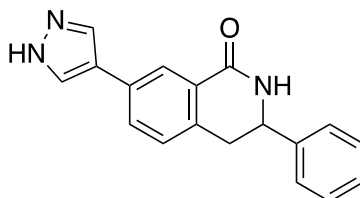
According to General Procedure A, {3-[1-(2,2-dimethylpropanoyl)-1H-pyrazol-4-yl]phenyl}formamido 2,2-dimethylpropanoate **3-42** (25.3 mg, 0.07 mmol), [Cp*RhCl$_2$]$_2$ (1.50 mg, 2.43 μmol, 3.5 mol%) and styrene (9 μl, 0.08 mmol) gave a crude material which was purified by flash column chromatography, eluting with 0:100 → 5:95 MeOH–CH$_2$Cl$_2$ to give the *isoquinolinone* (8 mg,

40%) as a colourless amorphous solid. δ_H (500 MHz, Chloroform-d) 8.28 (1H, d, J 1.9, 8–H), 8.02 – 7.89 (2H, br. s, pyrazolyl–H), 7.62 (1H, dd, J 7.8, 1.9, 6–H), 7.44-7.38 (4H, m, phenyl 2–, 3–, 5– and 6–H), 7.38-7.33 (1H, m, phenyl 1–H), 7.21 (1H, d, J 7.8, 5–H), 6.17 (1H, s, N–H), 4.88 (1H, ddd, J 10.9, 4.9, 1.2, 3–H), 3.31-3.08 (2H, m, 4–H). δ_C (126 MHz, Chloroform-d) 166.5, 141.0, 135.8, 131.8, 129.8, 129.2, 128.9, 128.6, 128.2, 126.6, 125.2, 56.4, 37.3. R_F 0.25 (5:95 MeOH–CH$_2$Cl$_2$). IR ν_{max} (film)/cm^{-1} 3255, 2959, 2928, 1651 and 1616. HRMS (ESI): C$_{18}$H$_{15}$N$_3$O requires [M+Na]$^+$, calculated 312.1107, found 312.1099.

4-Benzyl-7-(1H-pyrazol-4-yl)-1,2,3,4-tetrahydroisoquinolin-1-one and 3-benzyl-7-(1H-pyrazol-4-yl)-1,2,3,4-tetrahydroisoquinolin-1-one, 3-63

According to General Procedure A, [3-(1H-pyrazol-4-yl)phenyl]formamido 2,2-dimethylpropanoate **3-42** (80 mg, 0.28 mmol), [Cp*RhCl$_2$]$_2$ (6 mg, 9.70 µmol, 3.5 mol%) and allylbenzene (44 µl, 0.33 mmol) gave a crude material which was purified by flash column chromatography, eluting with 0:100 → 10:90 MeOH–CH$_2$Cl$_2$ to give the *isoquinolinones* (7 mg, 8%), as a 5:3 mixture of inseparable regioisomers, as an off-white amorphous solid. δ_H (500 MHz, Methanol-d_4) 8.16 (5H, d, J 2.0, 8–H *major*), 8.12 (3H, d, J 2.0 8–H *minor*), 7.99 (16H, app. br. s, pyrazolyl–H *major and minor*), 7.71 (3H, dd, J 7.8, 2.0, 6–H *minor*), 7.66 (5H, dd, J 7.9, 2.0, 6–H *major*), 7.35-7.26 (16H, m, benzyl–H *major and minor*), 7.26-7.19 (18H, m, 5–H *minor* and benzyl–H *major and minor*), 7.19-7.15 (11H, m, benzyl–H *major and minor*), 7.14 (5H, d, J 7.9, 5–H *major*), 3.90 (3H, dtd, J 7.7, 6.4, 5.3, 3–H *minor*), 3.53 (5H, dd, J 12.9, 4.4, 3–H$_A$ *major*), 3.30 (5H, app. d, J 2.8, 3–H$_B$ *major* peak under MeOD), 3.14 (5H, dddd, J 9.3, 6.8, 4.4, 2.8, 4–H *major*), 3.01–2.92 (11H, m, benzyl–H *major and minor*), 2.88 (5H, app. dd, J 13.4, 9.3, benzyl–H *major*), 2.83-2.75 (6H, m, 4–H *minor*). δ_C (126 MHz, Methanol-d_4) 166.7, 166.6, 140.8, 139.1, 137.3, 135.8, 131.9, 131.8, 129.3, 129.0, 129.0, 128.9, 128.6, 128.4, 128.3, 128.1,

128.1, 128.0, 126.4, 126.1, 123.9, 123.8, 121.4, 121.4, 52.2, 42.3, 40.5, 39.5, 39.3, 31.7. R_F 0.56 and 0.59 (10:90 MeOH–CH$_2$Cl$_2$). IR ν_{max} (film)/cm^{-1} 3208, 2974, 2929, 1654 and 1614. HRMS (ESI): C$_{19}$H$_{17}$N$_3$O requires [M+Na]$^+$, calculated 326.1264, found 326.1260.

7-(1*H*-Pyrazol-4-yl)-3-(pyridin-4-yl)-1,2,3,4-tetrahydroisoquinolin-1-one, 3-64
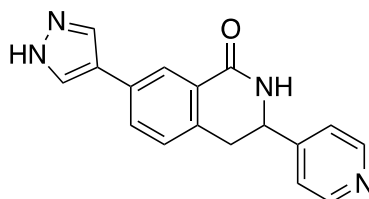
According to General Procedure A, [3-(1H-pyrazol-4-yl)phenyl]formamido 2,2-dimethylpropanoate **3-42** (80 mg, 0.28 mmol), [Cp*RhCl$_2$]$_2$ (6 mg, 9.70 µmol, 3.5 mol%) and 4-vinylpyridine (30 µl, 0.33 mmol) gave a crude material which was purified by flash column chromatography, eluting with 0:100 → 5:95 MeOH–CH$_2$Cl$_2$ to give the *isoquinolinone* (11 mg, 13%) as a light yellow amorphous solid. δ_H (500 MHz, DMSO-d_6) 13.00 (1H, s) 8.49 (2H, dd, *J* 4.4, 1.7, pyridinyl 2– and 6–H), 8.24 (1H, app. br. s, pyrazolyl–H), 8.06 (1H, d, *J* 2.0, 8–H), 7.92 (1H, app. br. s, pyrazolyl–H), 7.68 (1H, dd, *J* 7.8, 2.0, 6–H), 7.32 (1H, dd, *J* 5.9, 1.7, pyridinyl 3– and 5–H), 7.22 (1H, d, *J* 7.8, 5–H), 4.86 (1H, td, *J* 5.8, 3.1, 3–H), 3.37 (1H, dd, *J* 16.0, 5.8, 4–H$_A$), 3.10 (1H, dd, *J* 16.0, 5.8, 4–H$_B$). δ_C (126 MHz, DMSO-d_6) 165.2, 151.6, 150.1, 136.6, 134.6, 132.3, 129.7, 129.3, 128.8, 126.1, 123.6, 122.1, 120.9, 52.9, 34.8. R_F 0.09 (5:95 MeOH–CH$_2$Cl$_2$). IR ν_{max} (film)/cm^{-1} 3376, 2986, 2359, 2341, 1655 and 1615. HRMS (ESI): C$_{17}$H$_{14}$N$_4$O requires [M+Na]$^+$, calculated 313.1060, found 313.1059.

Methyl-1-oxo-7-(1*H*-pyrazol-4-yl)-1,2,3,4-tetrahydroisoquinoline-3-carboxylate, 3-65
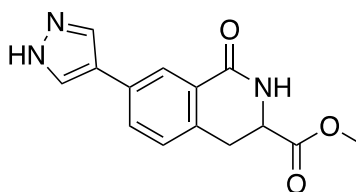
According to General Procedure A, [3-(1H-pyrazol-4-yl)phenyl]formamido 2,2-dimethylpropanoate **3-42** (80 mg, 0.28 mmol), [Cp*RhCl$_2$]$_2$ (6 mg, 9.70 μmol, 3.5 mol%) and methyl acrylate (30 μl, 0.33 mmol) gave a crude material which was purified by flash column chromatography, eluting with 0:100 → 5:95 MeOH–CH$_2$Cl$_2$ to give the *isoquinoline* (53 mg, 70%) as a colourless amorphous solid. δ_H (500 MHz, Acetone-d_6) 8.16 (1H, d, *J* 2.0, 8–H), 8.08 (2H, s, pyrazolyl–H), 7.73 (1H, dd, *J* 7.8, 2.0, 6–H), 7.30 (1H, d, *J* 7.8), 7.22 (1H, br. s, N–H), 4.50 (1H, ddd, *J* 6.2, 5.3, 3.6, 3–H), 3.66 (3H, s, methyl–H), 3.41 (1H, dd, *J* 16.0, 6.2, 4–H$_A$), 3.24 (1H, dd, *J* 16.0, 5.3, 4–H$_B$). δ_C (126 MHz, Acetone-d_6) 172.8, 165.4, 134.9, 133.3, 131.8, 130.3, 129.8, 129.1, 124.9, 122.1, 53.8, 52.7, 31.3. R_F 0.22 (5:95 MeOH–CH$_2$Cl$_2$). IR v_{max} (film)/cm^{-1} 3383, 2989, 2921, 2358, 1655 and 1437. HRMS (ESI): C$_{14}$H$_{13}$N$_3$O$_3$ requires [M+H]$^+$, calculated 272.1030, found 272.1025.

N-Methyl-1-oxo-7-(1*H*-pyrazol-4-yl)-1,2,3,4-tetrahydroisoquinoline-3-carboxamide, 3-71
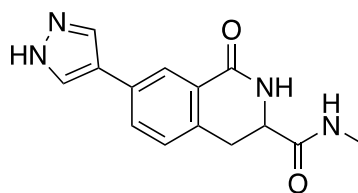
2 M methylamine in THF (0.8 ml, 1.6 mmol) was added to a solution of methyl-1-oxo-7-(1H-pyrazol-4-yl)-1,2,3,4-tetrahydroisoquinoline-3-carboxylate, **3-65** (13 mg, 0.048 mmol) in MeOH (0.3 ml, 0.16 M) and the reaction mixture was stirred at reflux overnight. After which, the mixture was cooled and concentrated under reduced pressure to give a crude product which was purified by flash column chromatography, eluting with 0:100 → 10:90 MeOH–CH$_2$Cl$_2$to give the *carboxamide* (11 mg, 85%) as a colourless amorphous solid. δ_H (500 MHz, Methanol-d_4) 8.12 (1H, d, *J* 1.9, 8–H), 8.09-7.88 (2H, br. m, pyrazolyl–H), 7.71 (1H, dd, *J* 7.9, 1.9, 6–H), 7.28 (1H, d, *J* 7.9, 5–H), 4.27 (1H, t, *J* 5.9, 3–H), 3.26 (2H, dd, *J* 15.8, 5.9, 4–H), 2.70 (3H, s, methyl–H). δ_C (126 MHz, Methanol-d_4) 173.7, 167.8, 137.5, 135.9, 133.5, 130.7, 129.9, 129.4, 126.8, 125.2, 122.7, 55.1, 32.0, 26.6. R_F 0.27 (10:90 MeOH–CH$_2$Cl$_2$). IR v_{max} (film)/cm^{-1} 3571, 3374, 2958, 1657 and 1617. HRMS (ESI): C$_{14}$H$_{14}$N$_4$O$_2$ requires [M+H]$^+$, calculated 271.1190, found 271.1197.

N-benzyl-1-oxo-7-(1*H*-pyrazol-4-yl)-1,2,3,4-tetrahydroisoquinoline-3-carboxamide, 3-66
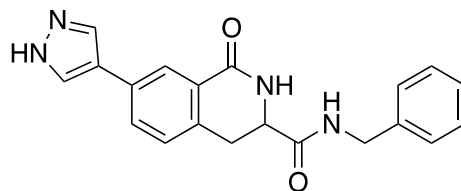
According to General Procedure A, {3-[1-(2,2-dimethylpropanoyl)-1H-pyrazol-4-yl]phenyl}formamido 2,2-dimethylpropanoate **3-51** (100 mg, 0.28 mmol), [Cp*RhCl$_2$]$_2$ (6 mg, 9.70 μmol, 3.5 mol%) and *N*-benzylacrylamide (49 mg, 0.33 mmol) gave a crude material which was purified by flash column chromatography, eluting with 0:100 → 10:90 MeOH–CH$_2$Cl$_2$ to give the *isoquinoline* (53 mg, 55%) as an off-white amorphous solid. δ_H (500 MHz, Methanol-d_4) 8.11 (1H, d, *J* 1.9, 8–H), 7.98 (2H, s, pyrazolyl–H), 7.73 (1H, dd, *J* 7.8, 1.9, 6–H), 7.27 (1H, d, *J* 7.8, 5–H), 7.18-7.08 (3H, m, benzyl–H), 6.98 (2H, app. dd, *J* 7.7, 1.9, benzyl–H), 4.40 (1H, d, *J* 15.1, benzyl–H$_A$), 4.32 (1H, dd, *J* 6.0, 5.0, 3–H), 4.25 (1H, d, *J* 15.1, benzyl–H$_B$), 3.31 (2H, m, 4–H peak under MeOD). δ_C (126 MHz, Methanol-d_4) 173.2, 167.9, 139.6, 135.9, 133.5, 132.1, 130.7, 130.2, 129.5, 129.4, 128.0, 128.0, 125.2, 122.7, 55.1, 44.1, 32.3. R_F 0.47 (10:90 MeOH–CH$_2$Cl$_2$). IR ν_{max} (film)/cm^{-1} 3254, 2970, 2359, 2341, 1656 and 1617. HRMS (ESI): C$_{20}$H$_{18}$N$_4$O$_2$ requires [M+Na]$^+$, calculated 369.1322, found 369.1320.

tert-Butyldimethyl(prop-2-en-1-yloxy)silane
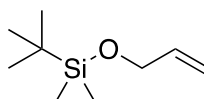
According to a modified procedure,[198] *tert*-butyl dimethylsilyl chloride (1.46 g, 9.68 mmol) followed by imidazole (5.4 ml, 97.68 mmol) was added to a solution of allyl alcohol (0.6 ml, 8.80 mmol) in DMF (17 ml, 0.5 M). After stirring at room temperature for 24 hours, H$_2$O (50 ml) and CH$_2$Cl$_2$ (50 ml) were added. The phases were separated and the aqueous layer was extracted with CH$_2$Cl$_2$ (3 x 50 ml). The combined organics were washed with ice-cold 1 M HCl (3 x 30 ml), H$_2$O (50 ml), LiCl (50 ml), dried (MgSO$_4$), filtered and concentrated under reduced pressure to give the *silane*[199] (1.3 g, 86%) as a

colourless oil. δ_H (500 MHz, Chloroform-*d*) 5.90 (1H, ddt, *J* 17.1, 10.4, 4.5, propenyloxy 2–H), 5.25 (1H, dq, *J* 17.1, 1.9, propenyloxy 3–H$_{trans}$), 5.06 (1H, dq, *J* 10.4, 1.9, propenyloxy 3–H$_{cis}$), 4.16 (2H, dt, *J* 4.5, 1.9, propenyloxy 1–H), 0.90 (9H, app. d, *J* 1.9, *t*Butyl–H), 0.06 (6H, s, dimethyl–H). δ_C (126 MHz, Chloroform-*d*) 136.5, 112.9, 63.1, 17.4, 24.9, -6.3. Spectroscopic data matched previously reported.[199]

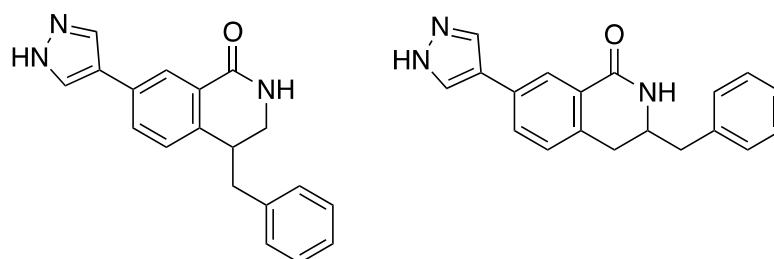### 3-(Hydroxymethyl)-7-(1*H*-pyrazol-4-yl)-1,2,3,4-tetrahydroisoquinolin-1-one, 3-67
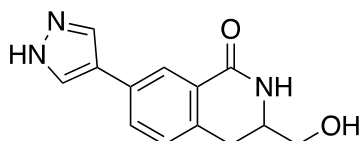
According to General Procedure A, [3-(1H-pyrazol-4-yl)phenyl]formamido 2,2-dimethylpropanoate **3-42** (80 mg, 0.28 mmol), [Cp*RhCl$_2$]$_2$ (6 mg, 9.70 μmol, 3.5 mol%) and tert-butyldimethyl(prop-2-en-1-yloxy)silane (71 μl, 0.33 mmol) gave a crude material which was purified by flash column chromatography, eluting with 0:100 → 5:95 MeOH–CH$_2$Cl$_2$ to give the TBS protected alcohol. The TBS protected alcohol was concentrated into a polypropylene Eppendorf tube and dissolved in anhydrous THF (1 ml, 0.13 M). HF•pyridine (50 μl) was added to the reaction followed by, after consumption of the starting material by TLC, methoxytrimethylsilane (300 μl). The reaction was stirred at room temperature for 18 hours and concentrated under reduced pressure to give the *isoquinolinone* (3 mg, 4% over two steps) as a yellow amorphous solid. δ_H (500 MHz, Methanol-*d*$_4$) 8.13 (1H, d, *J* 1.9, 8–H), 8.04 (1H, br s, pyrazolyl–H), 7.95 (1H, br s, pyrazolyl–H), 7.73 (1H, dd, *J* 7.9, 1.9, 6–H), 7.32 (1H, d, *J* 7.9, 5–H), 3.74 (1H, dq, *J* 8.4, 6.0, 3–H), 3.64-3.56 (2H, m, hydroxymethyl–H), 3.06 (1H, dd, *J* 16.0, 5.2, 4–H$_A$), 2.95 (1H, dd, *J* 16.0, 8.4, 4–H$_B$). δ_C (126 MHz, Methanol-*d*$_4$) 166.6, 136.1, 135.8, 131.8, 129.3, 128.5, 128.4, 125.3, 123.7, 121.4, 63.3, 52.4, 29.0. R_F 0.06 (5:95 MeOH–CH$_2$Cl$_2$). IR v_{max} (film)/cm^{-1} 3376, 2987, 2901, 2358, 2342 and 1648. HRMS (ESI): C$_{13}$H$_{13}$N$_3$O$_2$ requires [M+Na]$^+$, calculated 266.0900, found 266.0898.

[1-Oxo-7-(1*H*-pyrazol-4-yl)-1,2,3,4-tetrahydroisoquinolin-3-yl]methanaminium trifluoroacetate, 3-68

According to General Procedure A, {3-[1-(1-ethoxyethyl)-1H-pyrazol-4-yl]phenyl}formamido 2,2-dimethylpropanoate **3-57** (500 mg, 1.39 mmol), [Cp*RhCl$_2$]$_2$ (26 mg, 41.70 μmol, 3 mol%) and tert-butyl N-(prop-2-en-1-yl)carbamate (0.35 ml, 2.09 mmol) gave a crude material which was purified by mass-directed HPLC, eluting with 5:95 → 95:5 MeCN–H$_2$O plus 1% formic acid to give the bis-protected isoquinoline. According to General Procedure B, the bis-protected isoquinoline (232.5 mg, 0.56 mmol) gave the *methanaminium* (200 mg, 40% over two steps) as a yellow oil. δ$_H$ (500 MHz, Methanol-d_4) 8.14 (1H, d, *J* 2.0, isoquinolinyl 8–H), 8.02 (2H, app. d, *J* 4.3, pyrazolyl–H), 7.76 (1H, dd, *J* 7.9, 2.0, isoquinolinyl 6–H), 7.34 (1H, d, *J* 7.9 isoquinolinyl 5–H), 4.01 (1H, tt, *J* 6.7, 5.6, isoquinolinyl 3–H), 3.26 (1H, dd, *J* 16.0, 5.6, isoquinolinyl 4–H$_A$), 3.17-3.07 (2H, m, methan–H), 2.97 (1H, dd, *J* 16.0, 6.7 isoquinolinyl 4–H$_B$). δ$_C$ (126 MHz, Methanol-d_4) 167.5, 161.7 (q, *J* 38.0), 135.8, 133.5, 132.2, 131.1, 130.0, 129.5, 125.3, 122.7, 117.5 (app. d, *J* 289.5), 49.8, 43.7, 31.2. R_F 0.16 (10:90 7M NH$_3$ in MeOH–CH$_2$Cl$_2$). IR ν$_{max}$ (film)/cm^{-1} 3215, 2970, 2360, 1673 and 1617. HRMS (ESI): C$_{13}$H$_{14}$N$_4$O requires [M+H]$^+$, calculated 243.1240, found 243.1240.

[1-Oxo-7-(1*H*-pyrazol-4-yl)-1,2,3,4-tetrahydroisoquinolin-4-yl]methanaminium trifluoroacetate, 3-69

According to General Procedure A, {3-[1-(1-ethoxyethyl)-1H-pyrazol-4-yl]phenyl}formamido 2,2-dimethylpropanoate **3-57** (500 mg, 1.39 mmol), [Cp*RhCl$_2$]$_2$ (26 mg, 41.70 μmol, 3 mol%) and tert-butyl N-(prop-2-en-1-yl)carbamate (0.35 ml, 2.09 mmol) gave a crude material which was purified by mass-directed HPLC, eluting with 5:95 → 95:5 MeCN–H$_2$O plus 1% formic

acid to give the bis-protected isoquinoline. According to General Procedure B, the bis-protected isoquinoline (293.8 mg, 0.71 mmol) gave the *isoquinolinium* (253 mg, 51% over two steps) as a yellow oil. δ_H (500 MHz, Methanol-d_4) 8.19 (1H, d, *J* 2.0, isoquinolinyl 8–H), 8.05 (2H, s, pyrazolyl–H), 7.82 (1H, dd, *J* 7.9, 2.0, isoquinolinyl 6–H), 7.42 (1H, d, *J* 7.9, isoquinolinyl 5–H), 3.77 (1H, dd, *J* 13.6, 3.6, isoquinolinyl 3–H$_A$), 3.57 (1H, dd, *J* 13.6, 1.8, isoquinolinyl 2–H$_B$), 3.29 (2H, m, isoquinolinyl 4–H and methan–H$_A$), 3.15 (1H, app. dd, *J* 10.4, 6.2, methan–H$_B$). δ_C (126 MHz, Methanol-d_4) 167.3, 161.6 (q, *J* 37.8), 137.3, 134.5, 132.3, 131.1, 129.9, 129.6, 125.9, 122.5, 117.4 (q, *J* 289.8), 42.3, 42.2, 36.9. R_F 0.12 (10:90 7M NH$_3$ in MeOH–CH$_2$Cl$_2$). IR ν_{max} (film)/cm^{-1} 3195, 2970 2360, 1667 and 1615. HRMS (ESI): $C_{13}H_{14}N_4O$ requires [M+H]$^+$, calculated 243.1240, found 243.1238.

1'-Oxo-7'-(1*H*-pyrazol-4-yl)-2',4'-dihydro-1'H-spiro[azetidine-3,3'-isoquinolin]-1-ium trifluoroacetate, 3-70
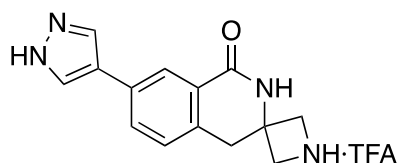
According to General Procedure A, {3-[1-(1-ethoxyethyl)-1H-pyrazol-4-yl]phenyl}formamido 2,2-dimethylpropanoate **3-57** (500 mg, 1.39 mmol), [Cp*RhCl$_2$]$_2$ (26 mg, 41.70 μmol, 3 mol%) and tert-butyl 3-methylideneazetidine-1-carboxylate (0.39 ml, 2.09 mmol) gave a crude material which was purified by flash column chromatography, eluting with 0:100 → 10:90 MeOH–CH$_2$Cl$_2$ to give the bis-protected isoquinoline. According to General Procedure B, the bis-protected isoquinoline (559 mg, 1.31 mmol) gave the *isoquinolinium* (481 mg, 94% over two steps) as a yellow amorphous solid. δ_H (500 MHz, Methanol-d_4) 8.14 (1H, d, *J* 2.0, isoquinolin 8–H), 8.04 (2H, br. s, pyrazolyl–H), 7.81 (1H, dd, *J* 7.8, 2.0, isoquinolin 6–H), 7.43 (1H, d, *J* 7.8, isoquinolin 5–H), 4.26 (1H, d, *J* 10.1, azetidine–H$_A$), 4.26 (1H, d, *J* 10.1, azetidine–H$_B$), 4.10 (1H, d, *J* 10.2, azetidine–H$_A$), 4.10 (1H, d, *J* 10.2, azetidine–H$_B$), 3.43 (2H, s, isoquinolin 4–H). δ_C (126 MHz, Methanol-d_4) 166.8, 161.0 (q, *J* 38.0), 134.1, 134.1, 132.3, 131.2, 130.3, 129.5, 125.3, 122.6, 117.2 (app. d, *J* 289.7), 58.6, 54.4, 37.4. R_F 0.09 (10:90 7M NH$_3$ in MeOH–CH$_2$Cl$_2$). IR ν_{max} (film)/cm^{-1} 3351, 3200, 2987, 2901, 2359, 2341, 1660

and 1617. HRMS (ESI): $C_{14}H_{14}N_4O$ requires $[M+H]^+$, calculated 255.1240, found 255.1240.

tert-Butyl N-methyl-N-(prop-2-en-1-yl)carbamate
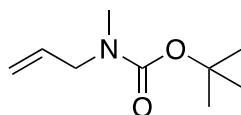
N-methyl ally amine (1.00 g, 14.0 mmol) followed by Et_3N (2.16 ml, 15.5 mmol) was added to a solution of di-*tert*-butyl dicarbonate (3.38 g, 15.5 mmol) in CH_2Cl_2 (35 ml, 0.4 M) and the reaction mixture was stirred overnight at room temperature. After which, the reaction was quenched with sat. $NaHCO_3$ soln. (35 ml) and the phases were separated. The organic layer was washed with sat. $NaHCO_3$ soln. (35 ml), H_2O (2 x 35 ml), and sat. brine soln. (35 ml) and dried ($MgSO_4$), filtered and concentrated under reduced pressure to give the *carbamate*[200], which was used without further purification, (1.98 g, 82%) as a colourless oil. δ_H (500 MHz, Chloroform-*d*) 5.69 (1H, ddt, *J* 16.3, 10.8, 5.7, propenyl 2–H), 5.12-4.97 (2H, m, propenyl 3–H), 3.73 (2H, br. s, propenyl 1–H), 2.75 (3H, s, methyl–H), 1.38 (9H, s, *t*butyl–H). δ_C (126 MHz, Chloroform-*d*) 155.7, 146.8, 133.7, 85.1, 79.3, 33.7, 28.4. Spectroscopic data matched previously reported.[200]

Methyl({[1-oxo-7-(1*H*-pyrazol-4-yl)-1,2,3,4-tetrahydroisoquinolin-3-yl]methyl})azanium trifluoroacetate, 3-72

According to General Procedure A, {3-[1-(1-ethoxyethyl)-1H-pyrazol-4-yl]phenyl}formamido 2,2-dimethylpropanoate **3-57** (125 mg, 0.35 mmol), [Cp*RhCl₂]₂ (6.5 mg, 10.5 μmol, 3 mol%) and tert-butyl N-methyl-N-(prop-2-en-1-yl)carbamate (90 mg, 0.53 mmol) gave a crude material which was purified by mass-directed HPLC, eluting with 5:95 → 95:5 MeCN–H_2O plus 1% formic acid to give the bis-protected isoquinoline. According to General Procedure B, the bis-protected isoquinoline (56 mg, 0.13 mmol) gave the *azanium* (48 mg, 43% over two steps) as a yellow oil. δ_H (500 MHz, Methanol-*d₄*) 8.13 (1H, d, *J* 1.9, isoquinolinyl 8–H), 8.00 (2H, s, pyrazolyl–H), 7.76 (1H,

dd, J 7.9, 1.9, isoquinolinyl 6–H), 7.34 (1H, d, J 7.9, isoquinolinyl 5–H), 4.07 (1H, ddd, J 12.1, 6.7, 5.7, isoquinolinyl 3–H), 3.29 (1H, d, J 5.7, isoquinolinyl 4–H$_A$), 3.20-3.15 (2H, m, isoquinolinyl-3-methyl–H), 2.95 (1H, dd, J 16.1, 5.7, isoquinolinyl 4–H$_B$), 2.75 (3H, s, methyl–H). δ_C (126 MHz, Methanol-d_4) 167.4, 161.9 (q, J 36.9), 135.7, 133.7, 132.2, 131.1, 130.0, 129.5, 125.4, 122.6, 117.5 (q, J 290.0), 53.4, 48.7, 34.2, 31.3. R_F 0.24 (10:90 7M NH$_3$ in MeOH–CH$_2$Cl$_2$). IR ν_{max} (film)/cm^{-1} 3234, 2971, 2925, 2361, 2342, 1670 and 1617. HRMS (ESI): C$_{14}$H$_{16}$N$_4$O requires [M+H]$^+$, calculated 257.1397, found 257.1398.

Methyl({[1-oxo-7-(1H-pyrazol-4-yl)-1,2,3,4-tetrahydroisoquinolin-4-yl]methyl})azanium trifluoroacetate, 3-73

According to General Procedure A, {3-[1-(1-ethoxyethyl)-1H-pyrazol-4-yl]phenyl}formamido 2,2-dimethylpropanoate **3-57** (125 mg, 0.35 mmol), [Cp*RhCl$_2$]$_2$ (6.5 mg, 10.5 μmol, 3 mol%) and tert-butyl N-methyl-N-(prop-2-en-1-yl)carbamate (90 mg, 0.53 mmol) gave a crude material which was purified by mass-directed HPLC, eluting with 5:95 → 95:5 MeCN–H$_2$O plus 1% formic acid to give the bis-protected isoquinoline. According to General Procedure B, the bis-protected isoquinoline (78 mg, 0.18 mmol) gave the *azanium* (67 mg, 52% over two steps) as a light yellow amorphous solid. δ_H (500 MHz, Methanol-d_4) 8.19 (1H, d, J 2.0, isoquinolinyl 8–H), 8.08 (2H, s, pyrazolyl–H), 7.82 (1H, dd, J 7.9, 2.0, isoquinolinyl 6–H), 7.42 (1H, d, J 7.9, isoquinolinyl 5–H), 3.77 (1H, dd, J 13.5, 3.6, isoquinolinyl 3–H$_A$), 3.56 (1H, dd, J 13.5, 1.8, isoquinolinyl 3–H$_B$), 3.42-3.34 (2H, m, isoquinolinyl 4–H and isoquinolinyl 4 methyl–H$_A$), 3.28-3.20 (1H, m, isoquinolinyl 4 methyl–H$_B$), 2.75 (3H, s, methyl–H). δ_C (126 MHz, Methanol-d_4) 167.2, 161.1 (q, J 38.1), 137.1, 134.5, 132.3, 131.1, 130.0, 129.6, 126.0, 122.6, 117.1 (q, J 288.2), 52.0, 42.5, 36.2, 34.5. R_F 0.16 (10:90 7M NH$_3$ in MeOH–CH$_2$Cl$_2$). IR ν_{max} (film)/cm^{-1} 3360, 2987, 2901, 2360, 2342, 1658 and 1614. HRMS (ESI): C$_{14}$H$_{16}$N$_4$O requires [M+H]$^+$, calculated 257.1397, found 257.1397.

Dimethyl({[1-oxo-7-(1*H*-pyrazol-4-yl)-1,2,3,4-tetrahydroisoquinolin-3-yl]methyl})azanium trifluoroacetate, 3-74
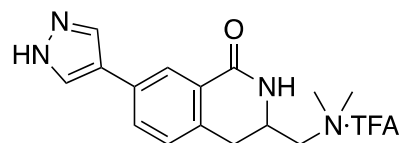
According to General Procedure A, {3-[1-(1-ethoxyethyl)-1H-pyrazol-4-yl]phenyl}formamido 2,2-dimethylpropanoate **3-57** (125 mg, 0.35 mmol), [Cp*RhCl₂]₂ (6.5 mg, 10.5 μmol, 3 mol%) and *N,N*-dimethylallylamine (0.16 ml, 1.33 mmol) stirred at 45 °C gave a crude material which was purified by flash column chromatography, eluting with 0:100 → 10:90 MeOH–CH₂Cl₂ to give the ethoxyethyl-protected pyrazole. According to General Procedure B, the ethoxyethyl-protected pyrazole (84 mg, 0.25 mmol) gave the *azanium* (96 mg, 71% over two steps) as an orange oil. δ$_H$ (500 MHz, Methanol-*d₄*) 8.07 (1H, d, *J* 2.0, isoquinolinyl 8–H), 7.97 (2H, s, pyrazolyl–H), 7.72 (1H, dd, *J* 7.9, 2.0, isoquinolinyl 6–H), 7.30 (1H, d, *J* 7.9, isoquinolinyl 5–H), 4.20 (1H, ddt, *J* 10.2, 5.7, 4.5, isoquinolinyl 3–H), 3.37-3.29 (2H, m, isoquinolinyl 4–H$_A$ and methyl–H$_A$), 3.21 (1H, dd, *J* 13.3, 4.5, methyl–H$_B$), 2.92 (6H, s, diemthyl–H), 2.88 (1H, dd, *J* 16.5, 4.5, isoquinolinyl 4–H$_B$). δ$_C$ (126 MHz, Methanol-*d₄*) 167.1, 161.8 (q, *J* 36.9), 135.6, 133.5, 132.2, 131.1, 130.1, 129.6, 125.5, 122.7, 117.5 (q, *J* 291.2), 61.9, 47.0, 45.2, 43.2, 31.5. R_F 0.49 (10:90 7M NH₃ in MeOH–CH₂Cl₂). IR ν$_{max}$ (film)/cm⁻¹ 3232, 2972, 2360, 1674 and 1618. HRMS (ESI): C₁₅H₁₈N₄O requires [M+H]⁺, calculated 271.1553, found 271.1550.

7-(1*H*-Pyrazol-4-yl)-2*H*,3*H*,3a*H*,4*H*,5*H*,9b*H*-furo[3,2-c]isoquinolin-5-one, 3-75

According to General Procedure A, {3-[1-(1-ethoxyethyl)-1H-pyrazol-4-yl]phenyl}formamido 2,2-dimethylpropanoate **3-57** (125 mg, 0.35 mmol), [Cp*RhCl₂]₂ (7.6 mg, 12.25 μmol, 3.5 mol%) and 2,3-dihydrofuran (0.1 ml,

1.33 mmol) stirred at 45 °C gave a crude material which was purified by flash column chromatography, eluting with 0:100 → 10:90 MeOH–CH$_2$Cl$_2$ to give the ethoxyethyl-protected pyrazole. According to General Procedure B, the ethoxyethyl-protected pyrazole (101.3 mg, 0.31 mmol) gave the *isoquinolinone* (56 mg, 61% over two steps) as a yellow oil. δ$_H$ (500 MHz, Methanol-*d*$_4$) 8.23 (1H, d, *J* 1.9, 6–H), 8.03 (2H, s, pyrazolyl–H), 7.81 (1H, dd, *J* 7.8, 1.9, 8–H), 7.47 (1H, d, *J* 7.8, 9–H), 4.79 (1H, d, *J* 4.3, 9b–H), 4.29 (1H, ddd, *J* 5.8, 4.3, 1.8, 3a–H), 3.99 (2H, dd, *J* 9.0, 5.4, 2–H), 2.43 (1H, dtd, *J* 13.0, 9.0, 5.8, 3–H$_A$), 2.25 (1H, dtd, *J* 13.0, 5.4, 1.8, 3–H$_B$). δ$_C$ (126 MHz, Methanol-*d*$_4$) 166.3, 135.5, 134.5, 131.3, 130.6, 129.0, 125.1, 122.5, 76.3, 67.5, 55.5, 35.1. *R*$_F$ 0.45 (10:90 MeOH–CH$_2$Cl$_2$). IR ν$_{max}$ (film)/cm^{-1} 3378, 3253, 2975, 2360, 2341, 1655 and 1615. HRMS (ESI): C$_{14}$H$_{13}$N$_3$O$_2$ requires [M+Na]$^+$, calculated 278.0900, found 278.0898.

9-Oxo-6-(1*H*-pyrazol-4-yl)-10,14-diazatetracyclo[10.2.1.0^{2,11}.0^{3,8}]pentadeca-3(8),4,6-trien-14-ium, 3-76
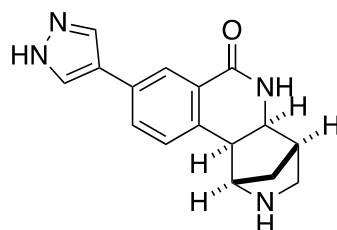
According to General Procedure A, {3-[1-(1-ethoxyethyl)-1H-pyrazol-4-yl]phenyl}formamido 2,2-dimethylpropanoate **3-57** (125 mg, 0.35 mmol), [Cp*RhCl$_2$]$_2$ (6.5 mg, 10.5 μmol, 3 mol%) and *tert*-butyl 2-azabicyclo[2.2.1]hept-5-ene-2-carboxylate (103 mg, 0.53 mmol) gave a crude material which was purified by flash column chromatography, eluting with 0:100 → 5:95 MeOH–CH$_2$Cl$_2$ to give the ethoxyethyl-protected pyrazole. According to General Procedure B, the ethoxyethyl-protected pyrazole (19 mg, 0.04 mmol) gave the *trienium* (17 mg, 12% over two steps) as a colourless amorphous solid. δ$_H$ (500 MHz, Methanol-*d*$_6$). δ$_H$ (501 MHz, Methanol-*d*$_4$) 8.25 (1H, d, *J* 2.0, 7–H), 8.03 (2H, s, pyrazolyl–H), 7.84 (1H, dd, *J* 8.0, 2.0, 5–H), 7.44 (1H, d, *J* 8.0, 4–H), 4.15 (1H, dd, *J* 9.0, 1.5, 11–H), 4.10 (1H, s, 1–H), 3.74 (1H, d, *J* 9.0, 2–H), 3.33-3.32 (1H, m, 13–H$_A$), 3.20 (1H, dd, *J* 11.8, 1.8, 13–H$_B$), 2.82-2.77 (1H, m, 12–H), 2.02 (1H, dt, *J* 11.8, 1.8, 15–H$_A$), 1.78 (1H,

dt, *J* 11.8, 1.8, 15–H$_B$). δ$_C$ (126 MHz, Methanol-*d*$_4$) 164.71, 134.19, 133.67, 132.32, 131.31, 130.43, 127.58, 125.19, 122.37, 65.87, 56.49, 47.72, 45.71, 41.51, 31.78. *R*$_F$ 0.05 (10:90 7M NH$_3$ in MeOH–CH$_2$Cl$_2$). IR ν$_{max}$ (film)/cm^{-1} 3387, 2959, 2929, 2360 and 1721. HRMS (ESI): C$_{16}$H$_{16}$N$_4$O requires [M+H]$^+$, calculated 281.1397, found 281.1395.

9-Oxo-6-(1*H*-pyrazol-4-yl)-10,13-diazatetracyclo[10.2.1.0^{2,11}.0^{3,8}]pentadeca-3(8),4,6-trien-13-ium, 3-77
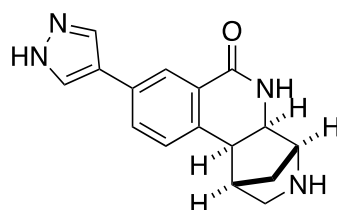
According to General Procedure A, {3-[1-(1-ethoxyethyl)-1H-pyrazol-4-yl]phenyl}formamido 2,2-dimethylpropanoate **3-57** (125 mg, 0.35 mmol), [Cp*RhCl$_2$]$_2$ (6.5 mg, 10.5 μmol, 3 mol%) and *tert*-butyl 2-azabicyclo[2.2.1]hept-5-ene-2-carboxylate (103 mg, 0.53 mmol) gave a crude material which was purified by flash column chromatography, eluting with 0:100 → 5:95 MeOH–CH$_2$Cl$_2$ to give the ethoxyethyl-protected pyrazole. According to General Procedure B, the ethoxyethyl-protected pyrazole (26 mg, 0.06 mmol) gave the *dione* (22 mg, 16% over two steps) as a colourless amorphous solid. δ$_H$ (501 MHz, Methanol-*d*$_4$) 8.22 (1H, d, *J* 2.0, 7–H), 8.01 (2H, br s, pyrazolyl–H), 7.83 (1H, dd, *J* 8.0, 2.0, 5–H), 7.45 (1H, d, *J* 8.0, 4–H), 4.25 (1H, dd, *J* 9.2, 1.8, 11–H), 3.97 (1H, s, 12–H), 3.64 (1H, d, *J* 9.2, 2–H), 3.41-3.30 (2H, m, 14–H), 2.86 (1H, d, *J* 3.3, 1–H), 2.00-1.90 (1H, m, 15–H$_A$), 1.77 (1H, dt, *J* 12.2, 1.8, 15–H$_B$). δ$_C$ (126 MHz, Methanol-*d*$_4$) 165.05, 136.86, 133.64, 131.51, 130.27, 126.95, 124.80, 122.43, 63.82, 55.20, 51.27, 46.79, 42.15, 31.75. *R*$_F$ 0.06 (10:90 7M NH$_3$ in MeOH–CH$_2$Cl$_2$). IR ν$_{max}$ (film)/cm^{-1} 3383, 3233, 2959, 2928, 2359, 1721 and 1637. HRMS (ESI): C$_{16}$H$_{16}$N$_4$O requires [M+H]$^+$, calculated 281.1397, found 281.1394.

Methyl (1*R*,3*S*,3a*R*,9b*R*)-1-amino-5-oxo-7-(1H-pyrazol-4-yl)-1*H*,2*H*,3*H*,3a*H*,4*H*,5*H*,9b*H*-cyclopenta[c]isoquinoline-3-carboxylate, 3-78
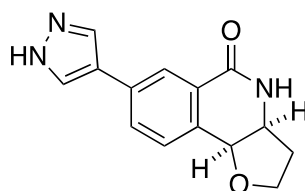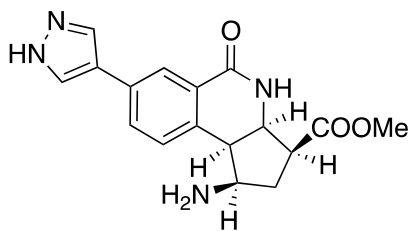
According to General Procedure A, {3-[1-(1-ethoxyethyl)-1H-pyrazol-4-yl]phenyl}formamido 2,2-dimethylpropanoate **3-57** (72 mg, 0.20 mmol), [Cp*RhCl$_2$]$_2$ (3.70 mg, 6.00 μmol, 3 mol%) and (1S,4R)-Methyl 4-((tert-butoxycarbonyl)amino)cyclopent-2-enecarboxylate (72 mg, 0.3 mmol) gave a crude material. TFA (0.25 ml, 3.27 mmol) was added to a solution of the crude material in CH$_2$Cl$_2$ (2 ml, 0.1 M) and stirred at room temperature for 18 hours to give a crude material which was purified by HPLC, eluting with 5:95 → 95:5 MeCN–H$_2$O plus 1% formic acid to give the *isoquinoline*, (21 mg, 23% over two steps) as a light yellow amorphous solid. δ$_H$ (501 MHz, Methanol-d_4) 8.26 (1H, d, *J* 2.0, 6–H), 8.06 (2H, app br s, pyrazolyl–H), 7.86 (1H, dd, *J* 7.9, 2.0, 8–H), 7.44 (1H, d, *J* 7.9, 9–H), 4.50 (1H, dd, *J* 6.7, 3.2, 3a–H), 3.86 (1H, q, *J* 8.4, 1–H), 3.79 (3H, s, methyl–H), 3.45 (1H, dd, *J* 8.4, 6.7, 9b–H), 3.23 (1H, ddd, *J* 9.1, 6.7, 3.2, 3–H), 2.70 (1H, dt, *J* 14.2, 8.4, 2–H$_A$), 2.15 (1H, ddd, *J* 14.2, 8.4, 6.7, 2–H$_A$). δ$_C$ (126 MHz, Methanol-d_4) 173.42, 164.69, 133.39, 133.28, 130.98, 129.78, 128.36, 127.24, 124.64, 57.57, 56.32, 51.72, 48.37, 45.10, 31.72. R_F 0.41 (10:90 7M NH$_3$ in MeOH–CH$_2$Cl$_2$). IR ν_{max} (film)/cm^{-1} 3397, 3233, 2958, 2921, 1728, 1669, and 1617. HRMS (ESI): C$_{17}$H$_{18}$N$_4$O$_3$ requires [M+Na]$^+$, calculated 349.1271, found 349.1267.

Methyl (1*S*,3*R*,3a*S*,9b*R*)-3-amino-5-oxo-7-(1*H*-pyrazol-4-yl)-1*H*,2*H*,3*H*,3a*H*,4*H*,5*H*,9b*H*-cyclopenta[c]isoquinoline-1-carboxylate, 3-79

According to General Procedure A, {3-[1-(1-ethoxyethyl)-1H-pyrazol-4-yl]phenyl}formamido 2,2-dimethylpropanoate **3-57** (72 mg, 0.20 mmol), [Cp*RhCl$_2$]$_2$ (3.70 mg, 6.00 μmol, 3 mol%) and (1S,4R)-Methyl 4-((tert-butoxycarbonyl)amino)cyclopent-2-enecarboxylate (72 mg, 0.3 mmol) gave a

crude material. TFA (0.25 ml, 3.27 mmol) was added to a solution of the crude material in CH_2Cl_2 (2 ml, 0.1 M) and stirred at room temperature for 18 hours to give a crude material which was purified by HPLC, eluting with 5:95 → 95:5 MeCN–H_2O plus 1% formic acid to give the *isoquinoline*, (8 mg, 12% over two steps) as a light yellow amorphous solid. δ_H (501 MHz, Methanol-d_4) 8.22 (1H, d, *J* 1.9, 6–H), 8.03 (2H, app s, pyrazolyl–H), 7.80 (1H, dd, *J* 8.0, 1.9, 8–H), 7.38 (1H, d, *J* 8.0, 9–H), 4.23 (1H, dd, *J* 6.7, 2.9, 3a–H), 3.84-3.78 (2H, m, 3–H and 9b–H), 3.75 (3H, s, methyl–H), 3.23 (1H, q, *J* 8.9, 1–H), 2.72 (1H, dt, *J* 14.5, 8.9, 2–H), 2.10 (1H, ddd, *J* 14.5, 8.9, 6.0, 2–H). δ_C (126 MHz, Methanol-d_4) 174.01, 164.78, 135.30, 132.97, 130.98, 129.70, 128.50, 126.57, 124.16, 59.16, 56.25, 51.49, 49.34, 42.94, 32.45. R_F 0.28 (10:90 7M NH_3 in MeOH–CH_2Cl_2). IR ν_{max} (film)/cm^{-1} 3379, 3248, 2960, 1665 and 1616. HRMS (ESI): $C_{17}H_{18}N_4O_3$ requires [M+H]$^+$, calculated 327.1452, found 327.1459.

(1*S*,3*R*,3a*S*,9b*S*)-1-amino-5-oxo-7-(1*H*-pyrazol-4-yl)-1*H*,2*H*,3*H*,3a*H*,4*H*,5*H*,9b*H*-cyclopenta[c]isoquinoline-3-carboxylic acid, 3-80
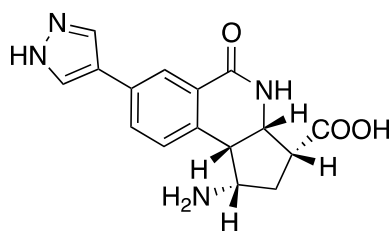
According to General Procedure A, {3-[1-(1-ethoxyethyl)-1H-pyrazol-4-yl]phenyl}formamido 2,2-dimethylpropanoate **3-57** (72 mg, 0.20 mmol), [Cp*RhCl$_2$]$_2$ (3.70 mg, 6.00 µmol, 3 mol%) and (1R,4S)-4-((tert-butoxycarbonyl)amino)cyclopent-2-enecarboxylic acid (68 mg, 0.3 mmol) gave a crude material. TFA (0.25 ml, 3.27 mmol) was added to a solution of the crude material in CH_2Cl_2 (2 ml, 0.1 M) and stirred at room temperature for 18 hours to give a crude material which was purified by HPLC, eluting with 5:95 → 95:5 MeCN–H_2O plus 1% formic acid to give the *isoquinoline*, (10 mg, 16% over two steps) as a colourless amorphous solid. δ_H (501 MHz, Methanol-d_4) 8.26 (1H, d, *J* 2.0, 6–H), 8.05 (2H, app s, pyrazolyl–H), 7.86 (1H, dd, *J* 8.0, 2.0, 8–H), 7.43 (1H, d, *J* 8.0, 9–H), 4.53 (1H, dd, *J* 6.2, 2.8, 3a–H), 3.83 (1H, q, *J* 8.7, 1–H), 3.43 (1H, dd, *J* 8.7, 6.2, 9b–H) 3.21 (1H, ddd, *J* 8.7, 6.4, 2.8, 3–H), 2.71 (1H, dt, *J* 14.0, 8.7, 2–H), 2.17 (1H, ddd, *J* 14.0, 8.7, 6.4, 2–H). δ_C

(126 MHz, Methanol-d_4) 174.58, 164.78, 133.43, 133.33, 130.95, 129.74, 128.39, 127.24, 124.64, 121.04, 57.83, 56.54, 48.45, 45.24, 31.85. IR v_{max} (film)/cm^{-1} 3391, 3250, 2924, 1673 and 1618. HRMS (ESI): $C_{16}H_{16}N_4O_3$ requires [M+H]$^+$, calculated 313.1295, found 313.1295.

(1*R*,3*S*,3a*R*,9b*S*)-3-Amino-5-oxo-7-(1*H*-pyrazol-4-yl)-1*H*,2*H*,3*H*,3a*H*,4*H*,5*H*,9b*H*-cyclopenta[c]isoquinoline-1-carboxylic acid, 3-81
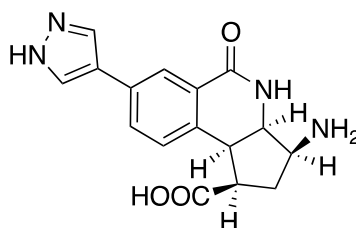
According to General Procedure A, {3-[1-(1-ethoxyethyl)-1H-pyrazol-4-yl]phenyl}formamido 2,2-dimethylpropanoate **3-57** (72 mg, 0.20 mmol), [Cp*RhCl$_2$]$_2$ (3.70 mg, 6.00 μmol, 3 mol%) and (1R,4S)-4-((tert-butoxycarbonyl)amino)cyclopent-2-enecarboxylic acid (68 mg, 0.3 mmol) gave a crude material. TFA (0.25 ml, 3.27 mmol) was added to a solution of the crude material in CH$_2$Cl$_2$ (2 ml, 0.1 M) and stirred at room temperature for 18 hours to give a crude material which was purified by HPLC, eluting with 5:95 → 95:5 MeCN–H$_2$O plus 1% formic acid to give the *isoquinoline*, (13 mg, 21% over two steps) as a colourless amorphous solid. δ$_H$ (501 MHz, Methanol-d_4) 8.22 (1H, d, *J* 2.0, 6–H), 8.04 (2H, app s, pyrazolyl–H), 7.80 (1H, dd, *J* 7.9, 2.0, 8–H), 7.45 (1H, d, *J* 7.9, 9–H), 4.24 (1H, dd, *J* 6.8, 3.2, 3a–H), 3.84 (1H, dd, *J* 8.9, 6.8, 9b–H), 3.79 (1H, ddd, *J* 7.8, 6.1, 3.2, 3–H), 3.17 (1H, q, *J* 8.9, 1–H), 2.71 (1H, ddd, *J* 14.4, 8.9, 7.8, 2–H$_A$), 2.10 (1H, ddd, *J* 14.4, 8.9, 6.1, 2–H$_B$). δ$_C$ (126 MHz, Methanol-d_4) 175.28, 164.82, 135.75, 132.70, 130.90, 129.74, 128.59, 126.51, 124.13, 121.17, 59.10, 56.45, 49.49, 42.69, 32.58. IR v_{max} (film)/cm^{-1} 3391, 3007, 2919, 1668 and 1618. HRMS (ESI): $C_{16}H_{16}N_4O_3$ requires [M+H]$^+$, calculated 313.1295, found 313.1296.

***tert*-Butyl 3-oxo-2-azabicyclo[2.2.1]hept-5-ene-2-carboxylate**
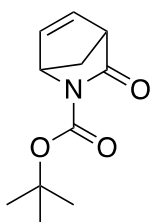
Et$_3$N (1.9 ml, 13.6 mmol) followed by di-*tert*-butyl decarbonate (2.4 g, 11 mmol) and DMAP (112 mg, 0.92 mmol) were added to a solution of 2-azabicyclo[2.2.1]hept-5-en-3-one (1 g, 9.2 mmol) in THF (10 ml, 0.9 M) and the reaction mixture was stirred overnight at room temperature. After which, the reaction was quenched with H$_2$O (50 ml) and extracted with EtOAc (3 x 50 ml). The combined organics were washed with sat. NaHCO$_3$ soln. (50 ml), H$_2$O (50 ml) and sat. brine soln. (50 ml), dried (MgSO$_4$), filtered and concentrated under reduced pressure to give a crude product which was purified by flash column chromatography, eluting with 0:100 → 10:90 EtOAc–CH$_2$Cl$_2$ to give the *carboxylate*[201] (1.6 g, 83%) as an off-white amorphous solid. δ$_H$ (500 MHz, Chloroform-*d*) 6.82 (1H, ddd, *J* 5.2, 2.3, 0.7, 5–H), 6.59 (1H, ddd, *J* 5.2, 3.5, 1.7, 6–H), 4.88 (1H, h, *J* 1.7, 4–H), 3.30 (1H, dh, *J* 3.5, 1.7, 1–H), 2.27 (1H, dt, *J* 8.5, 1.7, 7–H$_A$), 2.08 (1H, dt, *J* 8.5, 1.7, 7–H$_B$), 1.42 (9H, s, *t*butyl–H). δ$_C$ (126 MHz, Chloroform-*d*) 175.3, 149.3, 139.0, 137.2, 81.5, 61.4, 53.9, 53.4, 27.0. R_F 0.17 (10:90 EtOAc–petrol). IR ν$_{max}$ (film)/cm^{-1} 2979, 2360, 1753, 1702 and 1304. HRMS (ESI): C$_{11}$H$_{15}$NO$_3$ requires [2M+Na]$^+$, calculated 411.1996, found 411.1999.

6-(1*H*-Pyrazol-4-yl)-10,14-diazatetracyclo[10.2.1.0^{2,11}.0^{3,8}]pentadeca-3,5,7-triene-9,13-dione, 3-82
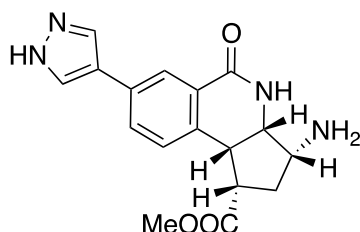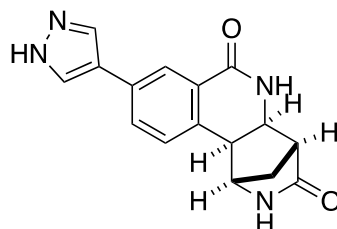

According to General Procedure A, {3-[1-(1-ethoxyethyl)-1H-pyrazol-4-yl]phenyl}formamido 2,2-dimethylpropanoate **3-57** (125 mg, 0.35 mmol), [Cp*RhCl$_2$]$_2$ (6.5 mg, 10.5 μmol, 3 mol%) and 2-azabicyclo[2.2.1]hept-5-en-3-one (57 mg, 0.53 mmol) gave a crude material which was purified by flash column chromatography, eluting with 0:100 → 10:90 MeOH–CH$_2$Cl$_2$ to give

the ethoxyethyl-protected pyrazole. According to General Procedure B, the ethoxyethyl-protected pyrazole (95 mg, 0.26 mmol) gave the *dione* (56 mg, 54% over two steps) as a yellow amorphous solid. δ_H (500 MHz, DMSO-d_6) 8.11 (3H, d, J 2.0, 7–H, pyrazolyl N–H, N–H$_A$), 8.10 (2H, br. s, pyrazolyl–H), 7.96 (1H, s, N–H$_B$), 7.79 (1H, dd, J 8.0, 2.0, 5–H), 7.37 (1H, d, J 8.0, 4–H), 4.00 (1H, dt, J 9.0, 1.8, 11–H), 3.85 (1H, d, J 1.8, 1–H), 3.49 (1H, d, J 9.0, 2–H), 2.62 (1H, d, J 1.8, 12–H), 1.76 (1H, dt, J 10.2, 1.8, 15–H$_A$), 1.53 (1H, dd, J 10.2, 1.8, 15–H$_B$). δ_C (126 MHz, DMSO-d_6) 176.8, 161.9, 134.5, 131.6, 129.1, 128.8, 126.5, 123.1, 120.4, 62.4, 54.1, 51.9, 43.7, 34.8. R_F 0.27 (10:90 MeOH–CH$_2$Cl$_2$). IR ν_{max} (film)/cm^{-1} 3201, 2985, 2360, 2341, 1684 and 1654. HRMS (ESI): $C_{16}H_{14}N_4O_2$ requires [M+Na]$^+$, calculated 317.1009, found 317.1007.

6-(1*H*-Pyrazol-4-yl)-10,13-diazatetracyclo[10.2.1.0^{2,11}.0^{3,8}]pentadeca-3,5,7-triene-9,14-dione, 3-83
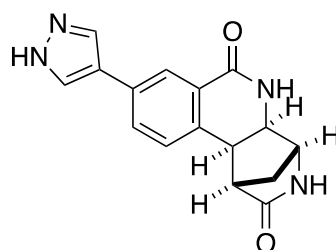
According to General Procedure A, {3-[1-(1-ethoxyethyl)-1H-pyrazol-4-yl]phenyl}formamido 2,2-dimethylpropanoate **3-57** (125 mg, 0.35 mmol), [Cp*RhCl$_2$]$_2$ (6.5 mg, 10.5 μmol, 3 mol%) and 2-azabicyclo[2.2.1]hept-5-en-3-one (57 mg, 0.53 mmol) gave a crude material which was purified by flash column chromatography, eluting with 0:100 → 10:90 MeOH–CH$_2$Cl$_2$ to give the ethoxyethyl-protected pyrazole. According to General Procedure B, the ethoxyethyl-protected pyrazole (33 mg, 0.09 mmol) gave the *dione* (17 mg, 17% over two steps) as a light yellow solid. δ_H (500 MHz, DMSO-d_6) 8.21 (1H, app. br. d, J 2.2, N–H$_A$), 8.10 (1H, d, J 2.1, 7–H), 7.97 (1H, s, pyrazolyl–H), 7.79 (1H, dd, J 8.0, 2.1, 5–H), 7.38 (1H, d, J 8.0, 4–H), 3.88 (1H, d, J 9.0, 11–H), 3.70 (1H, app. s, 12–H), 3.44 (1H, d, J 9.0, 2–H), 2.53 (1H, app. s, 1–H), 1.75 (1H, dt, J 10.0, 1.9, 15–H$_A$), 1.52 (1H, d, J 10.0, 15–H$_B$). δ_C (126 MHz, DMSO-d_6) 177.9, 161.8, 135.4, 131.6, 129.3, 129.3, 126.9, 122.8, 120.3, 60.2, 56.4, 53.9, 36.4, 34.6. R_F 0.19 (10:90 MeOH–CH$_2$Cl$_2$). IR ν_{max} (film)/cm^{-1} 3234,

2987, 2360, 1695 and 1661. HRMS (ESI): $C_{16}H_{14}N_4O_2$ requires $[M+Na]^+$, calculated 317.1009, found 317.1011.

N-{[1-Oxo-7-(1*H*-pyrazol-4-yl)-1,2,3,4-tetrahydroisoquinolin-3-yl]methyl}acetamide, 3-84
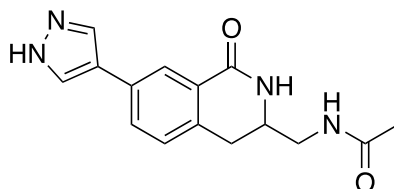
According to General Procedure G, [1-oxo-7-(1H-pyrazol-4-yl)-1,2,3,4-tetrahydroisoquinolin-3-yl]methanaminium trifluoroacetate, **3-68**, (50.0 mg, 0.14 mmol) gave a crude product which was purified by flash column chromatography, eluting with 0:100 → 10:90 MeOH–CH₂Cl₂ go give the *acetamide* (31 mg, 77%) as a colourless amorphous solid. δ_H (501 MHz, Methanol-*d₄*) 8.11 (1H, d, *J* 2.0, isoquinolinyl 8–H), 7.99 (2H, br s, pyrazolyl–H), 7.72 (1H, dd, *J* 7.9, 2.0, isoquinolinyl 6–H), 7.30 (1H, d, *J* 7.9, isoquinolinyl 5–H), 3.80 (1H, dq, *J* 7.5, 5.6, isoquinolinyl 3–H), 3.40-3.33 (2H, m, methyl acetamide–H), 3.09 (1H, dd, *J* 16.0, 5.6, isoquinolinyl 4–H), 2.88 (1H, dd, *J* 16.0, 7.5, isoquinolinyl 4–H), 1.94 (3H, s, acetamide–H). δ_C (126 MHz, Methanol-*d₄*) 174.09, 167.86, 137.51, 136.93, 133.21, 130.77, 129.85, 129.73, 126.74, 125.12, 122.77, 52.01, 43.93, 31.49, 22.54. R_F 0.19 (10:90 MeOH–CH₂Cl₂). IR ν_{max} (film)/cm⁻¹ 3233, 2950, 1649, 1617 and 1568. HRMS (ESI): $C_{15}H_{16}N_4O_2$ requires $[M+H]^+$, calculated 285.1346, found 285.1349.

N-methyl-*N*-{[1-oxo-7-(1*H*-pyrazol-4-yl)-1,2,3,4-tetrahydroisoquinolin-3-yl]methyl}acetamide, 3-85
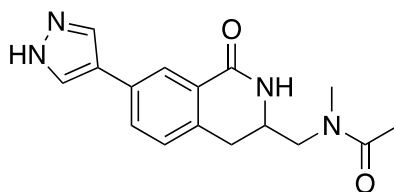
According to General Procedure G, Methyl({[1-oxo-7-(1H-pyrazol-4-yl)-1,2,3,4-tetrahydroisoquinolin-3-yl]methyl})azanium trifluoroacetate, **3-72**, (15.5 mg, 0.04 mmol) gave a crude product which was purified by flash column chromatography, eluting with 0:100 → 10:90 MeOH–CH₂Cl₂ go give the

acetamide (10 mg, 80%) as a 3:1 mixture of rotamers and a colourless amorphous solid. δ_H (501 MHz, Methanol-*d*) 8.16 (1H, d, *J* 2.0, isoquinolinyl 8–H$_{minor}$), 8.13 (3H, d, *J* 2.0, isoquinolinyl 8–H$_{major}$), 8.00 (8H, br s, pyrazolyl–H), 7.77 (1H, dd, *J* 7.9, 2.0, isoquinolinyl 6–H$_{minor}$), 7.73 (3H, dd, *J* 7.9, 2.0, isoquinolinyl 6–H$_{major}$), 7.35 (1H, d, *J* 7.9, isoquinolinyl 5–H$_{minor}$), 7.30 (3H, d, *J* 7.9, isoquinolinyl 5–H$_{major}$), 4.02-3.91 (4H, m, isoquinolinyl 3–H$_{major\ and\ minor}$), 3.59 (3H, dd, *J* 13.7, 7.4, methyl–H$_{major\ A}$), 3.52 (1H, dd, *J* 14.7, 8.2, methyl–H$_{minor\ A}$), 3.43-3.36 (4H, m, methyl–H$_{major\ and\ minor\ B}$), 3.31 (1H, m, isoquinolinyl 4–H$_{minor\ A}$), 3.15 (3H, ddd, *J* 16.0, 5.6, 0.9, isoquinolinyl 4–H$_{major\ A}$), 3.06 (9H, s, N-methyl–H$_{major}$), 2.94 (3H, s, N-methyl–H$_{minor}$), 2.90-2.83 (4H, m, isoquinolinyl 4–H$_{major\ and\ minor\ B}$), 2.07 (9H, s, acetamide–H$_{major}$), 1.93 (3H, s, acetamide–H$_{minor}$). δ_C (126 MHz, Methanol-*d*) 174.52, 173.60, 167.72, 167.41, 137.61, 136.89, 136.22, 133.60, 133.27, 130.99, 130.74, 130.16, 129.92, 129.87, 126.75, 125.24, 125.13, 122.80, 122.67, 54.90, 52.53, 50.49, 49.85, 38.21, 34.40, 31.47, 30.68, 21.68, 21.16. R_F 0.32 (10:90 MeOH–CH$_2$Cl$_2$). IR ν_{max} (film)/cm^{-1} 3218, 2941, 1651, 1615 and 1574. HRMS (ESI): C$_{16}$H$_{18}$N$_4$O$_2$ requires [M+H]$^+$, calculated 299.1503, found 299.1508.

N-{[1-oxo-7-(1*H*-pyrazol-4-yl)-1,2,3,4-tetrahydroisoquinolin-4-yl]methyl}acetamide, 3-86
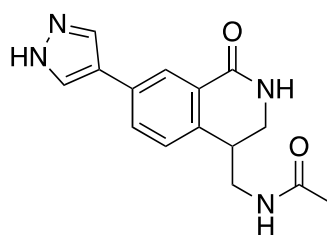
According to General Procedure G, [1-oxo-7-(1H-pyrazol-4-yl)-1,2,3,4-tetrahydroisoquinolin-4-yl]methanaminium trifluoroacetate, **3-69**, (73.6 mg, 0.21 mmol) gave a crude product which was purified by flash column chromatography, eluting with 10:90 → 15:85 MeOH–CH$_2$Cl$_2$ to give the *isoquinolinone* (20 mg, 34%) as a colourless amorphous solid. δ_H (500 MHz, Methanol-*d$_4$*) 8.16 (1H, d, *J* 2.0, isoquinolin 8–H), 8.00 (2H, s pyrazole–H), 7.77 (1H, dd, *J* 7.9, 2.0, isoquinolin 6–H), 7.35 (1H, d, *J* 7.9, isoquinolin 5–H), 3.65 (1H, dd, *J* 13.0, 4.5, isoquinolin 3–H$_A$), 3.46 (1H, dd, *J* 13.0, 2.5, isoquinolin 3–H$_B$), 3.42 (1H, dd, *J* 13.6, 8.7, methyl–H$_A$), 3.36 (1H, dd, *J* 13.6, 6.6, methyl–H$_B$), 3.12 (1H, dddd, *J* 8.7, 6.6, 4.5, 2.5, isoquinolin 4–H), 1.96

(3H, s, acetamide–H). δ_C (126 MHz, Methanol-d_4) 173.6, 167.7, 139.6, 133.8, 132.1, 130.6, 129.7, 129.7, 125.4, 122.7, 42.9, 42.7, 38.3, 22.6. R_F 0.18 (10:90 MeOH–CH$_2$Cl$_2$). IR ν_{max} (film)/cm^{-1} 3310, 3200, 2924, 1675, 1642 and 1617. HRMS (ESI): $C_{15}H_{16}N_4O_2$ requires [M+Na]$^+$, calculated 307.1165, found 307.1160.

4-[(Dimethylamino)methyl]-7-(1*H*-pyrazol-4-yl)-1,2,3,4-tetrahydroisoquinolin-1-one, 3-87
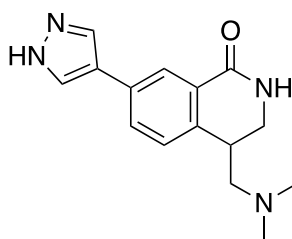
Et$_3$N (40 μl, 0.275 mmol) was added to a suspension of [1-oxo-7-(1H-pyrazol-4-yl)-1,2,3,4-tetrahydroisoquinolin-4-yl]methanaminium trifluoroacetate, **3-69**, (76.4 mg, 0.21 mmol) in MeOH (1 ml, 0.2 M) and the mixture stirred at room temperature. After 1 hour, aq. formaldehyde (37% w/v, 68 μl, 0.84 mmol) and glacial acetic acid (48 μl, 0.84 mmol) were added. The mixture was stirred for 5 minutes at room temperature before STAB (178 mg, 0.84 mmol) was added. The reaction mixture was stirred overnight at room temperature before it was concentrated to give a crude product which was purified by flash column chromatography, eluting with 0:100 → 10:90 sat. NH$_3$ in MeOH–CH$_2$Cl$_2$ to give the *isoquinolinone* (7 mg, 12%) as a colourless amorphous solid. δ_H (500 MHz, Methanol-d_4) 8.14 (1H, d, *J* 2.0, 8–H), 8.06 (2H, br s, pyrazolyl–H), 7.94 (2H, br s, pyrazolyl–H), 7.75 (1H, dd, *J* 7.9, 2.0, 6–H), 7.35 (1H, d, *J* 7.9, 5–H), 3.66-3.55 (2H, m, 3–H), 3.11 (1H, ddd, *J* 13.2, 6.0, 3.5, 4–H), 2.70 (1H, dd, *J* 12.5, 10.5 isoquinolin-4-methyl–H$_A$), 2.32 (6H, s, dimethylamino–H), 2.24 (1H, dd, *J* 12.5, 4.9, isoquinolin-4-methyl–H$_B$). δ_C (126 MHz, Methanol-d_4) 167.9, 140.8, 137.5, 133.5, 130.7, 129.8, 129.4, 126.8, 125.3, 122.7, 63.0, 46.0, 42.4, 36.7. R_F 0.35 (10:90 7M NH$_3$ in MeOH–CH$_2$Cl$_2$). IR ν_{max} (film)/cm^{-1} 3388, 2936 1657 and 1617. HRMS (ESI): $C_{15}H_{18}N_4O$ requires [M+Na]$^+$, calculated 293.1373, found 293.1368.

N-methyl-*N*-{[1-oxo-7-(1*H*-pyrazol-4-yl)-1,2,3,4-tetrahydroisoquinolin-4-yl]methyl}acetamide, 3-88
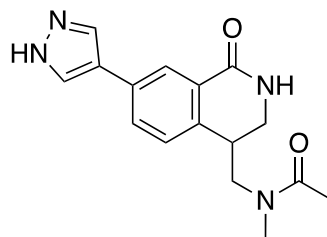
According to General Procedure G, Methyl({[1-oxo-7-(1H-pyrazol-4-yl)-1,2,3,4-tetrahydroisoquinolin-4-yl]methyl})azanium trifluoroacetate, **3-73**, (34.7 mg, 0.09 mmol) gave a crude product which was purified by flash column chromatography, eluting with 0:100 → 20:80 MeOH–CH₂Cl₂ go give the *isoquinolinone* (18 mg, 67%) as a colourless amorphous solid and a 9:7 mixture of rotamers.. δ_H (501 MHz, Methanol-d_4) 8.21 (7H, d, *J* 2.0, 8–H$_{minor}$), 8.17 (9H, d, *J* 2.0, 8–H$_{major}$), 8.01 (32H, br s, pyrazolyl–H$_{major\ and\ minor}$), 7.77 (16H, app ddd, *J* 7.9, 2.0, 1.3, 6–H$_{major\ and\ minor}$), 7.30 (9H, d, *J* 7.9, 5–H$_{major}$), 7.25 (7H, d, *J* 7.9, 5–H$_{minor}$), 3.75 (7H, dd, *J* 13.3, 4.5, 3–H$_{A\ minor}$), 3.71 (7H, dd, *J* 13.5, 8.6, methyl–H$_{A\ minor}$), 3.69-3.62 (7H, m, 3–H$_{B\ minor}$), 3.63-3.59 (18H, m, methyl–H$_{major}$), 3.45 (7H, dd, *J* 13.5, 7.0, methyl–H$_{B\ minor}$), 3.39 (18H, dt, *J* 13.2, 1.6, 3–H$_{major}$), 3.31 (16H, m, 4–H$_{major\ and\ minor}$), 2.98 (21H, s, N-methyl–H$_{minor}$), 2.95 (27H, s, N-methyl–H$_{major}$), 2.10 (27H, s, acetamide–H$_{major}$), 1.73 (21H, s, acetamide–H$_{minor}$). δ_C (126 MHz, Methanol-d_4) 173.98, 173.72, 167.60, 167.44, 139.52, 138.76, 137.55, 134.29, 133.89, 130.65, 130.62, 130.06, 129.90, 129.88, 129.60, 126.93, 125.58, 125.46, 122.69, 122.52, 54.38, 51.99, 42.62, 42.40, 38.17, 36.84, 36.69, 34.24, 21.78, 20.78. R_F 0.32 (10:90 MeOH–CH₂Cl₂). IR v_{max} (film)/cm⁻¹ 3216, 2932, 1651 and 1614. HRMS (ESI): $C_{16}H_{18}N_4O_2$ requires [M+Na]⁺, calculated 321.1322, found 321.1318.

1-Acetyl-7'-(1*H*-pyrazol-4-yl)-2',4'-dihydro-1'H-spiro[azetidine-3,3'-isoquinolin]-1'-one, 3-89
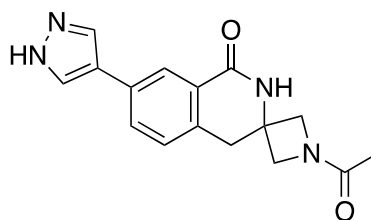
According to General Procedure G, 1'-oxo-7'-(1H-pyrazol-4-yl)-2',4'-dihydro-1'H-spiro[azetidine-3,3'-isoquinolin]-1-ium trifluoroacetate, **3-70**, (272.5 mg, 1.07 mmol) gave a crude product which was purified by flash column

chromatography eluting with 0:100 → 10:90 MeOH–CH$_2$Cl$_2$ to give the *isoquinolinone* (83 mg, 26%) as a colourless amorphous solid. δ$_H$ (500 MHz, Methanol-d_4) 8.16 (1H, app. d, *J* 0.8, pyrazolyl 5–H), 8.12 (1H, d, *J* 2.0, isoquinolin 8–H), 7.87 (1H, d, *J* 0.8, pyrazolyl 3–H), 7.76 (1H, dd, *J* 7.9, 2.0 isoquinolin 6–H), 7.39 (1H, d, *J* 7.9, isoquinolin 5–H), 4.25 (1H, d, *J* 9.2, azetidine–H$_A$), 4.19 (1H, d, *J* 9.2, azetidine–H$_B$), 4.05-3.98 (2H, m, azetidine–H), 3.31 (2H, s, isoquinolin 4–H), 1.90 (3H, s, acetyl–H). δ$_C$ (126 MHz, Methanol-d_4) 173.6, 167.6, 137.2, 135.1, 133.9, 130.8, 130.1, 129.6, 126.0, 125.0, 122.6, 63.5, 60.7, 51.8, 38.2, 18.8. R_F 0.57 (10:90 MeOH–CH$_2$Cl$_2$). IR ν$_{max}$ (film)/cm^{-1} 3377, 2988, 2901, 2360, 2340, 1654 and 1406. HRMS (ESI): C$_{16}$H$_{16}$N$_4$O requires [M+H]$^+$, calculated 297.1346, found 297.1345.

1-Methyl-7'-(1*H*-pyrazol-4-yl)-2',4'-dihydro-1'H-spiro[azetidine-3,3'-isoquinolin]-1'-one, 3-90

According to General Procedure H, 1'-oxo-7'-(1H-pyrazol-4-yl)-2',4'-dihydro-1'H-spiro[azetidine-3,3'-isoquinolin]-1-ium trifluoroacetate, **3-70**, (64.0 mg, 0.17 mmol), formaldehyde (37 wt. % in H$_2$O) (19.6 μl, 0.26 mmol) and STAB (110.0 mg, 0.52 mmol) gave a crude product which was purified by flash column chromatography, eluting with 0:100 → 10:90 7M NH$_3$ in MeOH–CH$_2$Cl$_2$ to give the *isoquinolinone* (33 mg, 70%) as a colourless amorphous solid. δ$_H$ (500 MHz, Methanol-d_4) 8.11 (1H, d, *J* 1.9, isoquinolin 8–H), 8.06 (1H, br. s, pyrazolyl–H), 7.94 (1H, br. s, pyrazolyl–H), 7.77 (1H, dd, *J* 7.9, 1.9, isoquinolin 6–H), 7.39 (1H, d, *J* 7.9, isoquinolin 5–H), 3.70 (2H, d, *J* 8.6, azetidine–H), 3.39 (2H, d, *J* 8.6, azetidine–H), 3.33 (2H, s, isoquinolin 4–H), 2.55 (3H, s, methyl–H). δ$_C$ (126 MHz, Methanol-d_4) 167.2, 137.5, 135.5, 133.7, 131.0, 130.1, 129.7, 126.8, 125.2, 122.7, 67.9, 51.8, 45.1, 37.9. R_F 0.21 (10:90 sat. NH$_3$ in MeOH–CH$_2$Cl$_2$). IR ν$_{max}$ (film)/cm^{-1} 3354, 3306, 3929, 3236, 1649 and 1617. HRMS (ESI): C$_{15}$H$_{16}$N$_4$O requires [M+H]$^+$, calculated 269.1397, found 269.1399.

1-(Propan-2-yl)-7'-(1*H*-pyrazol-4-yl)-2',4'-dihydro-1'*H*-spiro[azetidine-3,3'-isoquinolin]-1'-one, 3-91
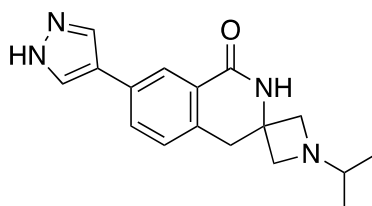
According to General Procedure H, 1'-oxo-7'-(1H-pyrazol-4-yl)-2',4'-dihydro-1'H-spiro[azetidine-3,3'-isoquinolin]-1-ium trifluoroacetate, **3-70** (purified by flash column chromatography, eluting with 0:100 → 10:90 7M NH₃ in MeOH–CH₂Cl₂ to give the free amine), (58 mg, 0.22 mmol), acetone (15 μl, 0.2 mmol) and STAB (47 mg, 0.22 mmol) gave a crude product which was purified by flash column chromatography, eluting with 0:100 → 10:90 7M NH₃ in MeOH–CH₂Cl₂ to give the *spiro-one* (11 mg, 19%) as a colourless amorphous solid. δ_H (501 MHz, Methanol-d_4) 8.10 (1H, d, *J* 1.9, 8'–H), 7.99 (2H, s, pyrazolyl–H), 7.75 (1H, dd, *J* 7.9, 1.9, 6'–H), 7.37 (1H, d, *J* 7.9, 5'–H), 3.46 (1H, d, *J* 7.1, azetidine–H$_A$), 3.46 (1H, d, *J* 7.1, azetidine–H$_B$), 3.31 (2H, s, 4'–H), 3.12 (1H, d, *J* 7.2, azetidine–H$_A$), 3.11 (1H, d, *J* 7.2, azetidine–H$_B$), 2.47 (1H, p, *J* 6.2, propanyl 2–H), 0.97 (6H, d, *J* 6.2, propanyl 1–H). δ_C (126 MHz, Methanol-d_4) 166.01, 134.69, 132.14, 129.47, 128.68, 128.37, 123.74, 121.33, 63.40, 58.68, 49.56, 36.68, 18.27. R_F 0.30 (10:90 7 M NH₃ in MeOH–CH₂Cl₂). IR ν_{max} (film)/cm⁻¹ 3219, 2966, 2848, 1655 and 1615. HRMS (ESI): $C_{17}H_{20}N_4O$ requires [M+Na]⁺, calculated 319.1529, found 319.1525.

1-[(Oxan-4-yl)methyl]-7'-(1*H*-pyrazol-4-yl)-2',4'-dihydro-1'*H*-spiro[azetidine-3,3'-isoquinolin]-1'-one, 3-92

According to General Procedure H, 1'-oxo-7'-(1H-pyrazol-4-yl)-2',4'-dihydro-1'H-spiro[azetidine-3,3'-isoquinolin]-1-ium trifluoroacetate, **3-70** (purified by flash column chromatography, eluting with 0:100 → 10:90 7M NH₃ in MeOH–CH₂Cl₂ to give the free amine), (58 mg, 0.22 mmol), 3,4,5,6-tetrahydro-2H-pyran-4-carbaldehyde (21 μl, 0.2 mmol) and STAB (47 mg, 0.22 mmol) gave

a crude product which was purified by flash column chromatography, eluting with 0:100 → 10:90 7M NH_3 in MeOH–CH_2Cl_2 to give the *spiro-one* (11 mg, 19%) as a light yellow amorphous solid. δ_H (501 MHz, Methanol-d_4) 8.11 (1H, d, *J* 1.8, 8'–H), 8.00 (2H, s, pyrazolyl–H), 7.76 (1H, dd, *J* 7.8, 1.8, 6'–H), 7.37 (1H, d, *J* 7.8 5'–H), 3.95-3.86 (2H, m, oxanyl 2–H), 3.78 (2H, app dt, *J* 7.8, 1.9, azetidine–H), 3.53-3.45 (2H, m, azetidine–H), 3.38 (2H, td, *J* 11.9, 2.0, oxanyl 2–H), 3.34 (2H, s, 4'–H), 2.68 (2H, dd, *J* 7.0, 1.5, methyl–H), 1.78-1.66 (1H, m, oxanyl 4–H), 1.63 (2H, ddd, *J* 13.0, 4.1, 2.0, oxanyl 3–H), 1.32-1.25 (2H, m, oxanyl 3–H). δ_C (126 MHz, Methanol-d_4) 167.19, 135.48, 133.68, 132.18, 130.96, 130.13, 129.61, 125.17, 122.63, 68.50, 66.87, 65.59, 52.47, 37.89, 34.46, 32.02. R_F 0.48 (10:90 7 M NH_3 in MeOH–CH_2Cl_2). IR ν_{max} (film)/cm^{-1} 3375, 3246, 2923, 2852, 1657 and 1617. HRMS (ESI): $C_{20}H_{24}N_4O_2$ requires $[M+Na]^+$, calculated 375.1792, found 375.1787.

1-Ethyl-7'-(1*H*-pyrazol-4-yl)-2',4'-dihydro-1'*H*-spiro[azetidine-3,3'-isoquinolin]-1'-one, 3-93

According to General Procedure H, 1'-oxo-7'-(1H-pyrazol-4-yl)-2',4'-dihydro-1'H-spiro[azetidine-3,3'-isoquinolin]-1-ium trifluoroacetate, **3-70**, (93 mg, 0.25 mmol), acetaldehyde (15 μl, 0.28 mmol), acetic acid (14 μl, 0.25 mmol) and STAB (58 mg, 0.28 mmol) gave a crude product which was purified by flash column chromatography, eluting with 0:100 → 10:90 7M NH_3 in MeOH–CH_2Cl_2 to give the *spiro-one* (30 mg, 43%) as a colourless amorphous solid. δ_H (501 MHz, Methanol-d_4) 8.10 (1H, d, *J* 1.9, 8'–H), 7.99 (2H, s, pyrazolyl–H), 7.74 (1H, dd, *J* 7.8, 1.9, 6'–H), 7.36 (1H, dd, *J* 7.8, 0.8, 5'–H), 3.47 (1H, d, *J* 7.1, azetidine–H_A), 3.47 (1H, d, *J* 7.1, azetidine–H_B), 3.30 (2H, s, 4'–H), 3.09 (1H, d, *J* 7.1, azetidine–H_A), 3.09 (1H, d, *J* 7.1, azetidine–H_B), 2.57 (2H, q, *J* 7.2, ethyl–H), 0.99 (3H, t, *J* 7.2, ethyl–H). δ_C (126 MHz, Methanol-d_4) 165.94, 136.15, 134.63, 132.14, 129.47, 128.68, 128.35, 125.62, 123.76, 121.33, 64.28, 52.91, 50.70, 36.74, 11.02. R_F 0.38 (10:90 7 M NH_3 in MeOH–CH_2Cl_2).

IR ν_{max} (film)/cm^{-1} 3194, 2937, 2839, 1654 and 1615. HRMS (ESI): C$_{16}$H$_{18}$N$_4$O requires [M+Na]$^+$, calculated 305.1373, found 305.1372.
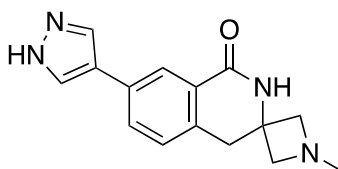
1-Benzyl-7'-(1*H*-pyrazol-4-yl)-2',4'-dihydro-1'*H*-spiro[azetidine-3,3'-isoquinolin]-1'-one, 3-94

According to General Procedure H, 1'-oxo-7'-(1H-pyrazol-4-yl)-2',4'-dihydro-1'H-spiro[azetidine-3,3'-isoquinolin]-1-ium trifluoroacetate, **3-70**, (83.53 mg, 0.23 mmol), benzaldehyde (25 μl, 0.25 mmol) and STAB (105 mg, 0.50 mmol) gave a crude product which was purified by flash column chromatography, eluting with 0:100 → 10:90 7M NH$_3$ in MeOH–CH$_2$Cl$_2$ to give the *spiro-one* (47 mg, 59%) as a colourless amorphous solid. δ$_H$ (501 MHz, Methanol-d_4) 8.10 (1H, d, *J* 1.9, 8'–H), 7.98 (2H, s, pyrazolyl–H), 7.73 (1H, dd, *J* 7.9, 1.9, 6'–H), 7.34 (1H, d, *J* 7.9, 5'–H), 7.33-7.28 (4H, m, phenyl 2– and 3–H), 7.27-7.22 (1H, m, phenyl 4–H), 3.70 (2H, s, benzyl–H), 3.45 (1H, d, *J* 7.1, azetidine–H$_A$), 3.44 (1H, d, *J* 7.1, azetidine–H$_B$), 3.30 (2H, s, 4'–H), 3.23 (1H, d, *J* 7.1, azetidine–H$_A$), 3.23 (1H, d, *J* 7.1, azetidine–H$_B$). δ$_C$ (126 MHz, Methanol-d_4) 165.99, 136.94, 134.68, 132.11, 129.46, 128.66, 128.49, 128.33, 128.15, 127.20, 123.75, 121.33, 64.58, 62.59, 51.03, 36.67. R_F 0.26 (10:90 7 M NH$_3$ in MeOH–CH$_2$Cl$_2$). IR ν_{max} (film)/cm^{-1} 3188, 2927, 2848, 1660 and 1615. HRMS (ESI): C$_{21}$H$_{20}$N$_4$O requires [M+Na]$^+$, calculated 367.1529, found 367.1525.

1-{[4-(Dimethylamino)phenyl]methyl}-7'-(1*H*-pyrazol-4-yl)-2',4'-dihydro-1'*H*-spiro[azetidine-3,3'-isoquinolin]-1'-one, 3-95
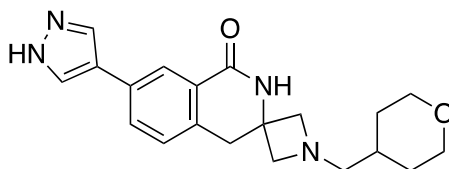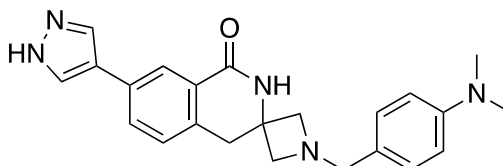

According to General Procedure H, 1'-oxo-7'-(1H-pyrazol-4-yl)-2',4'-dihydro-1'H-spiro[azetidine-3,3'-isoquinolin]-1-ium trifluoroacetate, **3-70**, (93 mg, 0.25 mmol), 4-dimethylamino-benzaldehyde (41 mg, 0.28 mmol), acetic acid (14

μl, 0.25 mmol) and STAB (58 mg, 0.28 mmol) gave a crude product which was purified by flash column chromatography, eluting with 0:100 → 10:90 7M NH$_3$ in MeOH–CH$_2$Cl$_2$ to give the *spiro-one* (34 mg, 35%) as a colourless amorphous solid. δ$_H$ (501 MHz, Methanol-d_4) 8.10 (1H, d, *J* 1.8, 8'–H), 7.98 (2H, s, pyrazolyl–H), 7.72 (1H, dd, *J* 7.8, 1.8, 6'–H), 7.33 (1H, dd, *J* 7.8, 0.8, 5'–H), 7.18-7.07 (2H, m, phenyl 2– and 6–H), 6.79-6.67 (2H, m, phenyl 3– and 5–H), 3.56 (2H, s, phenyl methyl–H), 3.38 (1H, d, *J* 7.1, azetidine–H$_A$), 3.37 (1H, d, *J* 7.1, azetidine–H$_B$), 3.27 (2H, s, 4'–H), 3.18 (1H, d, *J* 7.2, azetidine–H$_A$), 3.17 (1H, d, *J* 7.1, azetidine–H$_B$), 2.88 (6H, s, dimethyl–H). δ$_C$ (126 MHz, Methanol-d_4) 166.00, 150.42, 134.74, 132.08, 129.49, 129.45, 128.65, 128.34, 124.86, 123.74, 121.33, 112.64, 64.20, 62.15, 50.96, 39.63, 36.66. *R*$_F$ 0.48 (10:90 7 M NH$_3$ in MeOH–CH$_2$Cl$_2$). IR ν$_{max}$ (film)/cm^{-1} 3199, 2940, 2844, 1657 and 1614. HRMS (ESI): C$_{23}$H$_{25}$N$_5$O requires [M+H]$^+$, calculated 388.2132, found 388.2131.
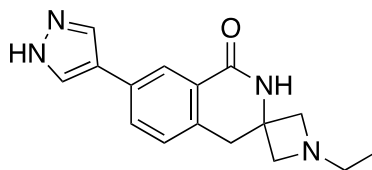
1-(Oxan-4-yl)-7'-(1*H*-pyrazol-4-yl)-2',4'-dihydro-1'*H*-spiro[azetidine-3,3'-isoquinolin]-1'-one, 3-96
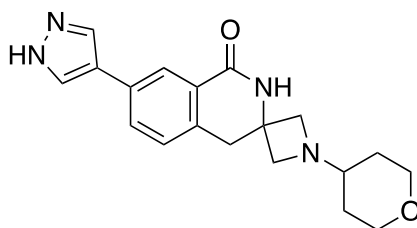
According to General Procedure H, 1'-oxo-7'-(1H-pyrazol-4-yl)-2',4'-dihydro-1'H-spiro[azetidine-3,3'-isoquinolin]-1-ium trifluoroacetate, **3-70**, (93 mg, 0.25 mmol), tetrahydro-4H-pyran-4-one (25 μl, 0.28 mmol), acetic acid (14 μl, 0.25 mmol) and STAB (58 mg, 0.28 mmol) gave a crude product which was purified by flash column chromatography, eluting with 0:100 → 10:90 7M NH$_3$ in MeOH–CH$_2$Cl$_2$ to give the *spiro-one* (38 mg, 45%) as a colourless amorphous solid. δ$_H$ (501 MHz, DMSO-d_6) 12.98 (1H, br s, pyrazole N–H), 8.47 (1H, s, amide N–H), 8.23 (1H, app br s, pyrazolyl–H), 8.00 (1H, d, *J* 1.9 8'–H), 7.93 (1H, app br s, pyrazolyl–H), 7.73 (1H, dd, *J* 7.8, 1.9, 6'–H), 7.37 (1H, d, *J* 7.8, 5'–H), 3.80 (2H, dt, *J* 11.4, 3.8, oxanyl 2–H), 3.31 (2H, app br s, azetidine–H), 3.25 (2H, td, *J* 11.4, 2.3, oxanyl 2–H), 3.21 (2H, s, 4'–H), 3.00 (2H, app br s, azetidine–H), 2.27 (1H, app br s, oxanyl 4–H), 1.57 (2H, dd, *J* 12.8, 3.8, oxanyl

3–H), 1.20-1.06 (2H, m, oxanyl 3–H). δ_C (126 MHz, DMSO-d_6) 164.05, 136.16, 134.50, 131.84, 129.01, 128.83, 125.62, 123.26, 120.56, 65.16, 62.59, 62.35, 50.28, 36.89, 29.57. R_F 0.40 (10:90 7 M NH$_3$ in MeOH–CH$_2$Cl$_2$). IR ν_{max} (film)/cm^{-1} 3201, 2939, 2846, 1654 and 1614. HRMS (ESI): C$_{19}$H$_{22}$N$_4$O$_2$ requires [M+Na]$^+$, calculated 361.1635, found 361.1634.
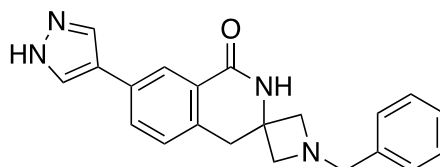
1-Cyclopentyl-7'-(1*H*-pyrazol-4-yl)-2',4'-dihydro-1'*H*-spiro[azetidine-3,3'-isoquinolin]-1'-one, 3-97
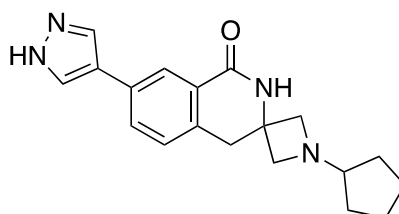
According to General Procedure H, 1'-oxo-7'-(1H-pyrazol-4-yl)-2',4'-dihydro-1'H-spiro[azetidine-3,3'-isoquinolin]-1-ium trifluoroacetate, **3-70**, (93 mg, 0.25 mmol), cyclopentanone (24 µl, 0.28 mmol), acetic acid (14 µl, 0.25 mmol) and STAB (58 mg, 0.28 mmol) gave a crude product which was purified by flash column chromatography, eluting with 0:100 → 10:90 7M NH$_3$ in MeOH–CH$_2$Cl$_2$ to give the *spiro-one* (62 mg, 77%) as a colourless amorphous solid. δ_H (501 MHz, Methanol-d_4) 8.10 (1H, d, *J* 1.9, 8'–H), 7.99 (2H, s, pyrazolyl–H), 7.73 (1H, dd, *J* 7.8, 1.9, 6'–H), 7.34 (1H, d, *J* 7.8, 5'–H), 3.40 (1H, d, *J* 7.2, azetidine–H$_A$), 3.40 (1H, d, *J* 7.2, azetidine–H$_B$), 3.27 (2H, s, 4'–H), 3.10 (1H, d, *J* 7.2, azetidine–H$_A$), 3.10 (1H, d, *J* 7.2, azetidine–H$_B$), 2.83 (1H, p, *J* 6.3, cyclopentyl 1–H), 1.77-1.60 (4H, m, cyclopentyl 2– and 3–H), 1.59-1.48 (2H, m, cyclopentyl 3–H), 1.36-1.23 (2H, m, cyclopentyl 2–H). δ_C (126 MHz, Methanol-d_4) 167.34, 137.49, 136.09, 133.46, 130.81, 130.05, 129.73, 126.86, 125.12, 122.71, 70.84, 65.05, 51.76, 38.11, 31.03, 25.46. R_F 0.45 (10:90 7 M NH$_3$ in MeOH–CH$_2$Cl$_2$). IR ν_{max} (film)/cm^{-1} 3196, 2946, 2864, 1656 and 1614. HRMS (ESI): C$_{19}$H$_{22}$N$_4$O requires [M+Na]$^+$, calculated 345.1686, found 345.1681.

1-(2-Methoxyethyl)-7'-(1*H*-pyrazol-4-yl)-2',4'-dihydro-1'*H*-spiro[azetidine-3,3'-isoquinolin]-1'-one, 3-98
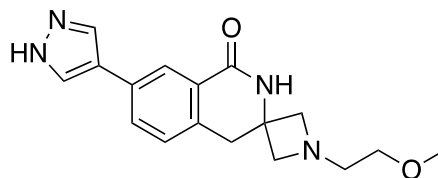
Bromo ethyl methyl ether (21 μl, 0.22 mmol) was added dropwise to a solution of 1'-oxo-7'-(1H-pyrazol-4-yl)-2',4'-dihydro-1'H-spiro[azetidine-3,3'-isoquinolin]-1-ium trifluoroacetate, **3-70**, (90.75 mg, 0.25 mmol) and NaHCO$_3$ (42.00 mg, 0.50 mmol) in DMF (0.8 ml, 0.3 M). After stirring at rt overnight, the mixture was concentrated under reduced pressure and purified by flash column chromatography, eluting with 0:100 → 10:90 7M NH$_3$ in MeOH–CH$_2$Cl$_2$ to give the *spiro-one* (20 mg, 29%) as a colourless amorphous solid. δ$_H$ (501 MHz, Acetone-d_6) 8.14 (1H, d, J 2.0, 8'–H), 8.08 (2H, br s, N–H and pyrazolyl–H), 7.75 (1H, dd, J 7.8, 2.0, 6'–H), 7.67 (1H, br s, pyrazolyl–H), 7.36 (1H, dt, J 7.8, 0.7, 5'–H), 3.50 (1H, d, J 7.0, azetidine–H$_A$), 3.50 (1H, d, J 7.0, azetidine–H$_A$), 3.37 (2H, t, J 5.6, ethyl 2–H), 3.30 (2H, s, 4'–H), 3.25 (3H, s, methoxy–H), 3.24-3.19 (2H, m, azetidine–H), 2.70 (2H, t, J 5.6, ethyl 1–H). δ$_C$ (126 MHz, Acetone-d_6) 164.36, 134.77, 132.31, 129.31, 128.99, 128.76, 123.99, 121.29, 70.96, 66.04 (d, J 3.5), 57.86, 57.70, 51.87, 37.21. R_F 0.41 (10:90 7 M NH$_3$ in MeOH–CH$_2$Cl$_2$). IR ν$_{max}$ (film)/cm^{-1} 3192, 2932, 2834, 1658 and 1615. HRMS (ESI): C$_{17}$H$_{20}$N$_4$O$_2$ requires [M+Na]$^+$, calculated 335.1479, found 335.1475.

tert-Butyl 7'-bromo-1'-oxo-2',4'-dihydro-1'*H*-spiro[azetidine-3,3'-isoquinoline]-1-carboxylate and tert-butyl 5'-bromo-1'-oxo-2',4'-dihydro-1'*H*-spiro[azetidine-3,3'-isoquinoline]-1-carboxylate, 3-99
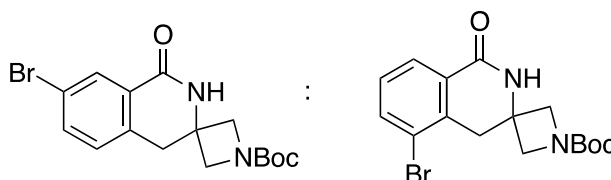
According to General Procedure A, (3-Bromophenyl)formamido 2,2-dimethylpropanoate, **3-15**, (5.39 g, 18.04 mmol) and tert-butyl 3-methylideneazetidine-1-carboxylate (3.36 ml, 19.84 mmol) gave a crude product which was purified by flash column chromatography, eluting with 0:100 → 50:50 EtOAc–hexane to give the *spiro-carboxylate* (4.42 g, 67%) as

a light yellow solid and a 5:3 inseparable mixture of regioisomers. δ_H (501 MHz, Chloroform-d) 8.18 (5H, d, J 2.1, 8'–H$_{Major}$), 8.04 (3H, dd, J 7.8, 1.3, 8'–H$_{Minor}$), 7.80 (5H, s, N–H$_{Major}$), 7.76-7.71 (6H, m, N–H$_{Minor}$ and 6'–H$_{Minor}$), 7.60 (5H, dd, J 8.0, 2.1, 6'–H$_{Major}$), 7.26 (3H, t, J 7.8, 7'–H$_{Minor}$), 7.16 (5H, d, J 8.0, 5'–H$_{Major}$), 4.01-3.89 (32H, m, azetidine–H$_{Major\ and\ minor}$), 3.36 (6H, s 4'–H$_{Minor}$), 3.20 (10H, s, 4'–H$_{Major}$), 1.44 (27H, s, *tert*-butyl–H$_{Minor}$), 1.43 (45H, s, *tert*-butyl–H$_{Major}$). δ_C (126 MHz, Chloroform-d) 165.06, 164.69, 156.21, 156.18, 136.70, 135.76, 135.68, 134.63, 131.12, 129.97, 129.77, 129.76, 128.78, 127.48, 123.67, 121.65, 80.29, 80.28, 61.34, 50.80, 50.42, 38.08, 37.63, 28.36, 28.34. R_F 0.29 (50:50 EtOAc–hexane). IR ν_{max} (film)/cm^{-1} 3233, 2974, 2881, 1669, 1396 and 1366. HRMS (ESI): $C_{16}H_{19}BrN_2O_3$ requires [M+H]$^+$, calculated 367.0652, found 367.0642.

tert-Butyl 3-methyl-4-(4,4,5,5-tetramethyl-1,3,2-dioxaborolan-2-yl)-1*H*-pyrazole-1-carboxylate, 3-100
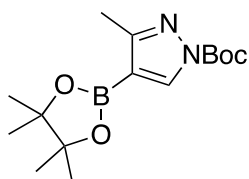
(Boc)$_2$O (0.53 g, 2.40 mmol) was added portion-wise to a solution of 3-Methyl-1H-pyrazole-4-boronic acid pinacol ester (0.50 g, 2.40 mmol) and triethylamine (0.33 ml, 2.40 mmol) in CH$_2$Cl$_2$ (12 ml, 0.2 M). The mixture was stirred at rt overnight, after which H$_2$O (25 ml) and CH$_2$Cl$_2$ (25 ml) were added. The aqueous layer was extracted with CH$_2$Cl$_2$ (3 x 25 ml) and the combined organics were washed with bicarb (sat. aq. soln., 25 ml), dried (MgSO$_4$), filtered and concentrated under reduced pressure. The resulting crude product was purified by flash column chromatography, eluting with 0:100 → 10:90 EtOAc–petrol to give the *pyrazole* (257 mg, 35%) as a colourless amorphous solid. δ_H (501 MHz, Chloroform-d) 8.25 (1H, d, J 0.6), 2.41 (3H, d, J 0.6), 1.60 (9H, s), 1.30 (12H, s). δ_C (126 MHz, Chloroform-d) 158.99, 147.34, 138.98, 109.98, 85.20, 83.63, 28.04, 24.93, 14.39. R_F 0.20 (10:90 EtOAc–petro). IR ν_{max} (film)/cm^{-1} 3233, 2978, 2933, 2359, 1763 and 1673. HRMS (ESI): $C_{15}H_{25}BN_2O_4$ requires [M+Na]$^+$, calculated 331.1800, found 331.1809.

7'-(3-Methyl-1*H*-pyrazol-4-yl)-1'-oxo-2',4'-dihydro-1'*H*-spiro[azetidine-3,3'-isoquinolin]-1-ium trifluoroacetate, 3-101

According to General Procedure D, tert-Butyl 7'-bromo-1'-oxo-2',4'-dihydro-1'H-spiro[azetidine-3,3'-isoquinoline]-1-carboxylate and tert-butyl 5'-bromo-1'-oxo-2',4'-dihydro-1'H-spiro[azetidine-3,3'-isoquinoline]-1-carboxylate, **3-99**, (267 mg g, 0.73 mmol) and tert-butyl 3-methyl-4-(4,4,5,5-tetramethyl-1,3,2-dioxaborolan-2-yl)-1H-pyrazole-1-carboxylate, (245 mg, 0.80 mmol) gave a crude product which was purified by flash column chromatography, eluting with 0:100 → 5:95 MeOH–CH$_2$Cl$_2$ to give the protected isoquinoline. According to General Procedure B, the protected isoquinoline (107 mg, 0.30 mmol) gave the *spiro-ium* (107 mg, 40% over two steps) as a red-brown amorphous solid. δ$_H$ (501 MHz, Methanol-*d$_4$*) 8.06-8.02 (2H, m 8'–H and pyrazolyl 5–H), 7.70 (1H, dd, *J* 7.8, 2.0, 6'–H), 7.49 (1H, d, *J* 7.8, 5'–H), 4.28 (1H, d, *J* 10.2, azetidine–H$_A$), 4.28 (1H, d, *J* 10.2, azetidine–H$_B$), 4.12 (1H, d, *J* 10.2, azetidine–H$_A$), 4.12 (1H, d, *J* 10.2, azetidine–H$_B$), 3.47 (2H, s, 4'–H), 2.49 (3H, s, methyl–H). δ$_C$ (126 MHz, Methanol-*d$_4$*) 165.20, 159.68 (q, *J* 38.0), 140.76, 133.53, 133.31, 131.86, 131.84, 128.94, 128.07, 125.99, 119.50, 115.74 (q, *J* 288.0), 57.12, 53.00, 35.97, 9.76. *R$_F$* 0.15 (10:90 7M NH$_3$ in MeOH–CH$_2$Cl$_2$). IR ν$_{max}$ (film)/cm^{-1} 3388, 3192, 2926, 2669, 2360, 1658 and 1617. HRMS (ESI): C$_{15}$H$_{16}$N$_4$O requires [M+H]$^+$, calculated 269.1397, found 269.1402.

5'-(3-Methyl-1*H*-pyrazol-4-yl)-1'-oxo-2',4'-dihydro-1'*H*-spiro[azetidine-3,3'-isoquinolin]-1-ium trifluoroacetate, 3-102

According to General Procedure D, tert-Butyl 7'-bromo-1'-oxo-2',4'-dihydro-1'H-spiro[azetidine-3,3'-isoquinoline]-1-carboxylate and tert-butyl 5'-bromo-1'-oxo-2',4'-dihydro-1'H-spiro[azetidine-3,3'-isoquinoline]-1-carboxylate, **3-99**, (267 mg g, 0.73 mmol) and tert-butyl 3-methyl-4-(4,4,5,5-tetramethyl-1,3,2-dioxaborolan-2-yl)-1H-pyrazole-1-carboxylate, (245 mg, 0.80 mmol) gave a crude product which was purified by flash column chromatography, eluting with 0:100 → 5:95 MeOH–CH$_2$Cl$_2$ to give the protected isoquinoline. According to General Procedure B, the protected isoquinoline (42 mg, 0.12 mmol) gave the *spiro-ium* (42 mg, 16% over two steps) as a yellow-orange amorphous solid. δ$_H$ (501 MHz, Methanol-d_4) 8.01 (1H, dd, *J* 7.6, 1.6, 8'–H), 7.86 (1H, d, *J* 2.3, pyrazolyl 5–H), 7.54 (1H, dd, *J* 7.6, 1.6, 6'–H), 7.49 (1H, t, *J* 7.6, 7'–H), 4.23 (1H, d, *J* 10.1, azetidine–H$_A$), 4.23 (1H, d, *J* 10.1, azetidine–H$_B$), 3.98 (1H, d, *J* 10.2, azetidine–H$_A$), 3.97 (1H, d, *J* 10.2, azetidine–H$_B$), 3.39 (2H, s, 4'–H), 2.30 (3H, s, methyl–H). δ$_C$ (126 MHz, Methanol-d_4) 165.42, 159.54 (q, *J* 40.1, 37.6), 141.91, 135.18, 134.53, 134.02, 131.64, 128.41, 127.26, 127.08, 117.62, 115.69 (q, *J* 288.6), 57.06, 52.69, 34.22, 9.06. R_F 0.06 (10:90 7M NH$_3$ in MeOH–CH$_2$Cl$_2$). IR ν$_{max}$ (film)/cm^{-1} 3379, 3234, 2973, 2360, 1661 and 1597. HRMS (ESI): C$_{15}$H$_{16}$N$_4$O requires [M+H]$^+$, calculated 269.1397, found 269.1400.

1-Methyl-7'-(3-methyl-1*H*-pyrazol-4-yl)-2',4'-dihydro-1'*H*-spiro[azetidine-3,3'-isoquinolin]-1'-one, 3-103
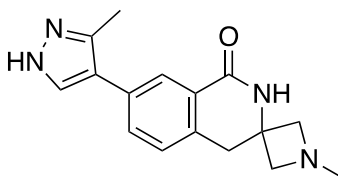
According to General Procedure H, 7'-(3-methyl-1H-pyrazol-4-yl)-1'-oxo-2',4'-dihydro-1'H-spiro[azetidine-3,3'-isoquinolin]-1-ium trifluoroacetate, **3-101**, (91 mg, 0.25 mmol), formaldehyde (37% aq., 28 μl, 0.38 mmol) and STAB (159 mg, 0.75 mmol) gave a crude product which was purified by flash column chromatography, eluting with 0:100 → 10:90 7M NH$_3$ in MeOH–CH$_2$Cl$_2$ to give the *spiro-one* (32 mg, 45%) as a colourless amorphous solid. δ$_H$ (501 MHz, Methanol-d_4) 7.99 (1H, d, *J* 1.9, 8'–H), 7.74 (1H, br s, pyrazolyl 5–H), 7.62 (1H, dd, *J* 7.8, 1.9, 6'–H), 7.40 (1H, d, *J* 7.8, 5'–H), 3.53 (1H, d, *J* 7.0,

azetidine–H$_A$), 3.53 (1H, d, J 7.0, azetidine–H$_B$), 3.32 (2H, s, 4'–H), 3.18 (1H, d, J 7.1, azetidine–H$_A$), 3.17 (1H, d, J 7.1, azetidine–H$_B$), 2.43 (3H, s, pyrazolyl methyl–H), 2.42 (3H, s, methyl–H). δ$_C$ (126 MHz, Methanol-d_4) 165.92, 137.99, 135.67, 134.38, 132.97, 131.26, 128.51, 128.15, 125.45, 118.52, 66.47, 50.40, 44.25, 36.59. R_F 0.40 (10:90 7M NH$_3$ in MeOH–CH$_2$Cl$_2$). IR ν$_{max}$ (film)/cm^{-1} 3202, 2943, 2847, 1656 and 1614. HRMS (ESI): C$_{16}$H$_{18}$N$_4$O requires [M+Na]$^+$, calculated 305.1373, found 305.1376.

1-Methyl-5'-(3-methyl-1*H*-pyrazol-4-yl)-2',4'-dihydro-1'*H*-spiro[azetidine-3,3'-isoquinolin]-1'-one, 3-104
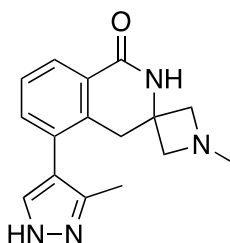
According to General Procedure H, 5'-(3-methyl-1H-pyrazol-4-yl)-1'-oxo-2',4'-dihydro-1'H-spiro[azetidine-3,3'-isoquinolin]-1-ium trifluoroacetate, **3-102**, (91 mg, 0.25 mmol), formaldehyde (37% aq., 28 µl, 0.38 mmol) and STAB (159 mg, 0.75 mmol) gave a crude product which was purified by flash column chromatography, eluting with 0:100 → 10:90 7M NH$_3$ in MeOH–CH$_2$Cl$_2$ to give the *spiro-one* (27 mg, 38%) as a colourless amorphous solid. δ$_H$ (501 MHz, Methanol-d_4) 7.93 (1H, dd, J 7.6, 1.6, 8'–H), 7.57 (1H, br s, pyrazolyl 5–H), 7.46 (1H, dd, J 7.6, 1.6, 6'–H), 7.42 (1H, t, J 7.6, 7'–H), 3.42 (1H, d, J 7.0, azetidine–H$_A$), 3.42 (1H, d, J 7.0, azetidine–H$_B$), 3.25 (2H, s, 4'–H), 3.11 (1H, d, J 7.1, azetidine–H$_A$), 3.11 (1H, d, J 7.1, azetidine–H$_B$), 2.32 (3H, s, methyl–H), 2.22 (3H, s, pyrazolyl methyl–H). δ$_C$ (126 MHz, Methanol-d_4) 167.48, 137.06, 136.18, 134.23, 129.95, 127.92, 127.68, 118.50, 67.81, 51.42, 45.48, 36.31. R_F 0.38 (10:90 7M NH$_3$ in MeOH–CH$_2$Cl$_2$). IR ν$_{max}$ (film)/cm^{-1} 3203, 2936, 2843 1656 and 1592. HRMS (ESI): C$_{16}$H$_{18}$N$_4$O requires [M+Na]$^+$, calculated 305.1373, found 305.1379.

5.2 Procedure for Activity Directed Synthesis

5.2.1 Mock Array 1

The mock reaction array was carried out in borosilicate glass vials (well volume ~750 µl). Fragments were dissolved in 50:50 CH_2Cl_2–MeOH 100 mM and 50 µl was added to the appropriate vials and the solvent was evaporated under room temperature and pressure. α-diazo amides were dissolved in CH_2Cl_2, to 220 mM and 25 µl was added to the appropriate vials followed by concentration. For the mock array of the fragments and α-diazo amides, 50 µl CH_2Cl_2 was added and the vials were sealed. The catalysts were dissolved in CH_2Cl_2 to 2.5 mM and sonicated for 10 min prior to the addition of 50 µl into the appropriate vials which were sealed. The mock array was incubated at room temperature without stirring. The final fragment, α-diazo amide and catalyst concentrations were 100 mM, 110 mM and 2.5 mM (2.5 mol % catalyst), respectively. After 48 h, each vial was scavenged with 30 mg of QuadraPure TU resin. After 24 h, the scavenged vials were filtered and washed 5 times with the corresponding solvent the substrates, co-substrate or catalyst was dissolved in. The resulting solutions were concentrated under reduced pressure and the crude product was dissolved in 50 µl DMSO to give a product mixture solution of $\sum[Pn] = 100$ mM which were assayed for activity against Nek7.

5.2.2 Reaction Array 1

The reaction array was carried out in borosilicate glass vials (well volume ~750 µl). Fragments were dissolved in 50:50 CH_2Cl_2–MeOH 100 mM and 50 µl was added to the appropriate vials and the solvent was evaporated under room temperature and pressure. α-diazo amides were dissolved in CH_2Cl_2, to 220 mM and 25 µl was added to the appropriate vials followed by concentration. The catalysts were dissolved in CH_2Cl_2 to 2.5 mM and sonicated for 10 min prior to the addition of 50 µl into the appropriate vials which were sealed and left to react at room temperature without stirring. The final fragment, α-diazo amide and catalyst concentrations were 100 mM, 110 mM and 2.5 mM (2.5 mol % catalyst), respectively. After 48 h, each reaction vial was scavenged with 30 mg of QuadraPure TU resin, incubated for 24 at

room temperature, filtered and washed 5 times with the corresponding solvent system the substrate was dissolved in. The resulting solutions were concentrated under reduced pressure and the crude product mixtures were dissolved in 50 µl DMSO to give a product mixture solution of $\sum[\text{Pn}] = 100$ mM which were assayed for activity against Nek7.

5.2.3 Mock Array 2

The mock reaction array was carried out as in Mock Array 1 (5.2.1).

5.2.4 Reaction Array 2

The reaction array was carried out as in reaction Array 1 (5.2.2).

5.2.5 Scale-up Reactions

Scale-up reactions were carried out on a ~10-fold or 50-fold scale following the reaction array procedure (5.2.2) in borosilicate glass vials (volume ~7 ml). The fragment was dissolved in 50:50 CH_2Cl_2–MeOH 100 mM and 600 µl (~10-fold) or 2.5 ml (50-fold) was added to the appropriate vials and the solvent was evaporated under room temperature and pressure. α-diazo amides were dissolved in CH_2Cl_2, to 220 mM and 300 µl or 1.25 ml was added to the appropriate vials followed by concentration. The catalysts were dissolved in CH_2Cl_2 to 2.5 mM and sonicated for 10 min prior to the addition of 600 µl or 2.5 ml into the appropriate vials which were sealed and left to react at room temperature without stirring. The final fragment, α-diazo amide and catalyst concentrations were 100 mM, 110 mM and 2.5 mM (2.5 mol % catalyst), respectively. After 48 h, each reaction vial was scavenged with 30 mg of QuadraPure TU resin, incubated for 24 at room temperature, filtered and washed 5 times with the corresponding solvent system the substrate was dissolved in. The resulting solutions were concentrated under reduced pressure and the crude product mixtures were dissolved in 600 µl d_6-DMSO or 2.5 ml DMSO to give a product mixture solution of $\sum[\text{Pn}] = 100$ mM.

5.3 EZ Reader II (Caliper) Mobility Shift Assay

5.3.1 General Experimental

Kinase assays were carried out with a Labchip EZ Reader II system (PerkinElmer, formerly Caliper Life Sciences) at room temperature using separation buffer (760367, PerkinElmer) containing Coating Reagent 8 (500 nM, 760278, PerkinElmer). The assay was carried out in 384-well plates (Corning) The substrate used was a fluorescein-labelled peptide [5-FAM-FLAKSFGSPNRAYKK-CONH$_2$] dissolved in 100 mM HEPES (pH 7.5), 0.003% (v/v) Brij-35, 0.004% (v/v) Tween-20 and 10 mM MgCl$_2$. Measurements of substrate phosphorylation were taken every two minutes for 30 cycles. All assays were carried out in duplicate using a 12-sipper chip (760404, PerkinElmer) with a 2% final DMSO concentration.

5.3.2 Protein Production and Purification

Nek7 (in pET30, *C*-terminal His$_6$-tag) expressing Codonplus RPIL (Stratagene) *Escherichia coli* were available in-house. The cell pellets containing recombinantly expressed Nek7 were lysed by sonication in lysis buffer containing 20 mM imidazole, 20 mM HEPES (pH 7.5), 200 mM NaCl, 1 mM MgCl$_2$ and 5% glycerol. The Clarified lysate was applied to a 5 ml HisTrap column, pre-charged with nickel, and eluted by FPLC across a gradient of 20 mM to 250 mM imidazole. The eluate corresponding to recombinant Nek7 was place in a 10 kDa membrane and dialysed in size exclusion buffer containing 50 mM (HEPES, pH 7.5), 200 mM NaCl, 1 mM MgCl$_2$ and 5% glycerol. The dialysed recombinant Nek7 was concentrated and applied to a Superdex 200 16/600 size exclusion column, equilibrated and eluting with size exclusion buffer.

5.3.3 Optimal Kinase Concentration Determination

The concentration of Nek7 for use in future assays was determined by the measurement of substrate conversion as a function of time over different concentrations of enzyme. Nek7 (1 μM) was subjected to a six-point two-fold serial dilution in Nek7 buffer containing 100 mM HEPES (pH 7.5), 0.003% (v/v) Brij-35, 0.004% (v/v) Tween-20, 10 mM MgCl$_2$ and 2% (v/v) DMSO to give 2 × Nek7 stock solutions, 14 μl of which were added to the appropriate

wells in the 384-well plate. A 2 × stock solution of substrate (3 μM) and ATP (from the previously determined K_M,[28] 80 μM) in Nek7 buffer was prepared and 14 μl was added to the wells containing enzyme in the 384-well plate to give six final Nek7 concentrations (500 nM – 15.63 nM), a final substrate concentration of 1.5 μM and a final ATP concentration of 40 μM in a final volume of 28 μl with 2% DMSO. The percentage conversion of substrate to product for each enzyme concentration was generated automatically by the EZ Reader software and was plotted against time using GraphPad Prism 7. An enzyme concentration of 250 nM was chosen for future assays.

5.3.4 Optimal ATP Concentration Determination

The Nek7 K_M ATP value was determined by subjection of ATP (12 mM) to a 12-point three-fold serial dilution in Nek7 buffer containing 100 mM HEPES (pH 7.5), 0.003% (v/v) Brij-35, 0.004% (v/v) Tween-20, 10 mM $MgCl_2$ and 2% (v/v) DMSO to give 4 × ATP stock solutions. A 4 × substrate stock concentration (6 μM) and 2 × Nek7 stock concentration (500 nM) were prepared. Each 4 × ATP stock solution were diluted two-fold in the 4 × substrate stock solution and 14 μl was added into the appropriate wells in the 384-well plate followed by 14 μl of the 2 × enzyme stock solution. This procedure gave 12 final ATP concentrations (3 mM – 17 nM) and final substrate and enzyme concentrations of 1.5 μM and 250 nM, respectively, in a final volume of 28 μl with 2% DMSO. The percentage conversion of substrate to product for each ATP concentration was generated automatically by the EZ Reader software and was plotted against time using GraphPad Prism 7. The initial rate at each ATP concentration was plotted against the corresponding concentration to generate a Michaelis-Menten plot. A Nek7 K_M ATP value of 32 ± 4 μM was determined.

5.3.5 IC$_{50}$ Determination

The activity for Nek7 was determined by subjection of the compound to a 10-point three-fold serial dilution in DMSO (150 mM, 100% DMSO) followed by dilution in Nek7 buffer containing 100 mM HEPES (pH 7.5), 0.003% (v/v) Brij-35, 0.004% (v/v) Tween-20 and 10 mM $MgCl_2$ to give 4 × fragment stock solutions (12 mM, 8% DMSO). A 4 × substrate and ATP stock solution, 6 μM and 120 μM, respectively, and a 2 × Nek7 stock solution (500 nM) were

prepared. Each of the 4 × fragment stock solutions were diluted two-fold in the substrate and ATP stock solution and 14 μl was added into the appropriate wells in the 384-well plate followed by 14 μl of the 2 × enzyme stock solution. This procedure gave 10 final fragment concentrations (3 mM – 152 nM), final substrate and ATP concentrations of 1.5 μM and 30 μM, respectively, and a final enzyme concentration of 250 nM in a final volume of 28 μl with 2% final DMSO. 2% DMSO in buffer was used as the negative control and 3 mM **4-3** in 2% DMSO buffer was used as the positive control. The percentage conversion of substrate to product for each compound concentration was generated automatically by the EZ Reader software and was plotted against time using GraphPad Prism 9. The initial rate at each compound concentration was plotted against the corresponding concentration to give the dose-response curve.

5.3.6 Mock Array 1

Each product mixture from the mock array (section x.x.x) was diluted in DMSO to 5 mM (assuming a product mixture solution of $\sum[\text{Pn}] = 100$ mM, relative to fragment) followed by dilution in Nek7 buffer containing 100 mM HEPES (pH 7.5), 0.003% (v/v) Brij-35, 0.004% (v/v) Tween-20 and 10 mM $MgCl_2$ to give 4 × product mixture stock solutions (400 μM, 8% DMSO). A 4 × substrate and ATP stock solution, 6 μM and 120 μM, respectively, and a 2 × Nek7 stock solution (500 nM) were prepared. Each of the 4 × product mixture stock solutions were diluted two-fold in the substrate and ATP stock solution and 14 μl was added into the appropriate wells in the 384-well plate followed by 14 μl of the 2 × enzyme stock solution. This procedure gave a final product mixture concentration of 100 μM, 2% DMSO, final substrate and ATP concentrations of 1.5 μM and 30 μM, respectively, and a final enzyme concentration of 250 nM in a final volume of 28 μl. For the case of reactions involving the phthalimide fragment, a final product mixture concentration of 30 μM 2% DMSO was used in the assay. 2% DMSO in buffer was used as the negative control and 3 mM **4-3** in 2% DMSO buffer was used as the positive control. The percentage conversion of substrate to product for each product mixture was generated automatically by the EZ Reader software and was plotted against time using GraphPad Prism 7. The initial rate for each product mixture was plotted against the components in each mock array vial.

5.3.7 Reaction Array 1

Each product mixture from the reaction array (section 4.2.3) was diluted in DMSO to 5 mM (assuming a product mixture solution of $\sum[\text{Pn}] = 100$ mM, relative to fragment) followed by dilution in Nek7 buffer containing 100 mM HEPES (pH 7.5), 0.003% (v/v) Brij-35, 0.004% (v/v) Tween-20 and 10 mM MgCl$_2$ to give 4 × product mixture stock solutions (400 μM, 8% DMSO). A 4 × substrate and ATP stock solution, 6 μM and 120 μM, respectively, and a 2 × Nek7 stock solution (500 nM) were prepared. Each of the 4 × product mixture stock solutions were diluted two-fold in the substrate and ATP stock solution and 14 μl was added into the appropriate wells in the 384-well plate followed by 14 μl of the 2 × enzyme stock solution. This procedure gave a final product mixture concentration of 100 μM, 2% DMSO, final substrate and ATP concentrations of 1.5 μM and 30 μM, respectively, and a final enzyme concentration of 250 nM in a final volume of 28 μl with 2% DMSO. For the case of reactions involving the phthalimide fragment, a final product mixture concentration of 30 μM 2% DMSO was used in the assay. 2% DMSO in buffer was used as the negative control and 3 mM **4-3** in 2% DMSO buffer was used as the positive control. The percentage conversion of substrate to product for each product mixture was generated automatically by the EZ Reader software and was plotted against time using GraphPad Prism 7. The initial rate for each product mixture was plotted against the components in each mock array vial.

5.3.8 Mock Array 2

The mock reaction array was assayed as in Mock Array 1 (5.3.6).

5.3.9 Reaction Array 2

The reaction array was assayed as in reaction Array 1 (5.3.7).

5.3.10 Scale-up Reactions

The Scale-up Reactions were assayed as previously described. For the reaction which was validated in the same manner as the reaction array assay see 5.3.6 and for the reaction which was validated by an IC$_{50}$ see 5.3.5.

List of References

1   P. Cohen and D. R. Alessi, *ACS Chem. Biol.*, 2013, 8, 96–104.

2   F. M. Ferguson and N. S. Gray, *Nat. Rev. Drug Discov.*, 2018, 17, 353–376.

3   O. Fedorov, S. Müller and S. Knapp, *Nat. Chem. Biol.*, 2010, 6, 166–169.

4   Understudied Proteins | NIH Common Fund, https://commonfund.nih.gov/idg/understudiedproteins, (accessed 18 August 2021).

5   G. Manning, D. B. Whyte, R. Martinez, T. Hunter and S. Sudarsanam, *Science (80-.).*, 2002, **298**, 1912–1934.

6   R. Kannaiyan and D. Mahadevan, *Expert Rev. Anticancer Ther.*, 2018, **18**, 1249.

7   G. Manning, G. D. Plowman, T. Hunter and S. Sudarsanam, *Trends Biochem. Sci.*, 2002, **27**, 514–520.

8   P. Cohen, *Trends Biochem. Sci.*, 2000, **25**, 596–601.

9   J. A. Ubersax and J. E. Ferrell, *Nat. Rev. Mol. Cell Biol.*, 2007, **8**, 530–541.

10   D. R. Knighton, J. Zheng, L. F. Ten Eyck, V. A. Ashford, N. H. Xuong, S. S. Taylor and J. M. Sowadski, *Science (80-.).*, 1991, **253**, 407–414.

11   A. P. Kornev, N. M. Haste, S. S. Taylor and L. F. Ten Eyck, *Proc. Natl. Acad. Sci. U. S. A.*, 2006, **103**, 17783–8.

12   S. S. Taylor and A. P. Kornev, *Trends Biochem. Sci.*, 2011, **36**, 65–77.

13   H. S. Meharena, P. Chang, M. M. Keshwani, K. Oruganty, A. K. Nene, N. Kannan, S. S. Taylor and A. P. Kornev, *PLoS Biol.*, 2013, **11**, e1001680.

14   R. Roskoski, *Pharmacol. Res.*, 2016, 103, 26–48.

15   L. Moniz, P. Dutt, N. Haider and V. Stambolic, *Cell Div.*, 2011, **6**, 18.

16   A. M. Fry, L. O'Regan, S. R. Sabir, R. Bayliss, B. Goh, A. C. Kim and

L. M. Quarmby, *J. Cell Sci.*, 2012, **125**, 4423–33.

17   C. E. Walczak and R. Heald, in *International review of cytology*, 2008, vol. 265, pp. 111–158.

18   L. O'Regan and A. M. Fry, *Mol. Cell. Biol.*, 2009, **29**, 3975–90.

19   E. A. Nigg, *Nat. Rev. Mol. Cell Biol.*, 2001, **2**, 21–32.

20   B. R. Oakley and N. R. Morris, *J. Cell Biol.*, 1983, **96**, 1155–8.

21   M. J. O'Connell, M. J. E. Krien and T. Hunter, *Trends Cell Biol.*, 2003, **13**, 221–8.

22   R. S. Hames, S. L. Wattam, H. Yamano, R. Bacchieri and A. M. Fry, *EMBO J.*, 2001, **20**, 7117–27.

23   G. Vaz Meirelles, D. C. Ferreira Lanza, J. C. da Silva, J. Santana Bernachi, A. F. Paes Leme and J. Kobarg, *J. Proteome Res.*, 2010, **9**, 6298–6316.

24   M. W. Richards, L. O'Regan, C. Mas-Droux, J. M. Y. Blot, J. Cheung, S. Hoelder, A. M. Fry and R. Bayliss, *Mol. Cell*, 2009, **36**, 560–570.

25   T. Haq, M. W. Richards, S. G. Burgess, P. Gallego, S. Yeoh, L. O'Regan, D. Reverter, J. Roig, A. M. Fry and R. Bayliss, *Nat. Commun.*, 2015, **6**, 8771.

26   A. M. Fry, R. Bayliss and J. Roig, *Front. Cell Dev. Biol.*, 2017, **5**, 102.

27   C. A. Dodson, S. Yeoh, T. Haq and R. Bayliss, *Sci. Signal.*, 2013, **6**, ra54.

28   M. J. Byrne, N. Nasir, C. Basmadjian, C. Bhatia, R. F. Cunnison, K. H. Carr, C. Mas-Droux, S. Yeoh, C. Cano and R. Bayliss, *Biochem. J.*, 2020, **477**, 1525–1539.

29   M. T. Bertran, S. Sdelci, L. Regué, J. Avruch, C. Caelles and J. Roig, *EMBO J.*, 2011, **30**, 2634–2647.

30   J. Rapley, M. Nicolàs, A. Groen, L. Regué, M. T. Bertran, C. Caelles, J. Avruch and J. Roig, *J. Cell Sci.*, 2008, **121**, 3912–3921.

31   S. Sdelci, M. T. Bertran and J. Roig, *Cell Cycle*, 2011, **10**, 3816–3817.

32   E. Laurell, K. Beck, K. Krupina, G. Theerthagiri, B. Bodenmiller, P.

Horvath, R. Aebersold, W. Antonin and U. Kutay, *Cell*, 2011, **144**, 539–550.

33   M. I. Linder, M. Köhler, P. Boersema, M. Weberruss, C. Wandke, J. Marino, C. Ashiono, P. Picotti, W. Antonin and U. Kutay, *Dev. Cell*, 2017, **43**, 141-156.e7.

34   R. Adib, J. M. Montgomery, J. Atherton, L. O'Regan, M. W. Richards, K. R. Straatman, D. Roth, A. Straube, R. Bayliss, C. A. Moores and A. M. Fry, *Sci. Signal.*, 2019, **12**, 2939.

35   B. R. Oakley, *Trends Cell Biol.*, 1992, **2**, 1–5.

36   L. O'Regan, J. Sampson, M. W. Richards, A. Knebel, D. Roth, F. E. Hood, A. Straube, S. J. Royle, R. Bayliss and A. M. Fry, *J. Cell Biol.*, 2015, **209**, 349.

37   C. Gutiérrez-Caballero, S. G. Burgess, R. Bayliss and S. J. Royle, *Biol. Open*, 2015, **4**, 170–179.

38   F. E. Hood, S. J. Williams, S. G. Burgess, M. W. Richards, D. Roth, A. Straube, M. Pfuhl, R. Bayliss and S. J. Royle, *J. Cell Biol.*, 2013, **202**, 463.

39   S. N. Cullati, L. Kabeche, A. N. Kettenbach and S. A. Gerber, *J. Cell Biol.*, 2017, **216**, 2339–2354.

40   S. Kim, S. Kim, K. Rhee and K. Rhee, *J. Cell Sci.*, 2011, **124**, 3760–3770.

41   H. J. Jee, A. J. Kim, N. Song, H.-J. Kim, M. Kim, H. Koh and J. Yun, *Cell Cycle*, 2010, **9**, 4703–4710.

42   R. Tan, S. Nakajima, Q. Wang, H. Sun, J. Xue, J. Wu, S. Hellwig, X. Zeng, N. A. Yates, T. E. Smithgall, M. Lei, Y. Jiang, A. S. Levine, B. Su and L. Lan, *Mol. Cell*, 2017, **65**, 818-831.e5.

43   H. Shi, Y. Wang, X. Li, X. Zhan, M. Tang, M. Fina, L. Su, D. Pratt, C. Hui Bu, S. Hildebrand, S. Lyon, L. Scott, J. Quan, Q. Sun, J. Russell, S. Arnett, P. Jurek, D. Chen, V. V Kravchenko, J. C. Mathison, E. M. Y. Moresco, N. L. Monson, R. J. Ulevitch and B. Beutler, *Nat. Immunol.*, 2016, **17**, 250–258.

44   M. Capra, P. G. Nuciforo, S. Confalonieri, M. Quarto, M. Bianchi, M. Nebuloni, R. Boldorini, F. Pallotti, G. Viale, M. L. Gishizky, G. F. Draetta and P. P. Di Fiore, *Cancer Res.*, 2006, **66**, 8147–54.

45   L. Zhou, Z. Wang, X. Xu, Y. Wan, K. Qu, H. Fan, Q. Chen, X. Sun and C. Liu, *Oncotarget*, 2016, **7**, 18620–30.

46   R. Wang, Y. Song, X. Xu, Q. Wu and C. Liu, *Clin. Transl. Oncol.*, 2013, **15**, 626–32.

47   H. Salem, I. Rachmin, N. Yissachar, S. Cohen, A. Amiel, R. Haffner, L. Lavi and B. Motro, *Oncogene*, 2010, **29**, 4046–4057.

48   C. I. Wells, N. R. Kapadia, R. M. Couñago and D. H. Drewry, *Medchemcomm*, 2018, **9**, 44–66.

49   A. Takeno, I. Takemasa, Y. Doki, M. Yamasaki, H. Miyata, S. Takiguchi, Y. Fujiwara, K. Matsubara and M. Monden, *Br. J. Cancer*, 2008, **99**, 1307–1315.

50   Y. J. Jeon, K. Y. Lee, Y. Y. Cho, A. Pugliese, H. G. Kim, C. H. Jeong, A. M. Bode and Z. Dong, *J. Biol. Chem.*, 2010, **285**, 28126–28133.

51   M. A. Jordan and L. Wilson, *Nat. Rev. Cancer*, 2004, **4**, 253–265.

52   J. R. Jackson, D. R. Patrick, M. M. Dar and P. S. Huang, *Nat. Rev. Cancer*, 2007, **7**, 107–117.

53   M. Soda, Y. L. Choi, M. Enomoto, S. Takada, Y. Yamashita, S. Ishikawa, S. Fujiwara, H. Watanabe, K. Kurashina, H. Hatanaka, M. Bando, S. Ohno, Y. Ishikawa, H. Aburatani, T. Niki, Y. Sohara, Y. Sugiyama and H. Mano, *Nat. 2007 4487153*, 2007, **448**, 561–566.

54   L. O'Regan, G. Barone, R. Adib, C. G. Woo, H. J. Jeong, E. L. Richardson, M. W. Richards, P. A. J. Muller, S. J. Collis, D. A. Fennell, J. Choi, R. Bayliss and A. M. Fry, *J. Cell Sci. 2020, 133, jcs.241505*.

55   C. G. Woo, S. Seo, S. W. Kim, S. J. Jang, K. S. Park, J. Y. Song, B. Lee, M. W. Richards, R. Bayliss, D. H. Lee and J. Choi, *Ann. Oncol.*, 2017, **28**, 791–797.

56   O. Hantschel, *ACS Chem. Biol.*, 2015, **10**, 234–245.

57   A. Gazit, P. Yaish, C. Gilon and A. Levitzki, *J. Med. Chem.*, 2002, **32**, 2344–2352.

58   D. M. Goldstein, N. S. Gray and P. P. Zarrinkar, *Nat. Rev. Drug Discov.*, 2008, **7**, 391–397.

59   C. V Miduturu, X. Deng, N. Kwiatkowski, W. Yang, L. Brault, P. Filippakopoulos, E. Chung, Q. Yang, J. Schwaller, S. Knapp, R. W. King, J.-D. Lee, S. Herrgard, P. Zarrinkar and N. S. Gray, *Chem. Biol.*, 2011, **18**, 868–879.

60   J. E. Maxson, M. L. Abel, J. Wang, X. Deng, S. Reckel, S. B. Luty, H. Sun, J. Gorenstein, S. B. Hughes, D. Bottomly, B. Wilmot, S. K. McWeeney, J. Radich, O. Hantschel, R. E. Middleton, N. S. Gray, B. J. Druker and J. W. Tyner, *Cancer Res.*, 2016, **76**, 127–138.

61   F. M. Ferguson, J. Ni, T. Zhang, B. Tesar, T. Sim, N. D. Kim, X. Deng, J. R. Brown, J. J. Zhao and N. S. Gray, *ACS Med. Chem. Lett.*, 2016, **7**, 908–912.

62   F. M. Ferguson, Z. M. Doctor, A. Chaikuad, T. Sim, N. D. Kim, S. Knapp and N. S. Gray, *Bioorganic Med. Chem. Lett.*, 2017, **27**, 4405–4408.

63   N. Kwiatkowski, X. Deng, J. Wang, L. Tan, F. Villa, S. Santaguida, H. C. Huang, T. Mitchison, A. Musacchio and N. Gray, *ACS Chem. Biol.*, 2012, **7**, 185–196.

64   X. Deng, N. Dzamko, A. Prescott, P. Davies, Q. Liu, Q. Yang, J. D. Lee, M. P. Patricelli, T. K. Nomanbhoy, D. R. Alessi and N. S. Gray, *Nat. Chem. Biol.*, 2011, **7**, 203–205.

65   X. Deng, Q. Yang, N. Kwiatkowski, T. Sim, U. McDermott, J. E. Settleman, J. D. Lee and N. S. Gray, *ACS Med. Chem. Lett.*, 2011, **2**, 195–200.

66   E. C. K. Lin, C. M. Amantea, T. K. Nomanbhoy, H. Weissig, J. Ishiyama, Y. Hu, S. Sidique, B. Li, J. W. Kozarich and J. S. Rosenblum, *Proc. Natl. Acad. Sci. U. S. A.*, 2016, **113**, 11865–11870.

67   X. Deng, J. M. Elkins, J. Zhang, Q. Yang, T. Erazo, N. Gomez, H. G.

Choi, J. Wang, N. Dzamko, J. D. Lee, T. Sim, N. Kim, D. R. Alessi, J. M. Lizcano, S. Knapp and N. S. Gray, *Eur. J. Med. Chem.*, 2013, **70**, 758–767.

68 F. M. Ferguson, Y. Liu, W. Harshbarger, L. Huang, J. Wang, X. Deng, S. J. Capuzzi, E. N. Muratov, A. Tropsha, S. Muthuswamy, K. D. Westover and N. S. Gray, *J. Med. Chem.*, 2020, **63**, 7817–7826.

69 F. M. Ferguson, B. Nabet, S. Raghavan, Y. Liu, A. L. Leggett, M. Kuljanin, R. L. Kalekar, A. Yang, S. He, J. Wang, R. W. S. Ng, R. Sulahian, L. Li, E. J. Poulin, L. Huang, J. Koren, N. Dieguez-Martinez, S. Espinosa, Z. Zeng, C. R. Corona, J. D. Vasta, R. Ohi, T. Sim, N. D. Kim, W. Harshbarger, J. M. Lizcano, M. B. Robers, S. Muthaswamy, C. Y. Lin, A. T. Look, K. M. Haigis, J. D. Mancias, B. M. Wolpin, A. J. Aguirre, W. C. Hahn, K. D. Westover and N. S. Gray, *Nat. Chem. Biol.*, 2020, **16**, 635–643.

70 J. Zimmermann, E. Buchdunger, H. Mett, T. Meyer, N. B. Lydon and P. Traxler, *Bioorganic Med. Chem. Lett.*, 1996, **6**, 1221–1226.

71 P. W. Manley, S. W. Cowan-Jacob, E. Buchdunger, D. Fabbro, G. Fendrich, P. Furet, T. Meyer and J. Zimmermann, *Eur. J. Cancer*, 2002, 38 Suppl 5, S19–S27.

72 R. Capdeville, E. Buchdunger, J. Zimmermann and A. Matter, *Nat. Rev. Drug Discov.*, 2002, 1, 493–502.

73 T. Schindler, W. Bornmann, P. Pellicena, W. T. Miller, B. Clarkson and J. Kuriyan, *Science (80-.).*, 2000, **289**, 1938–1942.

74 M. Bantscheff, D. Eberhard, Y. Abraham, S. Bastuck, M. Boesche, S. Hobson, T. Mathieson, J. Perrin, M. Raida, C. Rau, V. Reader, G. Sweetman, A. Bauer, T. Bouwmeester, C. Hopf, U. Kruse, G. Neubauer, N. Ramsden, J. Rick, B. Kuster and G. Drewes, *Nat. Biotechnol.*, 2007, **25**, 1035–1044.

75 U. Rix, O. Hantschel, G. Dürnberger, L. L. Remsing Rix, M. Planyavsky, N. V. Fernbach, I. Kaupe, K. L. Bennett, P. Valent, J. Colinge, T. Köcher and G. Superti-Furga, *Blood*, 2007, **110**, 4055–4063.

76   E. Buchdunger, J. Zimmermann, H. Mett, T. Meyer, M. Müller, B. J. Druker and N. B. Lydon, *Cancer Res.*

77   B. J. Druker, M. Talpaz, D. J. Resta, B. Peng, E. Buchdunger, J. M. Ford, N. B. Lydon, H. Kantarjian, R. Capdeville, S. Ohno-Jones and C. L. Sawyers, *N. Engl. J. Med.*, 2001, **344**, 1031–1037.

78   A. Levitzki, *Annu. Rev. Pharmacol. Toxicol.*, 2013, 53, 161–185.

79   O. Hantschel, F. Grebien and G. Superti-Furga, *Cancer Res.*, 2012, **72**, 4890–4895.

80   List of clinically approved kinase inhibitors | MRC PPU, https://www.ppu.mrc.ac.uk/list-clinically-approved-kinase-inhibitors, (accessed 10 August 2020).

81   D. Fabbro, *Mol. Pharmacol.*, 2015, 87, 766–775.

82   F. Zuccotto, E. Ardini, E. Casale and M. Angiolini, *J. Med. Chem.*, 2010, 53, 2681–2694.

83   Y. Liu and N. S. Gray, *Nat. Chem. Biol.*, 2006, 2, 358–364.

84   O. P. J. Van Linden, A. J. Kooistra, R. Leurs, I. J. P. De Esch and C. De Graaf, *J. Med. Chem.*, 2014, 57, 249–277.

85   G. Bollag, J. Tsai, J. Zhang, C. Zhang, P. Ibrahim, K. Nolop and P. Hirth, *Nat. Rev. Drug Discov.*, 2012, **11**, 873–886.

86   P. N. Mortenson, V. Berdini and M. O'Reilly, in *Methods in Enzymology*, Academic Press, 2014, vol. 548, pp. 69–92.

87   L. Xing, J. Klug-Mcleod, B. Rai and E. A. Lunney, *Bioorganic Med. Chem.*, 2015, **23**, 6520–6527.

88   P. I. Poulikakos, C. Zhang, G. Bollag, K. M. Shokat and N. Rosen, *Nature*, 2010, **464**, 427–430.

89   Z. Karoulia, E. Gavathiotis and P. I. Poulikakos, *Nat. Rev. Cancer 2017 1711*, 2017, **17**, 676–691.

90   C. Zhang, W. Spevak, Y. Zhang, E. A. Burton, Y. Ma, G. Habets, J. Zhang, J. Lin, T. Ewing, B. Matusow, G. Tsang, A. Marimuthu, H. Cho, G. Wu, W. Wang, D. Fong, H. Nguyen, S. Shi, P. Womack, M. Nespi,

R. Shellooe, H. Carias, B. Powell, E. Light, L. Sanftner, J. Walters, J. Tsai, B. L. West, G. Visor, H. Rezaei, P. S. Lin, K. Nolop, P. N. Ibrahim, P. Hirth and G. Bollag, *Nature*, 2015, **526**, 583–586.

91   Z. Yao, Y. Gao, W. Su, R. Yaeger, J. Tao, N. Na, Y. Zhang, C. Zhang, A. Rymar, A. Tao, N. M. Timaul, R. Mcgriskin, N. A. Outmezguine, H. Y. Zhao, Q. Chang, B. Qeriqi, M. Barbacid, E. de Stanchina, D. M. Hyman, G. Bollag and N. Rosen, *Nat. Med.*, 2019, **25**, 284–291.

92   X. M. Cotto-Rios, B. Agianian, N. Gitego, E. Zacharioudakis, O. Giricz, Y. Wu, Y. Zou, A. Verma, P. I. Poulikakos and E. Gavathiotis, *Nat. Commun. 2020 111*, 2020, **11**, 1–16.

93   L. Xing, J. Klug-Mcleod, B. Rai and E. A. Lunney, *Bioorg. Med. Chem.*, 2015, **23**, 6520–6527.

94   A. K. Ghose, T. Herbertz, D. A. Pippin, J. M. Salvino and J. P. Mallamo, *J. Med. Chem.*, 2008, 51, 5149–5171.

95   A.-Z. I and H. PJ, *Drug Discov. Today*, 2009, **14**, 291–297.

96   A. Gaulton, A. Hersey, M. Nowotka, A. P. Bento, J. Chambers, D. Mendez, P. Mutowo, F. Atkinson, L. J. Bellis, E. Cibrián-Uhalte, M. Davies, N. Dedman, A. Karlsson, M. P. Magariños, J. P. Overington, G. Papadatos, I. Smit and A. R. Leach, *Nucleic Acids Res.*, 2017, **45**, D945–D954.

97   J. Mui, A Fragment-based Approach towards Small-Molecule Inhibitors of Nek7 Kinase. Ph.D. Thesis, The Institute of Cancer Research, University of London, 2015.

98   M. Vieth, J. J. Sutherland, D. H. Robertson and R. M. Campbell, *Drug Discov. Today*, 2005, 10, 839–846.

99   G. Karageorgis, S. Warriner and A. Nelson, *Nat. Chem.*, 2014, **6**, 872–876.

100   G. Karageorgis, M. Dow, A. Aimon, S. Warriner and A. Nelson, *Angew. Chemie Int. Ed.*, 2015, **54**, 13538–13544.

101   A. Padwa and M. D. Weingarten, *Chem. Rev.*, 1996, **96**, 223–270.

102   A. Padwa and S. K. Bur, *Tetrahedron*, 2007, **63**, 5341–5378.

103 H. M. L. Davies and R. E. J. Beckwith, *Chem. Rev.*, 2003, **103**, 2861–2903.

104 H. M. L. Davies and D. Morton, *Chem. Soc. Rev.*, 2011, **40**, 1857.

105 A. Padwa, D. J. Austin, S. F. Hornbuckle, M. A. Semones, M. P. Doyle and M. N. Protopopova, *J. Am. Chem. Soc.*, 1992, **114**, 1874–1876.

106 A. I. Green, C. P. Tinworth, S. Warriner, A. Nelson and N. Fey, *Chem. – A Eur. J.*, 2021, **27**, 2402–2409.

107 B. Neises and W. Steglich, *Angew. Chemie Int. Ed. English*, 1978, **17**, 522–524.

108 R. Tanaka, H. Ikemoto, M. Kanai, T. Yoshino and S. Matsunaga, *Org. Lett.*, 2016, **18**, 5732–5735.

109 S. E. Boiadjiev and D. A. Lightner, *Monatshefte fur Chemie*, 2005, **136**, 553–565.

110 S. S. Kulkarni, S. Singh, J. R. Shah, W. K. Low and T. T. Talele, *Eur. J. Med. Chem.*, 2012, **50**, 264–273.

111 A. Card, C. Caldwell, H. Min, B. Lokchander, Hualin Xi, S. Sciabola, A. V. Kamath, S. L. Clugston, W. R. Tschantz, Leyu Wang and D. J. Moshinsky, *J. Biomol. Screen.*, 2009, **14**, 31–42.

112 Caliper Life Sciences, LabChip | EZ Reader Series Benchtop Readers for Enzymatic Assays and Selectivity Profiling, 2007, http://www.caliperls.com/assets/009/5903.pdf, (accessed 20 June 2018).

113 PerkinElmer, Mobility shift assay development guide, 2012, http://www.perkinelmer.com/lab-solutions/resources/docs/LabChip EZ Reader Assay Development Guide v2.pdf, (accessed 20 June 2018).

114 C. M. Ouimet, C. I. D'amico and R. T. Kennedy, *Expert Opin. Drug Discov.*, 2017, **12**, 213–224.

115 D. L. (David L. Nelson, D. L. (David L. Nelson, A. L. Lehninger and M. M. Cox, *Lehninger principles of biochemistry*, W.H. Freeman, New York, 5th ed., 2008.

116   S. Chow, A. I. Green, C. Arter, S. Liver, A. Leggott, L. Trask, G. Karageorgis, S. Warriner and A. Nelson, *Synth.*, 2020, **52**, 1695–1706.

117   H. O. House and C. J. Blankley, *J. Org. Chem.*, 1968, **33**, 53–60.

118   D. M. Hodgson and D. Angrish, *Chem. - A Eur. J.*, 2007, **13**, 3470–3479.

119   G. Fan, Z. Wang and A. G. H. Wee, *Chem. Commun.*, 2006, **0**, 3732–3734.

120   H. Lei and J. Atkinson, *J. Org. Chem.*, 2000, **65**, 2560–2567.

121   B. Miriyala and J. S. Williamson, *Tetrahedron Lett.*, 2003, **44**, 7957–7959.

122   M. Regitz, *Angew. Chemie Int. Ed. English*, 1967, **6**, 733–749.

123   M. P. Doyle, M. A. McKervey and T. Ye, *Modern catalytic methods for organic synthesis with diazo compounds : from cyclopropanes to ylides*, Wiley, 1998.

124   J. S. Baum, D. A. Shook, H. M. L. Davies and H. D. Smith, *Synth. Commun.*, 1987, **17**, 1709–1716.

125   L. Liu and J. Zhang, *Chem. Soc. Rev.*, 2016, 45, 506–516.

126   M. R. Fructos, M. M. Díaz-Requejo and P. J. Pérez, *Chem. Commun.*, 2016, **52**, 7326–7335.

127   P. De Frémont, E. D. Stevens, M. R. Fructos, M. Mar Díaz-Requejo, P. J. Pérez and S. P. Nolan, *Chem. Commun.*, 2006, 2045–2047.

128   A. Green, F. Hobor, C. Tinworth, S. Warriner, A. Wilson and A. Nelson, *Chem. – A Eur. J.*, 2020, chem.202002153.

129   J. Mui, The Institute of Cancer Research, University of London, 2015.

130   P. Shah and A. D. Westwell, *J. Enzyme Inhib. Med. Chem.*, 2007, 22, 527–540.

131   T. D. Heightman, V. Berdini, H. Braithwaite, I. M. Buck, M. Cassidy, J. Castro, A. Courtin, J. E. H. Day, C. East, L. Fazal, B. Graham, C. M. Griffiths-Jones, J. F. Lyons, V. Martins, S. Muench, J. M. Munck, D. Norton, M. O'Reilly, N. Palmer, P. Pathuri, M. Reader, D. C. Rees, S.

J. Rich, C. Richardson, H. Saini, N. T. Thompson, N. G. Wallis, H. Walton, N. E. Wilsher, A. J. A. Woolford, M. Cooke, D. Cousin, S. Onions, J. Shannon, J. Watts and C. W. Murray, *J. Med. Chem.*, 2018, **61**, 4978–4992.

132 S. D. Roughley and A. M. Jordan, *J. Med. Chem.*, 2011, **54**, 3451–3479.

133 J. Boström, D. G. Brown, R. J. Young and G. M. Keserü, *Nat. Rev. Drug Discov.*, 2018, **17**, 709–727.

134 G. B. Smith, G. C. Dezeny, D. L. Hughes, A. O. King and T. R. Verhoeven, *J. Org. Chem.*, 2002, **59**, 8151–8156.

135 D. N. Korolev and N. A. Bumagin, *Tetrahedron Lett.*, 2005, **46**, 5751–5754.

136 N. Kudo, M. Perseghini and G. C. Fu, *Angew. Chemie Int. Ed.*, 2006, **45**, 1282–1284.

137 T. A. Moss, M. S. Addie, T. Nowak and M. J. Waring, *Synlett*, 2012, **2012**, 285–289.

138 C. J. Hastie, H. J. McLauchlan and P. Cohen, *Nat. Protoc.*, 2006, **1**, 968–971.

139 K. R. Roesch and R. C. Larock, *J. Org. Chem.*, 1998, **63**, 5306–5307.

140 J. C. Lanter, J. J. Fiordeliso, V. C. Alford, X. Zhang, K. M. Wells, R. K. Russell, G. F. Allan, M.-T. Lai, O. Linton, S. Lundeen and Z. Sui, *Bioorg. Med. Chem. Lett.*, 2007, **17**, 2545–2548.

141 N. R. Curtis, J. J. Kulagowski, P. D. Leeson, M. P. Ridgill, F. Emms, S. B. Freedman, S. Patel and S. Patel, *Bioorg. Med. Chem. Lett.*, 1999, **9**, 585–588.

142 Y. Feng, Y. Wang, B. Landgraf, S. Liu and G. Chen, *Org. Lett.*, 2010, **12**, 3414–3417.

143 G. Zeni and R. C. Larock, *Chem. Rev.*, 2006, 106, 4644–4680.

144 N. Guimond, S. I. Gorelsky and K. Fagnou, *J. Am. Chem. Soc.*, 2011, **133**, 6449–6457.

145 D. R. Stuart, M. Bertrand-Laperle, K. M. N. Burgess and K. Fagnou, *J. Am. Chem. Soc.*, 2008, **130**, 16474–16475.

146 S. Rakshit, F. W. Patureau and F. Glorius, *J. Am. Chem. Soc.*, 2010, **132**, 9585–9587.

147 Y. Su, M. Zhao, K. Han, G. Song and X. Li, *Org. Lett.*, 2010, **12**, 5462–5465.

148 N. Guimond and K. Fagnou, *J. Am. Chem. Soc.*, 2009, **131**, 12050–12051.

149 T. K. Hyster and T. Rovis, *J. Am. Chem. Soc.*, 2010, **132**, 10565–10569.

150 S. Rakshit, C. Grohmann, T. Besset and F. Glorius, *J. Am. Chem. Soc.*, 2011, **133**, 2350–2353.

151 N. Guimond, C. Gouliaras and K. Fagnou, *J. Am. Chem. Soc.*, 2010, **132**, 6908–6909.

152 Z.-J. Jia, C. Merten, R. Gontla, C. G. Daniliuc, A. P. Antonchick and H. Waldmann, *Angew. Chemie Int. Ed.*, 2017, **56**, 2429–2434.

153 B. Ye and N. Cramer, *Science (80-.).*, 2012, **338**, 504–506.

154 H. S. Park, S. H. Nam, J. K. Lee, C. N. Yoon, B. Mannervik, S. J. Benkovic and H. S. Kim, *Science (80-.).*, 2006, **311**, 535–538.

155 E. A. Trifonova, N. M. Ankudinov, A. A. Mikhaylov, D. A. Chusov, Y. V. Nelyubina and D. S. Perekalin, *Angew. Chemie Int. Ed.*, 2018, **57**, 7714–7718.

156 N. J. Webb, S. P. Marsden and S. A. Raw, *Org. Lett.*, 2014, **16**, 4718–4721.

157 M. A. Düfert, K. L. Billingsley and S. L. Buchwald, *J. Am. Chem. Soc.*, 2013, **135**, 12877–12885.

158 N. Palmer, T. M. Peakman, D. Norton and D. C. Rees, *Org. Biomol. Chem.*, 2016, **14**, 1599–1610.

159 M. R. Biscoe, B. P. Fors and S. L. Buchwald, *J Am Chem Soc*, 2008, **130**, 6686–6687.

160   M. Presset, D. Oehlrich, F. Rombouts and G. A. Molander, *Org. Lett.*, 2013, **15**, 1528–1531.

161   J. R. Huckins, E. A. Bercot, O. R. Thiel, T. L. Hwang and M. M. Bio, *J. Am. Chem. Soc.*, 2013, **135**, 14492–14495.

162   W. Lossen, *Ann. der Chemie und Pharm.*, 1872, **161**, 347–362.

163   L. Bauer and O. Exner, *Angew. Chemie Int. Ed. English*, 1974, **13**, 376–384.

164   L. Jašíková, E. Hanikýřová, A. Škríba, J. Jašík and J. Roithová, *J. Org. Chem.*, 2012, **77**, 2829–2836.

165   M. P. Georgiadis, C. D. Apostolopoulos and S. A. Haroutounian, *J. Heterocycl. Chem.*, 1991, **28**, 599–604.

166   C. Y. Chern, Y. P. Huang and W. M. Kan, *Tetrahedron Lett.*, 2003, **44**, 1039–1041.

167   T. K. Hyster, D. M. Dalton and T. Rovis, *Chem. Sci.*, 2015, **6**, 254–258.

168   N. J. Webb, Development and Application of Rhodium(III)-Catalysed C-H Activation Methodologies. Ph.D. Thesis, University of Leeds, 2014.

169   S. Lee, N. Semakul and T. Rovis, *Angew. Chemie Int. Ed.*, 2020, **59**, 4965–4969.

170   J. G. Topliss, *J. Med. Chem.*, 2002, **15**, 1006–1011.

171   * Ahmed F. Abdel-Magid, Kenneth G. Carson, Bruce D. Harris, and Cynthia A. Maryanoff and R. D. Shah, *J. Org. Chem.*, 1996, **61**, 3849–3862.

172   G. Drewes, A. Ebneth, U. Preuss, E.-M. Mandelkow and E. Mandelkow, *Cell*, 1997, **89**, 297–308.

173   H. Lund, E. Gustafsson, A. Svensson, M. Nilsson, M. Berg, D. Sunnemark and G. von Euler, *Acta Neuropathol. Commun. 2014 21*, 2014, **2**, 1–15.

174   J. D. Goodreid, P. A. Duspara, C. Bosch and R. A. Batey, *J. Org.*

Chem., 2014, **79**, 943–954.

175   Q. Lin, D. Meloni, Y. Pan, M. Xia, J. Rodgers, S. Shepard, M. Li, L. Galya, B. Metcalf, T. N. Yue, P. Liu and J. Zhou, *Org. Lett.*, 2009, **11**, 1999–2002.

176   L. Zhang, X. jun Wang, J. Wang, N. Grinberg, D. K. Krishnamurthy and C. H. Senanayake, *Tetrahedron Lett.*, 2009, **50**, 2964–2966.

177   Q. Zhou, L. Jia, F. Du, X. Dong, W. Sun, L. Wang and G. Chen, *New J. Chem.*, 2020, **44**, 2247–2255.

178   S. Inel, R. Alan Jones and C. Ogretir, *Tetrahedron*, 1984, **40**, 3979–3986.

179   K. E. Coffey and G. K. Murphy, *Synlett*, 2015, **26**, 1003–1007.

180   * Magoichi Sako, Isamu Yaekura, and Souichi Oda and K. Hirota, *J. Org. Chem.*, 2000, **65**, 6670–6675.

181   V. A. Nikolaev, V. V. Shevchenko, M. S. Platz and N. N. Khimich, *Russ. J. Org. Chem. 2006 426*, 2006, **42**, 815–827.

182   M. Kitamura, N. Tashiro, S. Miyagawa and T. Okauchi, *Synthesis (Stuttg).*, 2011, **2011**, 1037–1044.

183   Z. Wang, X. Bi, P. Liao, R. Zhang, Y. Liang and D. Dong, *Chem. Commun.*, 2012, **48**, 7076–7078.

184   C. Zhai, D. Xing, C. Jing, J. Zhou, C. Wang, D. Wang and W. Hu, *Org. Lett.*, 2014, **16**, 2934–2937.

185   V. M. Muzalevskiy, E. S. Balenkova, A. V. Shastin, A. M. Magerramov, N. G. Shikhaliev and V. G. Nenajdenko, *Russ. Chem. Bull. 2011 6011*, 2012, **60**, 2343–2346.

186   P. Garcia, Y. Y. Lau, M. R. Perry and L. L. Schafer, *Angew. Chemie Int. Ed.*, 2013, **52**, 9144–9148.

187   P. A. Rist, R. S. Grainger and P. W. Davies, *Org. Lett.*, 2021, **23**, 642–646.

188   S. K. Bagal, K. Omoto, D. C. Blakemore, P. J. Bungay, J. G. Bilsland, P. J. Clarke, M. S. Corbett, C. N. Cronin, J. J. Cui, R. Dias, N. J.

Flanagan, S. E. Greasley, R. Grimley, E. Johnson, D. Fengas, L. Kitching, M. L. Kraus, I. McAlpine, A. Nagata, G. J. Waldron and J. S. Warmus, *J. Med. Chem.*, 2018, **62**, 247–265.

189   M. Michels, M. Follmann, A. Vakalopoulos, K. Zimmermann, N. Teusch, M. Lobell, D. Bierer and K. Engel, *Fluoro-substituted 3,5-dicyano-4-(1H-indazol-5-yl)-2,6-dimethyl-1,4-dihydropyridine derivatives and methods of use thereof, US 9422263 B2*, 2011.

190   A. Köhler, C. Welz, K. Börngen, D. Kulke, T. Ilg, J. Köbberling, W. Hübsch, H.-G. Schwarz, U. Görgens, U. Ebbinghaus-Kintscher, M. Hink, D. Nennstiel, K. Raming, M. Adamczewski And C. Böhm, *Pyrazolopyrimidine Derivatives, US10604525b2*, 2017.

191   L. Yan, J. Wu, H. Chen, S. Zhang, Z. Wang, H. Wang and F. Wu, *RSC Adv.*, 2015, **5**, 73660–73669.

192   E. J. Hanan, M. Baumgardner, M. C. Bryan, Y. Chen, C. Eigenbrot, P. Fan, X. H. Gu, H. La, S. Malek, H. E. Purkey, G. Schaefer, S. Schmidt, S. Sideris, I. Yen, C. Yu and T. P. Heffron, *Bioorganic Med. Chem. Lett.*, 2016, **26**, 534–539.

193   T. Zierke, J. Rheinheimer, M. Rack, S. P. Smidt, A. G. Altenhoff, J. Schmidt-Leithoff and N. Challand, *Method For The Production Of N-Substituted (3-Dihalomethyl-1-Methyl-Pyrazole-4-Yl) Carboxamides, WO/2008/145740*, 2008.

194   N. Luise and P. G. Wyatt, *Chem. – A Eur. J.*, 2018, **24**, 10443–10451.

195   E. Jones, Graham, J. Miles, Timothy and D. Pearson, Neil, *Pyrrolo-Quinoxalinone Derivatives As Antibacterials, WO/2007/115947*, 2007.

196   H. Chen, X. Han, N. Qin, L. Wei, Y. Yang, L. Rao, B. Chi, L. Feng, Y. Ren and J. Wan, *Bioorganic Med. Chem.*, 2016, **24**, 1225–1230.

197   Z. Chen, Y. Zheng and J. A. Ma, *Angew. Chemie - Int. Ed.*, 2017, **56**, 4569–4574.

198   L. Nielsen and T. Skrydstrup, *J. Am. Chem. Soc.*, 2008, **130**, 13145–13151.

199   M. E. Scheller and B. Frei, *Helv. Chim. Acta*, 1986, **69**, 44–52.

200   V. Chandrasekaran, S. Kalyan, V. Biel, M. Lettau, P. T. Nerdal, H.-H. Oberg, D. Wesch, T. K. Lindhorst and D. Kabelitz, *Medchemcomm*, 2015, **6**, 919–925.

201   M. Mahmoudian, A. Lowdon, M. Jones, M. Dawson and C. Wallis, *Tetrahedron: Asymmetry*, 1999, **10**, 1201–1206.

Appendix A

Appendices for Chapter 2
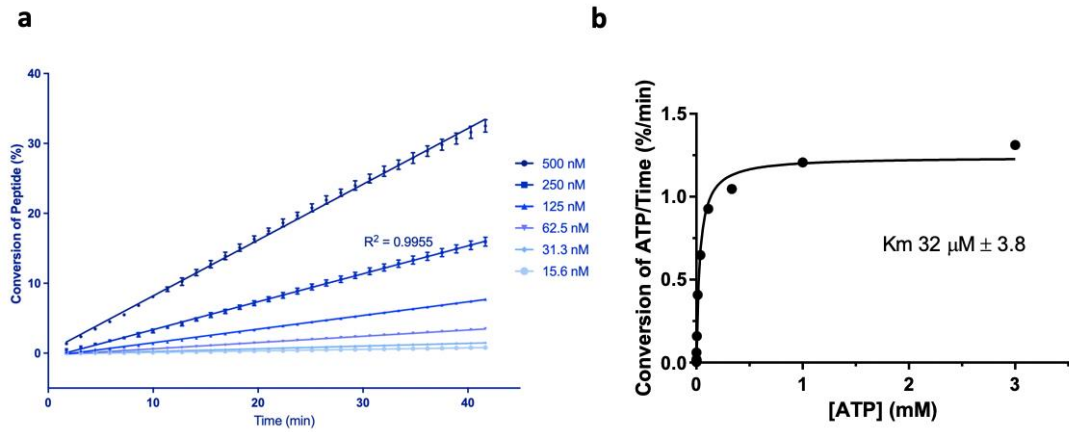
A.1 Optimal Assay Protein and ATP Concentration

Figure A-1. Optimal protein and ATP assay concentrations. (a) Nek7 titration to determine 250 nM suitable assay concentration. (b) ATP titration to measure the K_M of ATP for Nek7.

A.2 Fragment IC$_{50}$ Determination
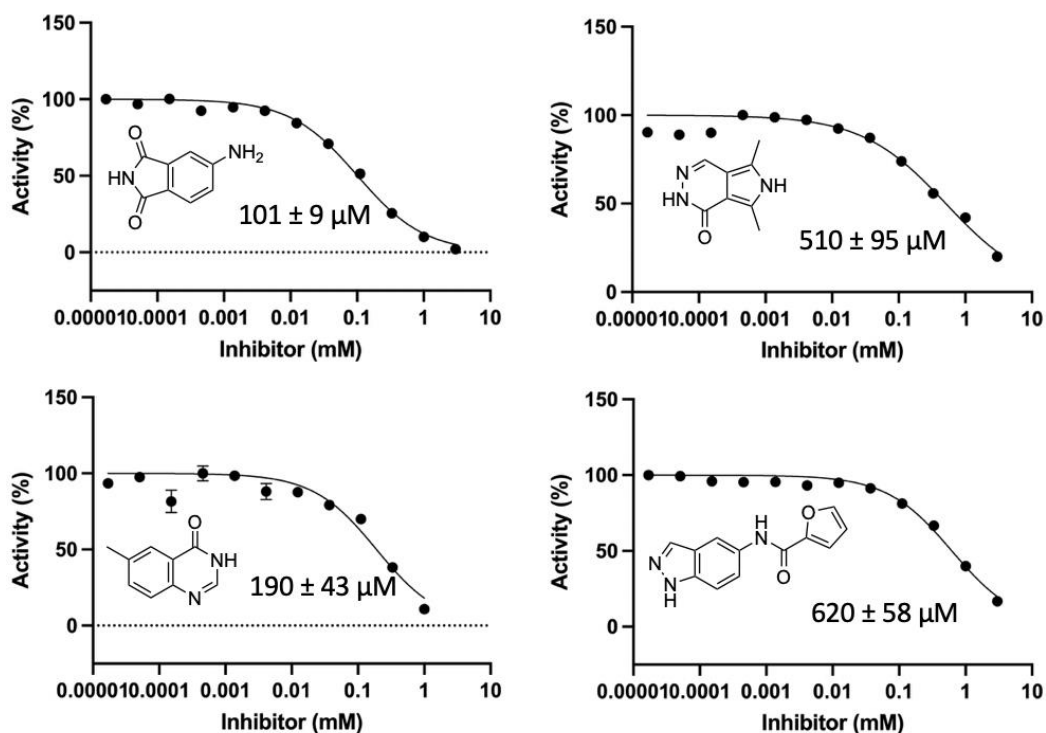
Figure A-2 Representative IC$_{50}$ curves. Each point n = 2 and SEM is shown (omitted where the error bars are smaller than the point). Normalised to the largest value and 0% activity.

A.3 Mock Array Round 1 and 2
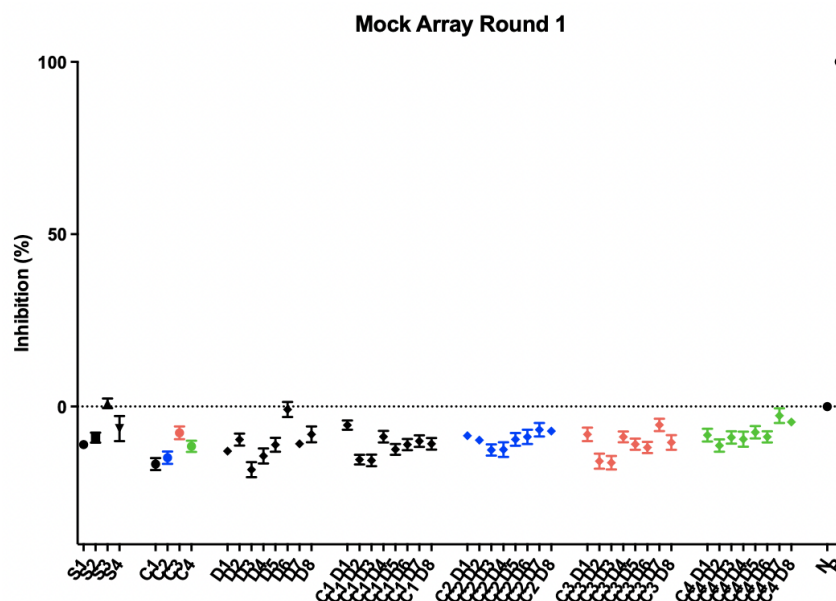
Figure A-3. Round 1 mock array showing that no component or combination of components are active under the assay conditions.
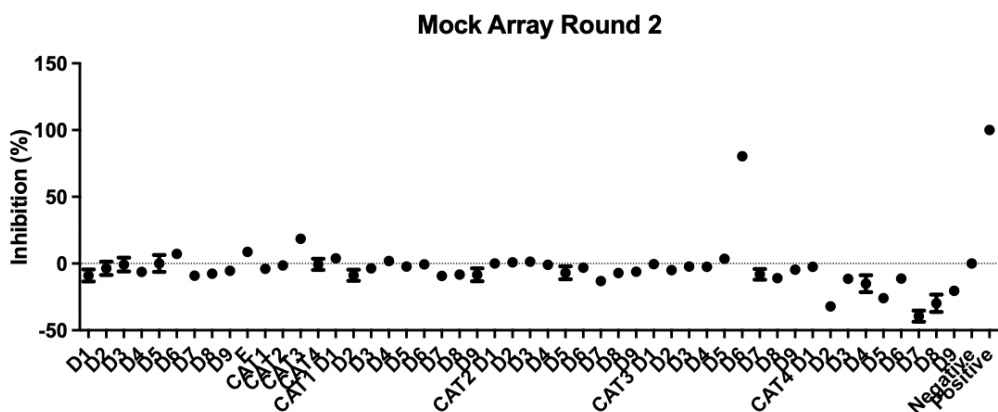
Mock Array Round 2

Figure A-4. Round 2 mock array showing only one combination of diazo-amide and catalyst is active under the assay conditions (see specific Chapter). Any reaction with this diazo-amide and catalyst combination was ignored.

A.4 Bioactive Product Mixture Validation

Table A-1. Validation of Bioactive Reaction Product Mixtures Post Scale-up

Entry	Fragment	α-Diazo amide	Catalyst	Solvent	Percentage Inhibition
1	**3-2**	**3-6**	$[Rh_2(cap)_4]$	CH_2Cl_2	97 (100 μM)
2		**3-6c**	$[Rh_2(cap)_4]$	CH_2Cl_2	187 ± 14 μM[a] (IC_{50})

[a]2-fold improvement over fragment alone. Note, this is the IC_{50} of the product mixture assuming a total product concentration relative to fragment.

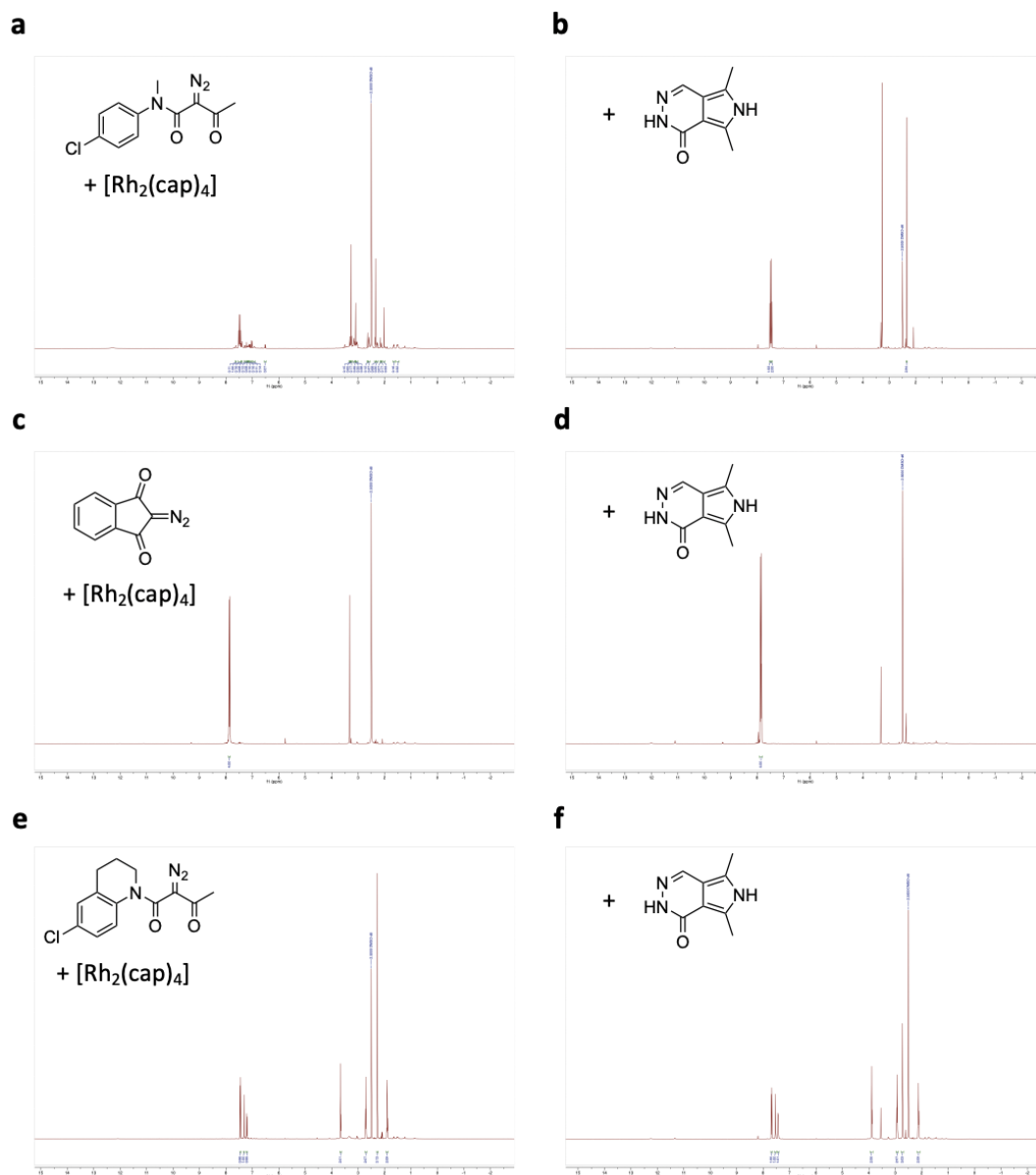## A.5 Bioactive Product Mixture NMR Analysis

Figure A-5. Bioactive product mixture NMR analysis. All reactions were subjected to the ADS workflow and re-dissolved in d_6-DMSO for analysis. (a) Diazo-amide and catalyst without and with (b) fragment. (c) Diazo-amide and catalyst without and with (d) fragment. (e) Diazo-amide and catalyst without and with (f) fragment. In all cases, no detectable reaction occurred except for in (a) when diazo-amide and catalyst were combined without fragment.

Appendix B

Appendices for Chapter 3

B.1 Representative IC$_{50}$ Curves
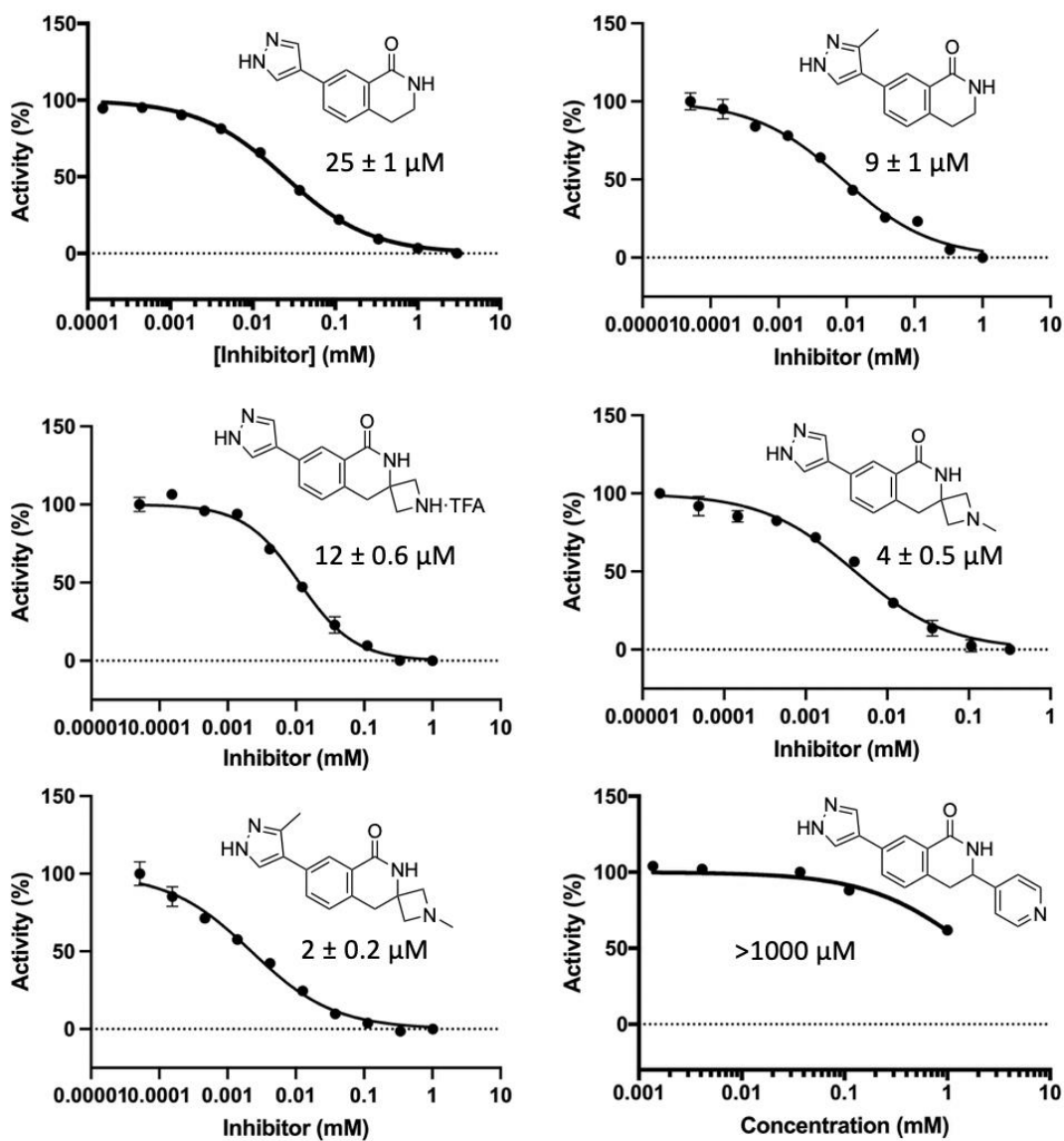
Figure B-1. Representative IC$_{50}$ curves. Each point n = 2 and SEM is shown (omitted where the error bars are smaller than the point). 2% DMSO was used as the negative control and 3 mM **4-3** was used as the positive.

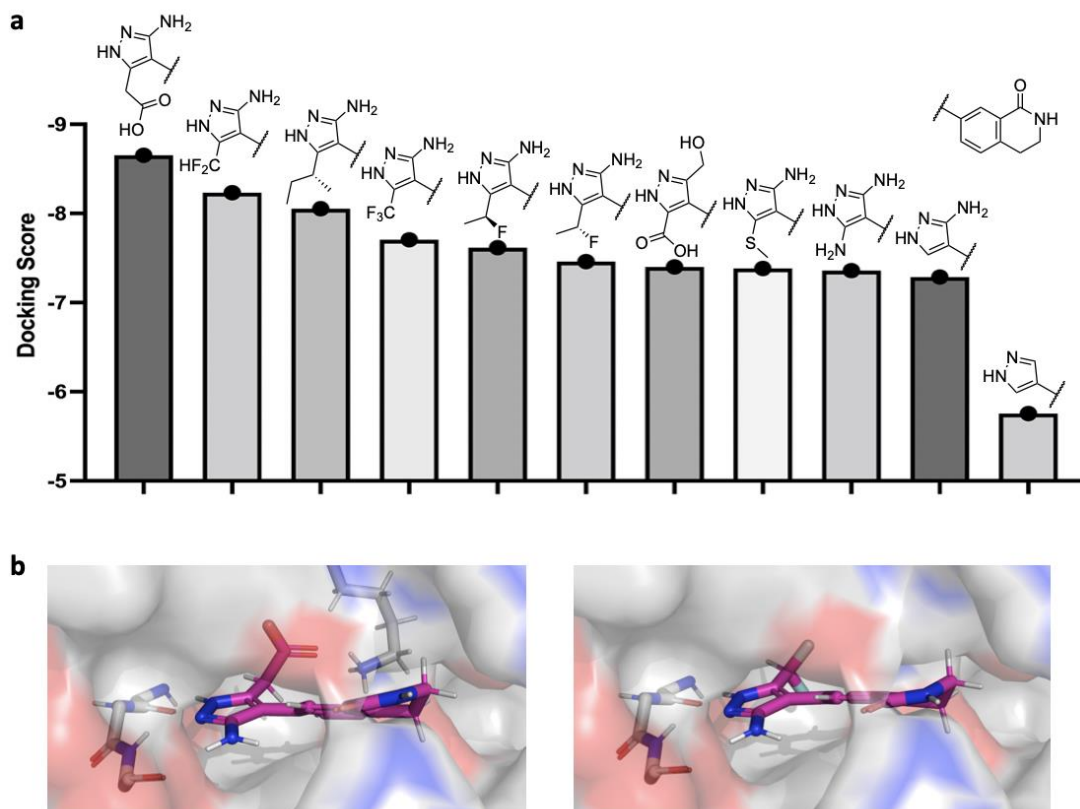## B.2 Docking Score and Poses for Top Ten Pyrazoles

Figure B-2. (a) Docking score of top ten compounds and (b) two representative poses.
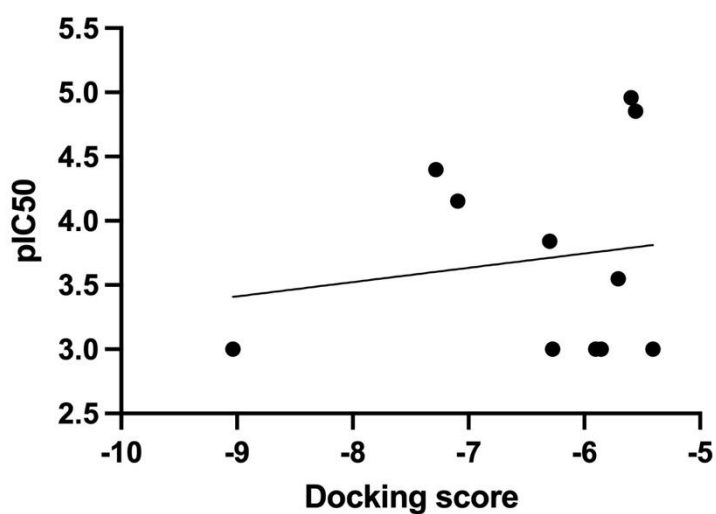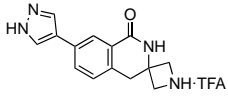
B.3 Docking Score *versus* pIC$_{50}$

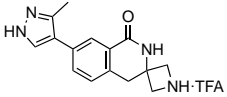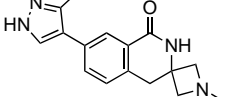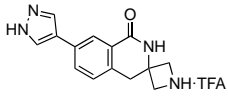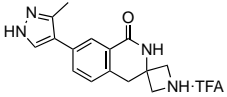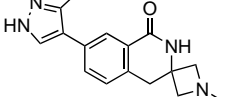**Figure B-3.** Docking score *versus* pIC$_{50}$ for the 3,5-pyrazole library of compounds.

B.4 Selectivity Data

Table B-1. Activity of 50 Enzymes Across the Kinome

Kinase			
	1 μM		
Kinase	Enzyme activity (%)		
AMPK (hum)	2	0	1
Aurora B	40	34	29
BTK	73	51	43
CAMK1	13	34	9
CAMKKb	12	12	16
CHK2	8	10	7
CK1δ	1	1	1
CK2	7	11	8
DYRK1A	7	9	8
EF2K	75	68	83
EPH-A2	29	45	65
GSK3b	0	0	0
HER4	9	6	26
HIPK2	1	3	2
IGF-1R	4	7	24
IRAK4	11	10	20
JAK3	2	2	2
JNK1	4	4	9
Lck	95	116	96
LKB1	17	20	15
MARK3§	1	0	3
MKK1	64	60	46
MLK3	31	28	26
MSK1	6	5	4
MST2	15	30	22
NEK6§*	62	67	121

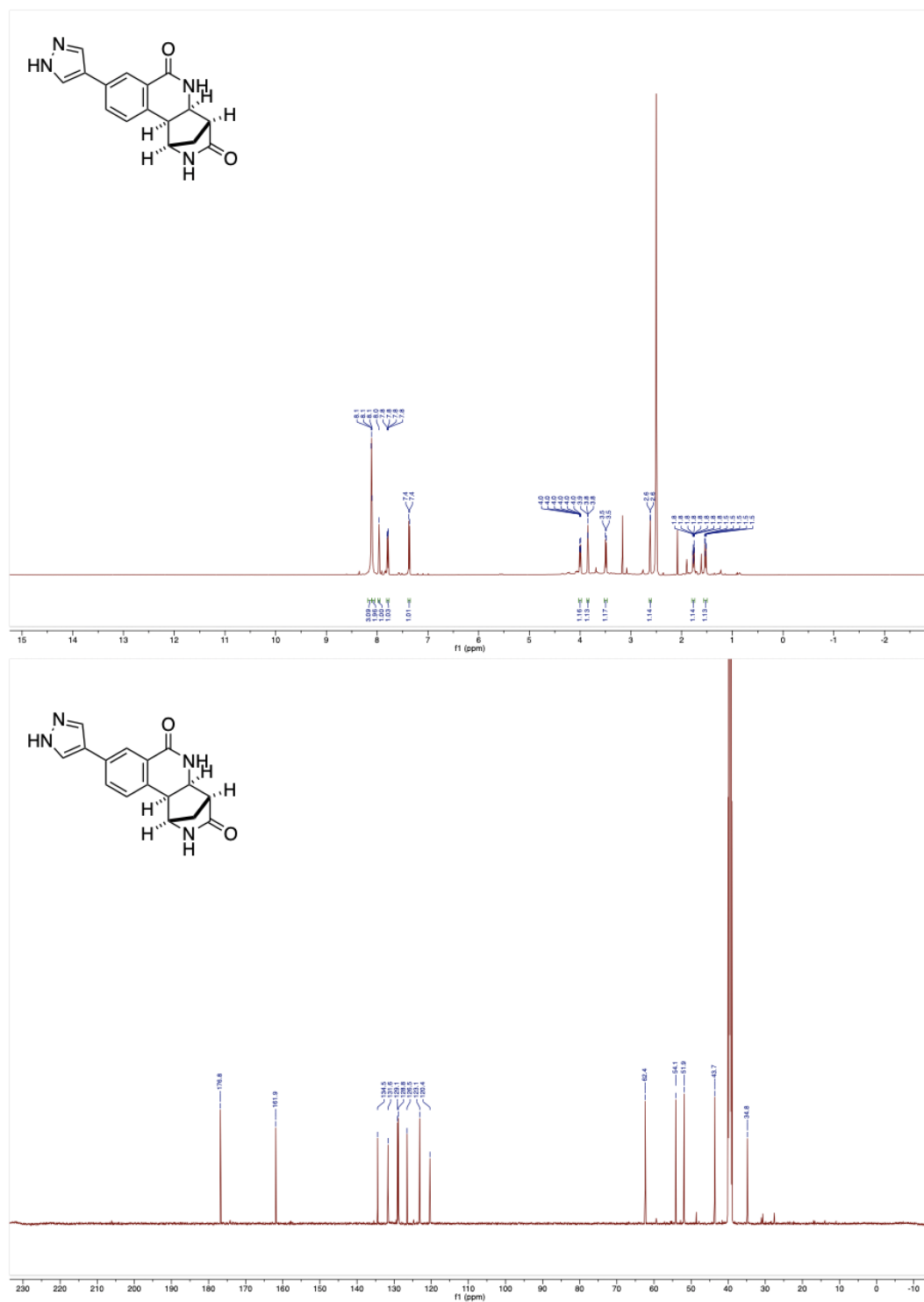|			
	1 μM		
Kinase	Enzyme activity (%)		
p38a MAPK	34	46	50
PAK4	2	2	9
PDK1	14	3	7
PIM1	2	2	2
PKA	2	2	1
PKBa	2	2	1
PKCa	2	4	5
PKD1	61	89	71
PLK1*	2	1	1
PRK2	1	0	0
RIPK2	17	14	23
ROCK 2	5	6	4
RSK1	36	27	19
S6K1	23	16	18
SGK1	11	9	7
SmMLCK^	102	57	109
Src	36	43	38
SRPK1	25	73	74
SYK	6	1	20
TAK1	1	1	1
TBK1	32	24	90
TrkA	99	32	43
TTK	10	9	19
VEG-FR	2	2	1

B.5 Representative NMR

Figure B-4. Representative ^{1}H and ^{13}C NMR for **3-82**. 2D experiments were used to aid assignment and omitted for clarity.